CHARACTERISING THE TETRASPANIN/ADAM10 'MOLECULAR SCISSORS' FOR THE PLATELET COLLAGEN AND FIBRIN RECEPTOR GPVI

by

CHEK ZIU KOO

A thesis submitted to the University of Birmingham for the degree of
DOCTOR OF PHILOSOPHY

School of Biosciences
College of Life and Environmental Sciences
University of Birmingham
September 2021

ABSTRACT

ADAM10 is a ubiquitous and essential transmembrane 'molecular scissor' that cleaves the ectodomains of >100 different membrane proteins. ADAM10 is regulated by interaction with six tetraspanins (Tspan5, Tspan10, Tspan14, Tspan15, Tspan17 or Tspan33) termed TspanC8s. Importantly, emerging evidence suggests that each TspanC8 promotes cleavage of different ADAM10 substrates, leading to proposal of the 'six scissors' hypothesis which suggests that each TspanC8/ADAM10 scissor has a distinct substrate repertoire. The platelet-activating collagen and fibrin receptor GPVI is a promising anti-thrombotic target that is also an ADAM10 substrate. Of the three scissors expressed on human platelets, Tspan15/ADAM10 and Tspan33/ADAM10 can cleave GPVI, whereas Tspan14/ADAM10 cannot. The overarching aim of this project was to examine the molecular basis behind the 'six scissors' hypothesis using GPVI as a model substrate. This thesis provided evidence of a novel mechanism where TspanC8s may differentially regulate ADAM10 substrate specificity by controlling the protease's access to the cut site of a substrate. Tspan15/ADAM10 was identified as the most efficient scissor for GPVI. The extracellular region of Tspan15 was essential for ADAM10 cleavage of GPVI and its cytoplasmic domain appeared to have a minor negative regulatory role. Analysis of non-coding *TSPAN15* polymorphisms revealed that high *TSPAN15* expression may confer protection against venous thrombosis. ADAM10 and Tspan15 regulated each other's expression at the protein level, and the cytoplasmic domain of ADAM10 was required for Tspan15 surface expression. Finally, this thesis provided evidence that functional redundancy of Tspan15/ADAM10 with other TspanC8/ADAM10 scissors was minimal, even at high expression levels. These findings may inform the feasibility and the design of future therapeutics that may allow substrate-specific modulation of ADAM10 activity by targeting the regulatory TspanC8 tetraspanin.

楽じゃなかったけど、楽しかったです。

It was not easy, but it was fun.

I dedicate this thesis to you
who inspired and supported me in this journey.

ACKNOWLEDGEMENTS

My supervisors, Mike Tomlinson and Natalie Poulter:

Mike, in May 2016, I got to know you for the first time (apart from recognising you as the lecturer who wore a red shirt to celebrate Liverpool winning a match and who referenced Luis Suárez's infamous biting habits when introducing platelets) when I had my first real research experience in your lab as part of my three-month MSc mini-project, thinking that this would be the only time that I would ever do any wet lab work. Little did I know that these tiny molecules called 'tetraspanins' and 'ADAM10' can be so addictive, so much that I didn't mind getting my feet (or gloved hands, rather) wet to learn and discover new things about them! And, before you say it… I won't forget that you taught me (almost) everything, apart from Fantasy Football, obviously, because I still couldn't beat your score even after playing Triple Captain!

Natalie, in January 2017, I met you for the first time during my interview for the one-year COMPARE Research Technician position with yourself and Mike on a snowy afternoon in the IBR. "How do you like to be managed?" you asked. "I like the idea of an open and honest communication," I answered. There is no doubt that we have achieved this, Natalie! You have always been there for me. All issues, regardless of whether they were experiment- or admin-related, had always been resolved quickly after speaking to you, because you always seem to have a solution! If there is an award for "the most caring and efficient supervisor", you will no doubt be the recipient. There is one thing that I do regret though – I don't seem to have mastered your super single-molecule microscopy skills yet!

Thank you both for putting up with me over the past few years. I will miss our regular meetings very much! Now, can we find the TspanC8/ADAM10 scissors that regulate shedding of tears?

My family, friends and colleagues:

Science cannot be done alone. I am very grateful to have met all 78 of you! Thank you for your patience, kindness and friendliness. This thesis would not have been completed without your generosity in sharing encouragement, compassion, knowledge, equipment, reagents, laughter, tears and most importantly… food!

Funding bodies:

This project was funded by a British Heart Foundation PhD studentship (FS/18/9/33388), a project grant from Mestag Therapeutics Limited, a COMPARE pump-priming grant, a COMPARE Team Science collaborative grant and tuition fee contributions from the College of Life and Environmental Sciences and the Birmingham Doctoral Scholarship Fund.

CONTENTS

FIGURES

Chapter 1 General introduction

Chapter 3 Investigating the mechanisms by which TspanC8s differentially regulate GPVI cleavage by ADAM10

Chapter 4 Analysis of *TSPAN15* and *GP6* variants associated with thrombosis

Chapter 5 How do Tspan15 and ADAM10 regulate each other?

Chapter 6 Investigating potential Tspan15 redundancy with other TspanC8s

Chapter 7 General discussion

Appendix

TABLES

Chapter 1 General introduction

Chapter 2 Materials and methods

Chapter 4 Analysis of *TSPAN15* and *GP6* variants associated with thrombosis

ABBREVIATIONS

ADAM	A disintegrin and metalloprotease
ANOVA	Analysis of variance
APP	Amyloid precursor protein
ATP	Adenosine triphosphate
BiFC	Bimolecular fluorescence complementation
BSA	Bovine serum albumin
cDNA	Complementary DNA
cpm	Counts per molecule
CRISPR/Cas9	Clustered regularly interspaced short palindromic repeats/CRISPR-associated protein 9
Cryo-EM	Cryo-electron microscopy
DAPT	N-[N-(3,5-Difluorophenacetyl-L-alanyl)]-(S)-phenylglycine t-butyl ester
EDTA	Ethylenediaminetetraacetic acid
EGF	Epidermal growth factor
EPCR	Endothelial protein C receptor
eQTL	Expression quantitative trait loci
ER	Endoplasmic reticulum
FBS	Foetal bovine serum
FcRγ	Fc receptor gamma chains
FCS	Fluorescence correlation spectroscopy
FITC	Fluorescein isothiocyanate
GPVI	Glycoprotein VI
GWAS	Genome-wide association study
HEK-293T	Human embryonic kidney cells expressing the simian virus 40 large T-antigen
HEL	Human erythroleukemia
Ig	Immunoglobulin
IL6R	Interleukin-6 receptor
ITAM	Immunoreceptor tyrosine-based activation motif
LB	Luria broth
LD	Linkage disequilibrium
mAb	Monoclonal antibody
MES	2-(N-morpholino)ethanesulfonic acid
N-cadherin	Neuronal cadherin
NEM	N-ethylmaleimide
NFAT	Nuclear factor of activated T-cells
pAb	Polyclonal antibody
PAGE	Polyacrylamide gel electrophoresis
PBS	Phosphate-buffered saline
PCH	Photon counting histogram

PDB	Protein Data Bank
PEI	Polyethylenimine
PMA	Phorbol myristate acetate
pNPP	p-Nitrophenyl phosphate
PS	Phosphatidylserine
qPCR	Quantitative polymerase chain reaction
RAGE	Receptor for advanced glycation end products
rsID	Reference SNP ID
RT	Reverse transcription
SDS	Sodium dodecyl sulfate
sfGFP	Superfolder green fluorescent protein
SH3	Src homology domain 3
SNP	Single-nucleotide polymorphism
TBS	Tris-buffered saline
TCA	Trichloroacetic acid
TIMP	Tissue inhibitor of metalloproteases
vWF	von Willebrand factor

PUBLICATIONS

Koo, C. Z.*, Harrison, N.*, Noy, P. J.*, Szyroka, J., Matthews, A. L., Hsia, H. E., Müller, S. A., Tüshaus, J., Goulding, J., Willis, K., Apicella, C., Cragoe, B., Davis, E., Keles, M., Malinova, A., McFarlane, T. A., Morrison, P. R., Nguyen, H. T. H., Sykes, M. C., Ahmed, H., Maio, A. di, Seipold, L., Saftig, P., Cull, E., Pliotas, C., Rubinstein, E., Poulter, N. S., Briddon, S. J., Holliday, N. D., Lichtenthaler, S. F. and Tomlinson, M. G. (2020) "The tetraspanin Tspan15 is an essential subunit of an ADAM10 scissor complex," *Journal of Biological Chemistry*, 295(36), pp. 12822–12839. doi: 10.1074/jbc.ra120.012601. *equal contribution

Seifert, A., Düsterhöft, S., Wozniak, J., **Koo, C. Z.**, Tomlinson, M. G., Nuti, E., Rossello, A., Cuffaro, D., Yildiz, D. and Ludwig, A. (2021) "The metalloproteinase ADAM10 requires its activity to sustain surface expression," *Cellular and Molecular Life Sciences*, 78(2), pp. 715–732. doi: 10.1007/s00018-020-03507-w.

Harrison, N., **Koo, C. Z.** and Tomlinson, M. G. (2021) "Regulation of ADAM10 by the TspanC8 family of tetraspanins and their therapeutic potential," *International Journal of Molecular Sciences*, 22(13), p. 6707. doi: 10.3390/ijms22136707.

Matthews, A. L., **Koo, C. Z.**, Szyroka, J., Harrison, N., Kanhere, A. and Tomlinson, M. G. (2018) "Regulation of leukocytes by TspanC8 tetraspanins and the 'molecular scissor' ADAM10," *Frontiers in Immunology*, 9, p. 1451. doi: 10.3389/fimmu.2018.01451.

Gavin, R. L., **Koo, C. Z.** and Tomlinson, M. G. (2020) "Tspan18 is a novel regulator of thrombo-inflammation," *Medical Microbiology and Immunology*, 209(4), pp. 553–564. doi: 10.1007/s00430-020-00678-y.

Noy, P. J., Gavin, R. L., Colombo, D., Haining, E. J., Reyat, J. S., Payne, H., Thielmann, I., Lokman, A. B., Neag, G., Yang, J., Lloyd, T., Harrison, N., Heath, V. L., Gardiner, C., Whitworth, K. M., Robinson, J., **Koo, C. Z.**, Maio, A. di, Harrison, P., Lee, S. P., Michelangeli, F., Kalia, N., Rainger, G. E., Nieswandt, B., Brill, A., Watson, S. P. and Tomlinson, M. G. (2019) "Tspan18 is a novel regulator of the Ca^{2+} channel Orai1 and von Willebrand factor release in endothelial cells," *Haematologica*, 104(9), pp. 1892–1905. doi: 10.3324/haematol.2018.194241.

CHAPTER 1
GENERAL INTRODUCTION

1.1 Overview

The proteolytic cleavage of membrane proteins, a process known as ectodomain shedding, is an essential and irreversible post-translational modification step to regulate their function and expression levels. It is estimated that around 400 membrane proteins, equivalent to around 2% of membrane proteins on the cell surface, undergo shedding (Hayashida *et al.*, 2010; Tien, Chen and Wu, 2017), although it has become apparent that shedding can also take place in intracellular compartments and extracellular vesicles (Lichtenthaler, Lemberg and Fluhrer, 2018). The molecular scissors that cleave these membrane proteins are referred to as sheddases, the majority of which are transmembrane proteases, although some soluble extracellular proteases, such as matrix metalloproteases, have also been classified as sheddases (reviewed extensively in Lichtenthaler, Lemberg and Fluhrer, 2018).

Members of a disintegrin and metalloprotease (ADAM) family, especially ADAM10 and ADAM17, are the most studied and are key sheddases with around 100 putative and confirmed substrates identified for each (Lichtenthaler, Lemberg and Fluhrer, 2018). They are widely expressed, evolutionarily conserved, and share 30% amino acid sequence identity, making them the most closely related among the 22 human ADAMs. ADAM10 and ADAM17 have distinct substrate pools and regulatory mechanisms, although a small overlap in their substrate repertoire exists (Caescu, Jeschke and Turk, 2009; Pruessmeyer and Ludwig, 2009). One notable example is Notch, where ADAM10 is responsible for its shedding physiologically when shedding is triggered by ligand binding, whereas ADAM17 has been found to participate only in non-physiological, ligand-independent shedding of Notch (Alabi *et al.*, 2021).

ADAM10 and ADAM17 typically cleave within the juxtamembrane stalk region of a substrate in the extracellular face, leading to the release of its ectodomain (Figure 1) (Lichtenthaler, Lemberg and Fluhrer, 2018). In addition to downregulation of proteins, shedding can lead to other functional consequences (Figure 1). Examples include generation of soluble mediators, such as the release of the epidermal growth factor receptor (EGFR) ligands from their membrane-bound precursors (Sahin *et al.*, 2004), or as a prerequisite for intramembrane proteolysis by another protease, such as permitting the release of the Notch intracellular domain by the γ-secretase complex, which can translocate to the nucleus to activate transcription of Notch target genes that control fundamental cellular processes (van Tetering *et al.*, 2009).

Because shedding of substrates by the ADAM molecular scissors underpins health and disease processes, tightly controlled mechanisms must exist to determine how and when one sheddase can cleave which out of the ~100 cleavable substrates in a cell. Regulation by partner proteins is one such mechanism. ADAM17 is primarily regulated by two members of the rhomboid-like superfamily (reviewed extensively in Düsterhöft *et al.*, 2019), whereas ADAM10, the sheddase of interest in this thesis, is regulated by six members of the tetraspanin superfamily (Matthews, Noy, *et al.*, 2017). This chapter will focus on a review of the latest understanding of the biology of ADAM10, tetraspanins, the six ADAM10-regulating tetraspanins, and finally the platelet glycoprotein receptor VI (GPVI), a novel anti-platelet target which is the ADAM10 substrate of interest in this project.

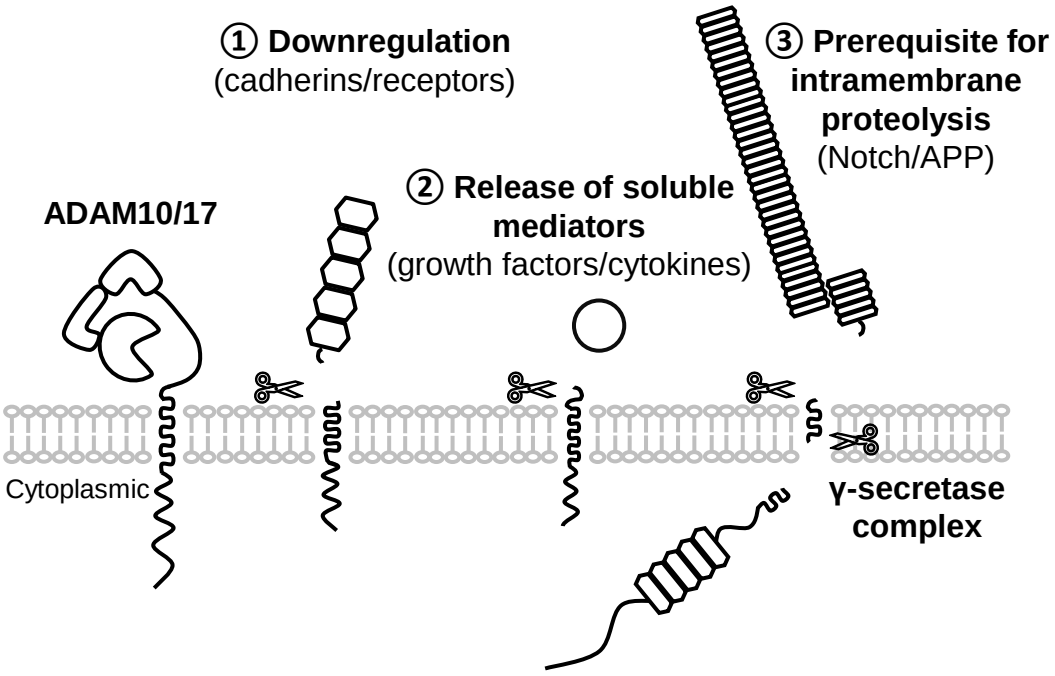

Figure 1. Consequences of ectodomain shedding. ADAM10/17-mediated shedding of different substrates may (1) downregulate protein levels, (2) release soluble mediators or (3) precede intramembrane proteolysis by the γ-secretase complex.

1.2 The molecular scissor ADAM10

1.2.1 ADAM10 has a unique ectodomain structure and a motif-rich tail

ADAM10 is a Zn^{2+}-dependent metalloprotease, characterised by the presence of Zn^{2+}-binding motifs in its catalytic site (Figure 2A). It is synthesised as an immature proform (~100 kDa) with an N-terminal prodomain that is required for correct folding of the catalytic site (Figure 2A) (Anders *et al.*, 2001). During its maturation in the Golgi, the prodomain is removed by furin and the proprotein convertase PCSK7, which uncovers its catalytic site in the metalloprotease domain that is otherwise masked by the prodomain, generating the catalytically active mature form of ~70 kDa (Figure 2A) (Anders *et al.*, 2001; Wong *et al.*, 2015). Indeed, recombinantly produced prodomain is a potent ADAM10-specific inhibitor (Moss *et al.*, 2007).

The crystal structure of the ADAM10 ectodomain reveals a globular structure with the metalloprotease domain surrounded by the non-catalytic domains consisting of the distintegrin, cysteine-rich and the membrane-proximal stalk regions (Figure 2B). Such an arrangement may be why the non-catalytic domains appear to have an auto-inhibitory role, perhaps by burying the catalytic site in an inactive ‘closed’ conformation, suggesting the possibility of control by a switch to an active ‘open’ conformation via an undetermined mechanism (Figure 2B). The positioning of the metalloprotease domain close to the membrane surface allows ADAM10 to cut substrates at a short distance from the membrane surface (Figure 2B) (Seegar *et al.*, 2017). It is important to highlight that there is no consensus cleavage site that is shared by all ADAM10 substrates. However, cleavage site profiling by mass spectrometry (Caescu, Jeschke and Turk, 2009; Tucher *et al.*, 2014; Scharfenberg *et al.*, 2020) and an analysis of the structure and residues lining the ADAM10 active site pocket suggests that ADAM10 may prefer substrates with a large hydrophobic or aromatic residue downstream of the cut site (Seegar *et al.*, 2017).

ADAM10 can exist as monomers and homodimers (Xu *et al.*, 2012). The cytoplasmic tail mediates ADAM10 dimerisation, but only in the presence of structural support from either a self or non-self transmembrane region (Deng *et al.*, 2014). The tail contains proline-rich Src homology domain 3 (SH3) domain-binding motifs at P708-P717 and R722-R728 (Figure 2A) that can interact with SH3 domain-containing proteins, many of which are non-receptor tyrosine kinases and adaptor proteins involved in regulating trafficking, membrane shaping or interaction with the cytoskeleton (Ebsen *et al.*, 2014). An arginine-rich endoplasmic reticulum (ER)-retention motif is also present at R722-R724 (Figure 2A), which controls its exit from the ER (Marcello *et al.*, 2010).

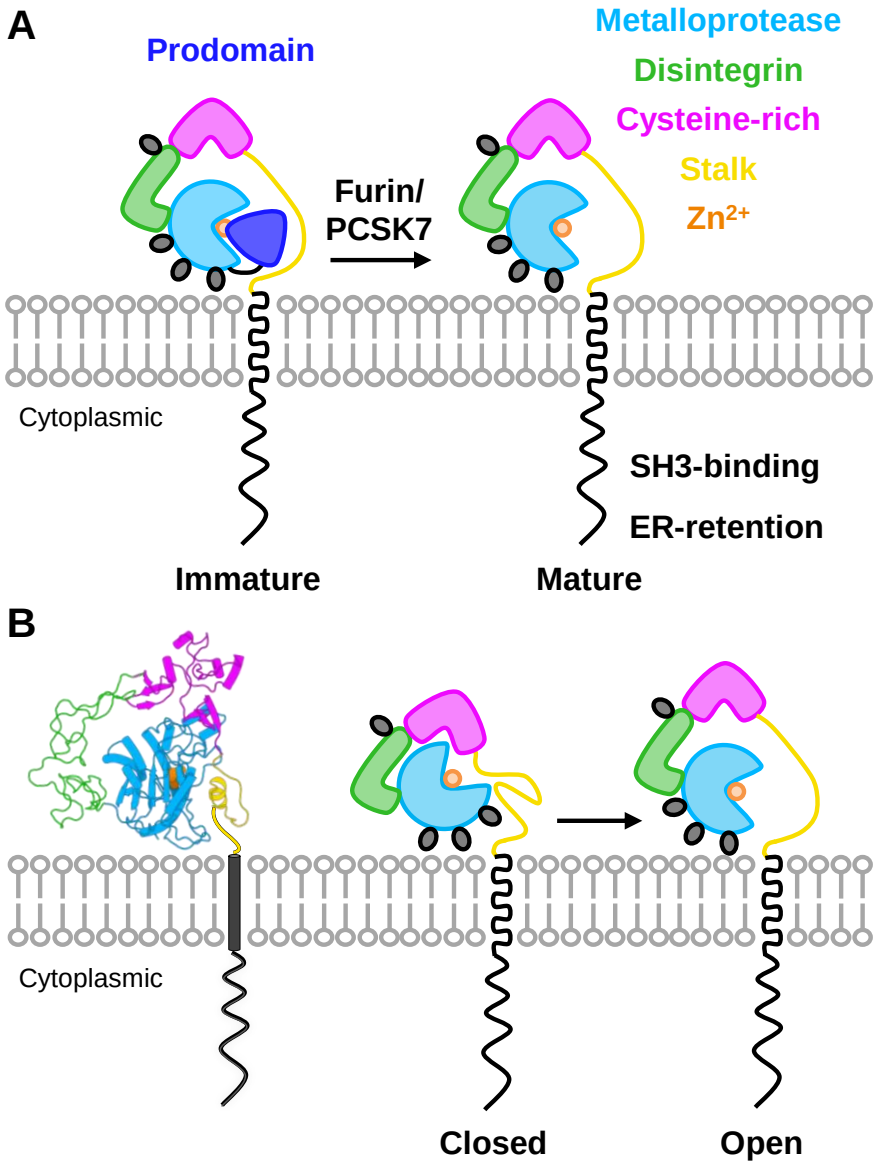

Figure 2. Structural features of ADAM10. (A) ADAM10 maturation requires the removal of the prodomain by furin and the proprotein convertase PCSK7, which unmasks its Zn^{2+}-containing active site. Dark ovals represent N-glycosylation sites. The cytoplasmic tail has SH3 domain-binding and ER-retention motifs. (B) The crystal structure of the ADAM10 ectodomain (Protein Data Bank ID: 6BE6) is represented on the left. The metalloprotease domain is enveloped by the non-catalytic domains consisting of the disintegrin, cysteine-rich and stalk regions. The requirement for a conformational switch from an inactive 'closed' (middle) to an active 'open' (right) state is predicted based on Seegar *et al.* (2017).

1.2.2 The role of ADAM10 and its substrates in health and disease

In human, deleterious ADAM10 variants are rare (minor allele frequency of < 0.01). One notable example is the association of five different coding mutations affecting the prodomain (missense and truncation), metalloprotease domain (frameshift) and disintegrin region (missense) with Reticulate acropigmentation of Kitamura, a rare skin hyperpigmentation disorder, but the causative ADAM10 substrate had not yet been identified (Kono *et al.*, 2013). The lack of common deleterious polymorphisms in *ADAM10* makes sense given the essential role of ADAM10 in development and disease, which is evident from the phenotypes of mice deficient in ADAM10. Of note, mouse and human ADAM10 share a striking 96% identity in amino acid sequence. ADAM10-knockout mice cannot survive beyond embryonic day 9.5 due to developmental defects in multiple organ systems, most notably in the central nervous and cardiovascular systems. The phenotypes leading to embryonic lethality are characteristic of defects in Notch signalling which regulate cell fate decisions, and indeed, are similar to mice deficient in Notch proteins or presenilins, components of the γ-secretase complex (Hartmann *et al.*, 2002). Follow-up investigations in tissue-specific conditional ADAM10 knockout mice have demonstrated that the essential role of ADAM10 in many organ systems is largely due to its role in promoting Notch signalling (Chaimowitz *et al.*, 2011; Weber *et al.*, 2011; Tsai *et al.*, 2014; Mizuno *et al.*, 2015; Alabi *et al.*, 2016). As an example, one study in neural progenitor-specific conditional ADAM10-knockout mice has established that the defects in neurogenesis can be attributed to the loss of ADAM10-mediated Notch shedding, and consequently impairment in Notch activation and signalling (Jorissen *et al.*, 2010). Furthermore, the same study has also provided *in vivo* evidence to support *in vitro* evidence that ADAM10 is the major sheddase for the disease-relevant substrates amyloid precursor protein (APP) and neuronal (N)-cadherin, which will be introduced further below.

ADAM10 shedding of APP is generally thought to have beneficial consequences in protecting against Alzheimer's disease (Manzine *et al.*, 2019). This is because ADAM10 shedding of APP may reduce the release of the disease-associated amyloid β peptides, which can only be generated when γ-secretase cleaves an alternative cleavage product originated from a separate amyloidogenic pathway (Figure 3). This pathway is mediated by β-secretase, which cuts APP at a neighbouring site upstream of the ADAM10 cut site (Figure 3) (Kuhn *et al.*, 2010). As less amyloid β peptides accumulate, the formation of amyloid plaques characteristic of Alzheimer's disease is reduced (Figure 3) (Postina *et al.*, 2004). Two ADAM10 missense variants in the prodomain (Q170H and R181G) have been reported to associate with late-onset Alzheimer's disease. These prodomain mutations result in decreased ADAM10 activity and APP shedding due to folding defects (Kim *et al.*, 2009; Suh *et al.*, 2013). Therefore, activating ADAM10 shedding of APP may have neuroprotective benefits.

Many members of the cadherin superfamily that mediate cell-cell adhesion and regulate the actin cytoskeleton are ADAM10 substrates, such as vascular endothelial (VE-) (Schulz *et al.*, 2008), epithelial (E-) (Maretzky, Reiss, *et al.*, 2005) and most notably N-cadherin (Reiss *et al.*, 2005) because of its role in central nervous and cardiovascular system development and function, and cancer progression (Radice, 2013). In addition to loosening cell-cell junctions, ADAM10 shedding of N-cadherin leads to subsequent γ-secretase cleavage of the membrane remnant and release of the cytoplasmic tail. This in turn releases the tail-associated β-catenin, which translocates to the nucleus to activate transcription of Wnt target genes that control key cellular processes such as differentiation, proliferation and migration (Reiss *et al.*, 2005). The soluble shed fragment of N-cadherin can also bind fibroblast growth factor receptor (FGFR) and affect FGFR signalling (Williams *et al.*, 2001; Lyon *et al.*, 2009; Lyon, Wadey and George, 2016).

In addition to GPVI (Section 1.5) and the best-characterised substrates described above, ADAM10 is responsible for shedding of ~100 other substrates (Kuhn *et al.*, 2016) that have physiological or pathological roles. These include precursors (loosely referred by their soluble forms thereafter) to the EGFR ligands betacellulin and EGF in embryonic development and cancer (Sahin *et al.*, 2004), and the receptor for advanced glycation end products (RAGE) (Raucci *et al.*, 2008), which is involved in a wide variety of diseases including cancer, cardiovascular, Alzheimer's and inflammatory diseases (Sorci *et al.*, 2013) and potentially coronavirus disease-2019 (COVID-19) (Roy, Ramasamy and Schmidt, 2021; Yalcin Kehribar *et al.*, 2021). Given the wide range of substrates and diseases that ADAM10 is involved in, non-strategic targeting of ADAM10 in a therapy would likely suffer from dangers of toxicity and poor efficacy due to off-target effects—a lesson learnt from the failure of matrix metalloprotease and ADAM inhibitors in clinical trials in the past 30 years (Fields, 2019). Therefore, there is a keen interest in the metalloprotease community to understand how the scissor activity of ADAM10 can be fine-tuned to harness its therapeutic potential to treat different diseases. Numerous post-translational regulatory mechanisms have been described, which will be introduced in the next section.

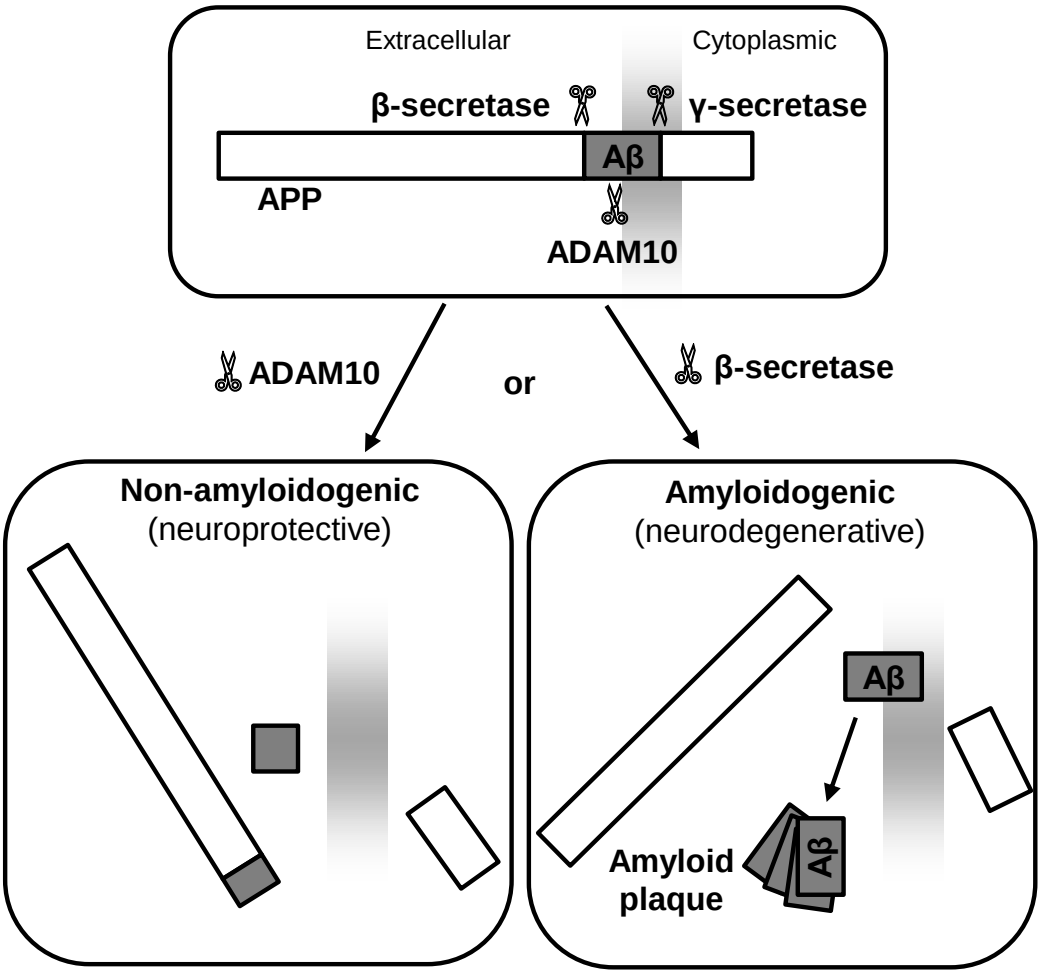

Figure 3. Activating ADAM10 shedding of APP may have neuroprotective benefits. APP can be shed via two separate pathways, which both lead to intramembrane proteolysis by γ-secretase. In the non-amyloidogenic pathway, cleavage of APP by ADAM10 does not lead to the generation of amyloid beta (Aβ) peptides, in contrast to cleavage of APP by β-secretase in the amyloidogenic pathway. Accumulation and aggregation of Aβ peptides lead to the formation of amyloid plaques characteristic of Alzheimer's disease. Figure is based on Manzine *et al.* (2019).

1.2.3 Post-translational regulation of ADAM10 activity

1.2.3.1 Constitutive *versus* stimulated shedding

It is generally thought that compared to ADAM17, ADAM10 scissor activity appears to be constitutive and does not require stimulation to occur (Lichtenthaler, Lemberg and Fluhrer, 2018) but can be rapidly activated in response to physiological or chemical stimuli that typically lead to a rise in intracellular Ca^{2+} levels (Horiuchi *et al.*, 2007). However, not all substrates can be constitutively shed. For instance, basal shedding has been observed for endogenous N-cadherin (Reiss *et al.*, 2005), E-cadherin (Maretzky, Reiss, *et al.*, 2005), VE-cadherin (Schulz *et al.*, 2008), as well as betacellulin and EGF in an overexpression cell-based system (Sahin *et al.*, 2004). In contrast, basal shedding has not been shown for endogenous GPVI in platelets (Gardiner *et al.*, 2004), even though ADAM10 is active on the surface of platelets as detected from its activity towards an ADAM10-specific cleavable sensor peptide (Facey *et al.*, 2016). Specific stimuli that can trigger GPVI shedding will be described further in Section 1.5.5. GPVI can, however, be constitutively cleaved by ADAM10 when overexpressed in cultured cells (Noy *et al.*, 2016). As another example, shedding of both endogenous and overexpressed Notch do not occur constitutively because its cleavage site is normally concealed and requires exposure via a conformational change induced by ligand binding to enable ADAM10 cleavage (van Tetering *et al.*, 2009; Alabi *et al.*, 2021).

1.2.3.2 Membrane environment

The membrane architecture, mediated by protein-lipid interactions, is a potential key regulator when considering that ADAM10 and its substrates are typically membrane-bound. Some of the earliest pieces of evidence supporting the role of membrane environment is that disruption of lipid rafts by depletion of cholesterol, which is enriched in these domains, activates ADAM10

shedding of APP (Kojro *et al.*, 2001) and other ADAM10 substrates including the interleukin-6 receptor (IL6R) (Matthews *et al.*, 2003) and CD44 (Murai *et al.*, 2011). On the other hand, targeting ADAM10 to lipid rafts inhibited ADAM10 shedding of APP (Harris, Pereira and Parkin, 2009; Kojro *et al.*, 2010). This suggests that ADAM10 is generally excluded from lipid rafts. Indeed, ADAM10 is associated with tetraspanin nanodomains (Arduise *et al.*, 2008), another type of membrane domains distinct from lipid rafts, that will be introduced in later sections (Sections 1.3 and 1.4).

Beyond confinement to distinct membrane domains, regulation by asymmetric distribution of membrane phospholipids in the lipid bilayer is an emerging concept that has recently been demonstrated experimentally (Bleibaum *et al.*, 2019). In this model, ADAM10 is activated by transient translocation of the phospholipid phosphatidylserine (PS), which normally resides at the cytoplasmic membrane face, to the extracellular face of the membrane, a process known as PS exposure or externalisation (Figure 4). Exposure of the negatively charged PS is proposed to facilitate interaction with positively charged residues (R656, K658 and K659) in the ADAM10 stalk region, which may relieve auto-inhibition by the non-catalytic domains as introduced in Section 1.2.1 (Figure 4). Indeed, Ca^{2+} influx, which activates ADAM10, induces PS externalisation (Nagata *et al.*, 2016).

On a larger scale, ADAM10 can also be activated in the context of loss of membrane structure when cells are challenged with bacterial infection. In addition to its major role as a sheddase, ADAM10 can also act as a receptor for *Staphylococcus aureus* α-toxin, which is a pore-forming toxin that punctures the plasma membrane, to mediate toxin-induced cytotoxicity in shedding-dependent and shedding-independent manners (Wilke and Wardenburg, 2010; Powers *et al.*, 2012; Ezekwe, Weng and Duncan, 2016; von Hoven *et al.*, 2016). Pore formation leads to Ca^{2+}

influx and subsequently cell death (Essmann *et al.*, 2003), which further activates ADAM10 shedding of substrates.

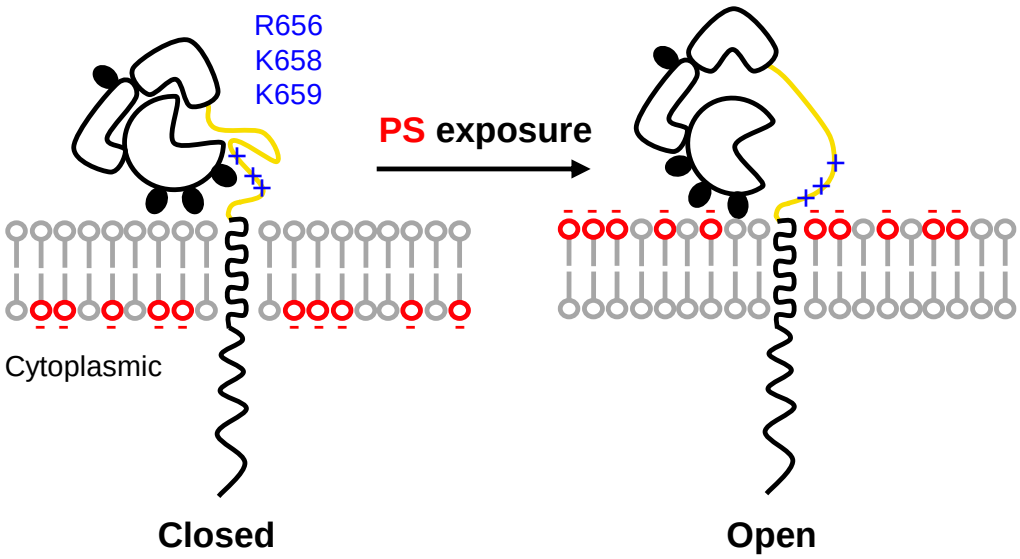

Figure 4. Activation of ADAM10 by phosphatidylserine (PS) exposure. In this model based on Bleibaum *et al.* (2019), translocation of negatively charged PS phospholipids from the inner leaflet of the lipid bilayer to the outer membrane leaflet attracts positively charged residues in the stalk region of ADAM10. This may relieve the autoinhibition from the non-catalytic domains and expose the metalloprotease domain to permit substrate cleavage.

1.2.3.3 Regulation by other proteins

ADAM10 activity can be inhibited physiologically by the tissue inhibitor of metalloproteases (TIMPs) TIMP-1, which is more selective towards ADAM10 as it does not inhibit ADAM17, and TIMP-3, which can also inhibit ADAM17 (Amour *et al.*, 2000). Binding of TIMP-3 to ADAM17 requires ADAM17 dimerisation (Xu *et al.*, 2012). It is currently unknown whether the same requirement applies to ADAM10, but the authors of the same study suggest that it may be different because ADAM10 has a higher level of monomers on the cell surface. Another physiological inhibitor of ADAM10 is the cell surface-anchored reversion-inducing cysteine-rich protein with Kazal motifs (RECK), which has been shown to inhibit ADAM10 shedding of Notch (Muraguchi *et al.*, 2007).

ADAM10 itself can be downregulated through shedding by ADAM9 or ADAM15. The membrane remnant of ADAM10 is further cleaved by the γ-secretase complex, releasing its intracellular domain which is proposed to act as a transcriptional regulator because of its preferential localisation to nuclear speckles which are rich in splicing machineries (Tousseyn *et al.*, 2009). On the other hand, the released soluble ectodomain of ADAM10 appears to retain its scissor activity when expressed recombinantly and can cleave the soluble counterparts of its substrates, such as the ectodomain of N-cadherin, and extracellular matrix components, although there is a difference in the substrate repertoire compared to membrane-bound ADAM10 (Scharfenberg *et al.*, 2020). However, a recent study detected soluble ADAM10 of ~50 kDa in plasma and cerebral spinal fluid samples but showed that it is inactive, although it is unknown whether this fragment corresponds to the shed form (Vanatabe *et al.*, 2021).

It is unclear how the various post-translational regulatory mechanisms described in this section, which regulate ADAM10 activity and expression in a broad sense, can address one crucial outstanding question: what restricts ADAM10 substrate repertoire? Therefore, the key mechanism may lie in the discovery that ADAM10 substrate specificity can be regulated by its interaction with tetraspanins.

1.3 The tetraspanin superfamily

1.3.1 Tetraspanins are structurally and functionally distinct four-pass transmembrane proteins

First described in 1990 from the discovery of CD81 (Oren *et al.*, 1990), tetraspanins are a superfamily of evolutionarily conserved four-pass transmembrane proteins consisting of 33 members in humans (Figure 5). Different cell types have different repertoires of tetraspanins; for example, leukocytes express around 20 tetraspanins (Tarrant *et al.*, 2003), whereas platelets have about 10 (Tomlinson, 2009). Some tetraspanins are widely expressed, for example, CD9 and CD81, whereas some are restricted to specific cell types, for example, peripherin-2 and ROM1, are only expressed in photoreceptor cells in the retina of the eye and are critical for retinal function because mutations in these tetraspanins result in retinal diseases (Charrin *et al.*, 2014).

Structurally, they are characterised by having one large and one small extracellular region, four transmembrane helices, one intracellular loop connecting transmembrane helices two and three, and cytoplasmic tails at each terminus (Figure 6A, Section 1.3.2). Key features will be detailed in Section 1.3.2. The defining feature of tetraspanins is the presence of a conserved CCG motif and at least another pair of cysteine residues that form structure-stabilising disulphide bridges in the large extracellular region (Charrin *et al.*, 2014; Hemler, 2014). It is worth noting that peripherin-2 and ROM1, unlike other tetraspanins, are unique in that they have an unpaired cysteine in the large extracellular region (Figure 5) (Charrin *et al.*, 2014). As such, tetraspanins can be classified according to the number of cysteine residues in their large extracellular regions, although only the six tetraspanins with eight cysteine residues that are most closely related by

their amino acid sequences have been named the TspanC8 subgroup (Figure 5) (Dornier *et al.*, 2012; Haining *et al.*, 2012).

Functionally, tetraspanins are dynamic molecular organisers on membranes. They interact with each other and with specific non-tetraspanin partner proteins to regulate their function by controlling their expression, trafficking to different membrane compartments, clustering, lateral mobility or activity (Charrin *et al.*, 2014). Tetraspanins and their associated proteins are generally considered to be organised into distinct ‘tetraspanin nanodomains’ in a large ‘tetraspanin web’ (Rubinstein, Charrin and Tomlinson, 2013; van Deventer, Arp and van Spriel, 2021). These concepts will be introduced further in Section 1.3.3.

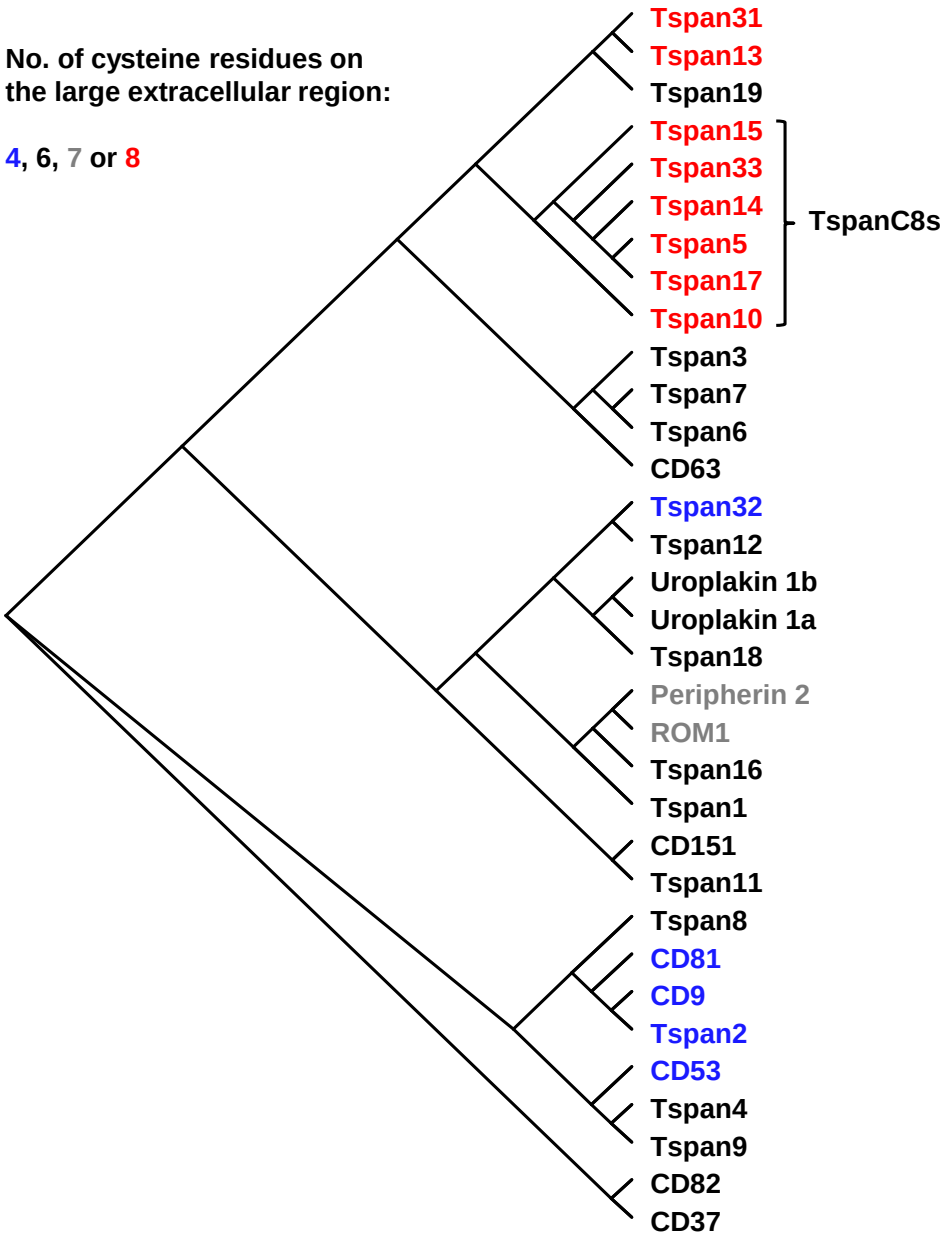

Figure 5. The tetraspanin superfamily consists of 33 members in human. A phylogenetic tree depicting the relationships among the 33 human tetraspanins generated with ClustalW2, using their amino acid sequence identities obtained from multiple sequence alignments with Clustal Omega with the web-based tools available from the European Bioinformatics Institute (EMBL-EBI) (Madeira *et al.*, 2019). The tree was displayed using the web-based tool Interactive Tree of Life (Letunic and Bork, 2021).

1.3.2 Tetraspanins undergo conformational changes and interact with proteins and lipids via different domains

Tetraspanins interact with their partner proteins primarily via their large extracellular regions, although the transmembrane regions may also have a role (Stipp, Kolesnikova and Hemler, 2003). Therefore, past structural studies have largely focused on the large extracellular region, which can be separated into two regions: (1) a conserved region consisting of three helices (A, B and E helices) forming a structural base that is highly conserved among tetraspanins and (2) a structurally variable region (C and D loops or helices depending on the tetraspanin) on the top that is also the least conserved region among tetraspanins (Matthews, Szyroka, *et al.*, 2017) (Figure 6A). The conserved CCG motif is located immediately after the B helix (Figure 6A) (Kitadokoro *et al.*, 2001; Rajesh *et al.*, 2012). Most tetraspanins have N-glycosylation sites on the large extracellular region (Figure 6C) (Stipp, Kolesnikova and Hemler, 2003).

A structural breakthrough emerged in 2016 when the first crystal structure of a full-length tetraspanin became available for CD81 in its ‘closed’ conformation, which revealed an inverted cone-shaped structure with a putative cholesterol-binding cavity formed within the four-transmembrane regions, capped off by the extracellular region (Figure 6B) (Zimmerman *et al.*, 2016). In the same study, molecular dynamics simulations predicted a conformational change where the large extracellular region swings open when cholesterol is removed from the cavity. Indeed, the same group has demonstrated this in their recent cryo-electron microscopy (cryo-EM) structure of CD81 in complex with its partner protein CD19, which revealed an extended, ‘open’ and cholesterol-free conformation of CD81 that is distinct to its ‘closed’ conformation in the absence of its partner protein (Figure 6B) (Susa *et al.*, 2021). Like most other tetraspanin/partner protein interactions, the same study shows that interaction with CD19 is largely mediated by the C and D helices in the variable region of CD81. Whether cholesterol

truly acts as the switch to conformational change remains undetermined, but this suggests the potential of a lipid-mediated conformational switch in tetraspanins.

In 2020, the crystal structures of CD9 and CD53, two other tetraspanins closely related to CD81 that also have four cysteine residues in the large extracellular region (Figure 5), were also resolved. The overall structures of both CD9 and CD53 are in general agreement with CD81, suggesting that this inverted cone-shaped shape could be a common feature in the tetraspanin superfamily (Figure 6A) (Umeda *et al.*, 2020; Yang *et al.*, 2020). Indeed, the structures of representative tetraspanins containing six or eight residues on the large extracellular region, that are more distantly related, are similar when predicted by homology modelling (Figure 7). Importantly, the structure of the small extracellular region was revealed for the first time in these two studies and showed that it is more than just a disordered loop (Figure 6A).

In particular, the structure of CD53 was captured in an 'open' conformation, capable for interactions with partner proteins with the large extracellular region rotated away from the membrane and with the base resting on top of the small extracellular region (Figure 6A). Indeed, follow-up functional and biochemical experiments in the same study with CD53 and CD81 small extracellular region mutants further support the structural observation that the 'open' conformation is stabilised by interactions between the large and small extracellular regions (Yang *et al.*, 2020).

The structure of CD9 was captured in a 'closed' conformation (Figure 6A), and molecular dynamics simulations suggest that it can exist in a third 'semi-open' state, which is akin to a transition between the 'closed' and 'open' conformation (Umeda *et al.*, 2020). In addition, palmitoylation of intracellular cysteine residues, which can contribute to tetraspanin-tetraspanin interactions (Berditchevski *et al.*, 2002; Charrin *et al.*, 2002; Yang *et al.*, 2002), could be

visualised in the structure of CD9 (Figure 6A). Clustering of individual CD9 molecules in the crystal show that the cone-shaped structures allow intrinsic organisation of the molecules into curvy layers in the lattice, which may explain how clustering of some tetraspanins affect membrane curvature and why some tetraspanins are enriched in exosomes (Umeda *et al.*, 2020).

Similar to CD81, the transmembrane cavities can house lipid molecules such as monoolein, a lipid used in the crystallisation of both CD9 and CD53 (Figure 6A-B). Unlike CD81, however, simulations suggest that lipid expulsion is not required for a conformational change (Umeda *et al.*, 2020; Yang *et al.*, 2020). Yang *et al.* (2020) proposed that lipid binding may act to stabilise the structure of the transmembrane helices. This conflicting observation highlights the need to examine the detailed structural contribution of the lipid-binding cavity in different tetraspanins to complement the functional importance of cholesterol (Charrin *et al.*, 2003; Silvie *et al.*, 2006; Huang *et al.*, 2020; Palor *et al.*, 2020) or other lipids.

The cytoplasmic domain, which consists of two intracellular tails of variable lengths and one short intracellular loop, is highly divergent, especially the C-terminal tail, and shares only 21-38% in amino acid sequence identity among tetraspanins (Stipp, Kolesnikova and Hemler, 2003). Besides containing palmitoylation sites, the tails of some tetraspanins also have intracellular sorting motifs (Berditchevski and Odintsova, 2007). Tetraspanin tails can bind either directly or indirectly to different intracellular proteins (Stipp, Kolesnikova and Hemler, 2003; Berditchevski and Odintsova, 2007) including adaptor proteins, e.g., CD63 and syntenin-1 (Latysheva *et al.*, 2006), signalling proteins, e.g., CD151 and phosphatidylinositol-4 kinase (Yauch *et al.*, 1998) and cytoskeletal proteins, e.g., CD81 and α-actinin (Gordón-Alonso *et al.*, 2012). Therefore, the cytoplasmic domain presents an attractive site for recruitment of proteins that affect the function of tetraspanins and their partner proteins in tetraspanin nanodomains.

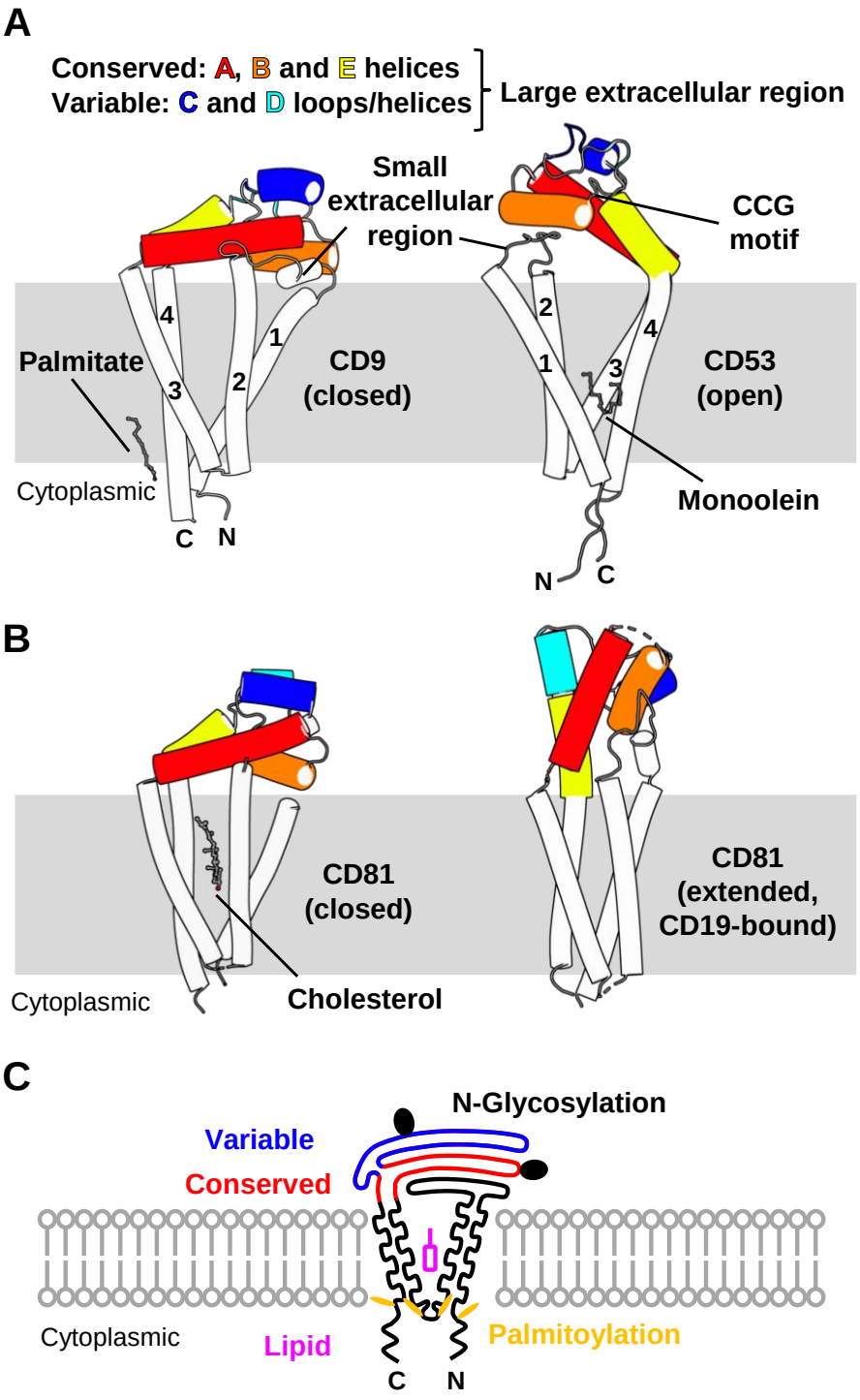

Figure 6. Structural features of tetraspanins. (A) The crystal structures of CD9 (Protein Data Bank (PDB) ID: 6K4J) in a 'closed' conformation (left) (Umeda *et al.*, 2020) and CD53 (PDB ID: 6WVG) in an 'open' conformation (right; relative to CD9, this is rotated 180º along the y-axis) (Yang *et al.*, 2020). The large extracellular region is represented by larger helices and consists of a conserved and a variable region. (B) The crystal structure of CD81 (PDB ID: 5TCX) in its 'closed' conformation (left) (Zimmerman *et al.*, 2016) and the cryo-EM structure of CD81 (PDB ID: 7JIC) in its extended, CD19-bound form (Susa *et al.*, 2021). (C) Schematic representation of a tetraspanin, adapted from Matthews, Szyroka *et al.* (2017).

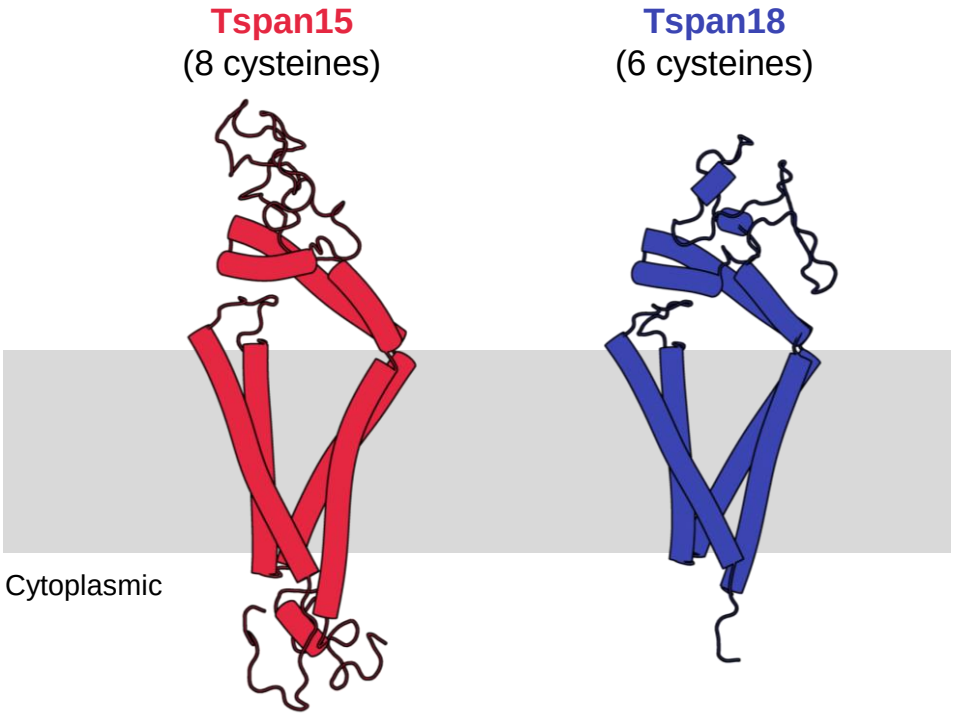

Figure 7. Predicted structures of Tspan15 and Tspan18. The structures of full-length Tspan15 and Tspan18 were predicted by homology modelling combined with *ab initio* methods with Phyre2 (Kelley *et al.*, 2015) based on the crystal structures of CD9 (PDB ID: 6K4J) (Umeda *et al.*, 2020) and CD53 (PDB ID: 6WVG) (Yang *et al.*, 2020). Numbers in brackets indicate the number of cysteine residues in the large extracellular region.

1.3.3 Tetraspanin and their associated proteins are organised into nanodomains in a large tetraspanin web

1.3.3.1 Tetraspanin web

In the tetraspanin community, detergent-based biochemical methods are typically used to identify and dissect interactions among tetraspanins and their partner proteins based on detergent strength. Direct tetraspanin-partner protein interactions are preserved in stronger detergents, e.g., digitonin, which on the other hand, disrupt weak tetraspanin-tetraspanin interactions that may occur between different tetraspanin/partner protein complexes. These weaker interactions can only be maintained in milder detergents, e.g., Brij. This demonstrates the different levels of interactions that tetraspanins facilitate to organise the membrane, termed the tetraspanin web (Rubinstein, 2011; Rubinstein, Charrin and Tomlinson, 2013).

1.3.3.2 Tetraspanin nanodomain

Single-molecule imaging of the tetraspanins CD37, CD53, CD81 and CD82 on human B cells (Zuidscherwoude *et al.*, 2015) revealed several key findings about the nanoscale organisation of tetraspanins and their associated partner proteins that led to the concept of tetraspanin nanodomains (van Deventer, Arp and van Spriel, 2021). Tetraspanins are organised into separate nanoclusters of ~120 nm in diameter consisting of less than 10 tetraspanins of a single type. Individual nanoclusters can aggregate into larger clusters (Figure 8A). Different tetraspanin nanoclusters do not overlap substantially with each other but their relative proximities to each other are not random, which is in line with the notion that tetraspanin nanodomains are dynamic and can interact weakly in the wider tetraspanin web. This contrasts with the apparent overlapping of a tetraspanin nanocluster with their associated partner proteins, for example, CD81 with CD19, at the border of CD81 nanoclusters, which suggests that these

primary interactions form the basis of a tetraspanin nanodomain (Figure 8A) (Zuidscherwoude *et al.*, 2015; van Deventer, Arp and van Spriel, 2021). Different organisation modes have also been described for different tetraspanins where the partner proteins are trapped within a tetraspanin nanodomain (Figure 8B) (Moretto *et al.*, 2019; van Deventer, Arp and van Spriel, 2021) or may be arranged in a string-like fashion as tetramer units consisting of tetraspanin/partner protein dimers (Figure 8C) (Oosterheert *et al.*, 2020). Therefore, the organisation of a tetraspanin nanodomain may be different for different tetraspanins.

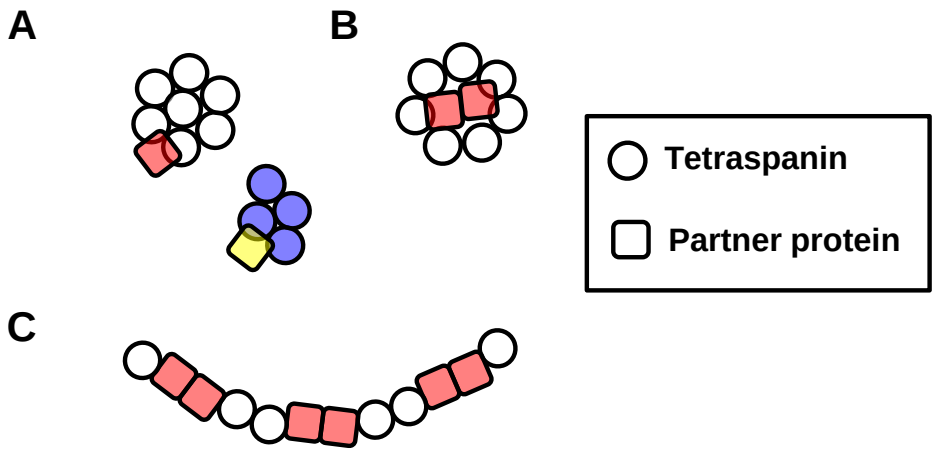

Figure 8. Different modes of tetraspanin nanodomain organisation. (A) Two tetraspanin nanodomains consisting different tetraspanin/partner proteins are depicted here. Each tetraspanin nanodomain consists of a cluster containing less than 10 tetraspanins and its associated partner protein overlapping at the border of the nanocluster. Tetraspanin nanodomains from different tetraspanin species do not overlap but may interact weakly in a larger tetraspanin web (Zuidscherwoude *et al.*, 2015). (B) In this tetraspanin nanodomain, partner proteins are clustered and trapped in the middle of a cluster of tetraspanins (Moretto *et al.*, 2019; van Deventer, Arp and van Spriel, 2021). (C) Based on Oosterheert *et al.* (2020), tetraspanin/partner protein dimers may form a tetramer unit with the tetraspanins sandwiching a partner protein dimer. The tetramer units may be arranged in a string-like fashion.

1.3.3.3 Tetraspanin deficiency disrupts partner protein function

Importantly, tetraspanin/partner protein complexes often act as one functional entity. This is best demonstrated by the consequences of tetraspanin deficiency. Two well-established disease-association examples in human, where the partner protein function is disrupted by a deficiency in its associated tetraspanin, include CD81 with CD19, and CD151 with integrins.

In B cells, CD81 promotes the trafficking of CD19 and its expression on the cell surface. CD81/CD19 forms a B cell co-receptor complex with CD21 and has an important role in signal transduction to regulate B cell activation (Levy, 2014). A patient who had an antibody deficiency disorder exhibited a complete loss of CD19 on the surface of B cells. This was accompanied by CD81 deficiency as a result of a homozygous mutation in a splice site in the *CD81* locus. Functional *in vitro* experiments demonstrated that the defect in CD19 expression was because of impaired trafficking due to the lack of CD81 (van Zelm *et al.*, 2010).

CD151 forms tight complexes with major laminin-binding integrins and regulates their function in cell adhesion, migration and signal transduction (Berditchevski, 2001). Three patients had the same frameshift mutation in the *CD151* locus, which coincides with a truncation in the middle of the large extracellular region and resulted in CD151 deficiency. They presented with broad symptoms including end-stage kidney disease, hearing loss and rare skin blistering conditions. Histological examination of a kidney biopsy sample from one patient revealed aberrant basement membrane assembly. These symptoms are associated with defects linked to the critical role of laminin-binding integrins in maintaining the integrity of basement membranes in the kidney and skin (Crew *et al.*, 2004). Indeed, it was later demonstrated in mice that CD151 deficiency led to kidney failure with phenotypes similar to what was observed in these patients (Sachs *et al.*, 2006, 2012).

Finally, perhaps the most striking phenotype that had ever been demonstrated in any tetraspanin-knockout mice can be seen in mice deficient in Tspan14, which is one of the six tetraspanins belonging to the TspanC8 subgroup that directly associate with and regulate the essential sheddase ADAM10. This is because Tspan14-knockout mice, like ADAM10-knockout mice, are embryonic lethal (Tomlinson and MRC Harwell, unpublished).

1.4 Six TspanC8 tetraspanins regulate ADAM10

1.4.1 TspanC8s are essential for ADAM10 maturation and expression

ADAM10 is a common tetraspanin-associated protein identified from proteomics of tetraspanin immunoprecipitates from cells lysed in mild detergents (André *et al.*, 2006; le Naour *et al.*, 2006; Arduise *et al.*, 2008). Some tetraspanins that interact indirectly with ADAM10 include CD9, CD81, CD151, CD63, CD82 (Arduise *et al.*, 2008) and Tspan12 (Xu, Sharma and Hemler, 2009), which likely stem from weak interactions in the wider tetraspanin web with nanodomains containing direct ADAM10 tetraspanin partners. Tspan3 was shown to interact with ADAM10 in relatively stringent detergent but did not affect ADAM10 maturation (Seipold *et al.*, 2017), unlike the six tetraspanins, Tspan5, 10, 14, 15, 17 and 33. These six tetraspanins interacted with ADAM10 in a digitonin-resistant and palmitoylation-independent manner, indicating their direct associations with ADAM10, which was further confirmed by chemical cross-linking on the cell surface (Dornier *et al.*, 2012; Haining *et al.*, 2012). They form the TspanC8 subgroup that are closely related by amino acid sequence identities compared to the rest of the superfamily (Figure 5, Section 1.3.1). Tspan5 and Tspan17 are the most similar, sharing 78% identity with each other, whereas Tspan10 is the most distant, sharing between 26-35% identity with the rest of the subfamily members (Matthews, Szyroka, *et al.*, 2017).

All six TspanC8s share the same role in promoting ADAM10 exit from the ER, its maturation to the catalytically active form in the Golgi, and its trafficking to different subcellular compartments (Dornier *et al.*, 2012; Haining *et al.*, 2012; Prox *et al.*, 2012). This has also been demonstrated *in vivo* in mice deficient in Tspan15 (Seipold *et al.*, 2018) or Tspan33 (Haining *et al.*, 2012), which have shown reduced ADAM10 expression in cells that express the TspanC8. It is worth noting that the only effective TspanC8 mAbs available to date are for Tspan5 (Saint-

Pol, Billard, *et al.*, 2017) and Tspan15 (Koo *et al.*, 2020). Using these mAbs, ADAM10 has recently been found to also reciprocally regulate the expression of endogenous Tspan5 and Tspan15 (Saint-Pol, Billard, *et al.*, 2017; Koo *et al.*, 2020). In addition, ADAM10 has been identified as the major interacting protein for endogenous Tspan15 (Koo *et al.*, 2020), and the majority of Tspan5 is also associated with ADAM10 (Saint-Pol, Billard, *et al.*, 2017), further demonstrating the intimate relationships between TspanC8s and ADAM10.

1.4.2 The 'six scissors' hypothesis: TspanC8s regulate ADAM10 substrate specificity

Importantly, TspanC8s can differentially regulate ADAM10 substrate specificity. Therefore, it was hypothesised that each TspanC8 constitutes an essential component of a functional ADAM10 complex, thus leading to the concept of ADAM10 existing as six different TspanC8/ADAM10 molecular scissors that can cleave distinct substrates (Figure 9) (Matthews, Noy, *et al.*, 2017; Matthews, Szyroka, *et al.*, 2017; Saint-Pol, Eschenbrenner, *et al.*, 2017; Matthews *et al.*, 2018; Harrison, Koo and Tomlinson, 2021).

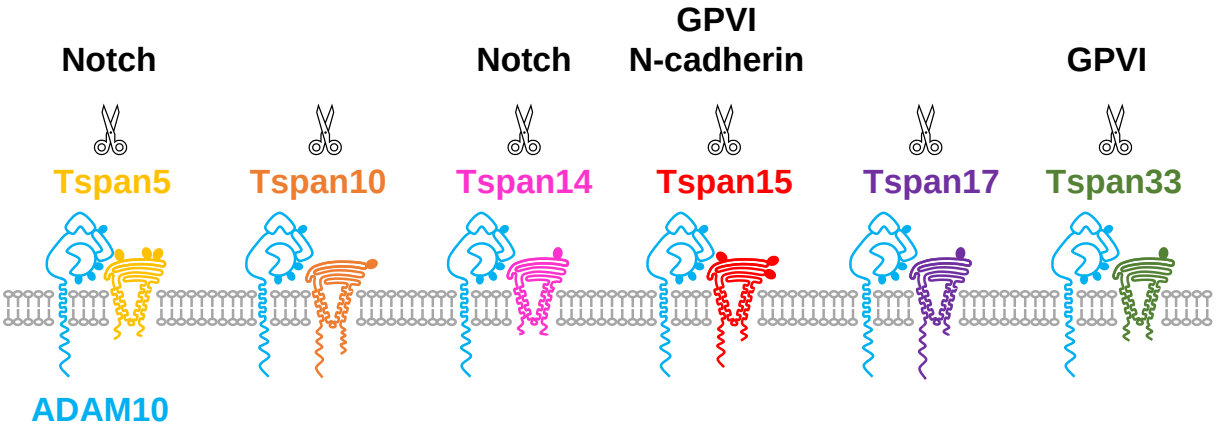

Figure 9. ADAM10 exists as six TspanC8/ADAM10 scissors with different substrate repertoires. In the 'six scissors' hypothesis, association of ADAM10 with different members of the TspanC8 tetraspanin subfamily allow ADAM10 to shed distinct substrates. For example, N-cadherin can only be cleaved by Tspan15/ADAM10 scissors, Notch can only be cleaved by Tspan5/ADAM10 and Tspan14/ADAM10 scissors, and GPVI can only be cleaved by Tspan15/ADAM10 and Tspan33/ADAM10 scissors. Figure is adapted from Harrison, Koo and Tomlinson (2021).

N-cadherin is the clearest example where Tspan15/ADAM10 has been shown to be its sole scissor by several independent studies in different cell types using different validation approaches (Prox *et al.*, 2012; Jouannet *et al.*, 2016; Noy *et al.*, 2016; Seipold *et al.*, 2018). Tspan15/ADAM10 scissors can also cleave other substrates such as betacellulin, EGF, RAGE and GPVI (Table 1). In addition, GPVI can also be cleaved by Tspan33/ADAM10 scissors (Matthews, 2019). The evidence that led to the identification of Tspan15/ADAM10 and Tspan33/ADAM10 as the scissors for GPVI will be detailed in Section 1.5.6.

Ligand-dependent Notch1 activation has been demonstrated in multiple cell types to be promoted by Tspan5 or Tspan14 (Dornier *et al.*, 2012; Jouannet *et al.*, 2016; Saint-Pol, Billard, *et al.*, 2017; Eschenbrenner *et al.*, 2020). Tspan5 has also recently been shown to promote Notch1 shedding in addition to Notch signalling in liver cancer (Xie *et al.*, 2021). These findings suggest that Notch proteins may be preferentially cleaved by Tspan5/ADAM10 and Tspan14/ADAM10 scissors. Notch activity in mouse was also shown to be promoted by Tspan5 and Tspan10 during differentiation of bone marrow macrophages to specialised osteoclasts (Zhou *et al.*, 2014), and Tspan33 during macrophage activation (Ruiz-García *et al.*, 2016), suggesting that Tspan10 and Tspan33 may play a role in Notch signalling in mouse macrophages.

The TspanC8/ADAM10 scissors for some substrates are less conclusive. One such example is APP, where different roles for different scissors have been shown depending on the validation approach and cell type (Table 1). Based on the evidence so far, and because the upregulation of Tspan15 in the brain of Alzheimer's disease patients and mouse models (Seipold *et al.*, 2018) contradicts with the finding that ADAM10 shedding of APP may be neuroprotective, Tspan15/ADAM10 scissor is likely to not be involved. It is possible that appropriate APP

shedding promotion involves a more complex mechanism that is dependent on both the TspanC8/ADAM10 scissor and other regulatory non-TspanC8 members like Tspan3 (Seipold *et al.*, 2017) or Tspan12 (Xu, Sharma and Hemler, 2009) in the tetraspanin web.

A detailed summary of the current known roles of TspanC8s in regulating shedding, activity or expression of different ADAM10 substrates compiled from the literature and unpublished data in the Tomlinson lab is presented in Table 1. Of note, studies where negative regulatory roles of TspanC8s were identified based on overexpression in the presence of endogenous TspanC8 regulator(s) should be interpreted with caution due to potential competition for ADAM10 association, depending on the expression levels of the TspanC8s. Competition for ADAM10 has been demonstrated between endogenous Tspan5 and Tspan15 (Eschenbrenner *et al.*, 2020), and overexpressed Tspan14 with endogenous Tspan15 (Tomlinson lab, unpublished). As such, an apparent inhibitory role of an overexpressed TspanC8 may be due to reduced formation of other TspanC8/ADAM10 scissor(s) that have a positive role, thus should be best concluded as having no effect unless the inhibitory effect can be validated by other approaches.

Although the demonstration of the substrate specificities of TspanC8/ADAM10 scissors is currently limited to a small number of substrates, future characterisation of the substrate repertoire of each TspanC8/ADAM10 scissor using high-throughput proteomics methods (Tüshaus *et al.*, 2020) would accelerate the filling of this knowledge gap, and to highlight opportunities where the regulatory TspanC8 can be targeted in place of ADAM10 to treat ADAM10-associated diseases in a substrate-specific manner. In the remainder of the introduction to TspanC8s, the differences among TspanC8s, from their expression in tissues, cells and organelles, down to their molecular interaction with ADAM10, some of which may contribute to the differential regulation of ADAM10 substrate specificity, will be highlighted.

Table 1. ADAM10 substrates with known regulatory TspanC8(s). The TspanC8 has a positive effect on substrate shedding unless otherwise indicated.

Substrate	TspanC8	Validation approach	Cell type	Comments	References
APP	Tspan15	Overexpression	HEK-293[a] and N2A[b]		(Prox *et al.*, 2012)
	Tspan14 (–) Tspan15 (–) Tspan33 (–)	Overexpression	U2OS-N1[c]	Effect strength: Tspan15>>33≈14. Tspan5 was tested in parallel and had no effect.	(Jouannet *et al.*, 2016)
	Tspan15 (–)	Knockdown	PC3[d]	Effect was minor. Tspan5 was tested in parallel and had no effect.	(Jouannet *et al.*, 2016)
		Overexpression	HEK-293		(Brummer *et al.*, 2019)
	Tspan15 (no effect)	Knockout	Mouse brain		(Seipold *et al.*, 2018)
Betacellulin	Tspan15	Knockout	HEK-293T[e]*	Tspan14 and Tspan33 were tested in parallel and had no effect.	(Tomlinson lab, unpublished)
		Overexpression (rescue)	HEK-293T*	Rescue by ADAM10 and Tspan15 overexpression had a greater effect than ADAM10 alone in ADAM10/Tspan15 double knockout cells.	(Koo *et al.*, 2020)
CD44	Tspan5	Knockdown	PC3	Effect was moderate. Tspan15 was tested in parallel and had no effect.	(Jouannet *et al.*, 2016)
Cellular prion protein	Tspan15	Knockout	Mouse brain		(Seipold *et al.*, 2018)
E-cadherin	Tspan15	Knockout	A549[f]		(Szyroka, 2019)
EGF	Tspan15	Knockout	HEK-293T*		(Tomlinson lab, unpublished)
GPVI	Tspan15 Tspan33	Knockout	HEK-293T* and HEL[g]	Completely abolished in Tspan15/33 double knockout cells. Tspan14 was tested in parallel and had no effect.	(Matthews, 2019)
	Tspan14 (–)	Overexpression	HEK-293T*	Moderate effect. All other TspanC8s were tested in parallel and had no effect.	(Noy *et al.*, 2016)
N-cadherin	Tspan15	Overexpression	Cos7[h]		(Prox *et al.*, 2012)
		Knockdown	PC3	Tspan5 was tested in parallel and had no effect.	(Jouannet *et al.*, 2016)
		Knockout	Mouse brain		(Seipold *et al.*, 2018)
		Overexpression	HEK-293T	All other TspanC8s were tested in parallel and had no effect.	(Noy *et al.*, 2016)
		Knockout	A549		(Szyroka, 2019)
		Knockout	HEK-293T	Tspan14 and Tspan33 were tested in parallel and had no effect.	(Tomlinson lab, unpublished)

Neuronal cell adhesion molecule	Tspan15	Overexpression	HEK-293*		(Brummer *et al.*, 2019)
Notch (activity)	Tspan5 Tspan14	Overexpression	HeLa[i]	Tspan15 was tested in parallel and had no effect.	(Dornier *et al.*, 2012)
		Knockdown	U2OS-N1*	Maximal reduction was achieved with combined depletion of Tspan5 and Tspan14.	(Dornier *et al.*, 2012) (Saint-Pol, Billard, *et al.*, 2017)
	Tspan15 (–) Tspan33 (–)	Overexpression	U2OS-N1*	Tspan5 and Tspan14 were tested in parallel and had no effect.	(Jouannet *et al.*, 2016) (Eschenbrenner *et al.*, 2020) for Tspan5 and Tspan15
	Tspan5 Tspan15 (–)	Knockdown	PC3	Combined Tspan5 and Tspan15 knockdown inhibited the increase seen in Tspan15 knockdown.	(Jouannet *et al.*, 2016)
	Tspan15 (no effect)	Knockout	Mouse brain		(Seipold *et al.*, 2018)
	Tspan5	Knockdown and overexpression	Hepatocellular carcinoma	Effect on Notch1 shedding was also demonstrated.	(Xie *et al.*, 2021)
	Tspan5 Tspan10	Knockdown	Mouse bone marrow macrophages	Also upregulated during osteoclast differentiation. Effect on Notch2 shedding was also demonstrated.	(Zhou *et al.*, 2014)
	Tspan5 Tspan33	Knockdown	HeLa*	Constitutively active Notch1 mutants, thus may be ADAM10-independent. Modulate γ-secretase activity.	(Dunn *et al.*, 2010)
	Tspan33	Knockdown and Overexpression	RAW 264.7[j]*	Modulate γ-secretase activity during macrophage activation.	(Ruiz-García *et al.*, 2016)
RAGE	Tspan15	Knockout	HEK-293T*	Tspan14 and Tspan33 were tested in parallel and had no effect.	(Tomlinson lab, unpublished)
VE-cadherin	Tspan15	Knockout	HEK-293T*		(Koo *et al.*, 2020)
	Tspan14	Knockdown	HUVEC[k]	Effect was minor.	(Haining *et al.*, 2012)
	Tspan15	Knockdown	HUVEC	Effect was minor.	(Szyroka, 2019)
VE-cadherin (expression)	Tspan5 Tspan17	Knockdown	HUVEC	Expression of Tspan5 or Tspan17 reduced surface expression but had no effect on shedding.	(Reyat, 2016; Reyat *et al.*, 2017)

[a] Human embryonic kidney 293; [b] Neuro 2A mouse neuroblastoma; [c] Human osteosarcoma expressing Notch1; [d] Human prostate adenocarcinoma; [e] HEK293 expressing the simian virus 40 (SV40) large T-antigen; [f] Human lung carcinoma; [g] Human erythroleukemia; [h] Monkey kidney fibroblast expressing SV40 T-antigen; [i] Human uterine cervical adenocarcinoma (Henrietta Lacks); [j] Mouse macrophage; [k] Human umbilical vein endothelial cells; * Transfected substrate.

1.4.3 Expression profiles of TspanC8s and their disease relevance

The expression of each TspanC8 in different tissue and cell types varies greatly, unlike the ubiquitous expression of their partner protein ADAM10 (Matthews, Szyroka, *et al.*, 2017; Matthews *et al.*, 2018; Harrison, Koo and Tomlinson, 2021). Figure 10 summarises the expression profiles of ADAM10 and TspanC8s in different healthy human tissues collated from publicly available proteomics datasets (Fishilevich *et al.*, 2016), and similarly, single-cell transcriptomic data in different human cell types in Figure 11 (Human Protein Atlas, 2021; Karlsson *et al.*, 2021). It is worth mentioning that the proteomics data presented here may under-represent the actual repertoire in each tissue because specific enrichment may be required for membrane proteins present at low levels; conversely, the transcriptomics data may over-represent the actual translated repertoire. Nevertheless, they provide a concise overview of the expression patterns of ADAM10 and TspanC8s.

1.4.3.1 Tspan5

The bulk expression of Tspan5 appears to be restricted to ovarian tissue (Figure 10), but its expression in the frontal cortex has been shown (Kim *et al.*, 2014), and it is also enriched in brain tissue at the RNA level (Aguet *et al.*, 2020). This correlates with its enhanced RNA expression in Horizontal cells, which are neurons in the retina (Figure 11). Its genetic association with non-responsiveness to treatments for clinical depression and alcohol use disorder, and function in promoting neurotransmitter release, also suggests its expression in the nervous system (Gupta *et al.*, 2016; Ho *et al.*, 2020). This is additionally supported by a recent study in rodents which shows the role of Tspan5 in promoting synapse maturation in neurons through clustering of the post synaptic cell-adhesion protein neuroligin-1, which is an ADAM10 substrate, but its shedding was not investigated in this study (Moretto *et al.*, 2019).

1.4.3.2 Tspan10

The expression of Tspan10, also known as oculospanin, is enriched in the retina (Figure 10) and in the Horizontal cells; expression in other cell types is considerably weak or absent (Figure 11). Coincidently, single-nucleotide polymorphisms (SNPs) surrounding the *TSPAN10* locus are associated with risk for several eye disorders, including a missense variant causing a C139Y substitution in the second transmembrane domain (Fritsche *et al.*, 2016; Shah and Guggenheim, 2018; Plotnikov *et al.*, 2019), although the direct biological link to Tspan10 has not been proven. It is also expressed in the lymph node and several internal and secretory tissues, and notably is the only TspanC8 expressed in uterus and cervix (Figure 10).

1.4.3.3 Tspan14

Like ADAM10, Tspan14 has the broadest tissue and cell type expression among TspanC8s (Figure 10 and Figure 11), which correlates with its role in Notch activation and embryonic lethality of Tspan14-knockout mice. It is the only TspanC8 detected in all ADAM10-expressing blood and immune cells including platelets (Figure 10), which is consistent with its high expression in transcriptomic profiles of the same cells (Figure 11). Indeed, there are reports of genetic associations of non-coding *TSPAN14* SNPs to susceptibility to chronic inflammatory diseases including inflammatory bowel diseases (Liu *et al.*, 2015; Ellinghaus *et al.*, 2016) and coronary artery disease (van der Harst and Verweij, 2018), suggesting the potential importance of Tspan14 in mediating immune cell function.

In addition, Tspan14 also appears to be the only TspanC8 detected in the heart tissue (Figure 10). Coinciding with this, it was reported recently in a short abstract that ADAM10 protein expression is upregulated in the heart tissue of patients with heart failure, and that ADAM10

inhibition in mouse models led to improved heart function and survival after heart attack due to reduced ADAM10 shedding of Notch1 (Klapproth *et al.*, 2020).

Lastly, the strong presence of Tspan14 in cerebrospinal fluid (Figure 10) is intriguing and plausible given that Tspan14 is one of the tetraspanins commonly found in extracellular vesicles (Keerthikumar *et al.*, 2015; Dozio and Sanchez, 2017; Silva *et al.*, 2021). Like ADAM10, it has also been detected in human plasma samples (Uhlén *et al.*, 2015; Human Protein Atlas, 2021). *TSPAN14* was recently identified as a novel risk locus for Alzheimer's disease in a comprehensive meta-analysis study (Schwartzentruber *et al.*, 2021) that also replicated previously identified associations with *ADAM10* (Marioni *et al.*, 2018; Jansen *et al.*, 2019; Kunkle *et al.*, 2019). Multiple *TSPAN14* risk alleles in non-coding regions were implicated but the predictions on expression changes were inconsistent (Schwartzentruber *et al.*, 2021). Given that full-length and soluble forms of ADAM10 have been detected in plasma and cerebrospinal fluid samples and the levels appear to change throughout the progression of Alzheimer's disease (Sogorb-Esteve *et al.*, 2018; Vanatabe *et al.*, 2021), it is possible that Tspan14 may contribute to the release of ADAM10 into extracellular vesicles.

1.4.3.4 Tspan15

Among the blood and immune cell types, Tspan15 appears to be present exclusively on platelets (Figure 10), but its RNA expression in other immune cells can also be detected at low levels (Figure 11), and at higher levels in some T cell subsets (Uhlén *et al.*, 2015; Human Protein Atlas, 2021). This suggests that its expression may be enhanced post-differentiation in T cells. Tspan15 is also expressed in the tissues in the central nervous system, in many internal and secretory tissues, and in male but not female reproductive tissues (Figure 10). At the RNA level, it is expressed at low levels in many different cell types but is remarkably enriched in many

secretory cells such as exocrine glandular, pancreatic endocrine and ductal cells (Figure 11). The latter coincides with it being the only TspanC8 expressed in the islet of Langerhans that contains pancreatic endocrine cells (Figure 10). Interestingly, several studies identified a non-coding SNP near the *TSPAN15* locus to associate with type 2 diabetes risk in East Asian populations (Ishigaki *et al.*, 2020; Spracklen *et al.*, 2020; Vujkovic *et al.*, 2020). However, it is currently unknown how the SNP affects *TSPAN15* or if neighbouring genes may be affected. Nevertheless, the high expression of Tspan15 in secretory cells highlights an area of underexplored ADAM10 biology and substrates in diabetes. For example, could Tspan15/ADAM10 cleavage of betacellulin and EGF, which appear to have opposite roles in controlling pancreatic endocrine cell differentiation (Hanley *et al.*, 2011; Santosa *et al.*, 2016), be important in maintaining glucose homeostasis?

Coinciding with Tspan15/ADAM10 being the scissor for N-cadherin, the most well-established disease relevance of Tspan15 is in cancer development, where both ADAM10 (Smith, Tharakan and Martin, 2020) and N-cadherin (Mrozik *et al.*, 2018) have long been identified as attractive therapeutic targets. Tspan15 has been shown to be upregulated and promote tumour formation in several cancer cell types and has a pro-invasive role (Zhang *et al.*, 2018; Hiroshima *et al.*, 2019; Sidahmed-Adrar *et al.*, 2019). In one study, Tspan15 promotion of cancer cell invasion was shown to be a direct effect via its interaction with the beta-transducin repeat-containing E3 ubiquitin protein ligase (β-TrCP) and subsequent activation of nuclear factor kappa B (NF-κB) signalling, suggesting that Tspan15 may have a dual role in promoting cancer progression via ADAM10-dependent and ADAM10-independent pathways (Zhang *et al.*, 2018).

Besides cancer, Tspan15 has also been shown to be upregulated in Alzheimer's disease (Seipold *et al.*, 2018). Among fibroblasts, Tspan15 expression appears to be limited to a specific

fibroblast subtype implicated in arthritis (Croft *et al.*, 2019). Lastly, non-coding *TSPAN15* SNPs had been identified to be associated with venous blood clotting risk (Germain *et al.*, 2015; Klarin *et al.*, 2017, 2019; Lindström *et al.*, 2019) and self-reported blood clotting events (Hinds *et al.*, 2016), but no biological link had been proposed or investigated.

1.4.3.5 Tspan17

Tspan17 is one of the least studied TspanC8s. Its expression is absent in the presented proteome (Figure 10), and its transcriptome profile suggests that it may be expressed at low levels in different cell types (Figure 11). Given that it shares 78% identity with Tspan5, and their redundancies have been demonstrated functionally (Reyat *et al.*, 2017) and in antibody recognition (Saint-Pol, Billard, *et al.*, 2017), could *TSPAN17* be a redundant gene that is only relevant in a diseased state? A search for its existential relevance revealed that it appears to be a target of a tumour-suppressing microRNA. High *TSPAN17* expression in glioblastoma patients is associated with poor prognosis; downregulation of *TSPAN17* via overexpression of the microRNA inhibited proliferation, migration and invasion and promoted cell death of glioblastoma cells *in vitro* (Guo *et al.*, 2019). ADAM10 also promotes the progression of glioblastoma (Siney *et al.*, 2017), and indeed, an ADAM10/17 inhibitor is currently in Phase I clinical trial for glioblastoma in children (US National Library of Medicine 2020). Therefore, it is possible that Tspan17 can contribute to the progression of glioblastoma by promoting ADAM10 expression or promoting cleavage of disease-relevant substrates, e.g. neuroligin-3 (Venkatesh *et al.*, 2015).

1.4.3.6 Tspan33

Other than platelets, Tspan33 expression appears to be restricted to B cells and kidney (Figure 10). This is reflected by its enhanced RNA expression in several kidney cell types such as

proximal tubular and peritubular cells, in B cells and additionally on monocytes and macrophages (Figure 11). Tspan33's roles in B cell activation (Luu *et al.*, 2013; Pérez-Martínez *et al.*, 2017; Navarro-Hernandez *et al.*, 2020) and macrophage activation (Ruiz-García *et al.*, 2016) have been demonstrated. Its expression is prominent in B cell lymphomas and in B cells of patients with autoimmune diseases (Luu *et al.*, 2013), which are diseases where monocytes and macrophages are involved (Ma *et al.*, 2019). In fact, the *TSPAN33* gene was first discovered in a chromosomal region containing hotspots for deletions in myeloid malignancies (Heikens *et al.*, 2007). Its role in red blood cell production has been shown in mice (Heikens *et al.*, 2007), but it is likely absent in human due to its absence in erythroid cells (Figure 11). Such species differences in expression have been shown before by the expression of Tspan33 on human platelets but not on mouse platelets (Haining *et al.*, 2012), which only have Tspan14 (Matthews, Noy, *et al.*, 2017).

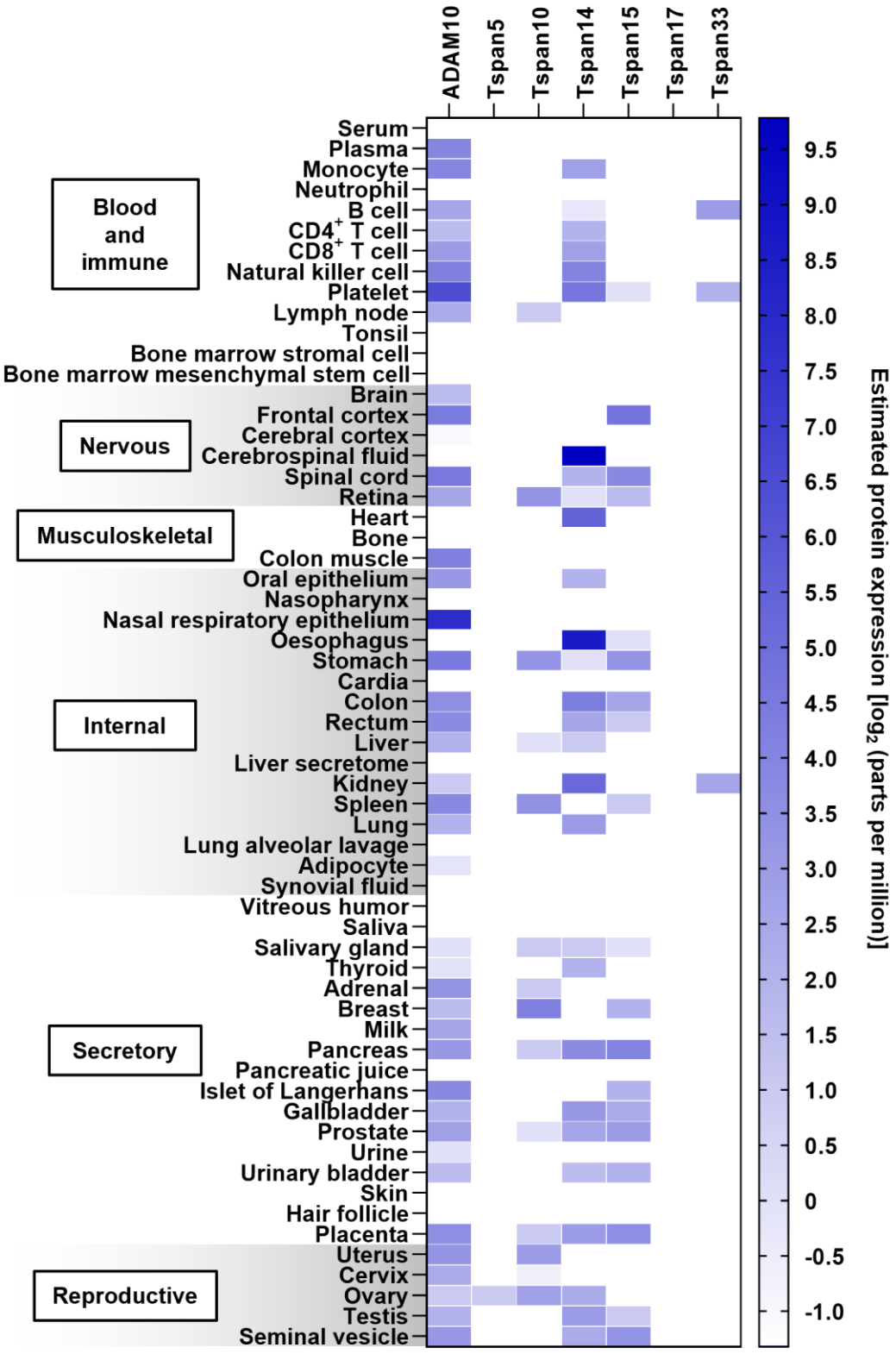

Figure 10. Protein expression profiles of ADAM10 and TspanC8s in human tissues. Data were extracted from a collation of publicly available mass spectrometry-based proteomics datasets in 60 healthy adult tissue and blood cell types, and categorised by tissue types: blood and immune, nervous, musculoskeletal, internal, secretory and reproductive tissues (Fishilevich *et al.*, 2016).

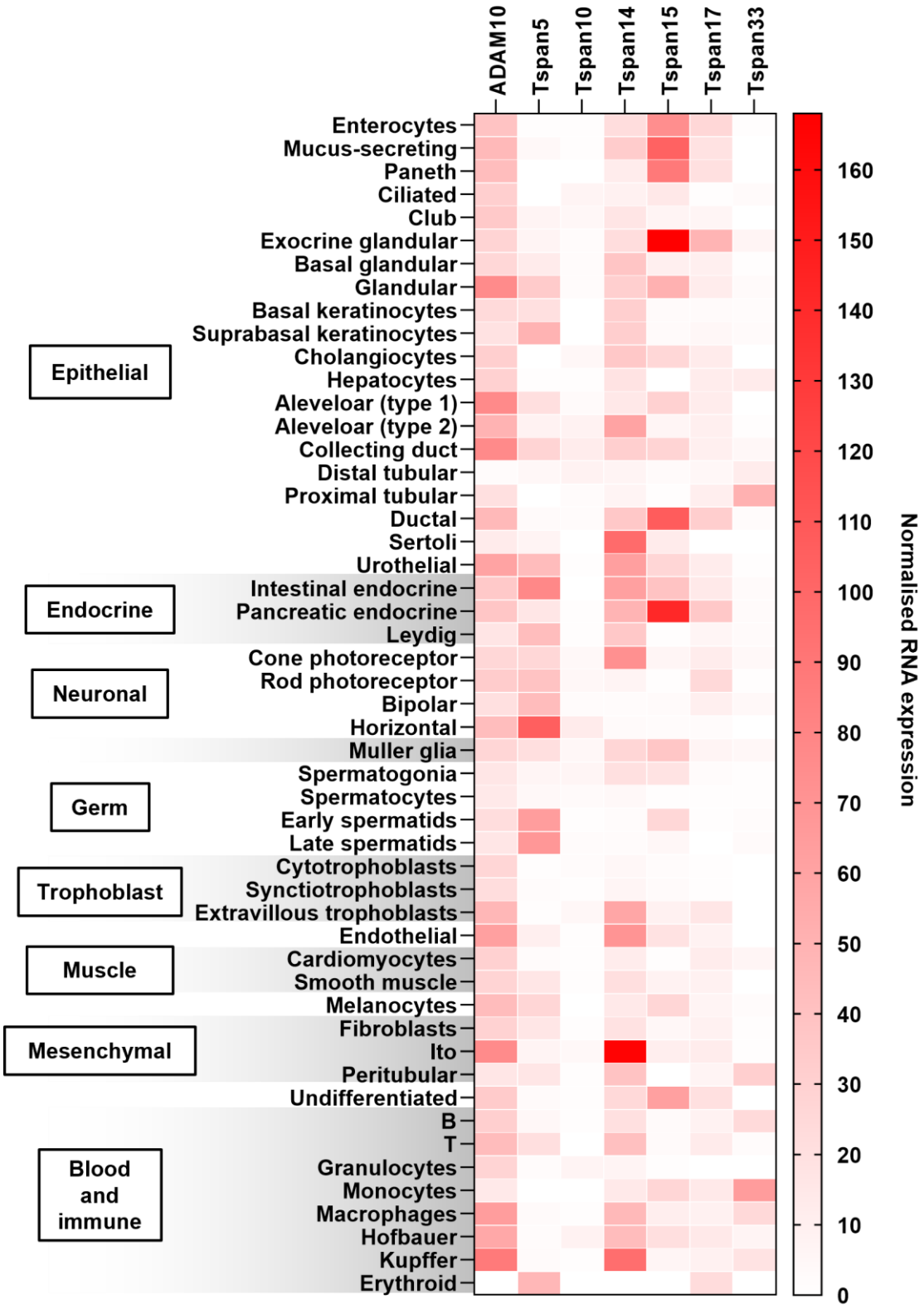

Figure 11. RNA expression profile of ADAM10 and TspanC8s in different human cell types. Data were extracted from a single-cell transcriptomic dataset from 51 cell types, and categorised by cell types: epithelial, endocrine, neuronal, glial, germ, trophoblast, muscle, mesenchymal, undifferentiated, and blood and immune cells (Human Protein Atlas, 2021; Karlsson *et al.*, 2021).

1.4.4 TspanC8s regulate ADAM10 subcellular distribution and dynamics

The individual effect of each TspanC8 on the subcellular distribution of ADAM10 was best demonstrated in one study using the HeLa epithelial cells which only express a minimal level of *TSPAN14* mRNA (Dornier *et al.*, 2012). This provided an almost TspanC8-free system in which the competition from endogenous TspanC8s for ADAM10 could be avoided when different TspanC8s were introduced by transfection. Flow cytometry and imaging showed that overexpression of Tspan5, Tspan14, Tspan15 or Tspan33 in HeLa cells promoted ADAM10 surface expression, accompanied by the striking colocalisation between ADAM10 and each TspanC8 on the plasma membrane and inside the cells. On the other hand, overexpressed Tspan10 and Tspan17 did not substantially affect ADAM10 surface expression as they preferentially localised ADAM10 to late endosomes. This demonstrates that TspanC8s can differentially regulate ADAM10 by affecting its subcellular localisation (Figure 12).

Subsequent imaging studies showed that the four TspanC8s that can promote cell surface expression had other distinctions in regulating ADAM10 subcellular localisation or dynamics. Overexpressed Tspan15 and Tspan33 exhibited strong localisation at the plasma membrane, and Tspan33 was demonstrated to also cluster ADAM10 at an apical region of the adherens junctions in densely packed epithelial cells (Figure 12) (Shah *et al.*, 2018). Overexpressed Tspan14 showed greater intracellular presence (Figure 12) (Noy *et al.*, 2016). Overexpressed Tspan5 increased ADAM10 localisation at the cell edges when the basal surface of cells was imaged, in contrast to overexpressed Tspan15 which did not (Jouannet *et al.*, 2016). This was also demonstrated similarly at the endogenous level, where strong colocalisation between ADAM10 and Tspan15 on the basal surface of cells was demonstrated throughout the membrane, which showed marked contrast with the preferential distribution of the non-TspanC8 CD9 at the periphery on the cell surface (Koo *et al.*, 2020).

Tspan5 and Tspan15 have also been demonstrated to regulate the dynamics of ADAM10. Overexpression of Tspan15 increased the lateral diffusion of ADAM10 compared to overexpression of Tspan5 (Jouannet *et al.*, 2016). In the most recent study, Tspan5 and Tspan15 differentially regulate ADAM10 endocytosis, with Tspan15 promoting ADAM10 stability on the cell surface better than Tspan5; reciprocal regulation by ADAM10 was also demonstrated (Eschenbrenner *et al.*, 2020). Given that Tspan5 and Tspan14 are closely related (58% amino acid sequence identity) and share the same role in promoting Notch activation (Matthews, Szyroka, *et al.*, 2017), it is possible that Tspan14 may also regulate ADAM10 endocytosis.

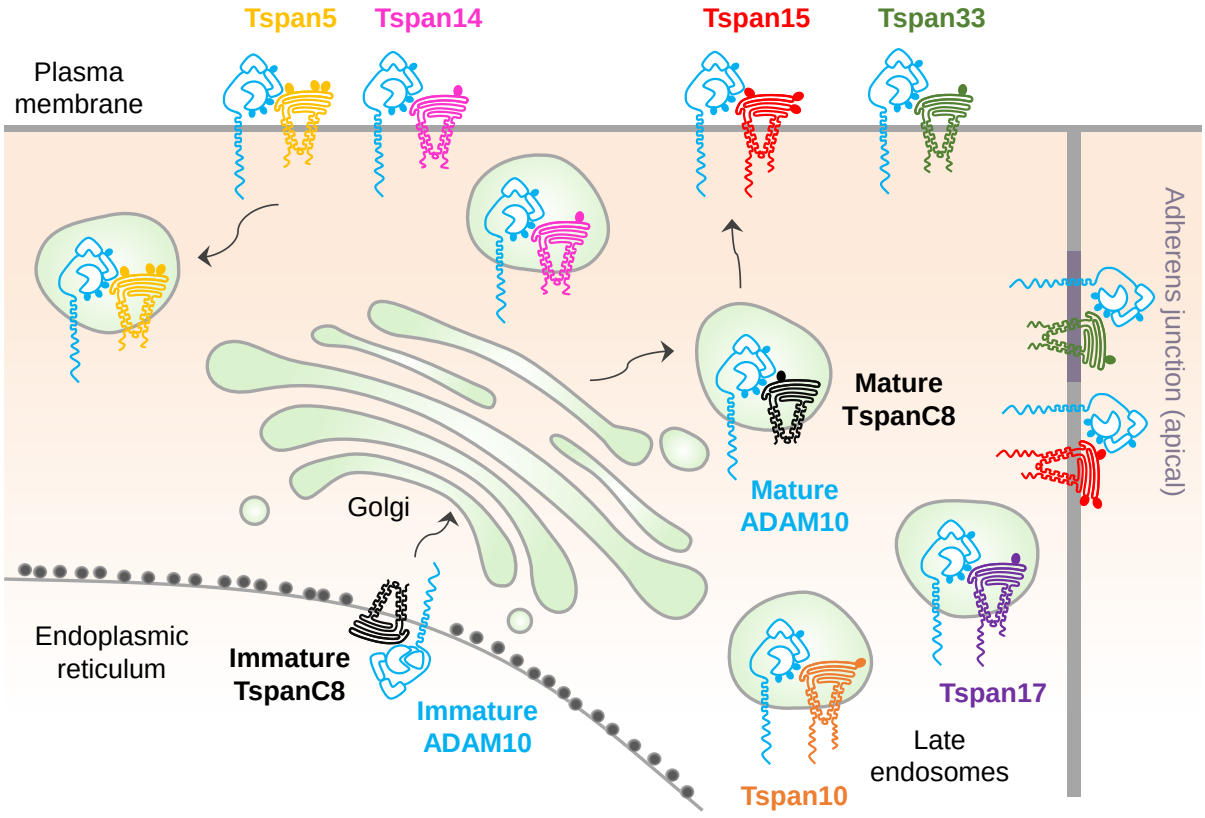

Figure 12. TspanC8s regulate ADAM10 subcellular localisation. TspanC8 is required to promote ADAM10 exit from the endoplasmic reticulum, its maturation in the Golgi and trafficking to different subcellular compartments (and *vice versa* for Tspan5 and Tspan15). Tspan10 and Tspan17 are predominantly localised to late endosomes. Tspan5 and Tspan14 are present on the plasma membrane but may predominantly localise to intracellular compartments. Tspan5 promotes ADAM10 endocytosis, whereas Tspan15 has the opposite role. Tspan15 and Tspan33 are predominantly expressed on the cell surface. Tspan33 can cluster ADAM10 at an apical region of the adherens junction in epithelial cells. Figure is adapted from Harrison, Koo and Tomlinson (2021).

1.4.5 TspanC8s interact with ADAM10 at their extracellular regions and may regulate ADAM10 conformation

TspanC8s have been shown to interact with ADAM10 at their extracellular regions. Using chimeras between CD9 and Tspan14 where the large extracellular region or the variable region alone was exchanged, it was shown that the entire large extracellular region of Tspan14 was required to interact with ADAM10 to promote its maturation and expression (Noy *et al.*, 2016). Using Tspan5 constructs encoding mutations in the large extracellular region, two motifs that are conserved in TspanC8s, RDD located between A and B helices in the conserved region, and NXYF (X denotes any amino acid; F is replaced by H in Tspan15) near the beginning of the variable region, were shown to be required for interaction with ADAM10 and promote its exit from the ER (Saint-Pol, Billard, *et al.*, 2017).

In addition, there is some evidence showing that interaction with different TspanC8s may affect the conformation that ADAM10 adopts. Each TspanC8 interacts with ADAM10 slightly differently; Tspan15 requires only the stalk region of ADAM10 for interaction, Tspan17 additionally requires the cysteine-rich region, whereas the other four TspanC8s also require the disintegrin region to interact with ADAM10 (Noy *et al.*, 2016). Furthermore, an analysis of known cleavage sites of ADAM10 substrates for which reliable evidence of the regulatory TspanC8(s) is available, suggests that there is an association between the TspanC8/ADAM10 identity and the cleavage site 'height' as estimated by the number of amino acids above the membrane surface (Table 2). Tspan15/ADAM10 scissors may prefer substrates with cut sites located closer to the membrane surface, e.g., betacellulin and N-cadherin, whereas cleavage of substrates with cut sites further away from the membrane surface, e.g., Notch1 and CD44, appear to be favoured by Tspan5/ADAM10 or Tspan14/ADAM10 scissors (Table 2).

Table 2. Substrates with known cleavage sites and evidence of TspanC8/ADAM10 scissor identities.

Substrate	**TspanC8/ADAM10 scissor(s)**	**ADAM10 cleavage site** (indicated with |)	**Estimated no. of residues above membrane surface**	**References**
Betacellulin	Tspan15	VDLFY | LRGDR	7	(Sunnarborg *et al.*, 2002)
CD44	Tspan5	HSHGS | QEGGA	19	(Nakamura *et al.*, 2004)
EGF	Tspan15	WWELR | HAGHG	9	(Sunnarborg *et al.*, 2002)
GPVI	Tspan15 and Tspan33	AGPAR | QYYTK	5	(Gardiner *et al.*, 2007)
N-cadherin	Tspan15	TDVDR | IVGAG	10	(Uemura *et al.*, 2006)
Notch1*	Tspan5 and Tspan14	YKIEA | VQSET	15	(Mumm *et al.*, 2000)
RAGE*	Tspan15	GPTAG | SVGGS	11	(Braley *et al.*, 2016)

* Based on sequence alignment with their mouse counterparts.

Based on the findings above and the insights from the structural features of ADAM10 (Section 1.2.1) and tetraspanins (Section 1.3.2), it is therefore tempting to hypothesise how TspanC8s may regulate ADAM10 substrate specificity at the protein structure level. An interaction between a TspanC8 with ADAM10, may lead to conformational changes in both proteins, which may or may not require a stimulus to occur, resulting in an 'open' conformation of a functional TspanC8/ADAM10 scissor (Figure 13A). The 'open' conformation of each TspanC8/ADAM10 scissor may be dependent on the 'open' conformation of individual TspanC8s, leading to their differential interactions with the non-catalytic domains on ADAM10 extracellular region, which in turn position the metalloprotease domain at different angles (Figure 13B). This restriction may affect whether a TspanC8/ADAM10 scissor can cut a substrate because of the differences in the distances of the ADAM10 cleavage site from the membrane surface among different substrates (Figure 13B). Could this be why among the three TspanC8/ADAM10 scissors expressed on platelets, only Tspan15/ADAM10 and Tspan33/ADAM10 scissors can cut GPVI, which has its cut site located five residues above the membrane surface, closer than other substrates, whereas Tspan14/ADAM10 scissors cannot? The final section in this chapter will introduce the main substrate of interest GPVI and its function in platelet biology and pathology.

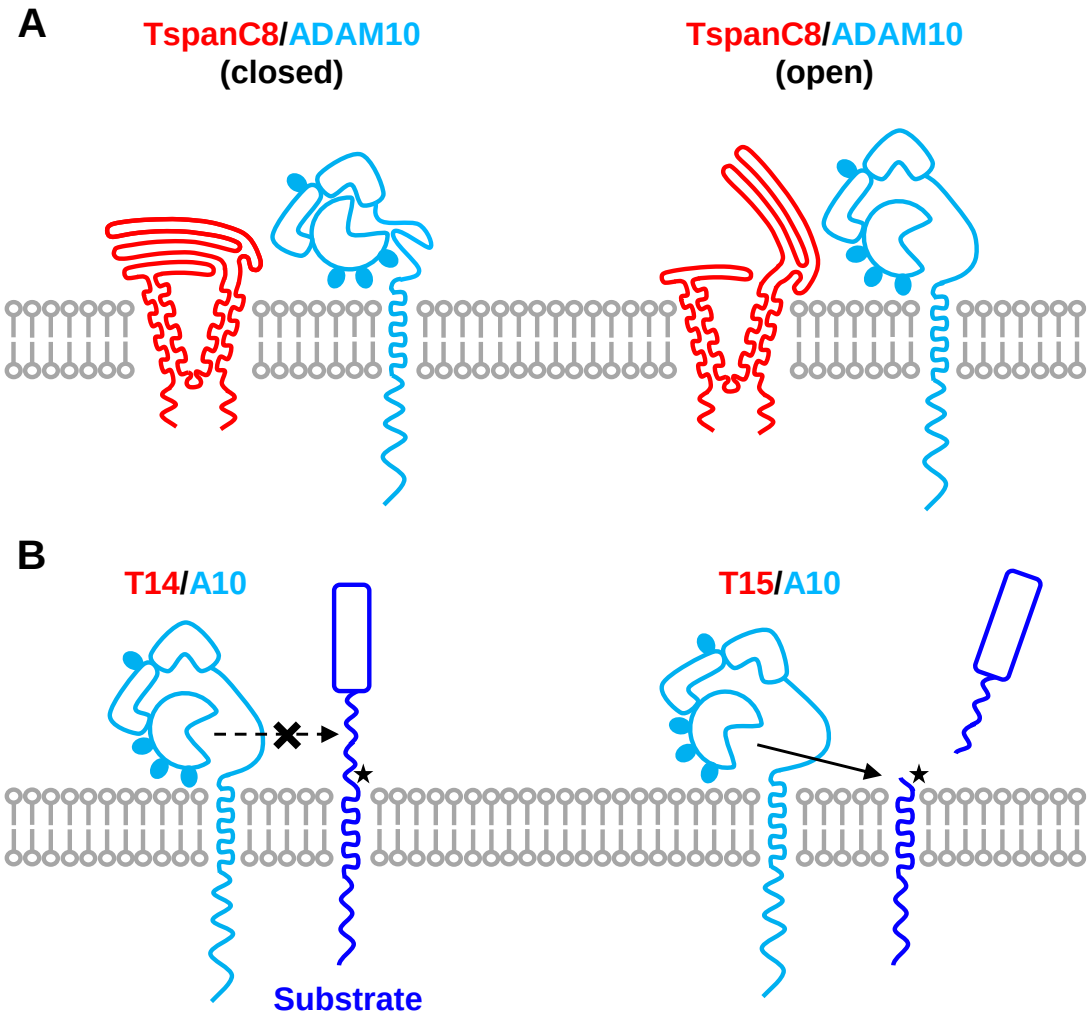

Figure 13. TspanC8s may restrict ADAM10 substrate repertoire by regulating ADAM10 conformation. (A) The interaction of a TspanC8 with ADAM10 may lead to conformational changes in both proteins, leading to the formation of an active 'open' conformation. (B) Depending on the associated TspanC8, e.g., Tspan14 (T14) or Tspan15 (T15) (not shown for clarity), the angle of the metalloprotease domain relative to the membrane surface may be different. Therefore, a substrate with an ADAM10 (A10) cut site (depicted by a star) located closer to the membrane surface cannot be cleaved by a Tspan14/ADAM10 scissor but can be cleaved by a Tspan15/ADAM10 scissor.

1.5 The platelet collagen and fibrin receptor GPVI

1.5.1 Platelets in haemostasis and thrombosis

Platelets are small, anucleate blood cells that originate from their larger precursor cells known as megakaryocytes. The major function of platelets is in regulating blood clot (thrombus) formation, although increasing evidence has shown that platelets can also act as immune cells and mediate other pathophysiological responses (Brass, Diamond and Stalker, 2016; Kapur and Semple, 2016; Braun *et al.*, 2021). Platelets respond to injury to blood vessels by becoming activated and initiate blood clotting to prevent excessive bleeding (haemostasis). In diseased blood vessels, unwanted platelet activation leads to the formation of excess blood clots that could obstruct blood flow (thrombosis) (Koupenova *et al.*, 2017; Mackman *et al.*, 2020).

Thrombosis in an artery (arterial thrombosis) may result in heart attack if it occurs in coronary arteries or stroke if it occurs in arteries providing blood supply to the brain (Figure 14A). Arterial thrombi are often characterised by the presence of platelet-rich white thrombi and the roles that platelets play are well-examined. On the other hand, thrombosis in a vein (venous thrombosis) results in fibrin- and red blood cell-rich red thrombi (Koupenova *et al.*, 2017; Mackman *et al.*, 2020). As such, the role of platelets in venous thrombosis is less well-studied but emerging genetic, experimental and clinical evidence suggest that platelet function is important in venous thrombosis (Takahashi *et al.*, 2009; Montoro-García *et al.*, 2016; Panova-Noeva *et al.*, 2020). Thrombosis in a deep vein, usually in the lower body, results in deep vein thrombosis; the thrombus may break off and travel (embolise) to the lungs, leading to pulmonary embolism (Figure 14B). Deep vein thrombosis and pulmonary embolism are collectively known as venous thromboembolism (Koupenova *et al.*, 2017; Mackman *et al.*, 2020).

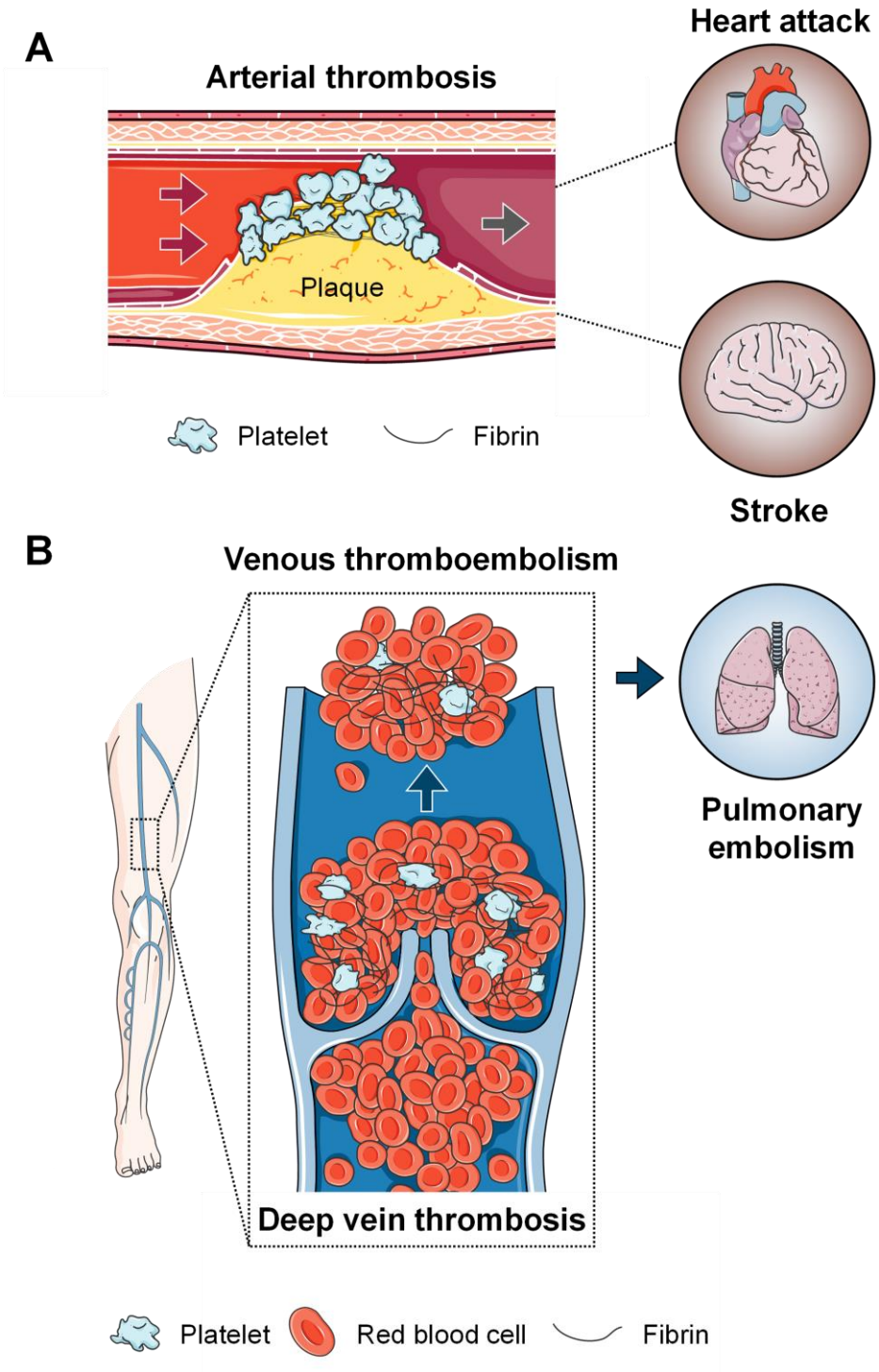

Figure 14. Platelets in arterial and venous thrombosis. (A) Unwanted platelet activation in a diseased artery, such as following the rupture of an atherosclerotic plaque, leads to arterial thrombosis, which can obstruct blood flow and cause heart attack or stroke depending on the location of the artery. Arrows indicate blood flow. (B) Unwanted activation of platelets and the coagulation cascade in a deep vein, such as due to a stagnation of blood flow in the thigh, leads to deep vein thrombosis. The clot can travel to the lungs, resulting in pulmonary embolism. Collectively, deep vein thrombosis and pulmonary embolism are referred to as venous thromboembolism. Diagrams of organs, vessels and blood components are adapted from Servier Medical Art (Servier Laboratories, 2020).

1.5.2 Mechanisms of platelet activation in haemostasis and thrombosis

Resting platelets circulate in the bloodstream and become activated in response to environmental stimuli. Platelets have many adhesion and signalling receptors on their surface that facilitate a complex network of activatory and inhibitory signalling machineries. In haemostasis, injury to the endothelium exposes the protein-rich subendothelial matrix (Figure 15). Binding of the platelet glycoprotein complex GPIb-IX-V to von Willebrand factor (vWF), immobilised on the collagen-rich matrix, tethers platelets to the site of injury. This allows collagen to bind to GPVI, which initiates platelet activation by triggering a signalling cascade through its associated Fc receptor gamma dimer chains (FcRɣ) that contain immunoreceptor tyrosine-based activation motifs (ITAMs) (Figure 15). Activation enhances platelet adhesion by activating the collagen-binding integrin receptor α2β1 and the fibrin(ogen)-binding platelet integrin αIIbβ3. In activated platelets, cytoskeletal rearrangements allow platelets to stretch and spread. Granules containing secondary mediators are also secreted to recruit other platelets in the bloodstream to the injury site, resulting in an aggregate of platelets (Figure 15). Activated platelets also augment the simultaneously active blood coagulation cascade by enhancing the production of the multi-functional protease thrombin, which converts fibrinogen to fibrin, resulting in a stable thrombus (Dütting, Bender and Nieswandt, 2012; Xu *et al.*, 2016).

In arterial thrombosis, excessive platelet activation can be triggered by damage to the vessel wall such as rupture of a subendothelial atherosclerotic plaque (Figure 14A, Section 1.5.1), which provides an attractive platform for platelet activation. In venous thrombosis, the endothelium often remains intact but endothelial dysfunction can occur due to blood flow stagnation (Figure 14B, Section 1.5.1). This results in a low-oxygen environment that can trigger the release of vWF from endothelial cells to recruit and activate platelets, and in

combination with other pro-coagulant mediators, lead to the formation of fibrin-rich clots (Koupenova *et al.*, 2017; Wang *et al.*, 2018; Mackman *et al.*, 2020).

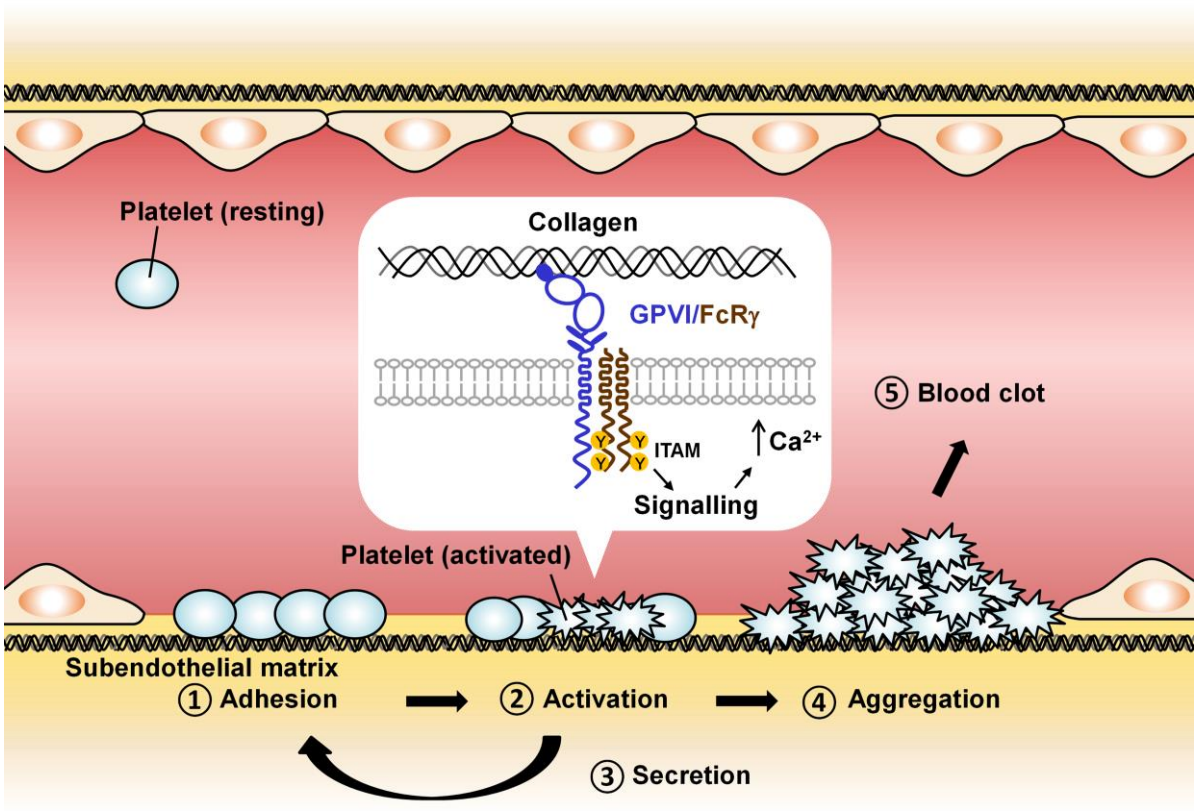

Figure 15. GPVI is a key receptor in platelet activation. (1) Platelets are recruited to the site of vessel injury following binding of platelet receptors to their substrates in the exposed subendothelial matrix. (2) Binding of GPVI to collagen initiates platelet activation by signalling through its associated ITAM-containing FcRɣ, resulting in a weak and sustained increase in intracellular Ca^{2+} levels. This triggers further inside-out signalling, activating integrins which enhance platelet adhesion and causes a shape change into spread, activated platelets. (3) Activated platelets secrete granules containing various chemotactic factors that recruit more platelets to their substrates at the injury site, (4) forming an aggregate of activated platelets and (5) together with the active blood coagulation cascade, produce a stable blood clot. Large, filled oval on GPVI depicts an N-glycosylation site, whereas smaller ovals on the stalk region depict O-glycosylation sites. Figure is based on Dütting, Bender and Nieswandt (2012).

1.5.3 GPVI is the major signalling receptor for collagen and can also bind fibrin

GPVI is a single-pass transmembrane protein with two extracellular immunoglobulin G (IgG) domains: an N-terminal domain that binds collagen (Lecut *et al.*, 2004; Smethurst *et al.*, 2004) and another domain that facilitates homodimerisation (Horii, Kahn and Herr, 2006; Slater *et al.*, 2021) (Figure 15, Section 1.5.2). Through its transmembrane and juxtamembrane intracellular regions, GPVI forms a complex with its signalling partner FcRγ (Berlanga *et al.*, 2002; Bori-Sanz *et al.*, 2003), which is also essential for its surface expression on platelets (Tsuji *et al.*, 1997). GPVI cytoplasmic tail contains motifs for binding to the Ca^{2+}-binding protein calmodulin (Andrews *et al.*, 2002), Src kinases (Suzuki-Inoue *et al.*, 2002) and tumour necrosis factor (TNF)-receptor associated factor 4 (TRAF4) (Arthur *et al.*, 2011).

GPVI is the major signalling receptor for collagen that initiates platelet activation (Figure 15, Section 1.5.2). Specifically, GPVI binds to type I, II and III fibrillar collagens (Jung *et al.*, 2008). The conventional view of GPVI dimerisation being a requirement for collagen binding has recently been challenged due to contradictions in the literature (Clark, Damaskinaki, et al. 2021) and evidence that endogenous GPVI exists as monomers and dimers on the platelet surface regardless of activation status, and that deletion or replacement of the dimerisation domain in the extracellular region did not impair collagen-induced signalling (Clark, Neagoe, et al. 2021). The authors proposed that GPVI dimerisation is not a conformational requirement for ligand binding but rather serves to increase avidity. Irrespective of dimerisation, it is clear that GPVI clustering upon collagen binding maintains collagen-induced ITAM signalling in platelets (Poulter *et al.*, 2017; Pallini *et al.*, 2021) to induce a weak and sustained rise in intracellular Ca^{2+} level (Tomlinson *et al.*, 2007).

GPVI can also bind other ligands, most notably the recently discovered fibrin which revealed another key role of GPVI in promoting thrombus growth and maintaining thrombus stability (Alshehri *et al.*, 2015; Mammadova-Bach *et al.*, 2015; Onselaer *et al.*, 2017; Induruwa *et al.*, 2018). The binding of GPVI to fibrin and whether it can bind fibrinogen is another subject of controversy (Slater *et al.*, 2018). A recent study attempted to address this using fibrin clots that more closely mimic the physiological condition and showed that GPVI binds fibrin but not fibrinogen (Moroi *et al.*, 2021). The authors also demonstrate that GPVI in resting platelets can bind fibrin and does not require activation of the major fibrin-binding receptor αIIbβ3. Similarly, another study compared fibrin- and collagen-induced platelet aggregation and showed that they are mechanistically different in that although binding of fibrin to GPVI can induce ITAM signalling, fibrin-mediated aggregation does not require ITAM signalling and is αIIbβ3-independent (Montague *et al.*, 2020). These findings support the role of GPVI-fibrin interaction in the propagation of collagen-poor thrombi such as venous thrombi (Lehmann *et al.*, 2018) or during septic thermal injury (Montague *et al.*, 2018).

1.5.4 GPVI is a promising anti-platelet target

Finding the right balance between maintaining haemostasis and reducing thrombosis is a key consideration when identifying novel anti-platelet targets or strategies (Mackman *et al.*, 2020). As such, GPVI is an attractive anti-platelet target not only because its expression is restricted to platelets and megakaryocytes, but also because its blockade or depletion reduces thrombosis but is not accompanied by severe haemostasis defects (Alenazy and Thomas, 2021; Harbi *et al.*, 2021). In human, this was best demonstrated by GPVI-deficient patients, who had mildly increased bleeding time; GPVI-deficient human platelets showed reduced adhesion to collagen, loss of aggregation in response to collagen and reduced thrombus formation on collagen (Sugiyama *et al.*, 1987; Moroi *et al.*, 1989; Dumont *et al.*, 2009; Hermans *et al.*, 2009). In

addition, *GP6* polymorphisms are associated with thrombotic disease risks (Arthur, Dunkley and Andrews, 2007).

Indeed, two novel biologics targeting GPVI are currently in clinical trials. The first is Revacept, developed by the biotech company advanceCOR. Revacept is a recombinant fusion protein consisting of the soluble ectodomain of a dimeric GPVI fused to the fragment crystallisable (Fc) region of human IgG1. It inhibited GPVI-dependent platelet adhesion and thrombus formation *in vitro* and in mice models *in vivo* by acting as a competitive antagonist to membrane-bound GPVI for collagen binding (Massberg *et al.*, 2004; Schönberger *et al.*, 2012). Phase II trials for the prevention and treatment of stroke and coronary heart disease with Revacept have recently been completed. In the trial for stroke, Revacept treatment reduced bleeding and stroke complications (US National Library of Medicine 2021a). In the trial for coronary heart disease, the safety of Revacept was demonstrated as it did not cause bleeding increase in patients. Although its clinical efficacy has not been demonstrated, a modest reduction in collagen-induced platelet aggregation was seen. The authors proposed that different clinical end-point measurements in a cohort of higher-risk patients is likely needed to realise the translation of platelet inhibition to clinical efficacy in future trials (Mayer *et al.*, 2021).

The second anti-GPVI agent is ACT017 (glenzocimab), developed by the company Acticor Biotech. It is a humanised antigen-binding fragment (Fab) of an anti-GPVI antibody 9O12. Administration in animal models reduced collagen-induced platelet aggregation and thrombus formation on collagen with no bleeding defects (Mangin *et al.*, 2012; Lebozec *et al.*, 2017). Its safety and anti-platelet effects have been demonstrated in healthy individuals in a completed Phase I trial (Voors-Pette *et al.*, 2019). Phase II clinical trials for stroke (and COVID-19) are at the patient recruitment stage (US National Library of Medicine 2021b).

These biologics demonstrate that anti-GPVI strategies may improve patient outcomes in thrombotic diseases without bleeding side effects.

1.5.5 GPVI can be downregulated by ADAM10-mediated shedding

Ectodomain shedding of GPVI is a mechanism that provides a means to rapidly downregulate GPVI expression on the surface of activated platelets. ADAM10 is the primary sheddase for human GPVI (Gardiner *et al.*, 2007). Of note, mouse GPVI, which only shares ~65% amino acid identity with its human counterpart (Jandrot-Perrus *et al.*, 2000), can also be cleaved by ADAM17 and additional unidentified proteases (Bender *et al.*, 2010). Other than GPVI, ADAM10 is estimated to have another 34 putative substrates that are expressed on platelets (Maurer *et al.*, 2020); of these, shedding of GPV (Gardiner *et al.*, 2007) and signalling lymphocyte activation molecule family 5 (SLAMF5) on platelets have been demonstrated (Hofmann *et al.*, 2012).

Shedding of GPVI (~60 kDa) generates a soluble ectodomain fragment (~50 kDa), leaving a membrane-bound fragment at the C-terminus (~10 kDa). The membrane remnant is not subjected to γ-secretase cleavage (Matthews, 2019). Due to the lack of constitutive GPVI shedding on resting platelets (Gardiner *et al.*, 2004), the ratio of soluble GPVI to membrane-bound GPVI may act as a marker for platelet activation (Montague, Andrews and Gardiner, 2018). This is because increased soluble GPVI levels have been detected in plasma samples of severely injured patients (Montague *et al.*, 2018; Vulliamy *et al.*, 2020) and patients with thrombotic diseases (Al-Tamimi, Gardiner, *et al.*, 2011; Yamashita *et al.*, 2014; Stack *et al.*, 2017).

Physiologically, GPVI shedding can be induced upon binding to its ligands (Gardiner *et al.*, 2004; Montague *et al.*, 2018). A recent study suggests that binding of collagen and fibrin induce

GPVI shedding by ADAM10 via different mechanisms in platelets. In contrast to collagen, fibrin-induced GPVI shedding occurs by increasing ADAM10 activity, is charge-dependent, and does not require activation of downstream ITAM signalling (Montague *et al.*, 2020). Shear stress (Al-Tamimi *et al.*, 2012) or activation of coagulation by factor Xa (Al-Tamimi, Grigoriadis, *et al.*, 2011) can also activate GPVI shedding. Shedding can also be triggered by external stimuli using ADAM-activating chemicals including the thiol-alkylating agent N-ethylmaleimide (NEM) (Gardiner *et al.*, 2007) and the Ca^{2+} ionophore ionomycin (Baaten *et al.*, 2018). It is worth noting that NEM is a potent metalloprotease activator, but the exact mechanism of activation remains unclear. It has been proposed that NEM triggers the "cysteine-switch" activation mechanism by alkylating a critical cysteine residue in the metalloprotease prodomain. Cysteine alkylation disrupts its interaction with Zn^{2+} in the catalytic site, allowing the prodomain to dissociate from the catalytic site to allow substrate access (van Wart and Birkedal-Hansent, 1990). Another unexplored possibility is that NEM may also indirectly activate metalloproteases by alkylating critical cysteine residues on their regulatory proteins, such as TspanC8 tetraspanins in the case of ADAM10. Inhibiting calmodulin can also activate GPVI shedding, which is accompanied by the dissociation of calmodulin from the cytoplasmic tail of GPVI (Gardiner *et al.*, 2004); it was proposed that this may increase the exposure of its cleavage site to ADAM10 (Gardiner, 2018).

A recent study has shown that in contrast to platelets in suspension, GPVI shedding is minimal on platelets adhered on immobilised collagen *in vitro.* Imaging shows that clustering of GPVI along collagen fibres may prevent access of ADAM10 to GPVI, thereby limiting its shedding (Pallini *et al.*, 2021). Another study has examined GPVI shedding in thrombus formed on collagen *in vitro* and has demonstrated that GPVI shedding occurs in loosely attached platelets in the outer region of a thrombus but not in aggregated platelets in the core of a thrombus

(Baaten *et al.*, 2018). These findings may represent homeostatic mechanisms whereby selective GPVI shedding on specific subpopulations acts to limit thrombus propagation, whereas prevention of GPVI shedding through its clustering acts to sustain platelet activation to maintain haemostasis. Therefore, could activating ADAM10 shedding of GPVI in platelets be useful to prevent thrombus growth?

1.5.6 Inducing GPVI cleavage by Tspan15/ADAM10 or Tspan33/ADAM10 scissors as a novel anti-platelet strategy?

A recent study in the lab provided evidence that of the three platelet TspanC8/ADAM10 scissors, Tspan15/ADAM10 and Tspan33/ADAM10 scissors can cleave human GPVI but Tspan14/ADAM10 scissor cannot. Because genetically modifying the anucleate human platelets is not a feasible option, the scissors were identified using a knockout approach in two different model cell lines: human embryonic kidney cells expressing the simian virus 40 large T-antigen (HEK-293T) transfected with human GPVI and phorbol ester-differentiated megakaryocyte-like human erythroleukemia (HEL) cells, which express endogenous GPVI. In both cell lines, shedding of human GPVI was unaffected in Tspan14-knockout cells but was completely abolished in Tspan15/33 double knockout cells, similar to what was observed in control ADAM10-knockout cells. Importantly, although ADAM10 surface expression was partially reduced to varying degrees in all cell lines, substantial levels of ADAM10 remained on the cell surface in Tspan15/33 double knockout cells, suggesting that the striking absence of shedding was contributed directly by the loss of Tspan15 and Tspan33 (Matthews, 2019).

These findings present an opportunity for a novel anti-GPVI strategy by specifically targeting Tspan15 or Tspan33 to modulate ADAM10 activity, rather than directly targeting ADAM10, which would affect shedding of all the other ~100 ADAM10 substrates. Specific activation of

Tspan15/ADAM10 or Tspan33/ADAM10 scissors would downregulate GPVI on the platelet surface and additionally release a Revacept-like soluble GPVI that can bind ligands to prevent further platelet activation (Figure 16). To determine whether such a strategy is feasible, it is therefore important to first understand the molecular mechanisms of how ADAM10-mediated shedding of GPVI is regulated by TspanC8s. In other words, why can Tspan15/ADAM10 and Tspan33/ADAM10 scissors cut GPVI, whereas Tspan14/ADAM10 scissors cannot?

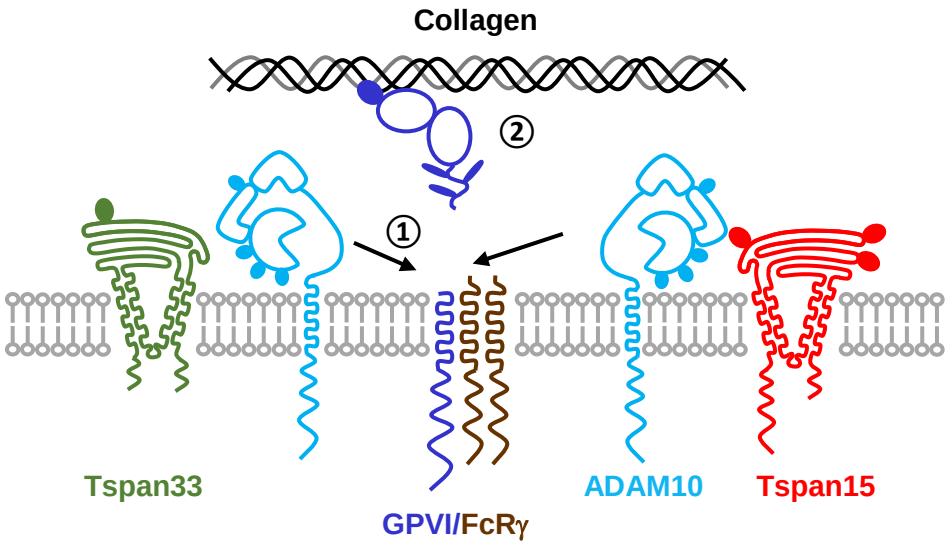

Figure 16. Potential anti-platelet strategy by targeting specific TspanC8/ADAM10 scissors. Specific targeting of Tspan15/ADAM10 or Tspan33/ADAM10 complexes may (1) downregulate platelet GPVI surface expression and (2) release soluble GPVI that can bind its ligands, e.g., collagen, to prevent further platelet activation.

1.6 Project aims and objectives

The overarching aim of this thesis is to characterise GPVI shedding by TspanC8/ADAM10 scissors to provide further evidence to the 'six scissors' hypothesis, i.e., how six TspanC8s differentially regulate ADAM10 substrate specificity. Understanding the molecular basis of this regulation is essential to guide future directions in designing therapeutics targeting TspanC8s to modulate ADAM10 activity, for example, to induce GPVI shedding as a novel anti-platelet strategy.

The objectives of this thesis are as follows:

- To investigate the mechanisms by which TspanC8s regulate GPVI cleavage by ADAM10 (Chapter 3).
- To analyse *TSPAN15* and *GP6* variants associated with thrombosis (Chapter 4).
- To investigate how Tspan15 and ADAM10 regulate each other (Chapter 5).
- To investigate potential Tspan15 redundancy with other TspanC8s (Chapter 6).

CHAPTER 2
MATERIALS AND METHODS

2.1 Antibodies

Antibodies for immunofluorescence microscopy (Section 2.12), immunoprecipitation (Section 2.6.1.3), flow cytometry (Section 2.6.3) and Western blotting (Section 2.6.2) are summarised in Table 3.

Table 3. Summary of antibodies. Antibodies are purified unless otherwise stated. IF: immunofluorescence microscopy; IP: immunoprecipitation; FC: Flow cytometry; WB: Western blot; mAb: monoclonal antibody; pAb: polyclonal antibody

	Source	Identifier	Working concentration/dilution
Primary antibodies			
Rabbit anti-FLAG pAb	Merck (Gillingham, UK)	F7425	IF: 1:800 WB: 1:5,000
Rabbit anti-GFP pAb	Merck	G1544	WB: 1:4,000
Mouse anti-HA mAb (6E2)	Cell Signaling Technology (CST; London, UK)	2367S	WB: 1:5,000
Mouse anti-myc mAb (9B11)	CST	2276S	IF: 1:8,000 WB: 1:5,000
Mouse anti-human ADAM10 mAb (11G2); ascites fluid	Dr. Eric Rubinstein (Paris, France)	(Arduise *et al.*, 2008)	FC: 10 µg/mL WB: 0.5 µg/mL
Mouse anti-human ADAM10 mAb (11G2)*	Abcam (Cambridge, UK)	ab59482*	IF: 1 µg/mL
Mouse anti-human ADAM17 mAb	R&D Systems (Abingdon, UK)	MAB9301	FC: 10 µg/mL
Mouse anti-human GPVI mAb (336A9)	Prof. Dr. Bernhard Nieswandt (Würzburg, Germany)	Unpublished	IF: 2.5 µg/mL FC: 10 µg/mL
Mouse IgG1κ mAb (MOPC-21)	MP Biomedicals (Santa Ana, US)	0850327	FC: 10 µg/mL
Mouse anti-N-cadherin mAb (cytoplasmic)	BD Biosciences (Wokingham, UK)	610921	IF: 2.5 µg/mL
Rabbit anti-N-cadherin mAb (extracellular)	Abcam (Cambridge, UK)	ab245117	WB: 1:1,000
Mouse anti-human Tspan15 mAb (1C12); hybridoma supernatant	In-house by Abpro (Woburn, US)	(Koo *et al.*, 2020)	FC: undiluted WB: 1:5
Mouse anti-human Tspan15 mAb (5D4)	Purified by Dr. Margaret Goodall (Birmingham, UK)	(Koo *et al.*, 2020)	IF: 5 µg/mL IP: 4 µg per reaction
Rabbit anti-human Tspan15 C-terminus pAb	Novus Biologicals (Abingdon, UK)	NBP1-92540	WB: 1:1,000
Secondary antibodies			
Sheep anti-mouse IgG-fluorescein isothiocyanate (FITC)	Merck	F2883	FC: 1:100
Goat anti-mouse IgG-allophycocyanin (APC)	Thermo Fisher Scientific (Loughborough, UK)	A10539	FC: 1:500

Donkey anti-mouse IgG-IRDye® 800CW	LI-COR Biosciences (Cambridge, UK)	926-32212	WB: 1:10,000
Goat anti-mouse IgG-IRDye® 680RD	LI-COR Biosciences	926-68070	WB: 1:10,000
Goat anti-rabbit IgG-IRDye® 800CW	LI-COR Biosciences	926-32211	WB: 1:10,000
Donkey anti-rabbit IgG-IRDye® 680RD	LI-COR Biosciences	926-68073	WB: 1:10,000
Goat anti-mouse IgG-Alexa Fluor® 488	Thermo Fisher Scientific	A-11001	IF: 1:300
Goat anti-mouse IgG-Alexa Fluor® 647	Thermo Fisher Scientific	A-21235	IF: 1:300
Goat anti-rabbit IgG-Alexa Fluor® 488	Thermo Fisher Scientific	A-11008	IF: 1:300
Fluorophore-conjugated primary antibodies			
Alexa Fluor® 647-conjugated mouse anti-human Tspan15 mAb (5D4)	Section 2.12.1	(Koo *et al.*, 2020)	IF: 5 µg/mL
Alexa Fluor® 647-conjugated mouse anti-human ADAM10 mAb (11G2)	Section 2.12.1	(Koo *et al.*, 2020)	IF: 1 µg/mL
FITC-conjugated rat anti-mouse ADAM10 mAb	R&D Systems	FAB946F	FC: 1:10
FITC-conjugated rat IgG2a mAb	R&D Systems	IC006F	FC: 1:10
FITC-conjugated mouse anti-human ADAM10 mAb	R&D Systems	IC1427F	FC: 1:10
FITC-conjugated mouse IgG2b mAb	R&D Systems	IC0041F	FC: 1:10

*Supplied in an ion-exchange purified format in phosphate-buffered saline (PBS) at the time of purchase in 2018 but is now supplied as tissue culture supernatant (2021).

2.2 Expression constructs

The pEF6 vector encoding human FcRɣ was as described (Tomlinson *et al.*, 2007). C-terminal GFP-tagged human RAGE in the pcDNA6.2 vector was a gift from Prof. Alexander Shekhtman (New York, US). N-terminal alkaline phosphatase-conjugated human betacellulin in the pAIPh vector was a gift from Prof. Shigeki Higashiyama (Matsuyama, Japan) and Prof. Carl Blobel (New York, US) (Sahin *et al.*, 2004). Nuclear factor of activated T-cells (NFAT)-luciferase reporter construct in the pΔODLO vector was described previously (Shapiro *et al.*, 1996; Tomlinson *et al.*, 2007). The pEF6 and pcDNA vectors used to generate new constructs were from Invitrogen (Thermo Fisher Scientific).

2.2.1 GPVI

C-terminal myc-tagged human GPVI expression constructs in pcDNA3.1 vectors were as described (Berlanga *et al.*, 2007). Wild-type GPVI refers to the more common isoform, GPVIa. The C-terminal myc-tagged GPVI stalk-extended mutants were generated with the Q5® site-directed mutagenesis kit (New England Biolabs, Hitchin, UK) using wild-type GPVI expression construct as the template. GPVI+5 and GPVI+10 had one and two sets of glycine-serine linkers (GGGGS) inserted at the predicted extracellular-transmembrane interface, respectively (Table 4).

2.2.2 TspanC8s

N-terminal FLAG-tagged pEF6 (pEF6 FLAG) vectors encoding TspanC8s were described previously (Noy *et al.*, 2016; Koo *et al.*, 2020). Table 4 summarises the list of N-terminal FLAG-tagged human Tspan14 and Tspan15 mutant constructs used in this project. Tspan14/15 extracellular region chimeras, Tspan14(15EC) and Tspan15(14EC) and the tails-truncated Tspan15 mutant, Tspan15(ΔNC) were as described (Szyroka, 2019). The Tspan14/15 cytoplasmic domain chimeras, Tspan14(15Cyto) and Tspan15(14Cyto) were generated by subcloning of synthesised fragments contained within pTWIST cloning vectors (Twist Bioscience, San Francisco, US) into the pEF6 FLAG expression vector by restriction digest. The Tspan14/15 C-terminal tail chimeras, Tspan14(15C) and Tspan15(14C) were generated by multi-step PCR using wild-type human Tspan14 and Tspan15 as templates (provided by Dr. Neale Harrison, Birmingham, UK).

2.2.3 ADAM10

C-terminal HA-tagged wild-type mouse ADAM10 (Maretzky, Schulte, et al. 2005) and ADAM10 lacking the cytoplasmic tail (ADAM10ΔC) (Maretzky *et al.*, 2015) in the pcDNA3.1

vectors had been described previously. C-terminal myc-tagged human ADAM10 in the pRK5M vector was a gift from Rik Derynck (Addgene plasmid #31717) (Liu *et al.*, 2009). The truncated human ADAM10 containing the disintegrin, cysteine-rich and stalk region (ADAM10DCS) in the pDisplay vector was as described (Noy *et al.*, 2016).

Table 4. Amino acid sequences of mutants. Insertions are depicted in red; substitutions are in blue; deleted residues are crossed out. EC: extracellular region; TM: transmembrane region; Cyto: cytoplasmic region; N: N-terminus; C: C-terminus.

Construct	Modified region(s)	Sequence(s)		
pcDNA3.1 GPVI-myc				
GPVI+5	EC-TM interface	N-	…QYYTKGGGGSGNLVR…	-C
GPVI+10	EC-TM interface	N-	…QYYTKGGGGSGGGGSGNLVR…	-C
pEF6 FLAG-Tspan				
14(15EC)	EC	TM1- TM3-	…LGVGLYAEVERQKYKTLESAFLAPVVLVL… …AVLAFTFRNQTIDF…IIWFMDNIYIVA…	-TM2 -TM4
15(14EC)	EC	TM1- TM3-	…SVGIYWAWSEKGVLSDLTKVTRMHGIDPAIILI… …GVVALLFQDWVG…ESWLPRNGILLG…	-TM2 -TM4
14(15Cyto)	Cyto	N- TM2- TM4-	…PRGDSEQVRYCARFSYLWLKFSLLFSY… …AGCVGSLRDNLYLLQFFCGT… …FGIFLTRVEDIIMEHSVTDGLL…AAGTGCCLCYPN	-TM1 -TM3 -C
15(14Cyto)	Cyto	N- TM2- TM4-	…HYYRYSNAKVSCWYKYLIIYS… …IGVLAALRENICLLNAFMYI… …TLLYIARTLISDIEAVKAGHHF	-TM1 -TM3 -C
15(ΔNC)	N and C	N- TM4-	…~~PRGDSEQVRYCARFSYL~~WLKFS… …TRVEDIIMEHSVTD~~GLLGPGAKPSVEAAGTGCCLCYPN~~	-TM1 -C
14(15C)	C	TM4-	… FGIFLTRVEDIIMEHSVTDGLL…AAGTGCCLCYPN	-C
15(14C)	C	TM4-	…TLLYIARTLISDIEAVKAGHHF	-C

2.2.4 Tspan15/ADAM10 bimolecular fluorescence complementation (BiFC)

A pair of Tspan15 and ADAM10 split superfolder GFP (sfGFP) constructs for bimolecular fluorescence complementation (BiFC) was generated by PCR cloning. The split sfGFP and CFP expression vectors were gifted by Dr. Nicholas Holliday (Nottingham, UK) (Kilpatrick, Briddon and Holliday, 2012). Tspan15 was linked to the N-terminal half of sfGFP at the C-terminus by amplifying the region encoding human Tspan15 on pEF6 FLAG Tspan15 and then subcloning into the pcDNA3.1/zeo split sfGFP vector. The C-terminal half of sfGFP was linked to the C-terminus of ADAM10 by PCR-mediated splicing of ADAM10-GFP fragments

generated by two separate PCR rounds from a pcDNA3.1/zeo split CFP vector and pcDNA3.1 mouse ADAM10 (Maretzky, Schulte, et al. 2005). The spliced ADAM10-GFP fragment was subcloned into pcDNA3.1 ADAM10.

2.3 Cell culture

Reagents were sourced from Merck unless otherwise stated. Complete media refers to growth media supplemented with 10% foetal bovine serum (FBS) (Thermo Fisher Scientific), 4 mM L-glutamine, 100 U/mL penicillin and 100 µg/mL streptomycin. Human embryonic kidney cells expressing the simian virus 40 large T-antigen (HEK-293T) and the human lung epithelial cell line A549 were cultured in complete high-glucose Dulbecco's modified Eagle's media (DMEM). Human erythroleukemia (HEL) cells and Jurkat T cells were cultured in complete Roswell Park Memorial Institute (RPMI) 1640 media. The chicken B cell line DT40 was cultured in complete RPMI 1640 media supplemented with 50 µM β-mercaptoethanol (Thermo Fisher Scientific). All cells were maintained at 37 ºC, 5% CO_2 in a humidified incubator.

2.4 Transfection

2.4.1 HEK-293T

HEK-293T cells were transfected with the cationic polymer polyethylenimine (PEI) (Merck) (Ehrhardt *et al.*, 2006). Cells were plated the day before transfection, such that they would be at 70-80% confluency on the day of transfection. Plasmid DNA and PEI were added at a 1:4 ratio by mass to the reduced serum media Opti-MEM® (Thermo Fisher Scientific), constituting 0.005% w/v of the mixture. The mixture was incubated for 10 minutes at room temperature to allow PEI/DNA complexes to form before adding to the cells.

2.4.2 DT40

DT40 cells were transfected by electroporation as described (Tomlinson *et al.*, 2007). Cells were passaged the day before to obtain a yield of 1.5×10^7 cells per transfection on the day of transfection. To remove cell culture supplements that may negatively impact electroporation, cells were washed in unsupplemented RPMI 1640 media, and resuspended in 400 µL of the same media before adding 20.5 µg of plasmid DNA. After 10 minutes of incubation at room temperature, the cells were electroporated at 350 V and 500 µF using a Gene Pulser electroporator (Bio-Rad, Watford, UK). The electroporated cells were allowed to rest for another 10 minutes before being added to 8 mL of complete RPMI 1640 media in one well of a 6-well plate.

2.5 Nucleic acid techniques

Reagents and kits were from Thermo Fisher Scientific unless otherwise stated. DNA and RNA concentrations were determined spectrophotometrically on a NanoPhotometer® UV/Vis spectrophotometer (Implen, München, Germany).

2.5.1 Genomic DNA extraction

Cells were incubated at 55 ºC overnight in a lysis buffer (5 mM ethylenediaminetetraacetic acid (EDTA), 0.2% w/v sodium dodecyl sulfate (SDS), 200 mM NaCl, 100 mM Tris, pH 8.5) containing 100 µg/mL Proteinase K (Merck) to lyse cells and remove proteins. Lysate was cleared by centrifuging at maximum speed for 3 minutes. An equal volume of isopropanol was mixed with the supernatant, and then centrifuged at 21,000 × g for 20 minutes at 4 ºC to precipitate genomic DNA. The resulting DNA pellet was resuspended in 10 mM Tris, pH 8.5.

2.5.2 RNA extraction and reverse transcription (RT)

RNeasy® Mini Kit (Qiagen, Hilden, Germany) was used to lyse cells and extract RNA using silica-based spin-columns, following manufacturer's instructions. Lysates were homogenised using QIAshredder columns (Qiagen) before RNA extraction to improve RNA binding to spin columns. RNA was eluted in sterile RNase-free water and converted to cDNA using the Applied Biosystems™ High-Capacity cDNA Reverse Transcription Kit.

2.5.3 End-point polymerase chain reaction (PCR)

PCR products used in downstream sequencing or cloning were generated using Phusion® High-Fidelity DNA Polymerase (New England Biolabs (NEB, Hitchin, UK)) using the manufacturer-recommended reaction setup and cycling conditions. REDTaq® DNA Polymerase (Merck) was used for other routine PCRs. All reactions were incubated in a SensoQuest Thermal Labcycler (Göttingen, Germany). PCR amplicons were visualised by gel electrophoresis on 1-2% w/v agarose gels containing 1:10,000 dilution of SYBR® Safe DNA Gel Stain and imaged using a U:Genius3 gel documentation system (Syngene, Cambridge, UK).

2.5.4 Quantitative polymerase chain reaction (qPCR)

Transcript levels of *TSPAN15* (Hs00202548_m1) and the internal control *GAPDH* (Hs02758991_g1) were determined from cDNA using TaqMan Gene Expression assays on an Agilent AriaMX real-time PCR system (Agilent Technologies, Santa Clara, US) with carboxyfluorescein (FAM™) detection. Manufacturer-recommended reaction setup and cycling conditions were used. Fluorescence was measured for 44 cycles. The threshold fluorescence was determined automatically on the AriaMx software (Agilent). The average cycle threshold (C_T) from technical duplicates was normalised to the *GAPDH* control (ΔC_T)

and to the experimental control ($\Delta\Delta C_T$). Expression fold change was presented as $2^{-\Delta\Delta C_T}$ (Livak and Schmittgen, 2001).

2.5.5 Subcloning

Synthesised DNA fragments contained within cloning vectors or PCR fragments were subcloned into plasmid vectors by restriction digest and ligation. Fragments for insertion were designed to include restriction sites for two different enzymes flanking either side, which were compatible with unique restriction sites on the vector's multiple cloning site. Both the insert and the vector were digested with the same pair of restriction enzymes following the recommended conditions for each enzyme pair (NEB). The digested fragments were subjected to gel electrophoresis on a 1% w/v agarose gel to separate fragments by size. The desired insert and vector were retrieved by gel purification using the QIAquick® Gel Extraction Kit (Qiagen). The insert was ligated into the vector at an insert:vector molar ratio of 3:1 using T4 DNA ligase and incubated overnight at 16 ºC (NEB). The ligated plasmid was transformed into *E. coli* to propagate for downstream screening and verification by sequencing.

2.5.6 Plasmid propagation

Plasmids were transformed into DH5α competent *E. coli* cells by heat shock following manufacturer's instructions. Transformed bacteria were spread on Luria broth (LB) agar plates containing the antibiotic matching the antibiotic resistance marker on the vector. Plates were incubated overnight in an enclosed 37 ºC incubator. Single colonies were picked for further culturing in LB containing the appropriate antibiotic. Plasmids were isolated from the bacteria by alkaline lysis, using the QIAprep® Miniprep Kit (Qiagen) or the GenElute™ HP Plasmid Midiprep Kit (Merck), depending on the required yield.

2.5.7 Sequencing and sequence analysis

PCR products were purified using the QIAquick® PCR Purification Kit (Qiagen). Purified PCR products and plasmids were sequenced by Sanger sequencing (Source BioScience, Nottingham, UK). Sequences were aligned to the template by Multiple Alignment using Fast Fourier Transform (MAFFT) (Katoh and Standley, 2013). To resolve mixed traces in heterozygous CRISPR/Cas9 knockout clones, sequences on individual alleles were determined using the web-based tools, Tracy (Indigo) (Rausch *et al.*, 2020) and CRISP-ID (Dehairs *et al.*, 2016).

2.6 Protein analysis techniques

Reagents were supplied by Thermo Fisher Scientific unless otherwise stated.

2.6.1 Protein extraction

2.6.1.1 Cell culture supernatant

Soluble proteins from cell culture supernatant were concentrated by trichloroacetic acid (TCA) precipitation and extracted as described with some modifications (Mentrup *et al.*, 2019). Supernatant was mixed with TCA at a final concentration of 20% w/v TCA and rotated overnight at 4 ºC. On the next day, the sample was centrifuged at 21,000 × g at 4 ºC for 10 minutes to pellet precipitated proteins. The pellet was washed with ice-cold acetone to remove residual TCA, and then resuspended in 2× sample buffer (non-reducing: 4% w/v SDS, 20% glycerol, 0.1 M Tris, 0.01% w/v bromophenol blue, pH 6.8; reducing: supplemented with 5% β-mercaptoethanol) and dissolved by gentle vortexing to achieve a final concentration of ~1× sample buffer in the resulting solution.

2.6.1.2 Whole cell

Cells were pelleted by centrifugation at 2,655 × g for 3 minutes and lysed in the desired ice-cold lysis buffer containing 1:100 dilution of a 100× protease inhibitor cocktail (Merck) for 30

minutes on ice. For the analysis of ADAM10, the lysis buffer was also supplemented with 5 μM of the ADAM10 inhibitor GI254023X (Merck) to prevent post-lysis degradation (Brummer *et al.*, 2018). Insoluble debris were pelleted by centrifuging at 21,000 × g at 4 ºC for 10 minutes. The resultant lysate was resuspended in an equal volume of 2× sample buffer.

2.6.1.3 Immunoprecipitation

For each reaction, 20 μL of Protein G Sepharose beads (50% slurry in PBS) (Generon, Slough, UK) was used. Antibodies were bound to Protein G Sepharose beads by incubating overnight at 4 ºC with rotation in 1% Triton X-100 lysis buffer (1% Triton X-100, 10 mM Tris, 150 mM NaCl, 1 mM EDTA, 0.02% NaN_3, pH 7.5) (Table 3). On the following day, the antibody-coated beads were washed by centrifugation at 2,655 × g for 20 seconds in the lysis buffer that the proteins were extracted in. Lysates were incubated at 4 ºC with rotation for 2 hours. Following four washes by centrifugation, the beads containing captured proteins were resuspended in 50 μL of 2× sample buffer.

2.6.2 Western blotting

To blot using tetraspanin or ADAM10 mAbs that bind to the extracellular region, protein samples were resuspended in non-reducing sample buffer to retain conformational epitopes for mAb recognition. Reducing samples were used when blotting with other mAbs that recognise linear epitopes. All samples were denatured at 95 ºC for 5 minutes before gel loading. For separation of proteins by SDS-polyacrylamide gel electrophoresis (PAGE), standard Tris-glycine gel and buffer system was used, except for GPVI, where a Bis-Tris gradient gel and 2-(N-morpholino)ethanesulfonic acid (MES) buffer system was used to resolve the ~60 kDa full-length and ~10 kDa C-terminal fragment simultaneously. Proteins were transferred from the gel onto low-fluorescence Immobilon-FL polyvinylidene difluoride (PVDF)

membranes (Merck) by wet transfer with the XCell II™ blot module system. Membranes were blocked in 5% w/v milk dissolved in Tris-buffered saline (TBS) (20 mM Tris, 137 mM NaCl, pH 7.6) for one hour at room temperature. Membranes were incubated with primary antibodies overnight at 4 ºC, before washing three times with high-salt TBST (TBST with a higher salt content at 500 mM NaCl) for 10 minutes to remove non-specific binding, followed by incubation with IRDye®-conjugated fluorescent secondary antibodies at room temperature for 1-2 hours. Primary and secondary antibodies were both diluted in 3% w/v bovine serum albumin (BSA) (First Link, Birmingham, UK) in TBST (TBS containing 0.1% Tween® 20) (Table 3). After three washes with high-salt TBST, membranes were washed with TBS to remove excess Tween® 20. The membranes were scanned using an Odyssey® infrared imaging system (LI-COR Biosciences). Band intensities were quantitated after background subtraction.

2.6.3 Flow cytometry

For staining of cell surface proteins, 2.5-5×10^5 cells were harvested and pelleted by centrifugation. Antibodies were diluted in 50 μL of PBS containing 0.2% BSA and 0.02% NaN_3; the same buffer was used for washes (Table 3). Cells were stained with primary antibody for 30 minutes on ice and then washed with 1 mL of buffer. After 30 minutes of incubation with secondary antibody on ice, cells were resuspended in the wash buffer before analysis. For two-colour staining, cells were washed with 1 mL of buffer, followed by a third 30-minute incubation step with a fluorophore-conjugated primary antibody and another wash step. For samples that could not be analysed within three hours of staining, cells were washed with 1 mL of buffer after secondary antibody incubation and then resuspended in PBS containing 1% formaldehyde (Merck), 2% FBS and 0.02% NaN_3 to preserve samples for storage at 4 ºC. Samples were processed on a FACSCalibur flow cytometer (BD Biosciences). Data were analysed on the CellQuest Pro software (BD Biosciences) or the Flowing Software (Turku

Bioscience Centre). Surface expression level was presented as geometric mean fluorescence intensity of the target antibody staining relative to the isotype control staining.

2.7 Generation of CRISPR/Cas9-knockout cell lines

HEK-293T cells deficient in ADAM17 and both ADAM10 and ADAM17 were generated using CRISPR/Cas9 genome editing technology (Ran *et al.*, 2013) from wild-type and previously validated ADAM10-knockout cells (Koo *et al.*, 2020), respectively. Tspan14/15 double knockout cells were generated from previously validated Tspan14-knockout cells (Matthews, 2019). These Tspan14/15 double knockout cells were subsequently used to generate cells deficient in Tspan14, Tspan15 and Tspan33. The guide oligos for Tspan15 (guide 1) and Tspan33 (guide 3) had been described previously (Matthews, 2019; Koo *et al.*, 2020). Guide oligos for ADAM17 are listed in Table 5. The oligos were annealed and cloned into the pSpCas9(BB)-2A-Puro (PX459) vector (Addgene plasmid #62988, a gift from Feng Zhang) (Ran *et al.*, 2013). Cells were transfected with the plasmid for 36 hours as described in Section 2.4.1 and treated with 2.5 µg/mL puromycin for three days to select for transfected cells. Monoclonal populations were isolated by limiting dilution at a starting concentration of one cell per well on a 96-well plate. ADAM17- and Tspan15-knockout clones were screened by flow cytometry. Tspan33-knockout clones were screened by Sanger sequencing of the targeted genomic region. To verify that any loss-of-function phenotype seen could be attributed to the knockout of a target of interest, experiments were repeated in an additional knockout clone generated from a second CRISPR/Cas9 guide targeting a different region on the same gene, where appropriate, as detailed in the respective figure legends.

Table 5. List of CRISPR/Cas9 oligos. F: forward; R: reverse. The genomic target sequence is in red.

Gene	Exon	Guide oligo (5' to 3')	Sanger Institute CRISPR ID
ADAM17 (Guide 1)	1	F: CACCGCCGAAGCCCGGGTCATCCGG R: AAACCCGGATGACCCGGGCTTCGGC	926027156
ADAM17 (Guide 2)	1	F: CACCGCGAAAGGAACCACGCTGGTC R: AAACGACCAGCGTGGTTCCTTTCGC	926027164

2.8 Substrate shedding or cleavage assays

HEK-293T cells were used in all assays and transfected for 24 hours to express GPVI/FcRγ, RAGE or betacellulin as described in Section 2.4.1. In some experiments, cells were also co-transfected with an equal amount of ADAM10 and/or TspanC8 expression constructs.

2.8.1 GPVI and RAGE

Cells on 6-well plates were transfected with expression constructs for either C-terminal myc-tagged GPVI (0.5 μg) and untagged FcRɣ (0.5 μg), or C-terminal GFP-tagged RAGE (1 μg). In the case of RAGE, cells were treated with 10 μM of the γ-secretase inhibitor, N-[N-(3,5-Difluorophenacetyl-L-alanyl)]-(S)-phenylglycine t-butyl ester (DAPT) (Cambridge Bioscience, Cambridge, UK) three hours post-transfection to prevent loss of the C-terminal fragment from γ-secretase cleavage (Zhang *et al.*, 2008). In some experiments, cells were treated with 2 mM N-ethylmaleimide (NEM) (Thermo Fisher Scientific) for 30 minutes before harvesting to activate metalloproteases. Cells were harvested by scraping in PBS and lysed in 1% Triton X-100 lysis buffer as described in Section 2.6.1.2. Lysates were subjected to anti-myc or anti-GFP Western blotting as described in Section 2.6.2 (Table 3). Band intensities of the full-length protein and the C-terminal fragment were quantitated. The percentage of substrate cleaved was calculated by expressing the amount of C-terminal fragment generated as a percentage of the total.

2.8.2 N-cadherin

Cells on 6-well plates were washed with PBS and media replaced with the reduced serum media Opti-MEM®. After 30 minutes of incubation, cells were treated with 2 mM NEM for one hour before harvesting. The supernatant was centrifuged at 2,655 × g for 3 minutes to remove any cell contamination. Protein was concentrated and extracted from the supernatant as described in Section 2.6.1.1. Cells were harvested by scraping in PBS and lysed in 1% Triton X-100 lysis buffer as described in Section 2.6.1.2. Supernatant and lysate samples were subjected to Western blotting as described in Section 2.6.2 with an antibody against the extracellular region of N-cadherin (Table 3). Band intensities of shed N-cadherin in the supernatant and full-length N-cadherin in the lysate were quantitated to calculate the amount of N-cadherin shed in the supernatant as a percentage of total.

2.8.3 Betacellulin

Cells were transfected with 0.2 μg of an N-terminal alkaline phosphatase-tagged betacellulin expression construct in 24-well plates. On the following day, cells were washed with PBS and incubated with the reduced serum media Opti-MEM® for 30 minutes. After 2.5 hours of stimulation with 2 mM NEM, the supernatant was harvested and centrifuged at maximum speed for 5 minutes to remove cells and debris. Cells were lysed while they are still attached on the plate with ice-cold 1% Triton X-100 lysis buffer containing a cocktail of protease inhibitors for 30 minutes on ice. Lysed cells were centrifuged at maximum speed for 10 minutes at 4 ºC to remove insoluble debris. Both the supernatant and lysate samples were diluted 10-fold with the assay buffer (100 mM Tris, 100 mM NaCl, 20 mM $MgCl_2$, pH 9.5). To measure alkaline phosphatase activity, the diluted samples were incubated at 37 ºC with the alkaline phosphatase substrate, p-nitrophenyl phosphate (pNPP) (Merck) at a final concentration of 1 mg/mL for 15 minutes to 1 hour, while monitoring the absorbance at 405 nm on an Anthos Zenyth 340rt

microplate reader (Biochrom, Cambridge, UK) to ensure the readings were within the linear detection range. The percentage of betacellulin shed was calculated from the absorbance of the supernatant sample as a percentage of total.

2.9 NFAT-luciferase assay

The assay was as described (Tomlinson *et al.*, 2007). DT40 cells were transfected with 20 µg of NFAT-luciferase reporter construct, 0.25 µg of GPVI construct and 0.25 µg of FcRɣ construct for 16 hours as described in Section 2.4.2. Cells were stimulated for 6 hours with 5 µg/mL collagen (Takeda, London, UK) or 50 ng/mL phorbol myristate acetate (PMA) (Merck) and 1 µM ionomycin (Merck) for maximum stimulation. Cells were lysed in 1% Triton X-100, 0.1 mM dithiothreitol (DTT) (Merck), 20 mM KH_2PO_4, pH 7.8 for 5 minutes at room temperature. Following lysis, the lysate was mixed with an equal volume of assay buffer (10 mM adenosine triphosphate (ATP) (Merck), 20 mM $MgCl_2$, 0.2 M KH_2PO_4, pH 7.8). Luciferase activity was measured using a Mithras LB 940 luminometer (Berthold Technologies, Harpenden, UK) following injection with 1 mM D-luciferin (Cambridge Bioscience). Data were quantitated as a percentage of the maximum luciferase activity from the PMA- and ionomycin-treated control for each transfection condition.

2.10 Lysosomal inhibition

A549 cells were treated with 50 mM NH_4Cl (Thermo Fisher Scientific) for 20 hours to inhibit lysosomal degradation (Jurkovitz *et al.*, 1992). Cells were lysed in 1% Triton X-100 lysis buffer, and Tspan15 was immunoprecipitated from the lysates using Tspan15 mAb 5D4 as described in Section 2.6.1.3.

2.11 Deglycosylation

Tspan15 immunoprecipitates from Section 2.10 were digested with the N-glycosidase PNGase F (NEB) under reducing condition following manufacturer's protocol. The digested samples were resuspended in 2×sample buffer for Western blotting.

2.12 Fluorescence microscopy

Materials were from Merck unless otherwise stated.

2.12.1 Antibody labelling

Purified antibodies in PBS were concentrated to 1 mg/mL using 0.5 mL Amicon Ultra Centrifugal Filters. Antibodies were conjugated to Alexa Fluor® 647 fluorophore by reacting with succinimidyl esters linked to the dye (Thermo Fisher Scientific). For optimal labelling, 100 µL of antibodies at 1 mg/mL were mixed with 1 M $NaHCO_3$, pH 8.3, before adding 10 µg of the dye to yield an antibody-to-dye ratio of 10:1 by mass. After one hour of incubation with rotation in the dark, excess dye was removed using Zeba Spin Desalting Columns (Thermo Fisher Scientific). The final concentration and degree of labelling of the conjugate was measured using a NanoPhotometer® UV/Vis spectrophotometer.

2.12.2 Immunostaining

Cells were cultured on 35 mm glass bottom dishes with glass diameter of 20 mm and thickness of #1.5 (MatTek Corporation, Ashland, US). All incubation steps were at room temperature. Cells were washed with PBS and fixed with 10% formalin for 15 minutes. To reduce autofluorescence from fixation, cells were washed three times with PBS and incubated with 50 mM NH_4Cl for 15 minutes, followed by another three PBS washes. Non-specific sites were blocked by incubating cells with block buffer (1% w/v high-purity BSA and 2% goat serum in PBS) for at least 20 minutes. Antibodies were diluted in block buffer (Table 3). After 1 hour of

incubation with primary antibodies, cells were washed three times with PBS and incubated with secondary antibodies in the dark for another hour. Cells were washed four times with PBS and stored in PBS in the dark at 4 ºC. In some experiments, a final step of one-hour incubation with a fluorophore-conjugated antibody raised in the same species as the primary antibody, was done after secondary antibody incubation to prevent false labelling. For experiments requiring cell permeabilisation, the block buffer was supplemented with 0.1% w/v saponin, which was used in all incubation steps.

2.12.3 Confocal microscopy

HEK-293T cells were transfected with expression constructs for Tspan15 and ADAM10 sfGFP BiFC halves for 24 hours as described in Section 2.4.1. Cells were fixed, permeabilised and stained for Tspan15 with Alexa Fluor® 647-conjugated Tspan15 mAb (Table 3). Dual-colour confocal images were acquired with 488 nm and 633 nm laser lines by sequential scanning on a Leica SP2 confocal microscope (Leica Biosystems, Wetzlar, Germany) equipped with a 63× 1.4 NA oil objective.

2.12.4 Airyscan confocal microscopy

HEL cells were differentiated into megakaryocyte-like cells by treating with 6.2 ng/mL PMA for 72 hours. Differentiation was monitored based on cell morphology, i.e., a shift from a small, rounded and semi-adherent state in an undifferentiated cell towards a larger and adherent phenotype in a differentiated cell. PMA-differentiated HEL cells were fixed, permeabilised and stained for GPVI and ADAM10 in a three-step incubation protocol using GPVI mouse mAb and Alexa Fluor® 488-conjugated secondary antibody, followed by Alexa Fluor®647-conjugated ADAM10 mouse mAb (Table 3). HEK-293T cells were transfected with expression constructs (detailed in figure legends) for 24 hours as described in Section 2.4.1. Fixed and

permeabilised cells were stained with rabbit and mouse primary antibodies simultaneously, and secondarily labelled with Alexa Fluor® 488-conjugated goat anti-rabbit and Alexa Fluor® 647-conjugated goat anti-mouse antibodies (Table 3). Dual-colour confocal images were captured sequentially with 488 nm and 640 nm laser lines using a 63× 1.4 NA oil objective in super-resolution mode on a Zeiss LSM 900 microscope with Airyscan 2 detector (Carl Zeiss, Oberkochen, Germany). The images were post-processed on ZEN software (Carl Zeiss) to obtain Airyscan images with improved lateral resolution at ~120 nm (Huff *et al.*, 2017).

2.12.5 Colocalisation analysis

Images were processed and analysed on Fiji software (Schindelin *et al.*, 2012). Images were processed by median filtering, rolling-ball background subtraction and Otsu or Li thresholding to isolate true signals. Colocalisation between two fluorescence channels on dual-colour images were analysed using Manders' coefficients to calculate the percentage of overlapping pixels in each channel (Manders, Verbeek and Aten, 1993; Pike *et al.*, 2017).

2.12.6 Fluorescence correlation spectroscopy (FCS)

HEK-293T cells were seeded on an 8-well glass-bottom chamber with a glass thickness of #1.0 (Thermo Fisher Scientific) pre-coated with 10 µg/mL poly-D-lysine (Thermo Fisher Scientific). On the following day, cells were transfected with equal amounts of expression constructs for Tspan15- and ADAM10-conjugated sfGFP BiFC halves for 24 hours as described in Section 2.4.1. The media was replaced with HEPES-buffered saline solution (2 mM sodium pyruvate, 10 mM D-glucose, 145 mM NaCl, 5 mM KCl, 1 mM $MgSO_4.7H_2O$, 10 mM HEPES, 1.3 mM $CaCl_2$, 1.5 mM $NaHCO_3$, pH 7.5). Cells were allowed to equilibrate to room temperature for 10 minutes. Fluorescence fluctuations on the cell surface were captured and recorded on a Zeiss LSM 510NLO Confocor 3 microscope (Carl Zeiss) equipped with a 40× 1.2 NA water objective

using a 488 nm laser line. The acquisition parameters, autocorrelation and photon counting histogram (PCH) analyses were as described (Ayling *et al.*, 2012; Koo *et al.*, 2020). Autocorrelation curves were fitted to a two-component, 2D diffusion model to obtain the number of particles per μm^2 and diffusion coefficients of the Tspan15/ADAM10 sfGFP BiFC complexes. The same traces were fitted to a one- or two-component PCH model to determine the molecular brightness of the complexes. FCS traces were collected under the supervision of Dr. Joëlle Goulding (Nottingham, UK), who also conducted the autocorrelation and PCH analyses.

2.13 Genotype-phenotype association analysis

Gene ATLAS, a repository containing genotype and phenotype data from the UK Biobank (Canela-Xandri, Rawlik and Tenesa, 2018) was used to analyse phenotypes associated with genetic variants of interest, or to identify variants associated with the phenotypes of interest. Gene expression level for each variant was retrieved from the Genotype-Tissue Expression (GTEx) portal (Aguet *et al.*, 2020). The web-based tool, LDlink was used to analyse linkage disequilibrium (LD) patterns to determine if the variants of interests were linked or were inherited independently of each other in the British population (Machiela and Chanock, 2015).

2.14 Statistics

All statistics were analysed in the GraphPad Prism 9 software (GraphPad Software, San Diego, US). Non-parametric data were normalised by arcsine transformation of the square root or log transformation before testing for differences in means using analysis of variance (ANOVA) tests and post-hoc multiple comparison tests at a 5% significance level. The exact statistical comparisons are detailed in each figure legend.

CHAPTER 3
INVESTIGATING THE MECHANISMS BY WHICH TSPANC8S DIFFERENTIALLY REGULATE GPVI CLEAVAGE BY ADAM10

3.1 Introduction

Human platelets express three of the six TspanC8s, Tspan14, Tspan15 and Tspan33 (Matthews, Noy, *et al.*, 2017). A recent study in the Tomlinson lab has identified Tspan15/ADAM10 and Tspan33/ADAM10, but not Tspan14/ADAM10, as the molecular scissors for both overexpressed GPVI in transfected HEK-293T cells and endogenous GPVI in megakaryocyte-like HEL cells. In both cell lines, GPVI cleavage was abolished in Tspan15/33 double knockout cells but was unaffected in Tspan14-knockout cells. However, the regulatory mechanism has not yet been defined (Matthews, 2019).

Tetraspanins interact with their partner proteins through the larger main extracellular region and/or transmembrane domains (Charrin *et al.*, 2014). The large extracellular domains of Tspan5 and Tspan14 have been shown to mediate ADAM10 interaction and maturation, which may be a common feature for all TspanC8s (Noy *et al.*, 2016; Saint-Pol, Billard, *et al.*, 2017). Interestingly, an exchange between the large extracellular domains of Tspan5 and Tspan15 was not sufficient to switch their roles in regulating ADAM10 stability at the cell surface, and ADAM10 function was only mildly affected (Eschenbrenner *et al.*, 2020). In line with this, recent insights from the crystal structures of the tetraspanins CD9 and CD53 have highlighted the importance of studying the extracellular region in its entirety, as the interaction between the small and the large extracellular regions may contribute to conformation switching of tetraspanins, a mechanism that has been proposed to facilitate partner protein function (Umeda

et al., 2020; Yang *et al.*, 2020). Indeed, besides the highly divergent cytoplasmic tails, the smaller extracellular region is the second least conserved region among TspanC8s (Matthews, Szyroka, *et al.*, 2017). Therefore, this chapter aimed to characterise the extracellular and cytoplasmic regions of TspanC8 tetraspanins to determine the regions responsible for regulating their subcellular localisation and ADAM10-mediated GPVI cleavage.

This chapter also aimed to study two potential mechanisms underlying how TspanC8s dictate substrate specificity of ADAM10, using GPVI as the model substrate. The first mechanism was whether TspanC8s regulate proximity of ADAM10 to substrates, since it is well established that TspanC8s determine ADAM10 subcellular localisation. In particular, Tspan15 and Tspan33 predominantly localise ADAM10 to the cell surface, whereas Tspan14 has a stronger intracellular localisation (Section 1.4.4). Therefore, it was hypothesised that the degree of colocalisation between TspanC8/ADAM10 scissors and GPVI would positively correlate with the shedding capacity of each scissor.

The second mechanism of interest was whether TspanC8s regulate ADAM10 accessibility to substrate cut sites, as detailed in Section 1.4.5. Previous co-immunoprecipitation experiments in the lab have identified different regions on the ADAM10 ectodomain that are required for interaction with each of the six TspanC8s (Noy *et al.*, 2016). Additionally, there is an association between the identity of the regulatory TspanC8 and the distance of ADAM10 cut site from the membrane surface for different substrates (Table 2, Chapter 1). Therefore, the substrate selectivity of ADAM10 may arise from interaction with different TspanC8s, which in turn positions the metalloprotease domain at different orientations to allow optimal cleavage of selected substrates with distinct cut site heights.

3.2 Results

3.2.1 Tspan15/ADAM10 is the most efficient scissor for GPVI

Tspan15/ADAM10 and Tspan33/ADAM10 have been identified as the scissors for both endogenous and overexpressed GPVI, but the regulatory mechanism remains unclear (Matthews, 2019). To investigate possible mechanisms, it was important to first determine if Tspan15 and Tspan33 differed in their abilities in mediating ADAM10 cleavage of GPVI. To do this, the extent of GPVI cleavage rescue by the three platelet TspanC8s, Tspan14, Tspan15 and Tspan33, was assessed in Tspan15/33 double knockout HEK-293T cells, where overexpressed GPVI could not be cleaved. Tspan15/33 double knockout cells were transfected with expression constructs for C-terminal myc-tagged GPVI and its associated FcRγ, or each of the FLAG-tagged human Tspan14, Tspan15 or Tspan33. To stimulate shedding, cells were treated with the metalloprotease activator NEM for 30 minutes before harvesting for lysis. GPVI cleavage was assessed by Western blotting with an anti-myc antibody to detect full-length GPVI (~63 kDa) and the membrane bound C-terminal fragment following cleavage (~10 kDa). Under both basal and NEM-stimulated conditions, reintroducing Tspan15 rescued GPVI cleavage maximally (Figure 17A-B). In contrast, Tspan33 restoration did not rescue GPVI cleavage to the same extent as Tspan15 despite comparable FLAG expression; the rescue was only marginally higher than Tspan14 overexpression, even with NEM treatment (Figure 17A-B). Therefore, it appears that Tspan15/ADAM10 was able to cleave GPVI substantially better than Tspan33/ADAM10.

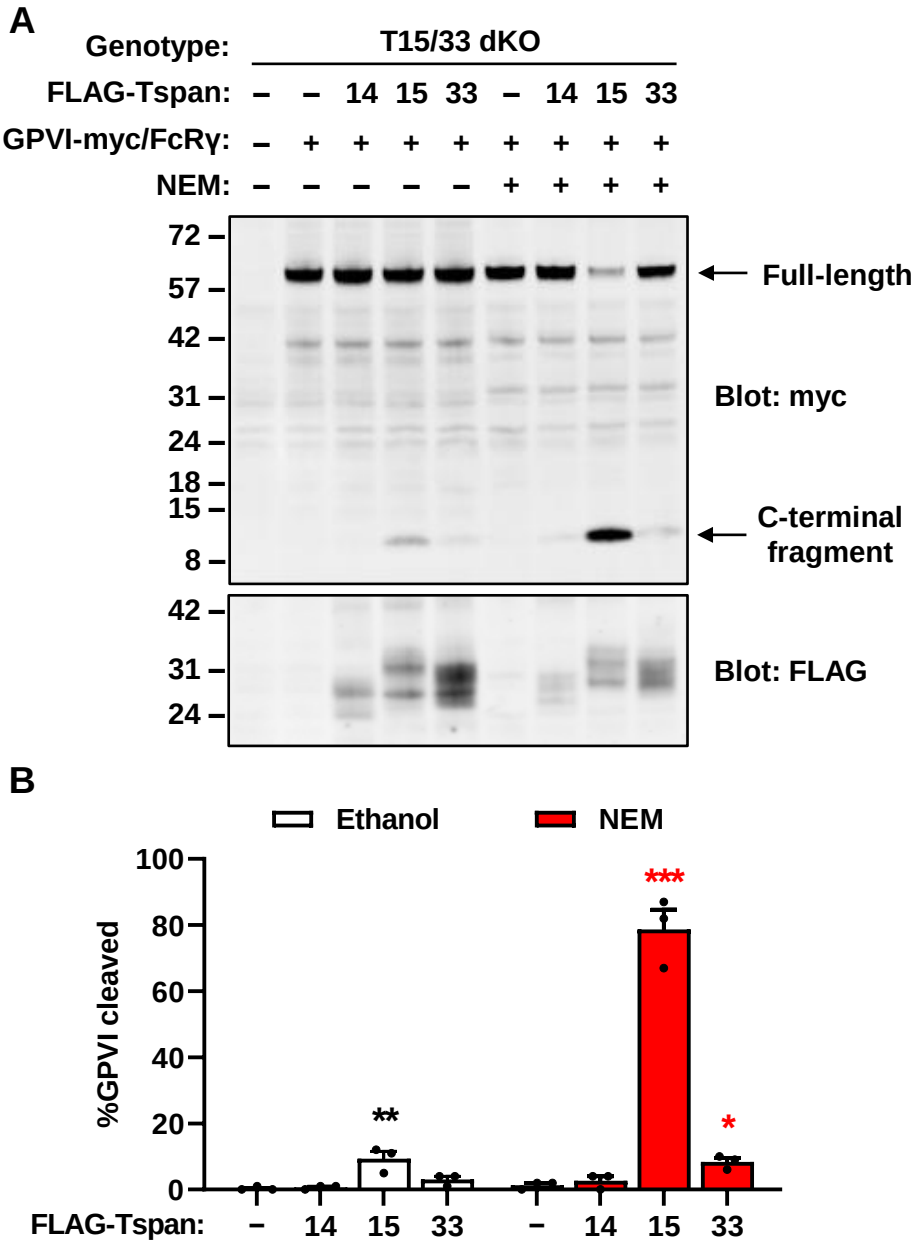

Figure 17. Tspan15/ADAM10 is the most efficient scissor for GPVI in HEK-293T cells. (A) Tspan15/33 double knockout (T15/33 dKO) HEK-293T cells were transfected with empty vector (–) or expression constructs for C-terminal myc-tagged human GPVI and FcRγ (+) and FLAG-tagged human Tspan14, Tspan15, Tspan33 or empty vector control (–) for 24 hours. In control wild-type cells, GPVI was cleaved similarly with or without co-expression of FcRγ (data not shown). To activate metalloproteases, cells were treated with 2 mM NEM (+), or ethanol as the vehicle control (–) for 30 minutes and lysed in 1% Triton X-100 lysis buffer. Lysates were subjected to anti-myc and anti-FLAG Western blotting. (B) The percentage of GPVI cleaved from panel A was quantitated, arcsine-transformed and statistically analysed by a two-way ANOVA with Dunnett's multiple comparisons test (*p<0.05, **p<0.01, ***p<0.001, compared to the corresponding empty vector controls in cells treated with ethanol (black) or NEM (red)). Error bars represent standard errors of the mean from three independent experiments.

3.2.2 The ectodomain of Tspan15, but not the cytoplasmic domain, is required for efficient GPVI cleavage

Based on the findings from the previous section, Tspan15/ADAM10 was selected as the representative GPVI scissor for mechanistic studies presented in the rest of this chapter. To examine the roles of the extracellular region and cytoplasmic domain of Tspan15 in regulating GPVI shedding by ADAM10, existing and newly generated Tspan15 mutants and chimeras between Tspan15 and Tspan14, the platelet TspanC8 that does not promote GPVI cleavage, were used (Figure 18A). These chimeras and mutants were analysed in their abilities to rescue GPVI cleavage. To prevent interference from endogenous Tspan14, Tspan14/15/33 triple knockout HEK-293T cells, which have a 90% reduction in ADAM10 surface expression, were generated by CRISPR/Cas9 for the rescue experiment (Figure A1B-C, Appendix). In addition to the FLAG-tagged Tspan14/15 constructs, cells were co-transfected with HA-tagged ADAM10 to ensure adequate supply of ADAM10 because it has been shown that ADAM10 facilitates Tspan5 and Tspan15 expression and maturation (Saint-Pol, Billard, *et al.*, 2017; Eschenbrenner *et al.*, 2020; Koo *et al.*, 2020), which could be a common feature for all TspanC8s.

GPVI cleavage was restored modestly to the extent seen in wild-type cells when wild-type Tspan14/ADAM10 was overexpressed, whereas overexpression of wild-type Tspan15/ADAM10 increased GPVI cleavage maximally (Figure 18Bi). Strikingly, substituting the extracellular region of Tspan15 with that of Tspan14 (Tspan15(14EC)) did not result in any GPVI cleavage rescue, in contrast to the reverse chimera (Tspan14(15EC)) that increased GPVI cleavage to a similar extent as wild-type Tspan15 (Figure 18Bi). Replacing the cytoplasmic domain of Tspan15 by that of Tspan14 (Tspan15(14Cyto)) did not diminish the shedding capacity of Tspan15/ADAM10 scissors (Figure 18Bi); the reverse chimera had also been made

and it did not cleave GPVI, but it was excluded from analysis because it was not functional (data not shown), unlike the other mutants which are functional as they promoted ADAM10 maturation (Figure 18Bii). In line with the findings so far that suggest that the extracellular region of Tspan15 is sufficient to promote GPVI shedding, maximal GPVI cleavage was retained with the truncation of the cytoplasmic tails on Tspan15 (Tspan15(ΔNC)) or replacement of the C-terminal tail with that of Tspan14 (Tspan15(14C)) (Figure 18Bi). Notably, replacing the C-terminal tail of Tspan14 with that of Tspan15 (Tspan14(15C)) was enough to abolish the minimal rescue achieved with wild-type Tspan14/ADAM10 overexpression, similar to what was observed with Tspan15(14EC) (Figure 18Bi).

Collectively, these data indicate that the extracellular region of Tspan15 is essential for promoting efficient GPVI cleavage by ADAM10; the cytoplasmic domain is dispensable, but the C-terminal tail may have a negative role.

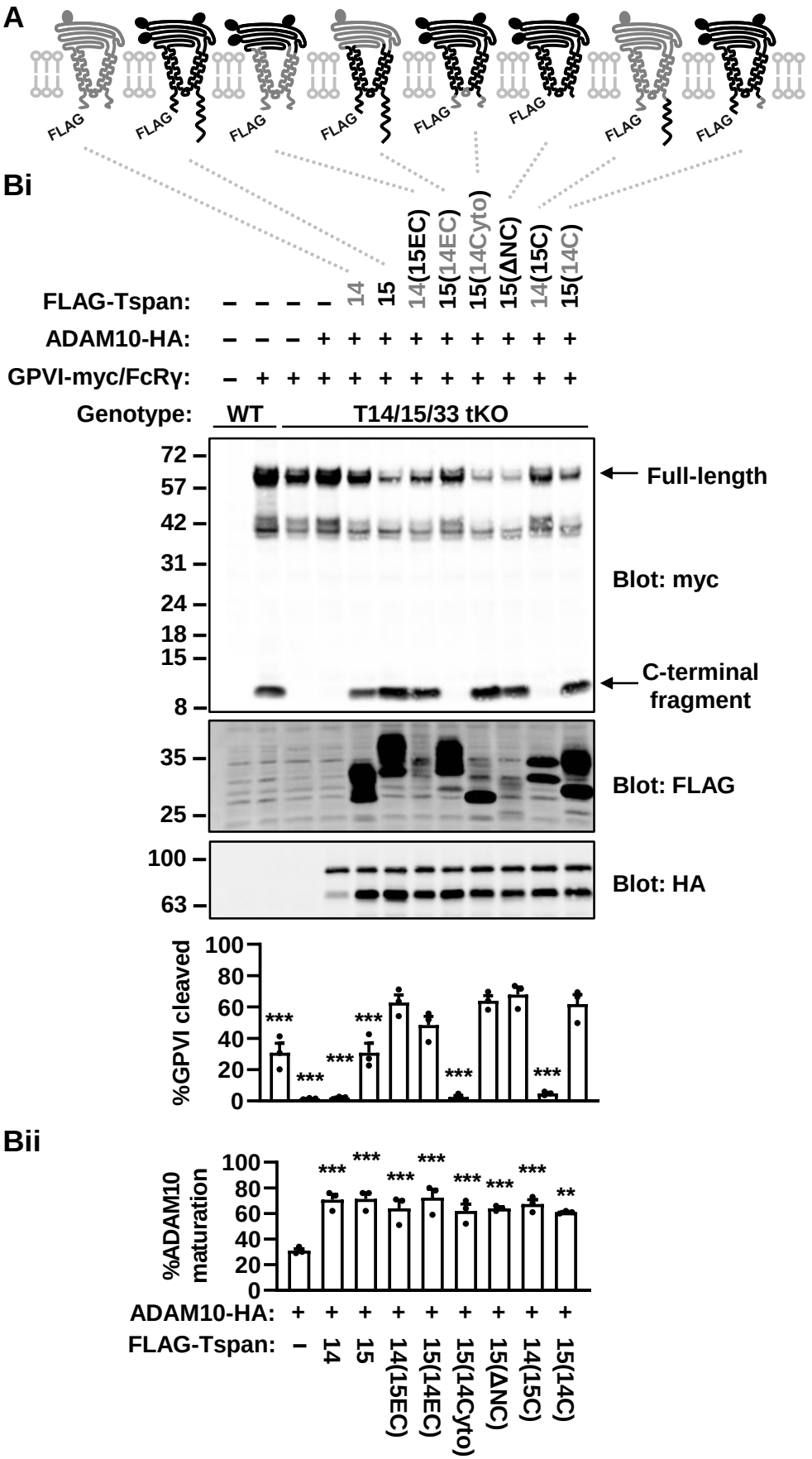
A
FLAG
Bi
FLAG-Tspan:
ADAM10-HA:
GPVI-myc/FcRγ:
Genotype:
WT
T14/15/33 tKO
14
15
14(15EC)
15(14EC)
15(14Cyto)
15(ΔNC)
14(15C)
15(14C)
72
57
42
31
24
18
15
8
Full-length
Blot: myc
C-terminal fragment
35
25
Blot: FLAG
100
63
Blot: HA
%GPVI cleaved
100
80
60
40
20
0
***
Bii
%ADAM10 maturation
**
ADAM10-HA:
FLAG-Tspan:

Figure 18. The ectodomain of Tspan15, but not the cytoplasmic domain, is required for efficient GPVI cleavage. (A) Schematic representation of N-terminal FLAG-tagged Tspan14 (grey) and Tspan15 (black) chimeras, where the extracellular region (EC), cytoplasmic domain (Cyto) or C-terminal tail (C) were exchanged. Truncation of both the N- and C-terminal tails is indicated by ΔNC. Ovals represent N-glycosylation sites. (Bi) Wild-type (WT) HEK-293T cells were transfected with expression constructs for C-terminal myc-tagged GPVI and FcRγ (+) or empty vector (–). In addition to GPVI and FcRγ, Tspan14/15/33 triple knockout (T14/15/33 tKO) HEK-293T cells were co-transfected with C-terminal HA-tagged ADAM10, or in combination with FLAG-tagged Tspan14 and Tspan15 constructs described in panel A. After 24 hours, cells were lysed in 1% Triton X-100 lysis buffer followed by anti-myc, anti-FLAG and anti-HA Western blotting (top panels). The percentage of GPVI cleaved was quantitated (bottom panel), arcsine-transformed and statistically analysed by a one-way ANOVA with Dunnett's multiple comparisons test (***p<0.001, compared to Tspan14/15/33 triple knockout cells transfected with wild-type Tspan15/ADAM10 scissors). Error bars represent standard errors of the mean from three independent experiments. (Bii) The percentage of mature ADAM10 in transfected Tspan14/15/33 triple knockout cells in panel Bi was calculated as a percentage of total (immature and mature). Data were arcsine-transformed and statistically analysed by a one-way ANOVA with Dunnett's multiple comparisons test (**p<0.01, ***p<0.001, compared to Tspan14/15/33 triple knockout transfected with ADAM10 only). Error bars represent standard errors of the mean from three independent experiments.

3.2.3 Extracellular and cytoplasmic domains determine Tspan14 and Tspan15 subcellular localisation

It is well established that TspanC8s determine the subcellular localisation of ADAM10 (Dornier *et al.*, 2012; Shah *et al.*, 2018; Eschenbrenner *et al.*, 2020). Tspan14 and Tspan15 have been shown to localise predominantly in intracellular compartments and on the cell surface, respectively, but the structural regions responsible for their distinct localisation have not yet been determined. To investigate this, the same setup described in the GPVI cleavage assay in the previous section (Section 3.2.2) was used. Tspan14/15/33 triple knockout cells transfected with Tspan14/15 expression constructs were immunostained for FLAG and myc to label Tspan14/15 and GPVI, respectively. Cells were imaged by Airyscan confocal microscopy in super-resolution mode to enhance lateral resolution to ~120 nm, and to improve sensitivity to detect mutants that showed weaker FLAG expression when lysates were immunoblotted (Figure 18Bi) (Huff *et al.*, 2017).

To describe the subcellular distribution of the Tspan14 and Tspan15 mutants, the percentage of colocalisation with GPVI, which predominantly resides at the cell surface (Matthews, 2019), was used as an objective metric. Wild-type Tspan15 exhibited the strongest plasma membrane localisation, in contrast to the more intracellularly localised wild-type Tspan14 (Figure 19Ai-ii). Exchanging the extracellular regions (Tspan14(15EC) and Tspan15(14EC)) resulted in the exchange of their localisations, as Tspan14(15EC) predominantly localised to the cell surface, whereas Tspan15(14EC) exhibited stronger intracellular localisation (Figure 19Ai-ii). All cytoplasmic domain mutants and chimeras were predominantly intracellular (Figure 19Ai-ii). These observations suggest that the cell surface localisation of Tspan15 and intracellular localisation of Tspan14 is determined by their extracellular regions, but their cytoplasmic domains also have supporting roles.

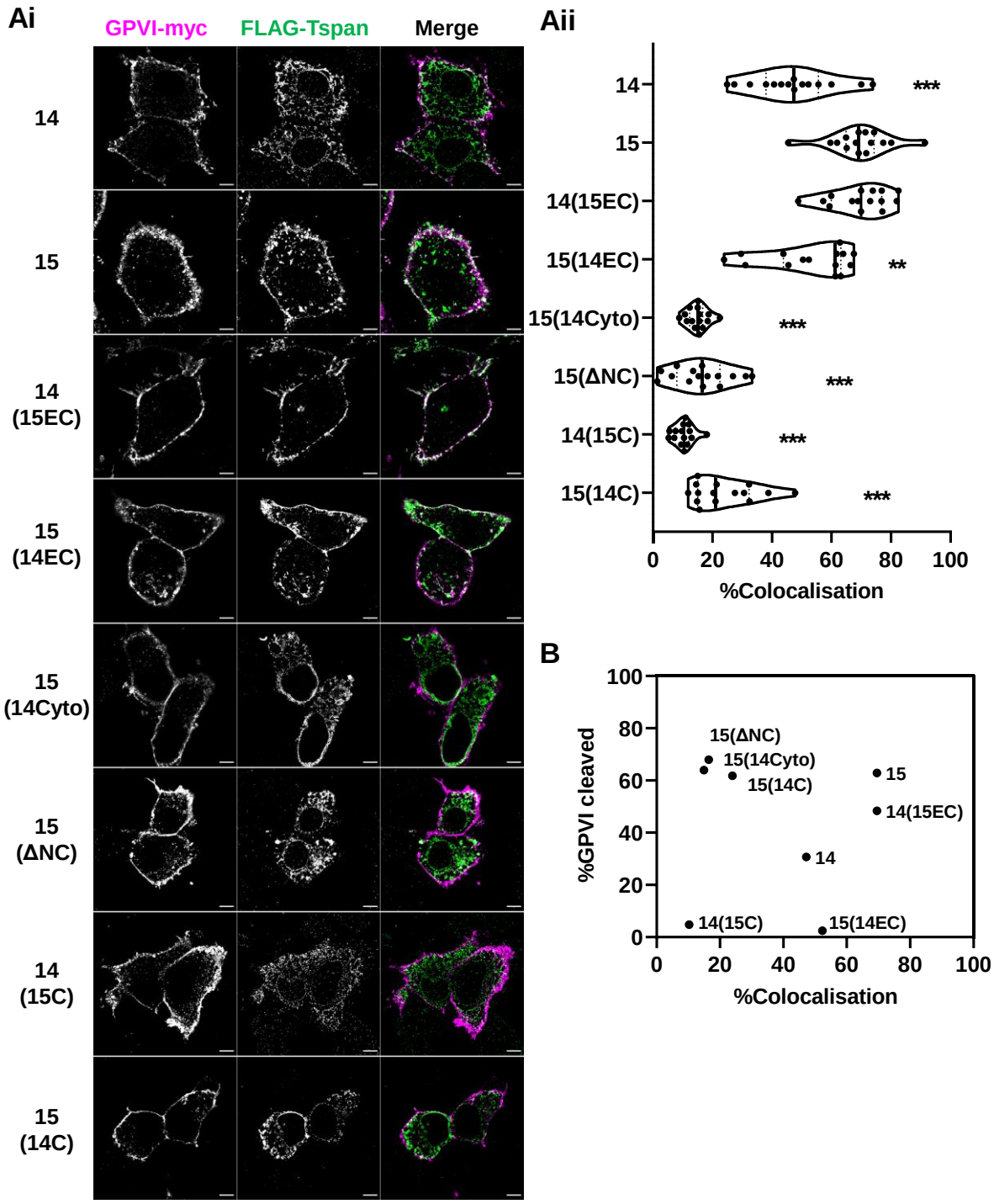

Figure 19. Location of Tspan14 and Tspan15 mutants in relation to GPVI. (Ai) Tspan14/15/33 triple knockout HEK-293T cells were transfected with expression constructs for C-terminal myc-tagged GPVI, FcRγ, ADAM10 and FLAG-tagged Tspan14 or Tspan15 mutants depicted in Figure 18A. After 24 hours, cells were fixed, permeabilised and immunostained for myc (GPVI-myc; magenta) and FLAG (FLAG-Tspan; green). Cells were imaged at the middle plane using Airyscan confocal microscopy in super-resolution mode. No signal was detected in either channel in the empty vector-transfected cells (data not shown). Images are representative of 15 fields of view, with each containing 1-2 cells, from three independent experiments. Scale bar: 5 μm. (Aii) The degree of colocalisation between GPVI-myc and FLAG-Tspan was expressed as the percentage of overlapping pixels in the GPVI-myc (magenta) channel. Data were arcsine-transformed and analysed by a one-way ANOVA, followed by Dunnett's

multiple comparison tests (**p<0.01, ***p<0.001, compared to the cells transfected with wild-type Tspan15/ADAM10 scissors). (B) Scatter plot summarising the relationship between the average of percentage of colocalisation from panel Aii and the average of percentage of GPVI cleaved in Figure 18Bi.

3.2.4 Degree of colocalisations with GPVI do not associate with scissor ability

The results so far showed that Tspan14, Tspan15 and their domain mutants have distinct abilities in mediating ADAM10 cleavage of GPVI (Section 3.2.2) and subcellular distributions (Section 3.2.3). To determine if proximity of a scissor to GPVI is critical for its cleavage, the relationship between the degree of colocalisation of the scissors with GPVI and the percentage of GPVI cleaved was assessed, and no association was found between the two (Figure 19B). The most striking example was demonstrated by Tspan15 with the cytoplasmic domain of Tspan14 (Tspan15(14Cyto)) which restored cleavage to the same degree as wild-type Tspan15, yet colocalised substantially less with GPVI (Figure 19B).

Next, HEL cells, which express GPVI, were used to address the same question, but for endogenously expressed proteins. HEL cells were treated with PMA for 72 hours to induce differentiation into an adherent, megakaryocyte-like state (Berlanga *et al.*, 2000). As no antibody against the GPVI tail suitable for imaging GPVI in HEL is available, cells were stained with an antibody recognising the extracellular domain of GPVI. To prevent loss of the GPVI ectodomain, cells were imaged under basal condition without shedding induction. Due to the lack of effective antibodies for Tspan14 and Tspan33 imaging, ADAM10 proximity to GPVI was compared between Tspan14-knockout cells, where GPVI can be cleaved, and Tspan15/33 double knockout cells, where GPVI cannot be cleaved (Matthews, 2019). It has been shown that GPVI is upregulated on the surface of HEL cells following PMA treatment, and that GPVI surface expression on PMA-differentiated wildtype and TspanC8-knockout cells are similar (Matthews, 2019). In addition, cell morphology was comparable among wildtype and PMA-

treated Tspan14-knockout and Tspan15/33 double knockout cells, suggesting that differentiation of HEL cells into megakaryocyte-like cells did not appear to be affected by the absence of these TspanC8s. Airyscan super-resolution confocal microscopy was used to image cells at the basal membrane (Figure 20Ai-ii) to analyse the lateral distribution on the cell surface, and at the middle plane (Figure 20Bi-ii) to detect differences in subcellular localisation. In both scenarios, there was no major difference between the percentage of colocalisation between ADAM10 and GPVI among the genotypes, suggesting that ADAM10 distribution was not different when different TspanC8s were knocked out and this could not account for the differences in GPVI shedding phenotypes in this experimental system.

Taken together, these data suggest that proximity of the scissors to GPVI, at least at a steady state, is not a critical factor in determining their abilities to cut GPVI.

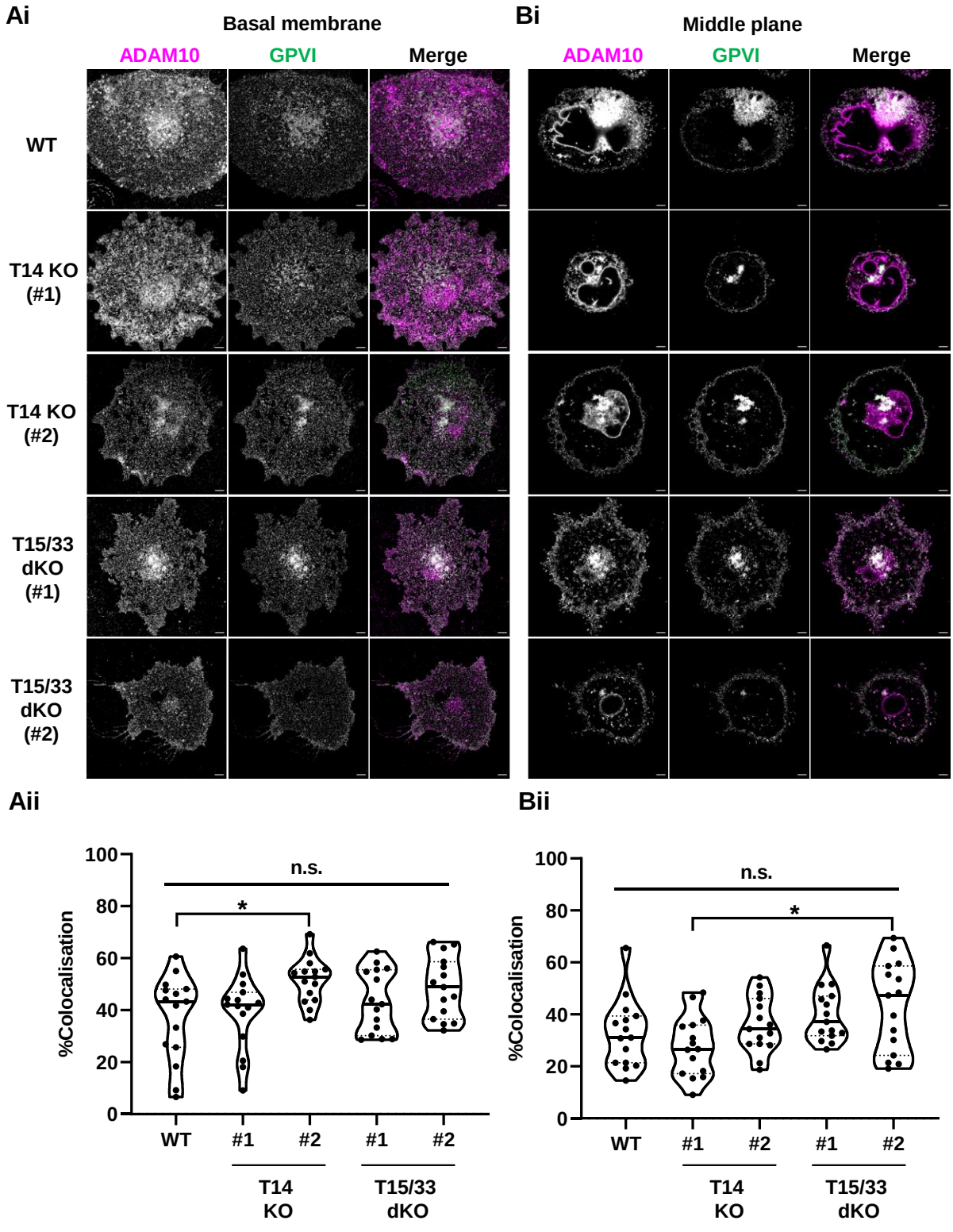

Figure 20. GPVI colocalises similarly with ADAM10 in wild-type, Tspan14-knockout and Tspan15/33 double knockout HEL cells. Wild-type (WT), Tspan14-knockout (T14 KO) and Tspan15/33 double knockout (T15/33 dKO) HEL cells were treated with 6.2 ng/mL PMA for 72 hours to induce megakaryocytic differentiation. Differentiated cells were fixed and immunostained for ADAM10 (magenta) and the extracellular region of GPVI (green). Cells were imaged at the (Ai) basal membrane and (Bi) middle plane using Airyscan confocal microscopy in super-resolution mode. No ADAM10 signal

was detected in control ADAM10-knockout cells and no GPVI signal was detected in control GPVI-knockout cells (data not shown). Images are representative of 15 fields of view from three independent experiments. Scale bar: 5 μm. The degree of colocalisation between ADAM10 and GPVI at the (Aii) basal membrane and (Bii) middle plane was expressed as the percentage of overlapping pixels in the ADAM10 (magenta) channel. Data were arcsine-transformed and statistically analysed by a one-way ANOVA, followed by Tukey's multiple comparison tests for all pairwise combinations (n.s., not significant; *p<0.05).

3.2.5 Generation of stalk-extended GPVI mutants to alter ADAM10 cut site position

Findings from the previous section did not yield evidence supporting the substrate proximity hypothesis. The second half of this chapter tested whether TspanC8s differentially regulate ADAM10 access to substrate cut site. The ADAM10 cleavage site for GPVI is located five residues above the membrane between R262 and Q263 (Figure 21A) (Gardiner *et al.*, 2007). Most substrates that can be cut by Tspan15/ADAM10 scissors, for example, N-cadherin, betacellulin, epidermal growth factor and RAGE have cut site positioned between 7-11 residues above the membrane, whereas Notch, the only substrate known to be cut by Tspan14/ADAM10 scissors so far, is cut at 15 residues above the membrane (Table 2, Chapter 1). Given the association of the scissor identity to the distance of cut site relative to the membrane surface, would altering the ADAM10 cut site position on GPVI change the TspanC8/ADAM10 scissor identity?

To test this hypothesis, the stalk region of GPVI was engineered to shift the ADAM10 cut site from five to ten (GPVI+5) or fifteen (GPVI+10) residues above the membrane surface. GPVI+5 and GPVI+10 had one or two sets of glycine-serine linkers (GGGGS) inserted at the extracellular-transmembrane interface (between K267 and G268), respectively (Figure 21A-B). The C-terminal myc tag from the parent wild-type expression construct was retained in the stalk extension mutants to enable GPVI cleavage to be assessed in transfected HEK-293T by anti-myc Western blotting as described in previous sections (Figure 21C). Expression of both

mutants at the cell surface were confirmed by flow cytometry using an anti-GPVI antibody (Figure 21D). In the next section, the mutants were characterised further in a functional assay.

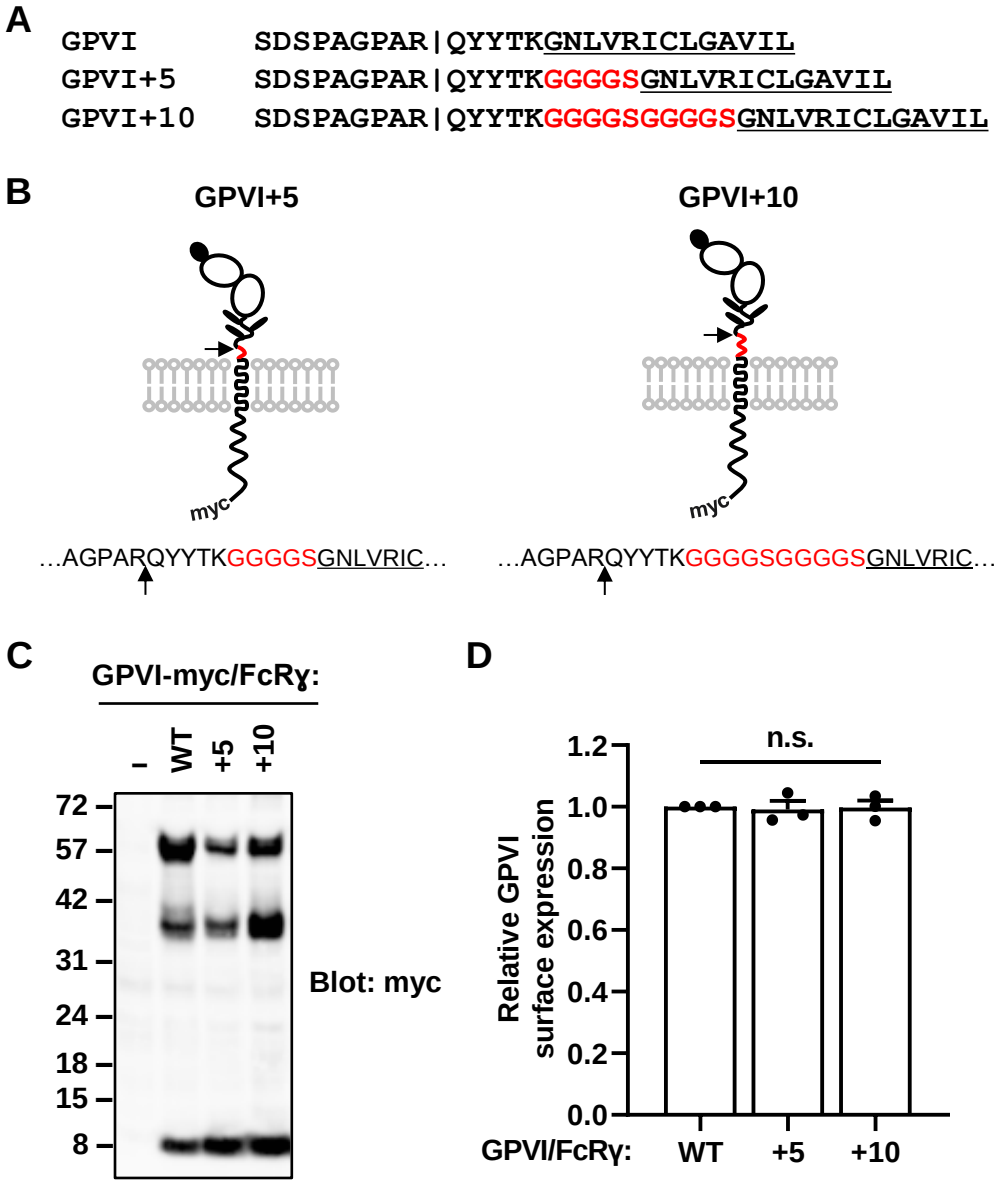

Figure 21. Validation of stalk-extended GPVI mutants. (A) Amino acid sequences of GPVI mutants with insertion of one (GPVI+5) or two (GPVI+10) sets of glycine-serine linkers (red) immediately before the predicted transmembrane region (underlined). ADAM10 cut site on GPVI is indicated by a 'I'. (B) Schematic representation of the GPVI mutants described in panel A. ADAM10 cut site on GPVI is indicated by an arrow. HEK-293T cells were transfected with empty vector control (–) or expression constructs for FcRγ and wild-type (WT) GPVI, GPVI+5 or GPVI+10 for 24 hours. (C) Cells were lysed in 1% Triton X-100 lysis buffer and subjected to anti-myc Western blotting. Blot shown is representative of three independent experiments. (D) Surface GPVI expression was analysed by flow cytometry with an anti-GPVI antibody. Geometric mean intensity was presented relative to WT GPVI-transfected cells. Data were arcsine-transformed and statistically analysed by a one-way ANOVA, followed by Tukey's multiple comparison tests for all pairwise combinations at a 5% significance level (n.s., not significant).

3.2.6 GPVI stalk extension mutants can signal in response to collagen

To determine if the stalk extension mutants, GPVI+5 and GPVI+10, are functional, their responses to collagen-induced ITAM signalling through their associated FcRɣ chains were investigated. An NFAT-luciferase reporter assay in the chicken B cell line DT40, suitable for the detection of weak and sustained collagen-induced signalling was used (Tomlinson *et al.*, 2007). In this assay, luciferase expression is driven by NFAT transcription factors, which are activated by an increase in Ca^{2+} levels, and through the mitogen-activated protein kinase (MAPK) signalling pathway. DT40 cells were co-transfected with the NFAT-luciferase reporter construct, and constructs encoding either GPVI, GPVI+5, GPVI+10 and FcRɣ for 16 hours. GPVI expression at the cell surface was confirmed by flow cytometry (Figure 22Ai-ii). Cells were stimulated with collagen, or a combination of the protein kinase C activator PMA and the Ca^{2+} ionophore ionomycin, as a positive control to maximally activate the NFAT reporter. After 6 hours, cells were lysed and assayed for luciferase activity. Collagen induced NFAT-luciferase activation in cells transfected with wild-type GPVI, GPVI+5 or GPVI+10, but not in cells transfected with empty vector controls (Figure 22B). This suggests that the GPVI stalk extension mutants are functional and could be used in downstream GPVI cleavage assays.

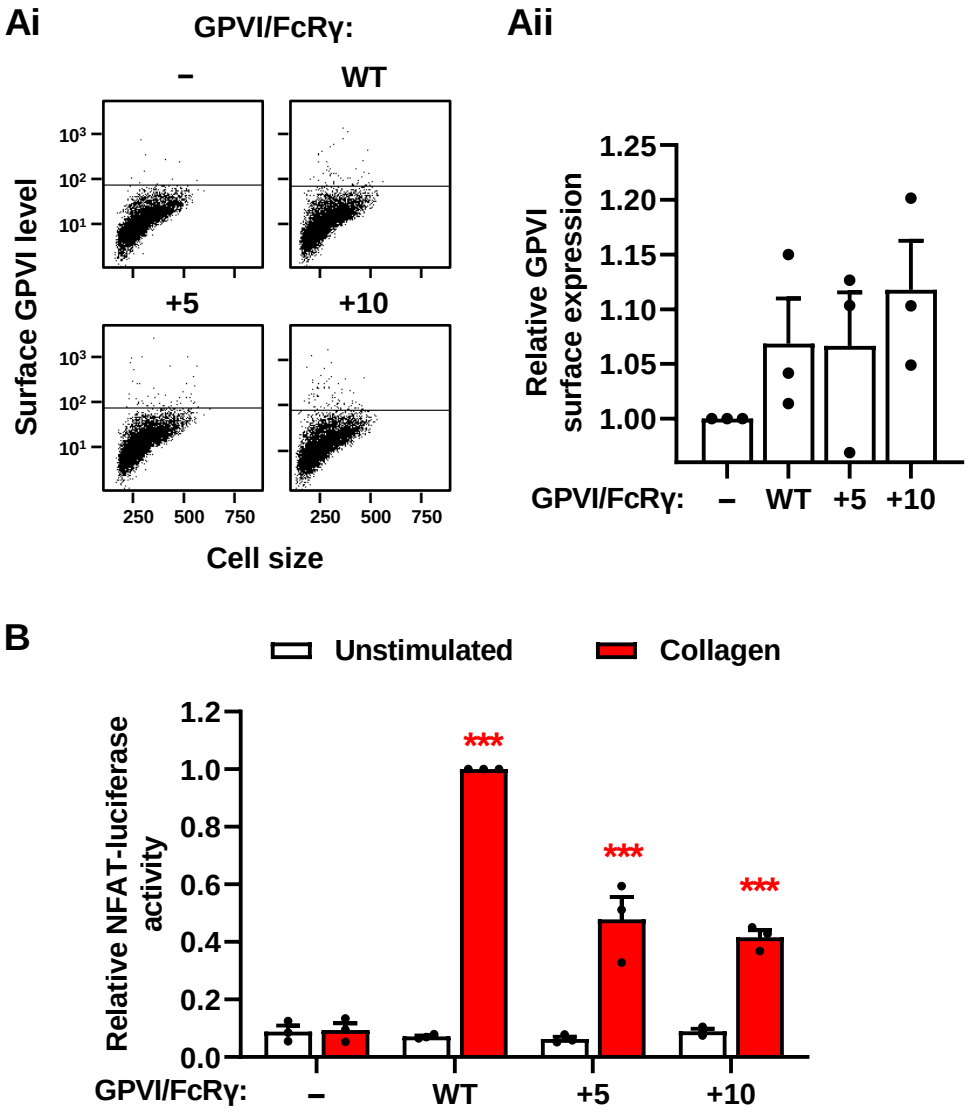

Figure 22. GPVI stalk extension mutants can signal in response to collagen. DT40 cells were transfected with an NFAT-luciferase reporter construct, FcRγ and the GPVI constructs described in Figure 21 or empty vector controls (–) for 16 hours. (Ai) Surface GPVI expression was analysed by flow cytometry with an anti-GPVI antibody. (Aii) Geometric mean intensity of GPVI staining in panel Ai was presented relative to empty vector-transfected cells. (B) Cells were left unstimulated, stimulated with 5 µg/mL collagen or 50 ng/mL PMA and 1 µM ionomycin for 6 hours, and then lysed and assayed for NFAT-luciferase activity. NFAT-luciferase activity was calculated as a percentage of PMA- and ionomycin-treated controls and presented relative to cells transfected with wild-type (WT) GPVI. Data were arcsine-transformed and statistically analysed by a two-way ANOVA with Dunnett's multiple comparisons test (***p<0.001, compared to collagen-stimulated empty vector-transfected control). Error bars represent standard errors of the mean from three independent experiments.

3.2.7 GPVI stalk extension enables ADAM10-independent cleavage

To investigate whether the cleavage of the GPVI stalk extension mutants was still ADAM10-dependent, GPVI cleavage was investigated in HEK-293T cells lacking ADAM10, or ADAM17, its closest relative, or both ADAMs; the latter two were generated as part of this study by CRISPR/Cas9 (Figure A2). In contrast to wild-type GPVI (Figure 23A), cleavage of both GPVI+5 (Figure 23B) and GPVI+10 (Figure 23C) was not completely abolished in ADAM10-knockout cells, especially when cells were treated with the metalloprotease activator NEM, albeit at lower percentages than in wild-type and in ADAM17-knockout cells. In the absence of both ADAM10 and ADAM17, GPVI+5 cleavage was abolished, but GPVI+10 could still be cleaved to a small extent (Figure 23B-C). These results suggest that although ADAM10 remains the primary protease, ADAM17 and potentially other proteases can cleave the stalk extension mutants in the absence of ADAM10.

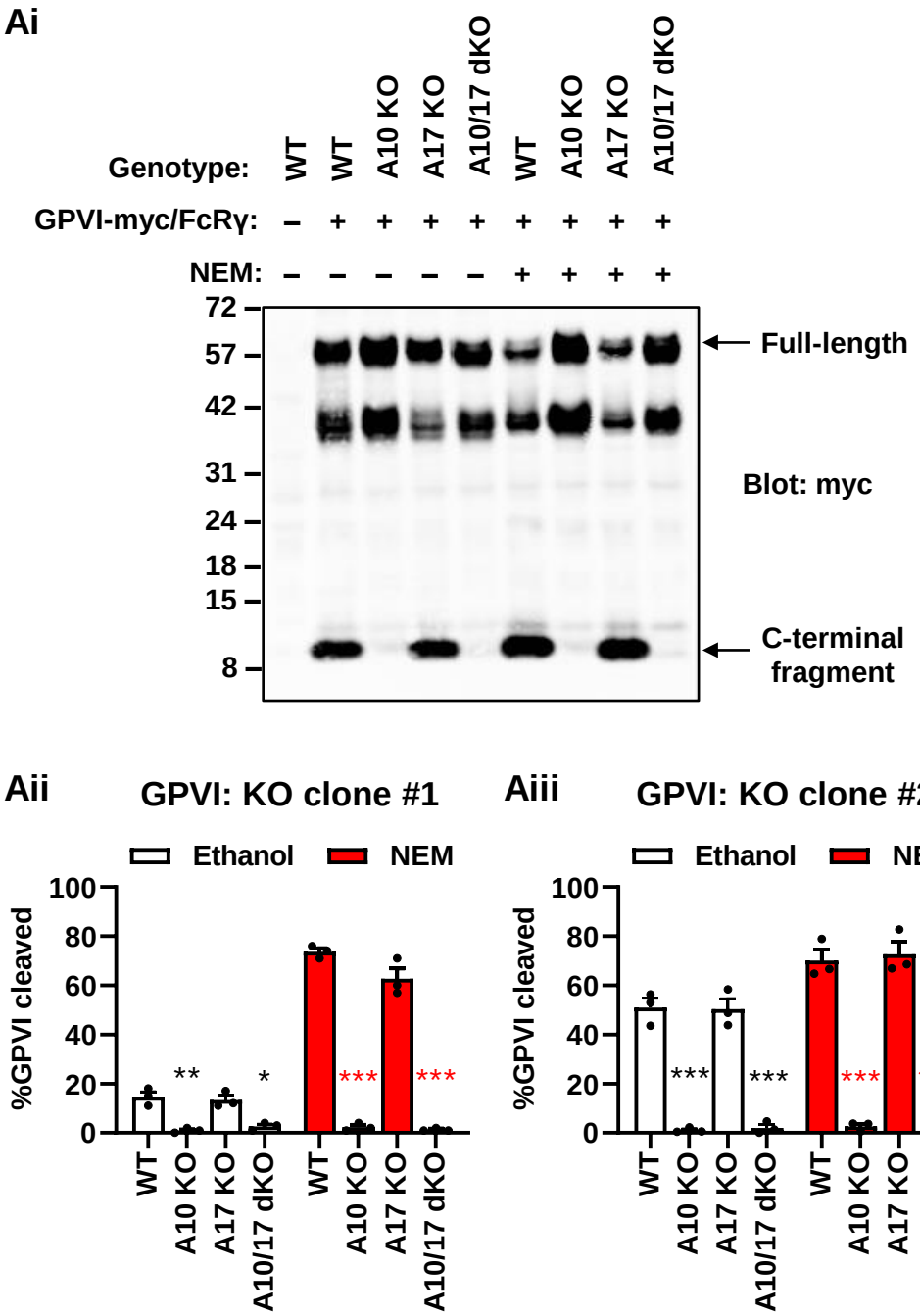
Ai
Genotype:
WT
WT
A10 KO
A17 KO
A10/17 dKO
WT
A10 KO
A17 KO
A10/17 dKO
GPVI-myc/FcRγ: – + + + + + + + +
NEM: – – – – – + + + +
72
57
42
31
24
18
15
8
Full-length
Blot: myc
C-terminal fragment
Aii
GPVI: KO clone #1
Ethanol
NEM
%GPVI cleaved
100
80
60
40
20
0
**
*
***
***
WT
A10 KO
A17 KO
A10/17 dKO
WT
A10 KO
A17 KO
A10/17 dKO
Aiii
GPVI: KO clone #2
Ethanol
NEM
%GPVI cleaved
100
80
60
40
20
0
***
***
***
***
WT
A10 KO
A17 KO
A10/17 dKO
WT
A10 KO
A17 KO
A10/17 dKO

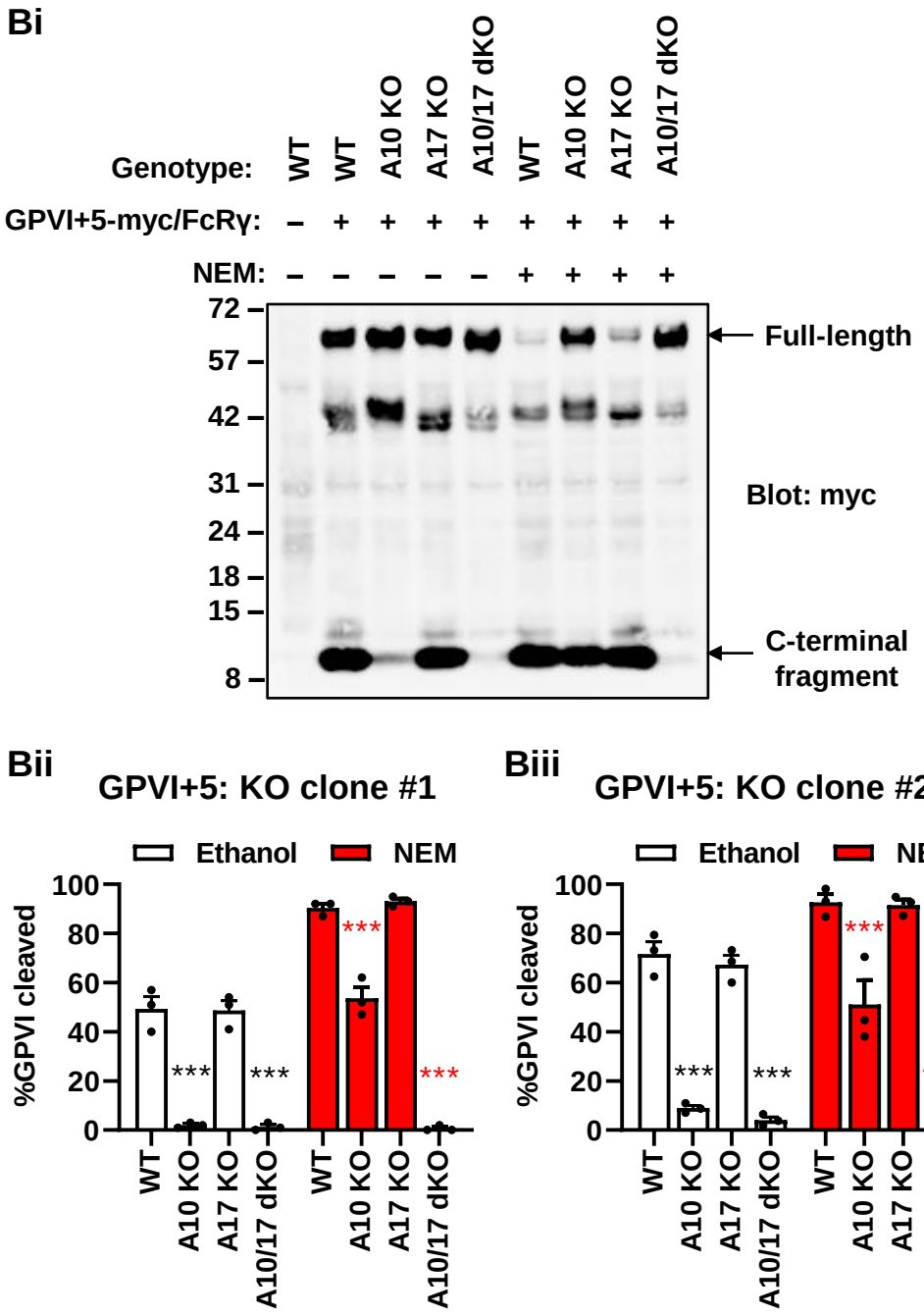
Bi
Genotype:
WT
WT
A10 KO
A17 KO
A10/17 dKO
WT
A10 KO
A17 KO
A10/17 dKO
GPVI+5-myc/FcRγ: – + + + + + + + +
NEM: – – – – – + + + +
72
57
42
31
24
18
15
8
Full-length
Blot: myc
C-terminal fragment
Bii
GPVI+5: KO clone #1
Ethanol
NEM
%GPVI cleaved
100
80
60
40
20
0
***
***
***
***
WT
A10 KO
A17 KO
A10/17 dKO
WT
A10 KO
A17 KO
A10/17 dKO
Biii
GPVI+5: KO clone #2
Ethanol
NEM
%GPVI cleaved
100
80
60
40
20
0
***
***
***
***
WT
A10 KO
A17 KO
A10/17 dKO
WT
A10 KO
A17 KO
A10/17 dKO

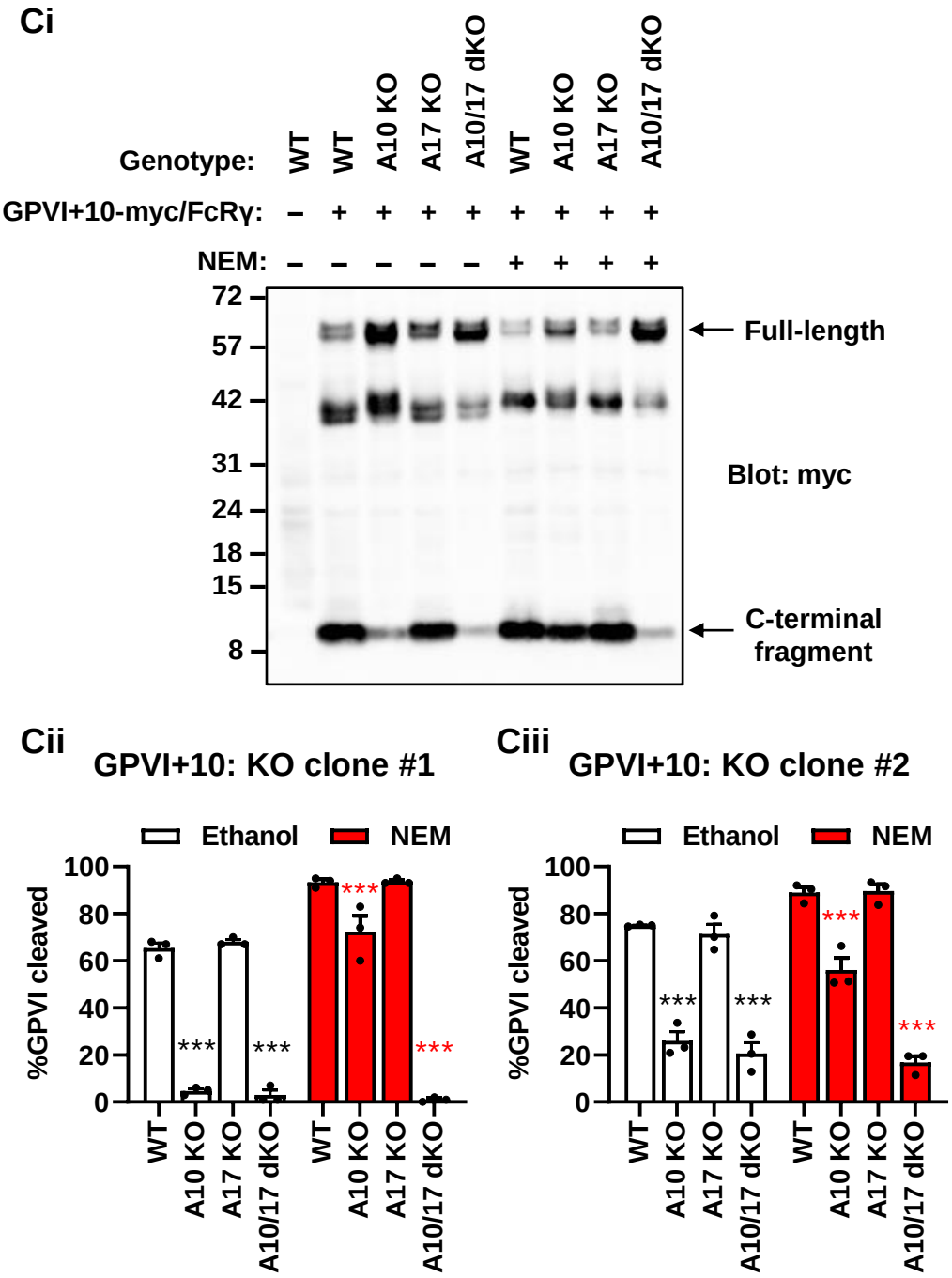

Figure 23. GPVI stalk extension mutants can be cleaved by ADAM17 and other proteases in the absence of ADAM10. Wild-type (WT), ADAM10 (A10)-knockout (KO), ADAM17 (A17) KO and ADAM10/17 (A10/17) double knockout (dKO) HEK-293T cells were transfected with empty vector control (–) or C-terminal myc-tagged (A) WT GPVI, (B) GPVI+5 or (C) GPVI+10 and FcRɣ expression constructs. After 24 hours, cells were treated with 2 mM NEM (+) or ethanol as vehicle control (–) for 30 minutes and lysed in 1% Triton X-100 lysis buffer. Lysates were subjected to anti-myc Western blotting. Representative blots are shown in sub-panels i. The percentage of GPVI cleaved was calculated from two different sets of knockout clones (sub-panels ii and iii). Data were arcsine-transformed and statistically analysed by a two-way ANOVA with Dunnett's multiple comparisons test (*p<0.05, **p<0.01, ***p<0.001, compared to the corresponding empty vector controls in cells treated with ethanol (black) or NEM (red)). Error bars represent standard errors of the mean from three independent experiments.

3.2.8 GPVI stalk extension alters the TspanC8/ADAM10 scissor profile

To determine the scissor identities for the GPVI stalk extension mutants, the most logical approach would be to perform subsequent cleavage assays in TspanC8-knockout cells without NEM stimulation. However, the additional background cleavage by other proteases hindered results interpretation because of the low percentages of basal cleavage (data not shown). Therefore, to circumvent the issue of non-specific cleavage by other proteases, ADAM10/17 double knockout HEK-293T cells were transfected with each of the six TspanC8/ADAM10 scissors as an alternative approach to more accurately quantify the cleavage of GPVI stalk extension mutants. Wild-type GPVI served as a key control for the interpretation of the results. Compared to overexpression of ADAM10 alone, a significant ($p<0.05$) increase in wild-type GPVI was only seen with the overexpression of Tspan15/ADAM10 and Tspan33/ADAM10, which are the true scissors for GPVI (Figure 24A). The magnitudes of these increases were only 2.2-fold and 1.8-fold, respectively, possibly because this is an overexpression system and ADAM10 overexpression alone yielded a substantial GPVI cleavage of 28% (Figure 24A). In the case of GPVI+5, all six scissors, apart from Tspan33/ADAM10, significantly ($p<0.05$) increased cleavage, although the magnitudes of these increases were relatively subtle, between 1.2- and 1.4-fold, in part because ADAM10 overexpression alone yielded 67% GPVI cleavage (Figure 24B). For GPVI+10, only Tspan5/ADAM10, Tspan14/ADAM10 and Tspan17/ADAM10 increased cleavage, and again the increases were subtle, between 1.1- and 1.2-fold (Figure 24C). A subtle 1.2-fold decrease in cleavage was seen with Tspan33/ADAM10 overexpression, compared to overexpression of ADAM10 alone (Figure 24C).

These results show that shifting the cut site to a different position changed the TspanC8/ADAM10 scissors responsible for its cleavage. Therefore, this suggests the possibility that each TspanC8/ADAM10 scissor has an optimal cleavage range and that TspanC8s may

differentially regulate ADAM10 by limiting access to substrates with distinct cut site positions (Figure 24D).

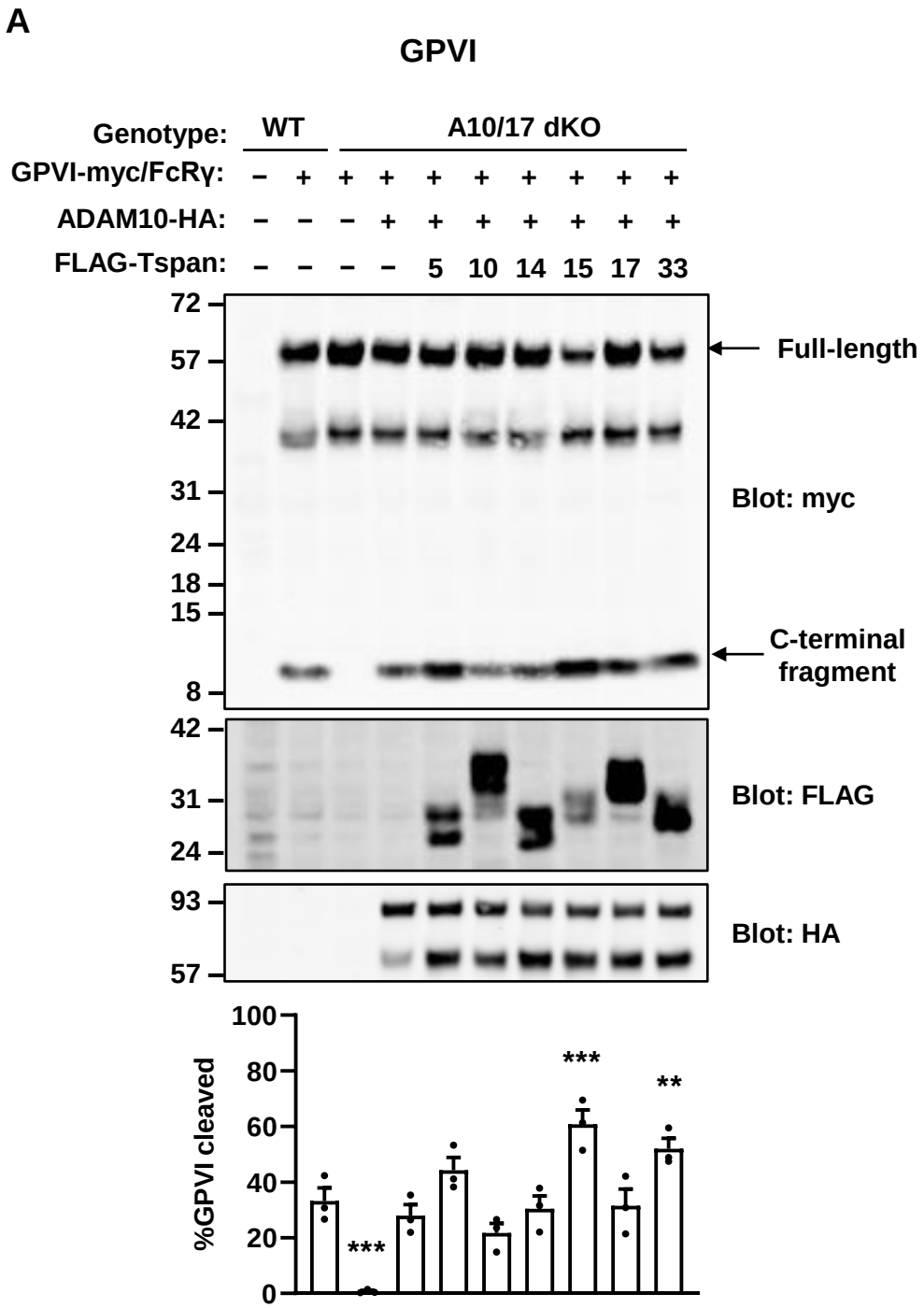

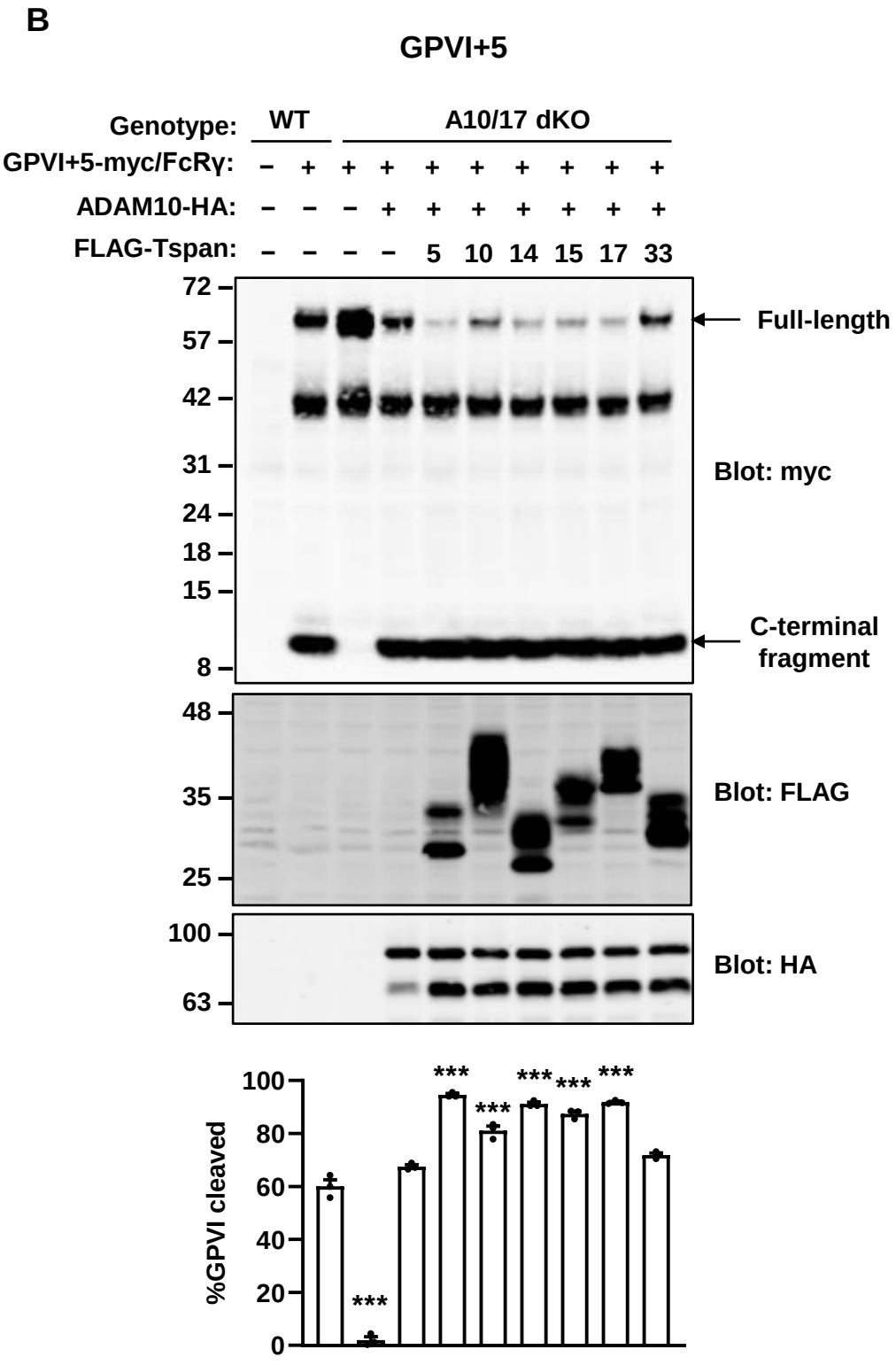
B
GPVI+5
Genotype: WT A10/17 dKO
GPVI+5-myc/FcRγ: – + + + + + + + + +
ADAM10-HA: – – – + + + + + + +
FLAG-Tspan: – – – – 5 10 14 15 17 33
72
57
42
31
24
18
15
8
Full-length
Blot: myc
C-terminal fragment
48
35
25
Blot: FLAG
100
63
Blot: HA
%GPVI cleaved
100
80
60
40
20
0
***

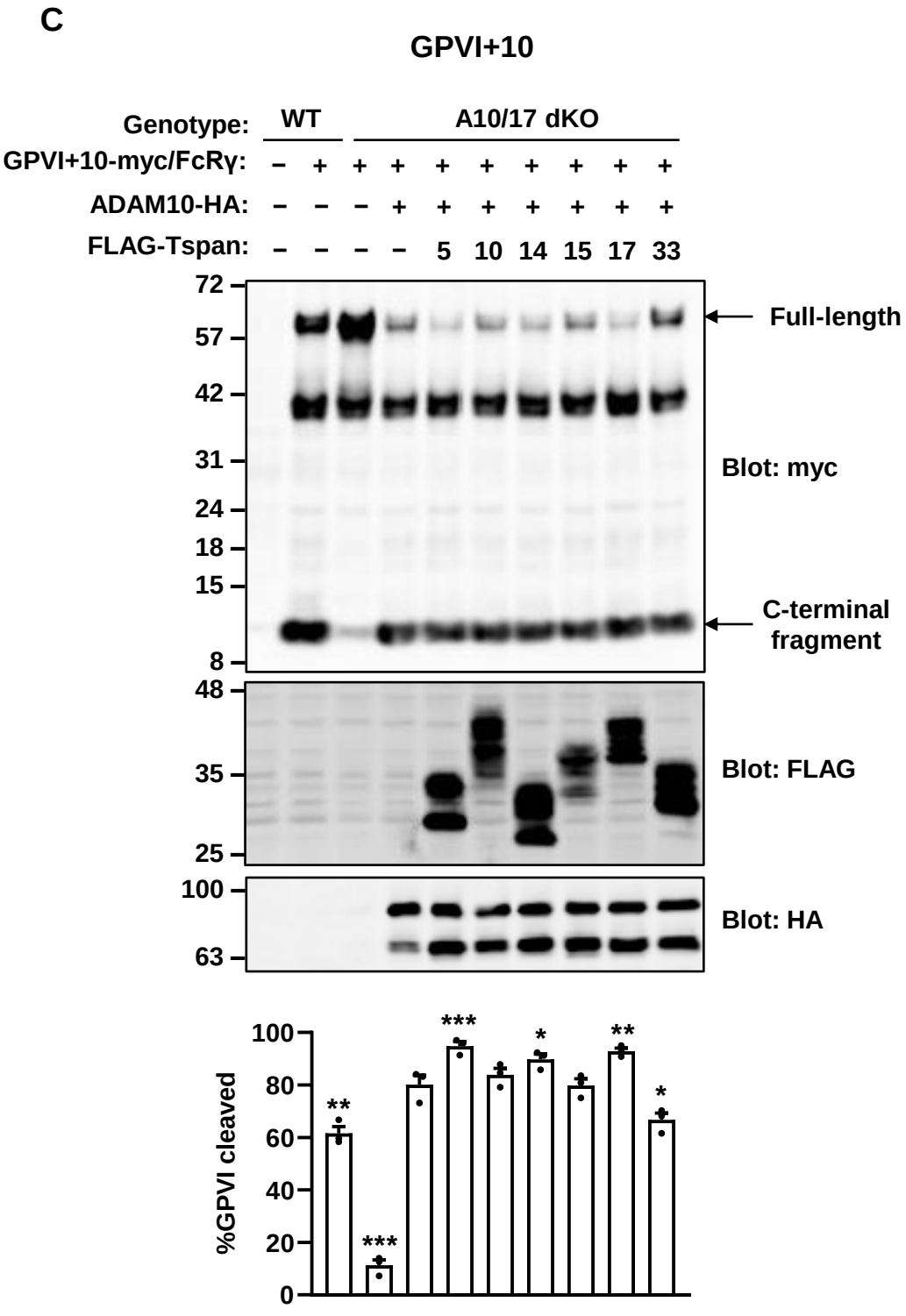
C
GPVI+10
Genotype: WT A10/17 dKO
GPVI+10-myc/FcRγ: – + + + + + + + + +
ADAM10-HA: – – – + + + + + + +
FLAG-Tspan: – – – – 5 10 14 15 17 33
72
57
42
31
24
18
15
8
Full-length
Blot: myc
C-terminal fragment
48
35
25
Blot: FLAG
100
63
Blot: HA
%GPVI cleaved
100
80
60
40
20
0
**
***
***
*
**
*

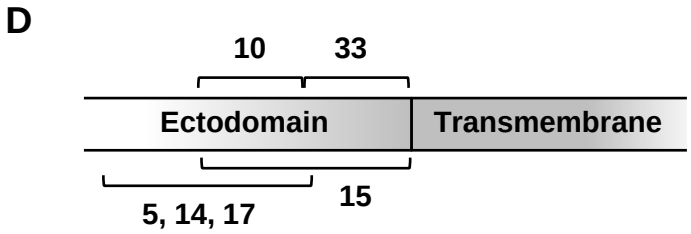

Figure 24. GPVI stalk extension changes the TspanC8/ADAM10 scissor profile. (A) Wildtype (WT) and ADAM10/17 double knockout (A10/17 dKO) HEK-293T cells were transfected with expression constructs for C-terminal myc-tagged wild-type GPVI and FcRγ (+) or empty vector (–). In addition to GPVI/FcRγ, cells were co-transfected with C-terminal HA-tagged ADAM10, or in combination with each of the FLAG-tagged TspanC8s for 24 hours. Cells were lysed in 1% Triton X-100 lysis buffer. Lysates were subjected to anti-myc, anti-FLAG and anti-HA Western blotting. There were no substantial differences in the levels of ADAM10 maturation among TspanC8-expressing cells (data not shown). The percentage of GPVI cleaved was calculated, arcsine-transformed and statistically analysed by a one-way ANOVA with Dunnett's multiple comparisons test (*p<0.05, **p<0.01, ***p<0.001, compared to A10/17 dKO cells transfected with ADAM10 alone). Error bars represent standard errors of the mean from three independent experiments. The experiment described in panel A was performed for (B) GPVI+5 and (C) GPVI+10. (D) Schematic representation of the predicted optimal range (indicated by square brackets) of cut site position for each TspanC8/ADAM10 scissor.

3.3 Discussion

What allows Tspan15/ADAM10 and Tspan33/ADAM10 scissors to cut GPVI, in contrast to the Tspan14/ADAM10 scissor which cannot? This chapter set out to address this question mechanistically and provided evidence that (1) Tspan15/ADAM10 is the most efficient scissor, (2) the extracellular region of Tspan15 is important for determining its subcellular localisation and regulating ADAM10 activity, with minor contribution from the cytoplasmic domain, (3) degree of colocalisations with GPVI do not determine scissor specificity, and (4) TspanC8s may confer ADAM10 substrate specificity by regulating the protease's access to substrate cut sites.

The first major finding revealed that Tspan15/ADAM10 is the strongest scissor for GPVI because Tspan15 was able to rescue GPVI shedding substantially better than Tspan33 when expressed at comparable levels in Tspan15/33 double knockout HEK-293T cells. This finding is consistent with the lab's recent observation that knocking out Tspan15 had a more prominent effect on GPVI cleavage reduction than knocking out Tspan33 in both HEK-293T cells and HEL cells (Matthews, 2019), when considering that the relative mRNA expression of Tspan33 to Tspan15 is higher in both cell lines, particularly in HEL cells which have approximately six times more Tspan33 (Matthews, Szyroka, *et al.*, 2017). Whether Tspan15/ADAM10 is the most efficient GPVI scissor in human platelets remains unknown; however, given that genome-wide association studies on thrombosis reported links to non-coding SNPs in *TSPAN15* (Germain *et al.*, 2015; Hinds *et al.*, 2016; Klarin *et al.*, 2017, 2019; Lindström *et al.*, 2019) and *GP6* (Bezemer *et al.*, 2008; Trégouët *et al.*, 2009; Klarin *et al.*, 2019; Lindström *et al.*, 2019) but not *TSPAN33*, Tspan15 may indeed be the most relevant TspanC8 for regulating GPVI cleavage.

In this chapter, generation of a HEK-293T cell line lacking all three human platelet TspanC8s enabled structure-function analysis of Tspan15 using cytoplasmic mutants and chimeras between Tspan14 and Tspan15, without interference from endogenous proteins. Consistent with previous reports, Tspan15 localises preferentially to the cell surface, whereas Tspan14 is predominantly intracellular (Dornier *et al.*, 2012; Noy *et al.*, 2016). This study revealed that the extracellular domain of Tspan15 and Tspan14 is the main determinant of their preferential subcellular localisation because of the clear localisation exchange seen with the extracellular region chimeras. This observation highlighted the importance of studying the extracellular region in its entirety as mentioned in the introduction of this chapter (Section 3.1). However, the cytoplasmic domain may also play a supporting role because of the strong intracellular localisation seen with all cytoplasmic domain mutants. Similar to the study from the Rubinstein group that saw increased ADAM10 stability on the cell surface when the C-terminus tail of Tspan5 was replaced by that of Tspan15 (Eschenbrenner *et al.*, 2020), replacing Tspan15 C-terminus with that of Tspan14 was sufficient to abrogate the strong plasma membrane localisation, supporting the notion that Tspan15 C-terminus is important for maintaining cell surface localisation. However, in contrast to the same study, the C-terminus of Tspan15 caused a stronger shift towards intracellular localisation in the reverse Tspan14 chimera. The reason for this conflicting observation is unclear, but it is possible that the contribution from the Tspan14 extracellular region is stronger and can override the contribution from Tspan15 C-terminus.

More importantly, functional characterisation of these mutants in their abilities to rescue GPVI cleavage in Tspan14/15/33 triple knockout cells revealed several interesting findings. Remarkably, the mutants displayed unambiguous shedding phenotypes. The extracellular region of Tspan15, but not its cytoplasmic domain, is required for efficient GPVI cleavage. The

observation that wild-type Tspan14 could rescue GPVI cleavage minimally when co-expressed with ADAM10 in Tspan14/15/33 triple knockout cells was unexpected. One possible explanation for this is that overexpression increased the chances of scissor-substrate encounter, therefore allowing any TspanC8/ADAM10 scissor to cleave GPVI, albeit at much lower efficiencies compared to the true scissors (explored further in Chapter 6). However, if this were the case, one would not have expected an all-or-none shedding phenotype from every mutant; therefore, an intrinsic negative regulatory role must exist to enable the Tspan15 C-terminus to abolish the minimal GPVI cleavage seen with overexpression of wild-type Tspan14 when the C-terminal tail was replaced. The negative effect from the C-terminal tail was suppressed in the presence of the Tspan15 extracellular region, as seen in wild-type Tspan15, but not when the extracellular region was replaced by that of Tspan14, suggesting that Tspan15 extracellular region is the dominant positive regulator. It is possible that the C-terminal tail of Tspan15 exerts its negative regulatory effect through an interaction with intracellular regulatory proteins. As a precedence, the PLEKHA7/PDZD11 complex binds to the C-terminal tail of Tspan33, which in turn regulates clustering of ADAM10 at specialised apical junctions to facilitate alpha toxin binding (Shah *et al.*, 2018).

This chapter did not provide evidence supporting the hypothesis that TspanC8s regulate ADAM10 substrate specificity by limiting its substrate repertoire through differential subcellular localisation. The degree of colocalisation of neither the Tspan14/15 mutants described previously in this section with overexpressed GPVI in HEK-293T, nor endogenous ADAM10 with GPVI in Tspan14-knockout and Tspan15/33 double knockout HEL cells, associated with their distinct shedding phenotypes. The results in this chapter suggest that the proximity of a TspanC8/ADAM10 scissor with a substrate, at least at a steady state, does not determine the specificity of the scissor. Although spatial resolution was improved with the use

of Airyscan super-resolution imaging, temporal resolution was a key limitation in the current investigation, given the dynamic nature of TspanC8/ADAM10 complexes (Jouannet *et al.*, 2016; Koo *et al.*, 2020). However, the Rubinstein group's study, which investigated the relationship between ADAM10 endocytosis and Notch activity, also did not report strong association between the two (Eschenbrenner *et al.*, 2020). In the future, investigating the relationship between GPVI shedding and GPVI interaction with TspanC8/ADAM10 scissors in real-time with live-cell single-molecule imaging would help shed more light on the extent to which substrate proximity affects scissor specificity.

Finally, this chapter provided the first evidence that TspanC8s may confer substrate specificity by regulating access of ADAM10 to substrate cut sites. The specificities of Tspan15/ADAM10 and Tspan33/ADAM10 were lost when the ADAM10 cut site on GPVI was shifted synthetically by adding either five or ten residues above the membrane surface. In line with the lab's previous report that each TspanC8 binds to different regions on ADAM10 (Noy *et al.*, 2016), the changes in the TspanC8/ADAM10 scissor profile for each GPVI stalk extension mutant suggest that each TspanC8 may physically constrain ADAM10's metalloprotease domain at a certain angle or position, thus only allowing access to cut sites at a particular distance from the plasma membrane. Tspan10/ADAM10 and Tspan33/ADAM10 appear to be more rigid scissors that are limited to narrower optimal cleavage ranges. This could imply that Tspan33/ADAM10 may preferentially cleave only substrates with cut sites very close to the membrane surface, such as GPVI (Gardiner *et al.*, 2007). The rest of the four scissors are more flexible and can access a wider range of cut sites. The results are consistent with the observation that Tspan5/ADAM10 and Tspan14/ADAM10 are the major scissors for Notch (Dornier *et al.*, 2012; Jouannet *et al.*, 2016; Saint-Pol, Billard, *et al.*, 2017; Eschenbrenner *et al.*, 2020), which has its cut site located at 15 residues above the membrane (Mumm *et al.*, 2000). Similarly, this

could explain why Tspan15/ADAM10 cannot cleave Notch because the cut site for Notch is located beyond its access range, which is closer to the membrane surface. The greater flexibility of Tspan15/ADAM10 compared to Tspan33/ADAM10 may also be why both scissors can cut GPVI, but only Tspan15/ADAM10 can cut substrates with cut sites located slightly higher above the membrane, such as N-cadherin, which has its cut site located at 10 residues above the membrane (Uemura *et al.*, 2006).

It is important, however, to address the limitations of the GPVI stalk extension strategy used in the current study. Firstly, it is unknown whether the insertion of flexible glycine-serine linkers would be representative of increasing the distance of the cut site from the membrane. However, the observation that ADAM17 can cleave both stalk extension mutants in the absence of ADAM10 is consistent with a similar study investigating IL6R shedding, which showed that ADAM17 is restricted to cut sites further away from the membrane surface compared to ADAM10 (Riethmueller *et al.*, 2016), inferring that the cut site may indeed be shifted further away from the membrane in the GPVI stalk extension mutants. Another consideration is whether ADAM10 still cleaves the mutants at the original GPVI cleavage site. Given that ADAM10 prefers larger residues at its active site (Caescu, Jeschke and Turk, 2009; Tucher *et al.*, 2014), it is unlikely that ADAM10 would prefer to cleave within the small glycine-serine linkers, but it may be necessary to identify the cleavage products by mass spectrometry to confirm. Lastly, the effects seen with the overexpression of TspanC8/ADAM10 scissors were subtle due to the limitations of the overexpression system in ADAM10/17 double knockout cells, where endogenous TspanC8s are still present; therefore, overexpression of ADAM10 alone could already rescue cleavage substantially. The ideal cell line for this experiment would be one that lacks ADAM10, ADAM17 and all six TspanC8s. Future studies should aim to gather additional evidence from other ADAM10 substrates, for example, by studying whether

bringing the ADAM10 cut site of Notch closer towards the membrane surface would remove the specificities of Tspan5/ADAM10 and Tspan14/ADAM10 scissors.

In summary, this chapter provided further insights into the complex multi-factorial regulation of ADAM10 substrate specificity by TspanC8 tetraspanins, which will be discussed further in Chapter 7. The discovery that Tspan15/ADAM10 is the most efficient GPVI scissor laid a foundation for the thesis, which primarily investigated the role of Tspan15.

CHAPTER 4
ANALYSIS OF *TSPAN15* AND *GP6* VARIANTS ASSOCIATED WITH THROMBOSIS

4.1 Introduction

Recent genome-wide association studies (GWASs) of thrombotic disease have uncovered *TSPAN15* as a novel gene associated with venous thromboembolism (Germain *et al.*, 2015; Klarin *et al.*, 2017, 2019; Lindström *et al.*, 2019) and self-reported blood clots (Hinds *et al.*, 2016). However, no biological follow-up studies have been reported so far as the identified SNPs are in the intron region, and none of the studies identified links to putative causal variant(s). In addition, the role of Tspan15 in vascular biology is largely unknown in the field. The primary aim of this chapter was to identify and characterise novel *TSPAN15* variants associated with venous thrombosis using publicly available genotype-phenotype association and gene expression datasets.

GP6 polymorphisms and their links to platelet function and disorders have been extensively studied (Arthur, Dunkley and Andrews, 2007; Jandrot-Perrus, Hermans and Mezzano, 2019). In human, two common missense variants of GPVI, GPVIa and GPVIb, had been identified (Croft *et al.*, 2001). These two variants arise from SNPs, resulting in five amino acid substitutions (S219P, K237E, T249A, Q317L and H322N) in the rarer GPVIb (frequency of ~0.13) (Joutsi-Korhonen *et al.*, 2003; Jandrot-Perrus, Hermans and Mezzano, 2019). GPVIb has been reported to associate with an increased risk in heart attack and stroke (Takagi *et al.*, 2002; Cole *et al.*, 2003; Ollikainen *et al.*, 2004), sticky platelet syndrome (Sokol *et al.*, 2018) and non-responsiveness to antiplatelet therapies (Lepäntalo *et al.*, 2006; Pandey *et al.*, 2019). Conversely, emerging evidence suggest that the more common GPVIa associates with venous

thromboembolism (Bezemer *et al.*, 2008; Trégouët *et al.*, 2009; Kotuličová *et al.*, 2012; Klarin *et al.*, 2019; Lindström *et al.*, 2019). The expression and functional differences between GPVIa and GPVIb have been well characterised, but not their cleavage. Platelets with GPVIb appear to have reduced signalling and thrombus formation in response to collagen (Joutsi-Korhonen *et al.*, 2003; Jones *et al.*, 2007; Trifiro *et al.*, 2009; Petersen *et al.*, 2017; van Geffen *et al.*, 2019). A reduction in GPVI expression in individuals with the *GP6b* haplotype has been described (Joutsi-Korhonen *et al.*, 2003; Jones *et al.*, 2007; Petersen *et al.*, 2017), but a conflicting observation, where there is no difference in GPVI expression between individuals with *GP6a* and *GP6b*, has also been reported (Trifiro *et al.*, 2009). Therefore, a secondary aim of this chapter was to determine whether GPVIa and GPVIb are differentially cleaved by TspanC8/ADAM10 scissors, which may explain their respective associations with venous and arterial thrombosis, in light of the findings from the association of *TSPAN15* with venous thrombosis.

4.2 Results

4.2.1 Non-coding *TSPAN15* variants are associated with venous thromboembolism

Each variant is assigned a unique reference SNP ID (rsID) by the National Center for Biotechnology Information (NCBI) (Sherry, Ward and Sirotkin, 1999). The two *TSPAN15* variants that have been reported in GWASs of thrombotic diseases are rs78707713 for venous thromboembolism (Germain *et al.*, 2015; Klarin *et al.*, 2017, 2019; Lindström *et al.*, 2019) and rs17490626 for self-reported blood clots (Hinds *et al.*, 2016); both are SNPs in different intron regions of *TSPAN15*, with a minor allele frequency of ~0.05 in the global population (Auton *et al.*, 2015). In all studies, the major alleles were identified as the risk alleles. All studies examined individuals of European ancestry, except for the study by Klarin *et al.* (2019), which also included African, Hispanic and Latino Americans.

As GWASs commonly report only the most significantly associated variant for each locus, also known as the lead variant, it was important to consider whether unreported *TSPAN15* variants exist that could be the causal variants for thrombosis. To identify other *TSPAN15* variants, data from the genotype-phenotype association database, Gene ATLAS, were mined and analysed. The database contains associations among 30 million variants and 778 phenotypes from 452,264 white British individuals from the UK Biobank cohort (Canela-Xandri, Rawlik and Tenesa, 2018).

The only variants that significantly ($p<1\times10^{-8}$) associated with venous thromboembolism on chromosome 10 were close to the *TSPAN15* locus (Figure 25A). Other than the two published lead variants, an additional 21 variants in the region surrounding the *TSPAN15* locus (±15 kb) were discovered; these included another 12 intron variants and nine variants upstream of the locus (Figure 25B). Two of these intergenic variants, rs77784890 and rs7475662, were mapped to regulatory regions in the genome annotation from the Ensembl project (Howe *et al.*, 2021).

In particular, rs77784890 overlaps with a predicted transcription factor binding site, whereas rs7475662 is located within a promoter.

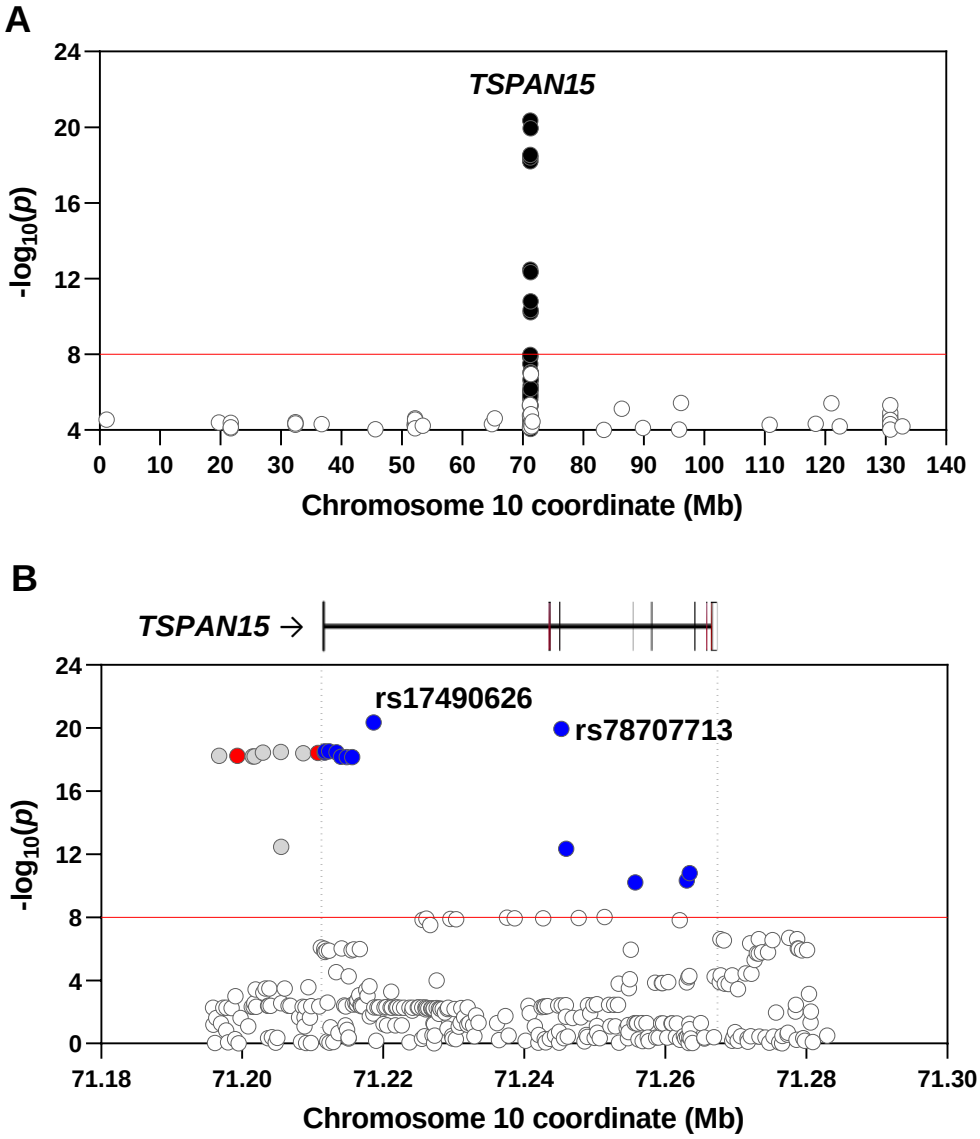

Figure 25. Twenty-three single-nucleotide polymorphisms around the *TSPAN15* locus are associated with venous thrombosis. Regional association plots for venous thrombosis showing the association strength of individual single-nucleotide polymorphisms (SNPs) with venous thrombosis risk. Data were extracted from the genotype-phenotype association database, Gene ATLAS, which analysed 11,636 cases of venous thromboembolism and 440,628 controls from the UK Biobank cohort (Canela-Xandri, Rawlik and Tenesa, 2018). Each dot represents a single SNP. The red line indicates the statistical threshold of $-\log_{10}(p)$ of 8 ($p=1\times10^{-8}$). (A) Association plot for the entire chromosome 10 showing SNPs with at least a $-\log_{10}(p)$ of 4 ($p=1\times10^{-4}$) for simplicity. *TSPAN15* SNPs are highlighted in black. (B) In the region surrounding the *TSPAN15* locus (±15 kb), 23 variants were identified: 7 intergenic (grey), 2 regulatory (red) and 14 intronic (blue) variants.

4.2.2 Minor alleles of the *TSPAN15* variants negatively associate with venous thrombosis traits and may link to increased platelet size

The minor alleles of all 23 variants negatively associated with venous thromboembolism, as indicated by the negative β coefficients, which measure the slope of the linear regression analysis computed by Gene ATLAS (Table 6). The odds ratio provides a more intuitive description of the effect size of each variant (Pirinen, Donnelly and Spencer, 2013), and suggests that the probability of venous thromboembolism events was 10-19% less in individuals with the minor alleles compared to individuals with the major alleles (Table 6).

Next, phenome-wide association analysis data were extracted from Gene ATLAS to determine other phenotypes associated with the *TSPAN15* variants (Figure 26). Strikingly, the minor alleles of most variants negatively associated with other phenotypes characteristic of venous blood clots: deep vein thrombosis, pulmonary embolism, pulmonary heart and vascular disease, vein inflammation (phlebitis) and vein inflammation due to blood clots (thrombophlebitis). Interestingly, the minor alleles of 18 of the 23 variants associated with a larger mean platelet volume, but the magnitude of increase could not be determined from this analysis. Associations with other platelet quantitative traits, namely platelet count, platelets as a percentage of blood cells and variation in platelet size distribution were not reported to be significant ($p<1\times10^{-8}$) in the analyses.

Table 6. *TSPAN15* variants associated with venous thromboembolism. Variants are identified by their unique reference SNP IDs (rsIDs) assigned by the National Center for Biotechnology Information (NCBI) (Sherry, Ward and Sirotkin, 1999). Statistics are for the effect allele. Data were compiled from Gene ATLAS (Canela-Xandri, Rawlik and Tenesa, 2018) and Ensembl (Howe *et al.*, 2021).

Variant	Position on chromosome 10 (Mb)	Type	Alleles (major/minor)	Minor allele frequency	Effect allele	β coefficient	Odds ratio	*p*-value	-$\log_{10}(p)$
rs78677622	71.196698	intergenic	C/T	0.14	T	-0.0042	0.85	5.73×10^{-19}	18.2
rs77784890	71.199295	regulatory	G/C	0.14	C	-0.0042	0.85	5.72×10^{-19}	18.2
rs12242391	71.201504	intergenic	C/T	0.14	T	-0.0042	0.85	6.27×10^{-19}	18.2
rs10998780	71.201735	intergenic	T/A	0.14	A	-0.0042	0.85	6.25×10^{-19}	18.2
rs55892803	71.202929	intergenic	A/T	0.14	T	-0.0043	0.84	3.61×10^{-19}	18.4
rs79069746	71.205473	intergenic	T/C	0.14	C	-0.0043	0.84	3.32×10^{-19}	18.5
rs77356330	71.205544	intergenic	T/C	0.05	C	-0.0053	0.81	3.38×10^{-13}	12.5
rs76628955	71.208625	intergenic	C/T	0.14	T	-0.0042	0.84	3.9×10^{-19}	18.4
rs7475662	71.210744	regulatory	G/C	0.14	C	-0.0042	0.84	3.81×10^{-19}	18.4
rs112843485	71.211707	intronic	T/C	0.14	C	-0.0043	0.84	3.60×10^{-19}	18.4
rs77602872	71.211734	intronic	G/A	0.14	A	-0.0043	0.84	2.98×10^{-19}	18.5
rs2033372	71.212333	intronic	C/G	0.14	G	-0.0043	0.84	2.95×10^{-19}	18.5
rs13377102	71.213386	intronic	T/A	0.14	A	-0.0042	0.84	3.45×10^{-19}	18.5
rs12258136	71.213995	intronic	C/T	0.14	T	-0.0042	0.85	6.73×10^{-19}	18.2
rs75583483	71.214798	intronic	A/G	0.14	G	-0.0042	0.85	7.05×10^{-19}	18.2
rs28463525	71.215578	intronic	A/T	0.14	T	-0.0042	0.85	6.85×10^{-19}	18.2
rs17490626	71.218646	intronic	G/C	0.13	C	-0.0046	0.83	4.40×10^{-21}	20.4
rs78707713	71.245276	intronic	T/C	0.13	C	-0.0046	0.83	1.14×10^{-20}	19.9
rs80118685	71.245942	intronic	G/T	0.05	T	-0.0053	0.81	4.60×10^{-13}	12.3
rs3829182	71.251384	intronic	A/G	0.24	G	-0.0022	0.92	9.53×10^{-9}	8.0
rs1864589	71.255747	intronic	T/C	0.24	C	-0.0025	0.90	6.04×10^{-11}	10.2
rs78855907	71.263061	intronic	T/A	0.06	A	-0.0047	0.83	4.59×10^{-11}	10.3
rs77364098	71.263455	intronic	G/T	0.12	T	-0.0035	0.87	1.60×10^{-11}	10.8

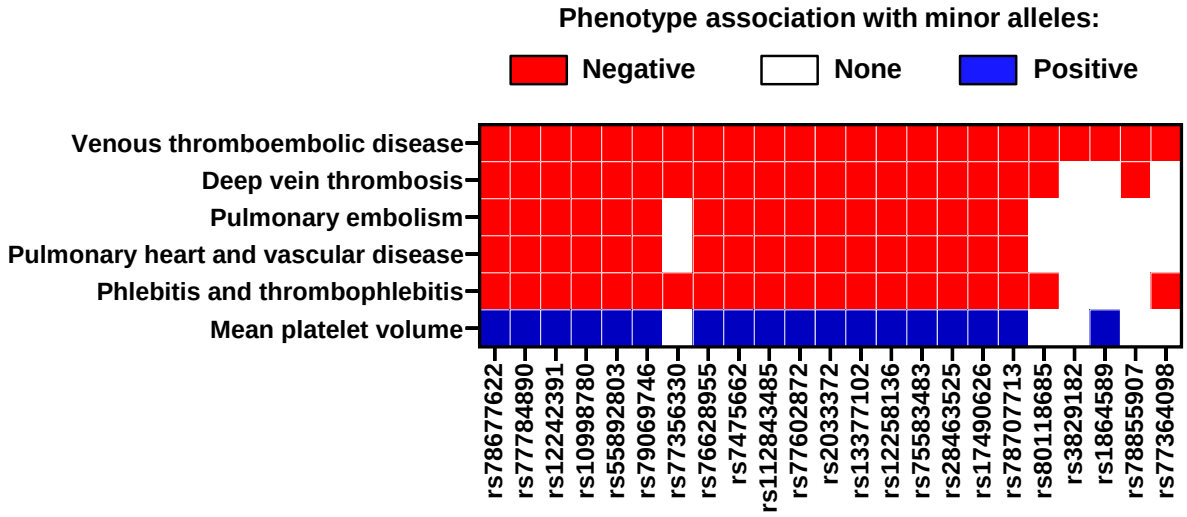

Figure 26. Phenotypes associated with *TSPAN15* variants. Phenome-wide association analysis data for the 23 venous thrombosis-associated single-nucleotide polymorphisms (SNPs) in the region surrounding the *TSPAN15* locus (±15 kb) were extracted from Gene ATLAS (Canela-Xandri, Rawlik and Tenesa, 2018). Phenotypes significantly ($p<1\times10^{-8}$) associated with the minor alleles were summarised for each variant. The direction of association was differentiated by colour: red for negative, blue for positive, and white for non-significant associations.

4.2.3 *TSPAN15* variants are in tight genetic linkage

The data in previous sections demonstrate similarities in the trend of genotype-phenotype association, providing some evidence that most of the *TSPAN15* variants are likely to be inherited together as a haplotype. To investigate this further, the web-based tool, LDlink, was used to analyse the variants for linkage disequilibrium, a term used to describe non-random inheritance of alleles and a measure of the genetic linkage of alleles in a population (Machiela and Chanock, 2015). Since the association data from Gene ATLAS were from white British individuals in the UK Biobank, the linkage disequilibrium pattern for the 23 variants was assessed in the British population. Two metrics were used to describe linkage: (1) R^2 to measure the correlation of each allele from two SNPs, whereby a high R^2 value indicates that having the major allele for one SNP would predict the inheritance of the major allele for the other SNP; and (2) D' to determine whether a pair of SNPs are in genetic linkage due to physical proximity on the chromosome, whereby a high D' value indicates that two SNPs are tightly linked (Machiela and Chanock, 2015).

All pairwise comparisons had high D' values, suggesting that all variants are in tight genetic linkage and are likely to be inherited together (Figure 27). However, six of the 23 variants had lower R^2 values with the rest of the variants (Figure 27), which coincide with the deviation of their minor allele frequencies from the common value of 0.14 for most variants (Table 6). In fact, these variants were also the most dissimilar in their phenotype pattern and association significance (Table 6) (Figure 26). This divergence suggests that these SNPs likely emerged separately in the British populations at a different time point or within a specific sub-population. Together, the linkage disequilibrium patterns suggest that the 17 highly correlated *TSPAN15* variants may constitute two common haplotypes in the British population.

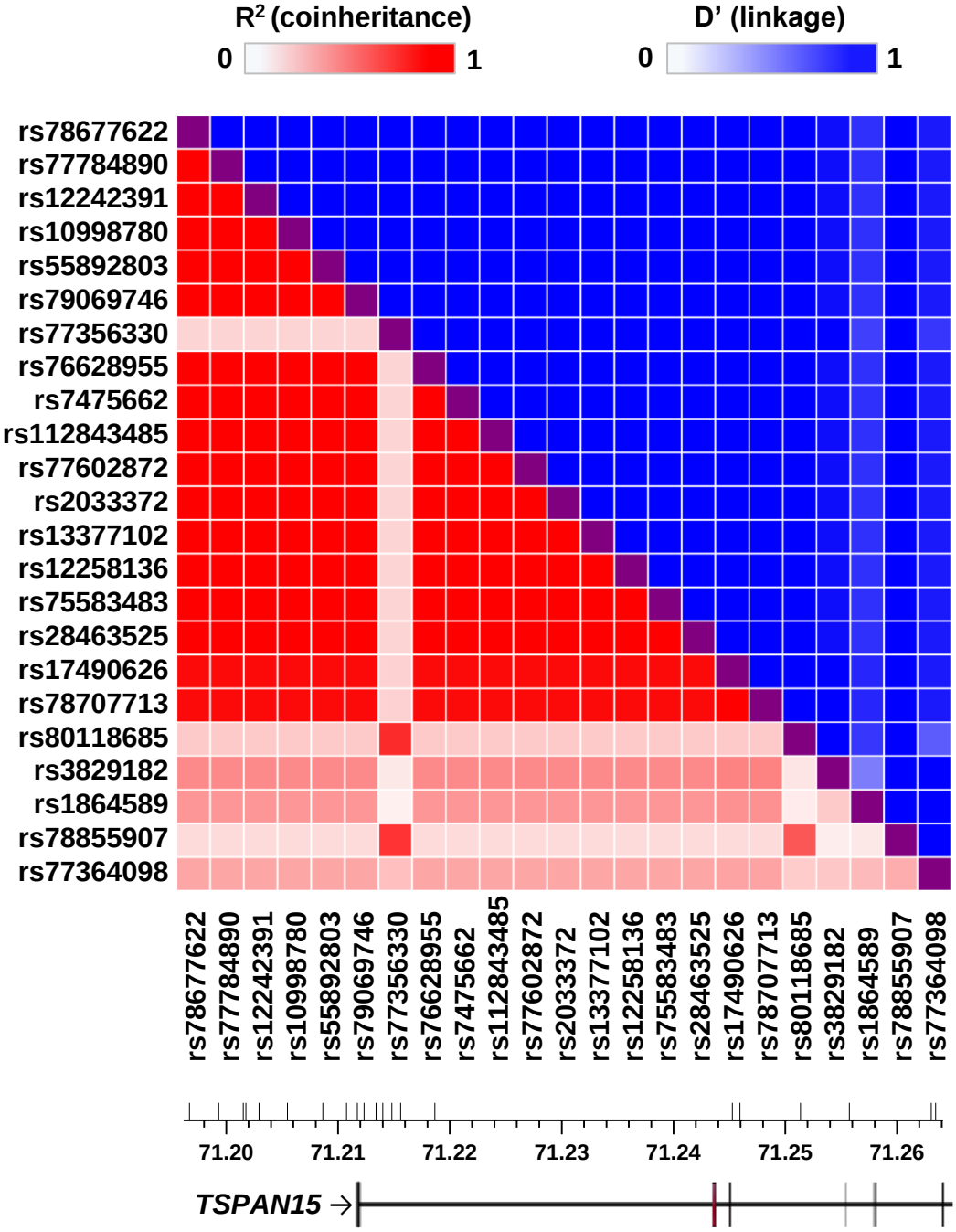

Figure 27. *TSPAN15* single-nucleotide polymorphisms associated with venous thrombosis are in tight genetic linkage. The 23 venous thrombosis-associated single-nucleotide polymorphisms (SNPs) in the region surrounding the *TSPAN15* locus (±15 kb) were analysed for linkage disequilibrium in the British population. Two metrics were used for all pairwise comparisons: R^2 (red) to predict whether each allele from two SNPs would be inherited together and D' (blue) to determine whether a pair of SNPs are in genetic linkage due to physical proximity on the chromosome. Data were extracted from the web-based tool, LDlink (Machiela and Chanock, 2015).

4.2.4 Protective minor alleles are associated with higher *TSPAN15* gene expression

Given that two SNPs, rs77784890 and rs7475662, are in the regulatory region, the possibility that the SNPs would affect *TSPAN15* expression was investigated. This was achieved by analysing expression quantitative trait loci (eQTL) mapping data from the Genotype-Tissue Expression (GTEx) project, which studied the effects of genetic polymorphisms on the transcriptomes of 49 healthy tissue samples from 838 individuals (Aguet *et al.*, 2020). A genetic variant is a *cis*-eQTL for a gene if the genetic polymorphism associates with the variation in mRNA expression levels of genes within ±1 Mb of its locus, and a *trans*-eQTL if it affects the expression of a distant gene (Aguet *et al.*, 2017; Mohammadi *et al.*, 2017).

The analysis revealed that all 23 *TSPAN15* variants are *cis*-QTLs for *TSPAN15* in multiple tissues, including whole blood, with the strongest effect seen in oesophagus mucosa (Figure 28A). No *trans*-eQTLs were identified, and all *cis*-QTLs were specific for *TSPAN15*, apart from five variants (indicated by an asterisk in Figure 28A) which were also weak (p=1.2×10^{-4}, normalised effect size=0.15) *cis*-QTLs for a neighbouring gene, *TACR2*, in one tissue (oesophagus muscularis). In all cases, the minor alleles associated with increased mRNA expression, as indicated by the positive normalised effect size, which is a measure of the slope of the linear regression computed by GTEx (Figure 28A). This was confirmed by visualising the distribution of *TSPAN15* expression in individuals homozygous or heterozygous for the alleles of the lead SNP, rs78707713, in oesophagus mucosa (Figure 28B). As the normalised effect size is a better measure for statistical strength than for biological effect size, the allelic fold change in each tissue was analysed as a more representative metric of the true magnitude of the *TSPAN15* eQTLs (Mohammadi *et al.*, 2017), which revealed similar results (Figure 28C). Collectively, these data provide evidence of higher *TSPAN15* mRNA expression in individuals with the *TSPAN15* minor haplotype that confers lower venous thrombosis risk.

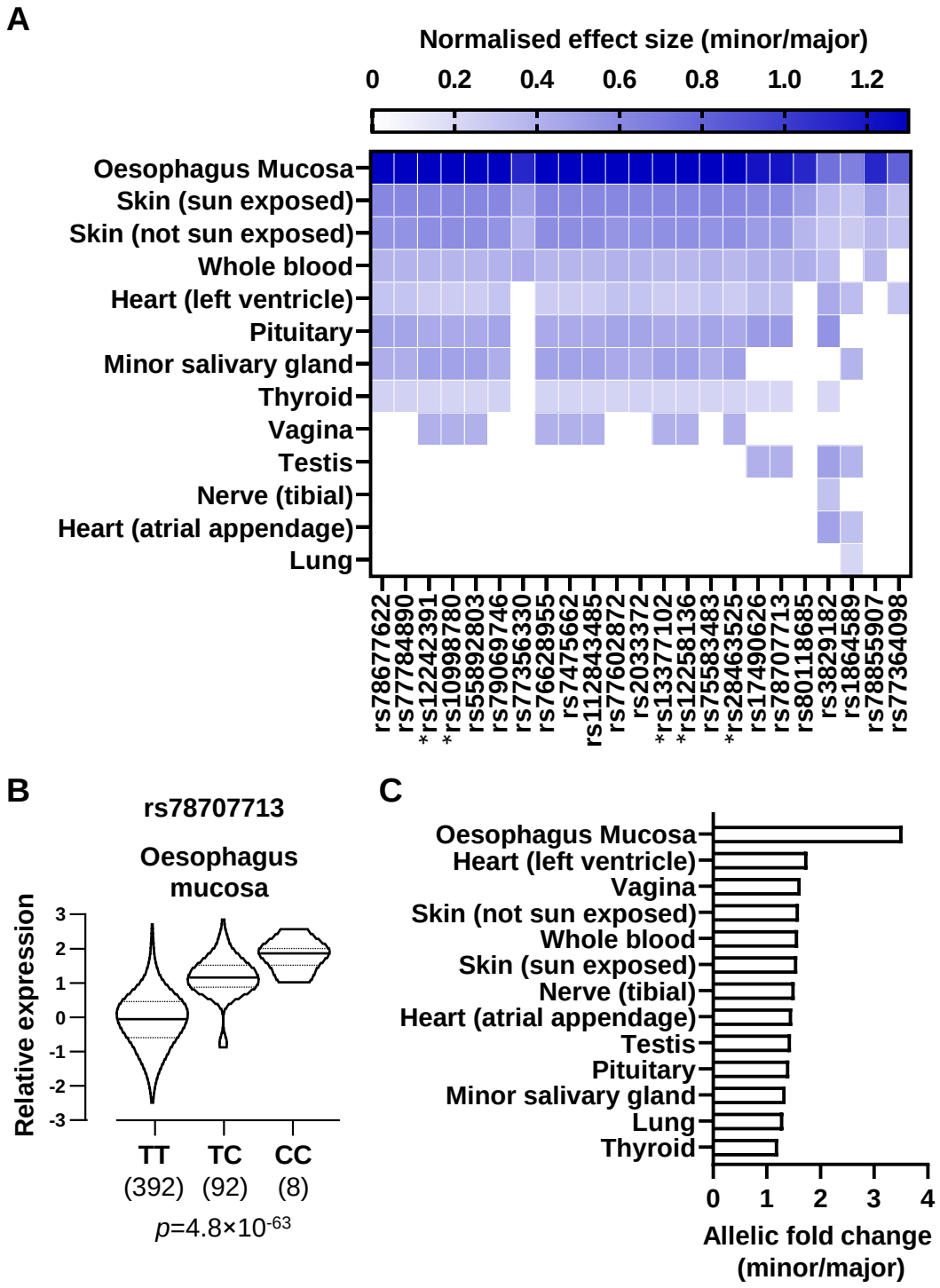

Figure 28. Minor alleles of *TSPAN15* are associated with higher *TSPAN15* gene expression. Expression quantitative trait loci (eQTL) analysis data were extracted from the Genotype-Tissue Expression (GTEx) project (Aguet *et al.*, 2020) to examine the relationship between venous thrombosis-associated *TSPAN15* variants and mRNA expression. (A) Summary of tissues where *TSPAN15* expression were significantly (nominal *p*-value thresholds calculated from permutation-based methods) affected by each SNP. The normalised effect size describes the direction and strength of the association trend, i.e., a positive value indicates increased expression relative to the major reference allele, and a higher value indicates a steeper linear regression slope. Variants marked by an asterisk also weakly affect a nearby gene, *TACR2,* in oesophagus muscularis. (B) Relative *TSPAN15* expression data in

oesophagus mucosa in individuals homozygous or heterozygous for the alleles of the lead *TSPAN15* variant, rs78707713. Number in brackets represents the number of samples per genotype. (C) Allelic fold change for each tissue, expressed as the ratio of *TSPAN15* expression of the minor haplotype to the major haplotype, was used to describe the biological effect size of the *TSPAN15* eQTLs (Mohammadi *et al.*, 2017).

4.2.5 HEL cells express GPVIa

In the second part of this chapter, the potential contribution of *GP6* polymorphisms to thrombosis was investigated by examining whether GPVI isoforms are differentially cleaved by TspanC8/ADAM10 scissors. The two most common haplotypes of *GP6, GP6a* and *GP6b*, are missense variants that result in five amino acid substitutions in the rarer GPVIb: S219P, K237E, and T249A in the extracellular region, and Q317L and H322N in the cytoplasmic region (Jandrot-Perrus, Hermans and Mezzano, 2019) (Figure 29A). GPVIa and GPVIb electrophorese at similar molecular weights when separated by SDS-PAGE (Figure 29B). In the lab's previous study, Tspan15/ADAM10 and Tspan33/ADAM10 were identified as the scissors for GPVI in PMA-differentiated HEL cells and GPVIa in transfected HEK-293T cells (Matthews, 2019). The scissors for GPVIb have yet to be identified, and the GPVI isoform HELs express is unknown.

To determine the GPVI variant that HELs express, the cells were genotyped by sequencing the cDNA region flanking the polymorphic sites from T177 to H333. Alignment of the translated sequence to consensus GPVIa and GPVIb sequences revealed that HEL cells express GPVIa (Figure 29C), further confirming that Tspan15/ADAM10 and Tspan33/ADAM10 are the scissors for GPVIa.

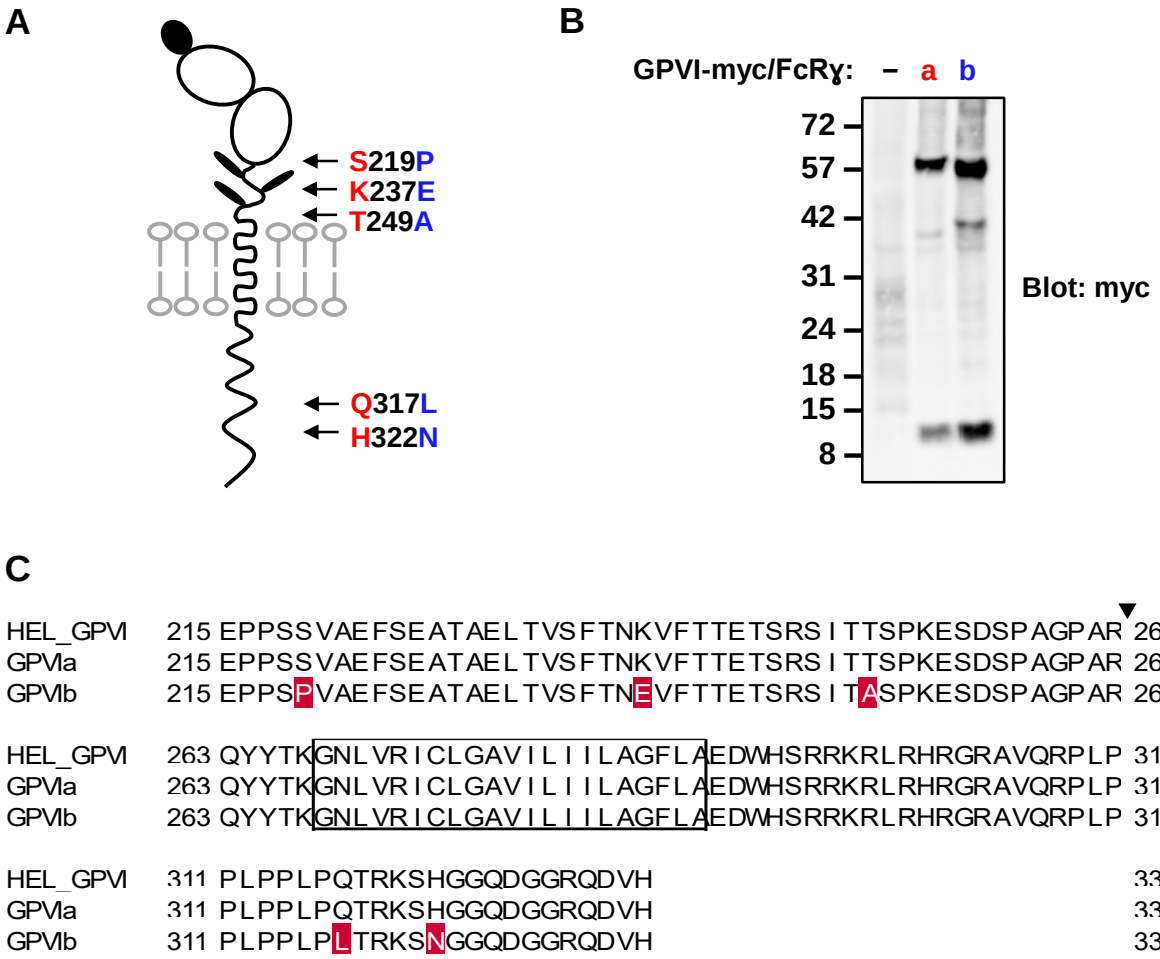

Figure 29. HEL cells express the GPVIa isoform. (A) Schematic representation of the amino acid differences between GPVIa (red) and GPVIb (blue). (B) HEK-293T cells were transfected with empty vector (–) or expression constructs for human FcRγ and either GPVIa or GPVIb, both with a myc epitope tag at the C-terminus. Whole cell lysates extracted with 1% Triton X-100 lysis buffer were Western blotted with an anti-myc antibody. (C) RNA was extracted from HEL cells and reverse transcribed into cDNA. The cDNA region containing differences in GPVIa and GPVIb was amplified by PCR and sequenced. The cDNA sequences were translated into amino acid sequences (between amino acids 215 to 333) and aligned with GPVIa and b consensus. Sequence differences are highlighted in red. ADAM10 cleavage site is indicated with a triangle. Boxed region represents transmembrane domain.

4.2.6 Tspan15/ADAM10 and Tspan33/ADAM10 are the scissors for GPVIb

It has been shown that there is no difference between the extent of cleavage of GPVIa and GPVIb in transfected wild-type HEK-293T cells, but the specific TspanC8/ADAM10 scissor was not determined (Matthews, 2019). To determine the scissors for GPVIb, expression constructs encoding FcRγ and either C-terminal myc-tagged GPVIa or GPVIb were transfected into wild-type, ADAM10-knockout, Tspan15-knockout, Tspan33-knockout and Tspan15/33 double knockout HEK-293T cells. Cells were stimulated with the metalloprotease activator NEM for 30 minutes, and cleavage was assessed as described in previous chapters (Section 2.8.1 and 3.2.1).

The cleavage patterns were comparable between GPVIa and GPVIb across all cell types (Figure 30). Similar to GPVIa, GPVIb cleavage was also reduced by 50% in Tspan15-knockout cells and was reduced to a level comparable to ADAM10-knockout cells in Tspan15/33 double knockout cells. In NEM-stimulated cells, GPVIb cleavage in Tspan33-knockout cells was ~20% lower, suggesting that GPVIb may be less susceptible to cleavage by Tspan15/ADAM10 scissors than GPVIa in the absence of Tspan33. Nevertheless, the results suggest that the scissor identities for GPVIa and GPVIb are the same.

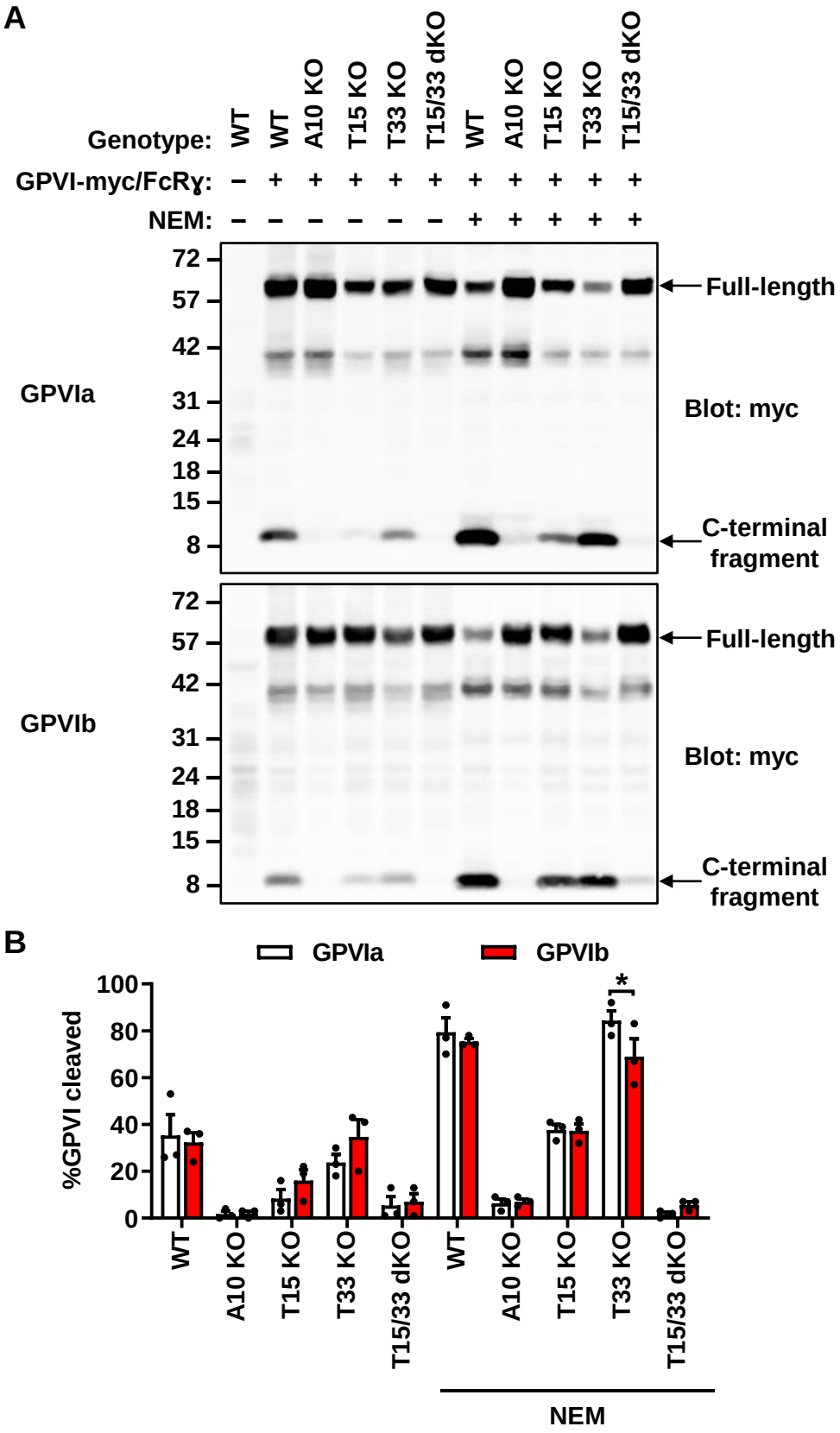
A
Genotype:
WT
WT
A10 KO
T15 KO
T33 KO
T15/33 dKO
WT
A10 KO
T15 KO
T33 KO
T15/33 dKO
GPVI-myc/FcRγ:
NEM:
GPVIa
GPVIb
Blot: myc
Full-length
C-terminal fragment
72
57
42
31
24
18
15
8
B
GPVIa
GPVIb
%GPVI cleaved
100
80
60
40
20
0
*
NEM

Figure 30. GPVIa and GPVIb are not differentially cleaved by TspanC8/ADAM10 complexes in transfected HEK-293T cells. (A) Wild-type (WT), ADAM10 (A10)-knockout (KO), Tspan15 (T15) KO, Tspan33 (T33) KO and Tspan15/33 (T15/33) double KO (dKO) HEK-293T cells were transfected with constructs encoding C-terminal myc-tagged human GPVI of either variant a (GPVIa; top panel) or variant b (GPVIb; bottom panel) and FcRɣ, or an empty vector control (–). After 24 hours, cells were treated with 2 mM NEM (+) or ethanol as vehicle control (–) for 30 min and lysed in 1% Triton X-100 lysis buffer. Lysates were subjected to anti-myc Western blotting. (B) The percentage of GPVI cleaved from panel A was quantitated, arcsine-transformed and statistically analysed by a two-way ANOVA with a Bonferroni's multiple comparisons test (*p<0.05). Error bars represent standard errors of the mean from three independent experiments.

4.3 Discussion

This chapter analysed *TSPAN15* and *GP6* variants associated with thrombosis and revealed that (1) a *TSPAN15* minor haplotype consisting of non-coding variants is associated with reduced venous thrombosis risk and higher *TSPAN15* expression; and (2) the two common GPVI haplotypes associated with thrombosis risk, GPVIa and GPVIb, are both cleaved by Tspan15/ADAM10 and Tspan33/ADAM10 scissors.

The first part of this chapter confirmed the association of the two previously reported SNPs, rs78707713 and rs17490626, with venous thromboembolism and other traits related to venous blood clots in the UK Biobank cohort, and identified 15 other non-coding variants that are in strong linkage disequilibrium. Therefore, these variants are likely to be inherited together to constitute a common haplotype in the British population. How does the minor haplotype confer protection to venous thrombosis? Although the meta-analysis by Germain *et al.* (2015) found an association of rs78707713 to *TSPAN15* expression in endothelial cells, macrophages and oesophagus mucosa, and DNA methylation in blood, the authors did not report the direction and specificity of the associations. This chapter revealed that individuals with the minor haplotype have increased mRNA expression that is specific to *TSPAN15* in multiple tissues, including whole blood, the tissue which is most relevant to venous thrombosis. This effect could be attributed to the two regulatory variants located within 15 kb upstream of the *TSPAN15* locus, rs77784890 and rs7475662. Changes at the epigenetic level, such as histone modification and transcription factor binding, could arise from these SNPs; indeed, SNPs in the regulatory region of other genes have been shown to alter histone modification, which in turn affects gene expression and lead to disease (Becanovic *et al.*, 2015; Gu *et al.*, 2017). It is interesting to note that individuals with the minor haplotype have increased platelet size, which contrasts with reduced risk for venous thromboembolism because of its positive association with higher mean

platelet volume (Brækkan *et al.*, 2010; Kovács *et al.*, 2019). However, the significance of mean platelet volume as a marker of platelet activation and clinical relevance is highly debatable as it is affected by multiple variables, including time of sample collection and measurement methodologies (Noris, Melazzini and Balduini, 2016; Lippi, Sanchis-Gomar and Favaloro, 2020). In fact, a decrease in mean platelet volume was found in venous thromboembolism patients whose samples were collected at least one day after the diagnosis (Lippi, Buonocore and Cervellin, 2016). Future studies should aim to examine whether individuals with the minor *TSPAN15* haplotype have increased Tspan15 protein expression in platelets, other blood cells and endothelial cells, and to determine whether epigenetic control or transcription in the affected cell types is modified by the regulatory SNPs with chromatin immunoprecipitation (ChIP) or transcriptional reporter assays.

The second part of this chapter examined whether differential ADAM10 cleavage by TspanC8s would explain the association of the *GP6* coding SNPs with thrombosis. The results show that Tspan15/ADAM10 and Tspan33/ADAM10 are also the scissors for the rarer GPVIb, although interestingly, GPVIb cleavage was lower than GPVIa only in NEM-stimulated Tspan33-knockout cells, suggesting that GPVIb may be less susceptible to cleavage by Tspan15/ADAM10 scissors. As basal cleavage was not different and given the modest difference in NEM-stimulated cells, follow-up experiments in cell lines were not pursued. In terms of ADAM10-mediated proteolysis, one would not predict differential cleavage between GPVIa and GPVIb based on sequence variation and findings from Chapter 3, as the closest T249A substitution is far from the ADAM10 cut site (between R262 and Q263). On the other hand, however, the result is, to a small extent, in line with the hypothesis by Trifiro *et al.* (2009), who proposed that the extent of GPVIb cleavage may be less than GPVIa due to increased binding of GPVIb to calmodulin by the Q317L substitution in the cytoplasmic tail, making it

less susceptible to ADAM10 cleavage. To rule this out, the ideal experiment would be a direct comparison of the effects of Ca^{2+}-dependent and Ca^{2+}-independent GPVI cleavage in individuals with the two haplotypes.

Based on the results of this chapter, it is unlikely that differential cleavage by Tspan15/ADAM10 and Tspan33/ADAM10 scissors would contribute to the association of GPVIa and GPVIb with venous and arterial thrombosis, respectively. Indeed, this is consistent with the study by Trifiro *et al.* (2009) that showed no difference in expression level or ligand-binding capacities between the two variants, even though GPVIb has impaired signalling, suggesting that variations in the ectodomain did not substantially affect GPVI function or cleavage. The reason why GPVIa and GPVIb are differentially associated with increased venous and arterial thrombosis risks remains unclear, owing to conflicts in the literature. It was demonstrated that white, non-Hispanic Americans with *GP6a*, *GP6b* or heterozygotes have similar levels of total and surface GPVI (Trifiro *et al.*, 2009). However, other studies conducted in the British population reported reduced GPVI expression in individuals with the *GP6b* haplotype (Joutsi-Korhonen *et al.*, 2003; Jones *et al.*, 2007; Petersen *et al.*, 2017). Since *GP6* is highly polymorphic (Jandrot-Perrus, Hermans and Mezzano, 2019), additional effects on GPVI expression could be contributed by other polymorphisms found exclusively in each donor population. In line with this, could this mean that the differential associations of GPVIa and GPVIb with higher risks of venous and arterial thrombosis, respectively, are also indirect contributions from other polymorphisms? Despite the conflict in expression phenotypes, all studies reported reduced platelet activation or ligand-mediated signalling responses with GPVIb, which was also demonstrated elegantly in a study showing the contribution of GPVIb to impaired collagen-mediated thrombus formation (van Geffen *et al.*, 2019). Although arterial and venous thrombi are structurally and mechanistically distinct, both are contributed by

unwanted platelet activation (Section 1.5.2). Therefore, it would make more sense if individuals with GPVIb are associated with lower risk of thrombosis. Extending the investigations of the effects of *GP6* polymorphisms on ligand-mediated signalling and thrombus formation to GPVI-fibrin interaction may provide additional clues to the differential associations of GPVIb and GPVIa with arterial and venous thrombosis. Given that cardiovascular disease is complex and multifactorial, increased statistical power with greater sample sizes in future GWASs, or further stratification into different groups such as according to cancer status (Skille *et al.*, 2020), may also help determine the extent of the contributions from *GP6* polymorphisms. Importantly, regardless of whether *GP6* polymorphisms contribute to thrombosis, downregulation of GPVI remains a promising anti-platelet strategy (Section 1.5.4).

Finally, taking into consideration of the association of *GP6* and *TSPAN15* with venous thrombosis, could individuals with the minor *TSPAN15* haplotype confer protection against venous thrombosis via their higher Tspan15 levels on platelets, which in turn lead to increased GPVI shedding and reduced platelet activation? This and other potential mechanisms will be discussed in Chapter 7.

CHAPTER 5
HOW DO TSPAN15 AND ADAM10 REGULATE EACH OTHER?

5.1 Preface

Most data related to this chapter were published as part of a larger study in Koo *et al.* (2020). This study includes data generated during my employment as a Research Technician in 2017 and during my PhD studentship in 2018-2019. My specific contributions during each period are listed below.

Research Technician:

1. Validation of the first Tspan15 mAbs (verifying previous data with new mAbs for Figure 1B; Figure 1C).
2. Optimisation of Tspan15 mAbs for ADAM10 co-immunoprecipitation in Jurkat T cells (related to Figure 1D; unpublished).
3. Epitope mapping of the Tspan15 mAbs (Figure 2A).
4. Colocalisation of Tspan15 and ADAM10 on the cell surface (Figure 4).
5. Assessment of Tspan15 protein expression in ADAM10-knockout cells (Figure 6C and 6F; repeating and verifying previous data with new mAbs for Figure 6A).

PhD studentship:

1. Epitope mapping of the Tspan15 mAbs (Figure 2B; repeating and rectifying previously generated data for Figure 2D; Tspan15 structure prediction in Figure 2E).
2. Assessment of *TSPAN15* mRNA expression in ADAM10-knockout cells (Figure 6D).

3. Assessment of the effect of inhibiting lysosomal degradation in Tspan15 expression in ADAM10-knockout cells (Figure 6E).
4. Assessment of the dynamics of ADAM10 and Tspan15 complexes (Figure 8, in collaboration with Joëlle Goulding, Steve Briddon and Nicholas Holliday at the University of Nottingham).
5. Presentation and writing of all figures and their legends.
6. Writing of relevant sections of the original draft and editing of other sections.

This chapter will therefore only include some published data generated during my PhD studentship (items 2-4) and additional related unpublished data, some of which were contributions to Seifert *et al.* (2021) (Sections 5.3.4 and 5.3.5).

5.2 Introduction

The six TspanC8s are well characterised for their essential roles in promoting ADAM10 exit from the ER, its maturation in the Golgi and trafficking to the cell surface or intracellular compartments (Dornier *et al.*, 2012; Haining *et al.*, 2012). Generating tetraspanin mAbs has traditionally been challenging (Rubinstein, Charrin and Tomlinson, 2013). To date, the only effective TspanC8 mAbs available are for Tspan5 and Tspan15 (Saint-Pol, Billard, *et al.*, 2017; Koo *et al.*, 2020). Using the first Tspan5 and Tspan15 mAbs, emerging evidence suggest that ADAM10 also reciprocally regulates Tspan5 and Tspan15 expression and trafficking at the endogenous level (Saint-Pol, Billard, *et al.*, 2017; Eschenbrenner *et al.*, 2020; Koo *et al.*, 2020). Since Tspan15 promotes GPVI shedding by ADAM10 (Chapter 3) and because low *TSPAN15* expression may be linked to increased venous thrombosis risk (Chapter 4), this chapter aimed to provide more insights into the mechanism of how ADAM10 regulates Tspan15 expression.

The second aim of this chapter was to compare how Tspan15 regulates ADAM10 expression on the cell surface in comparison to the other two platelet TspanC8s, Tspan14 and Tspan33. It was recently discovered that ADAM10 activity is required to maintain its expression on the cell surface (Seifert *et al.*, 2021). Given that TspanC8s are essential components of ADAM10 scissor complexes, the hypothesis that TspanC8s differentially affect ADAM10 downregulation on the cell surface following inhibition was investigated.

Previous studies have examined the dynamics of either ADAM10 or a TspanC8, but without knowing whether these proteins were in isolation, or together in a complex (Jouannet *et al.*, 2016; Eschenbrenner *et al.*, 2020). Therefore, the final aim of this chapter was to establish a live-cell single-molecule spectroscopy technique to characterise Tspan15/ADAM10 scissor complexes on the cell surface.

5.3 Results

5.3.1 ADAM10 does not regulate *TSPAN15* transcription

ADAM10 is required for Tspan15 expression on the cell surface in multiple cell lines (Eschenbrenner *et al.*, 2020; Koo *et al.*, 2020) and primary cells (Koo *et al.*, 2020). This has also been demonstrated at the whole cell level in Jurkat T cells, as total Tspan15 expression in ADAM10-knockout cells is similarly reduced by ~80% (Koo *et al.*, 2020). Cleavage of Notch by ADAM10 is a prerequisite for the subsequent γ-secretase cleavage and release of the Notch intracellular domain into the nucleus, where it acts as a master transcriptional regulator of many downstream target genes (Wang *et al.*, 2015). ADAM10 itself or its intracellular domain can also translocate to the nucleus, suggesting its potential role in regulating transcription (Arima *et al.*, 2007; Tousseyn *et al.*, 2009). To determine if ADAM10 affects *TSPAN15* transcription, *TSPAN15* mRNA expression was assessed by RT-qPCR in three ADAM10-knockout cell lines: HEK-293T, A549 and Jurkat cells. In all three cell lines, *TSPAN15* mRNA expression in ADAM10-knockout cells was comparable to wild-type cells (Figure 31). This suggests that ADAM10 does not regulate *TSPAN15* transcription.

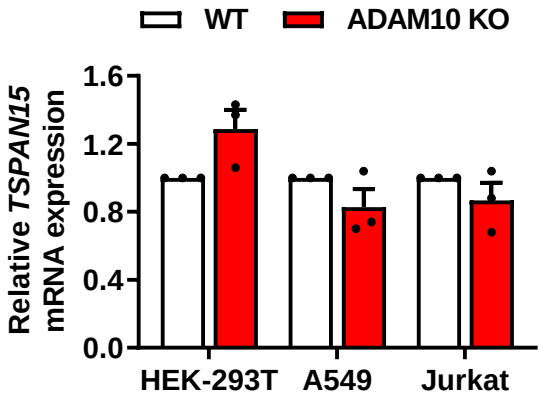

Figure 31. *TSPAN15* mRNA expression is not affected by ADAM10 deficiency. RNA was extracted from wild-type (WT) and ADAM10-knockout (KO) HEK-293T, A549 and Jurkat cells. The reverse transcribed cDNA was subjected to quantitative PCR to measure *TSPAN15* expression. Expression was normalised to the housekeeping control *GAPDH* and WT cells. Data were arcsine-transformed prior to a two-way ANOVA with Bonferroni's multiple comparisons test at the 5% significance level. Error bars represent standard errors of the mean from three independent experiments.

5.3.2 Tspan15 is degraded by lysosomes in the absence of ADAM10

Membrane proteins are primarily degraded by lysosomes (Jin, Kiral and Hiesinger, 2018). To investigate whether the reduction in Tspan15 protein expression in the absence of ADAM10 was due to protein degradation, cells were treated with ammonium chloride (NH_4Cl) for 20 hours to inhibit lysosomal proteolysis. A549 was chosen as the representative cell line as it has one of the highest Tspan15 expression levels among the cell lines used in the previous section (Koo *et al.*, 2020). Cells were harvested for flow cytometry to measure Tspan15 expression at the cell surface. Whole cell lysates were subjected to Tspan15 immunoprecipitation and Western blotting to measure total Tspan15 expression. Tspan15 expression at the cell surface was reduced by ~70% in ADAM10-knockout cells and was unaffected when cells were treated with NH_4Cl (Figure 32A). At the whole cell level, Tspan15 expression was reduced by ~80% in the absence of ADAM10, and this was increased by ~2.5-fold in NH_4Cl-treated ADAM10-knockout cells, but not in wild-type cells (Figure 32B). Inhibition of proteasomal degradation with the proteasome inhibitor MG132 in one experiment did not contribute to Tspan15 rescue, despite the accumulation of polyubiquitinated proteins in the cell lysate, which acted as a positive control for MG132 (Figure A3, Appendix). Interestingly, two extra Tspan15 bands, one slightly above and one slightly below the band in wild-type cells, were observed in ADAM10-knockout cells (Figure 32Bi and Figure A3, Appendix). The rescued Tspan15 in NH_4Cl-treated ADAM10-knockout cells also appeared predominantly at a higher molecular weight (Figure 32Bi). To investigate if the changes in molecular weight were due to altered N-glycosylation, Tspan15 immunoprecipitates were digested with the N-glycosidase, PNGaseF. In all conditions, the Tspan15 band collapsed to the same molecular weight at ~25 kDa, indicating that the absence of ADAM10 altered Tspan15 N-glycosylation (Figure 32C).

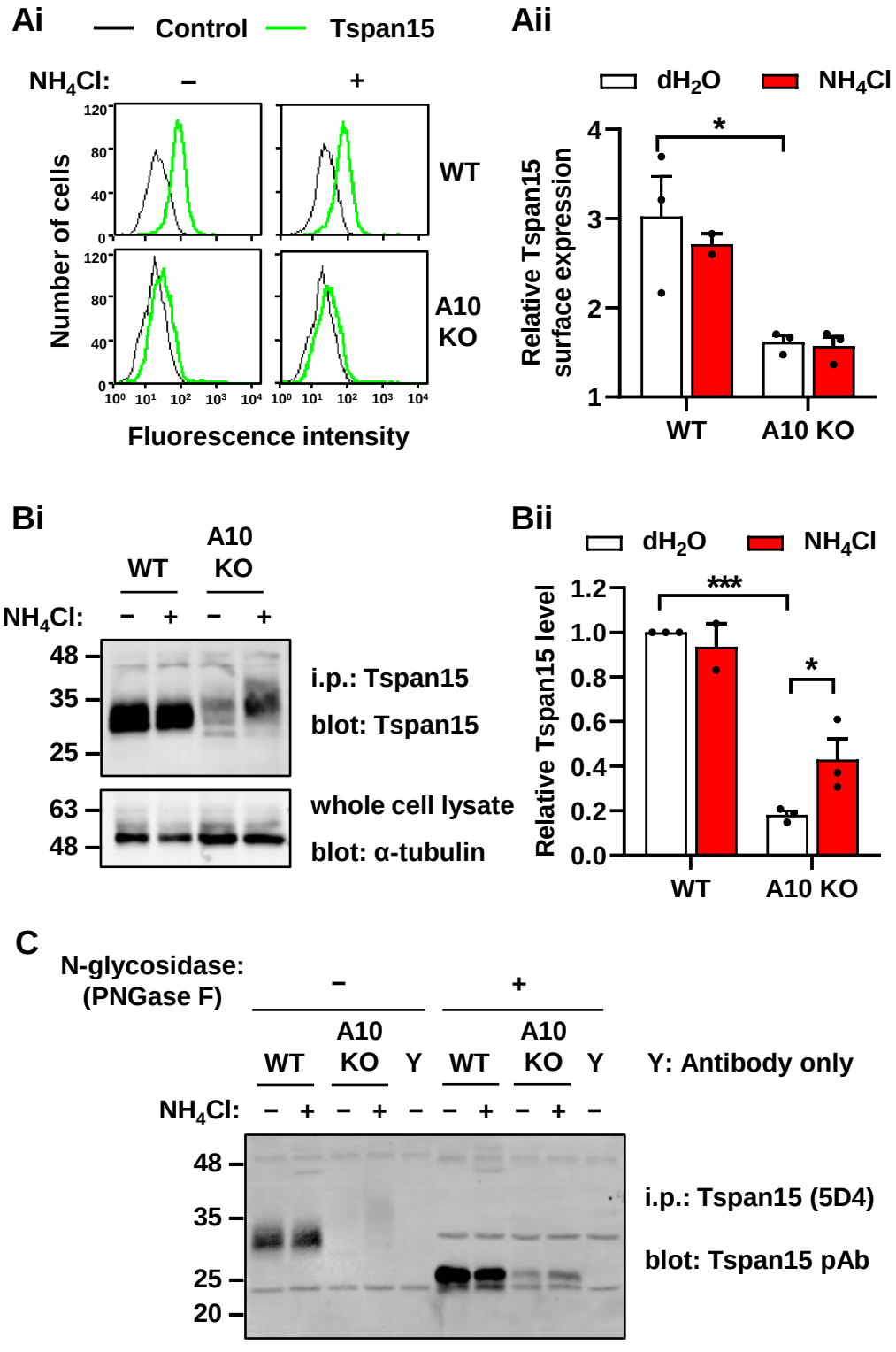

Figure 32. Lysosomal inhibition partially rescues Tspan15 expression in ADAM10-knockout cells. Wild-type (WT) and ADAM10-knockout (A10 KO) A549 cells were treated with 50 mM NH_4Cl (+) or dH_2O as the vehicle control (–) for 20 hours to inhibit lysosomal degradation. (Ai) Cells were stained with Tspan15 mAb (green) and isotype control (black) and analysed by flow cytometry. (Aii) Tspan15 surface expression was quantitated and presented as geometric mean intensity of Tspan15 staining relative to the isotype control staining. Data were log-transformed and statistically analysed by a two-way ANOVA with Bonferroni's multiple comparisons test (*p<0.05). Error bars represent standard errors of the mean

from three independent experiments. (Bi) Cells were lysed in 1% Triton X-100 lysis buffer. Lysates were immunoprecipitated and Western blotted with Tspan15 mAbs. Lysates were also blotted for α-tubulin as a loading control. (Bii) The amount of immunoprecipitated Tspan15 was quantitated, normalised to tubulin expression, and presented relative to WT cells. Data were arcsine-transformed and statistically analysed by a two-way ANOVA with Bonferroni's multiple comparisons test (*p<0.05, ***p<0.001). Error bars represent standard errors of the mean from three independent experiments. (C) Tspan15 immunoprecipitates and control Tspan15 mAb-coated beads were left undigested (–) or digested with the N-glycosidase, PNGase F (+) under reducing conditions. Undigested and digested samples were subjected to Western blotting with Tspan15 pAb against the C-terminus. The blot is representative of two independent experiments.

5.3.3 ADAM10 cytoplasmic domain is required for Tspan15 surface expression

Previous data in the Tomlinson lab have shown that ADAM10 can rescue Tspan15 expression on the cell surface when reintroduced into ADAM10-knockout HEK-293T cells. Evidence so far suggests that Tspan15 cytoplasmic tails have supporting roles in maintaining ADAM10 surface expression (Chapter 3) (Eschenbrenner *et al.*, 2020). To determine whether the reverse is true, dual-colour flow cytometry was used to assess Tspan15 surface expression in ADAM10-knockout HEK-293T cells transfected with expression constructs for wild-type ADAM10 or two different ADAM10 cytoplasmic domain mutants (Figure 33A).

The first ADAM10 mutant was ADAM10(DCS), which consists of the disintegrin, cysteine-rich and stalk region (DCS) of ADAM10. It was expressed using a pDISPLAY vector that has an N-terminal secretion signal sequence and the transmembrane domain of the platelet-derived growth factor receptor (PDGFR) at the C-terminus to target ADAM10(DCS) to the cell surface, which has been shown to be sufficient for Tspan15 interaction via co-immunoprecipitation experiments (Noy *et al.*, 2016). Both wild-type full-length ADAM10 and ADAM10(DCS) were expressed at comparable levels (Figure 33B). Tspan15 surface expression was reduced by 75% in ADAM10-knockout cells, and was increased by 2.1-fold in the ADAM10-knockout cells transfected with wild-type ADAM10, although this increase was not statistically significant (Figure 33B). Tspan15 surface expression was also rescued to a lesser extent in

ADAM10(DCS)-transfected cells (Figure 33B). This suggests that interaction via the ADAM10 DCS region may be sufficient to deliver Tspan15 to the cell surface. However, ADAM10(DCS) must be expressed in the pDISPLAY vector because it does not get to the cell surface otherwise, as determined previously when expressed on an ADAM17 backbone (Noy *et al.*, 2016). Therefore, one limitation was that the small increase in rescued Tspan15 could be an artifact from increased stability by the cell-surface anchored ADAM10(DCS).

To address the above limitation, a second ADAM10 mutant that lacks the cytoplasmic tail but retained the rest of the protein was used (ADAM10(ΔC)) (Figure 33A), as it was shown to be able to reach the cell surface in a standard pcDNA3.1 expression vector (Maretzky *et al.*, 2015). Interestingly, Tspan15 surface expression was reduced by a further 2.3-fold in ADAM10-knockout cells transfected with ADAM10(ΔC), in contrast to the 2.3-fold rescue seen with wild-type ADAM10, when both mutants were expressed at a comparable level when reconstituted in ADAM10-knockout cells (Figure 33C).

Together, these data suggest that the cytoplasmic tail of ADAM10 may have a role in maintaining Tspan15 expression on the cell surface.

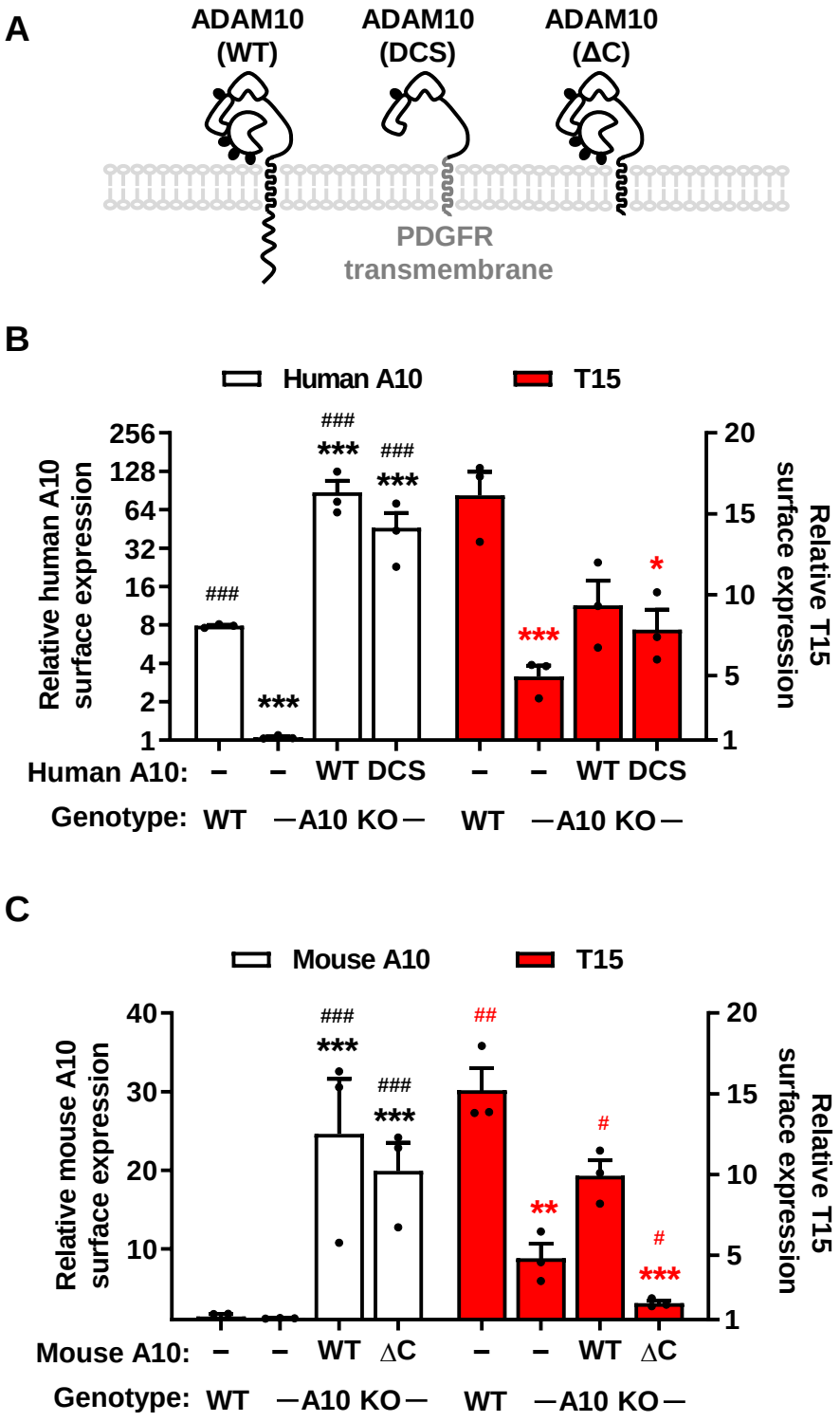

Figure 33. ADAM10 cytoplasmic domain is required for Tspan15 surface expression. (A) Schematic representation of wild-type (WT) ADAM10 and mutants: the disintegrin, cysteine-rich and stalk region (DCS) of ADAM10 (linked to the transmembrane domain of the platelet-derived growth factor receptor (PDGFR) in a pDISPLAY vector) and ADAM10 lacking the cytoplasmic tail (ΔC). (B) ADAM10-knockout (A10 KO) HEK-293T cells were transfected with expression constructs for human WT ADAM10 and ADAM10(DCS) or empty vector (–) for 40 hours. Cells were double-stained for ADAM10 and Tspan15 (T15) and analysed by flow cytometry to measure the surface expression of ADAM10 and Tspan15 in ADAM10-transfected cells. Surface expression of ADAM10 and Tspan15 in

WT cells were also quantitated as a control. Expression was presented as geometric mean intensity of target protein staining relative to the isotype control staining. Data were log-transformed and statistically analysed by a two-way ANOVA with Tukey's multiple comparisons test (*p<0.05, **p<0.01, ***p<0.001, compared to WT cells; $^{\#}p$<0.05, $^{\#\#}p$<0.01, $^{\#\#\#}p$<0.001, compared to empty vector-transfected ADAM10 KO cells). Error bars represent standard errors of the mean from three independent experiments. (C) Experiment design and analysis were as described in panel B, but cells were transfected with expression constructs for mouse ADAM10 and ADAM10(ΔC).

5.3.4 ADAM10 inhibition reduces ADAM10 and Tspan15 surface expression

A previous study observed that the ADAM10 inhibitor GI254023X reduced ADAM10 surface expression in the myeloid cell lines THP-1 and U937, in a time-dependent manner (Ezekwe, Weng and Duncan, 2016). Given that Tspan15 regulates ADAM10 expression and *vice versa*, the possibility that Tspan15 surface expression was also downregulated following GI254023X treatment was investigated. Jurkat and A549 cells, which have high levels of ADAM10 and Tspan15 on the cell surface (Koo *et al.*, 2020), were treated with 2.5 μM GI254023X (IC_{50}<2 μM for membrane-bound ADAM10) (Ludwig *et al.*, 2005) for an extended period of 48 hours. Flow cytometry analysis revealed that surface ADAM10 and Tspan15 was reduced by ~50% and ~20% in Jurkat cells, and ~70% and ~80% in A549 cells, respectively (Figure 34). During the investigation, the Ludwig group has also demonstrated similar observations described in Ezekwe *et al.* (2016) in multiple cell lines (THP-1, A549 and HEK-293 cells) and *in vivo* in mice; they showed that the effect was time- and dose-dependent, with maximal reduction in ADAM10 surface expression seen when THP-1 cells were treated with 10 μM GI254023X for 24 hours (Seifert *et al.*, 2021). Using this optimised condition, HEK-293T cells, which express lower levels of ADAM10 and Tspan15 (Koo *et al.*, 2020), were found to have ~50% and ~40% reduction in surface ADAM10 and Tspan15, respectively (Figure 34). These data suggest that Tspan15 was downregulated together with ADAM10 in multiple cell types.

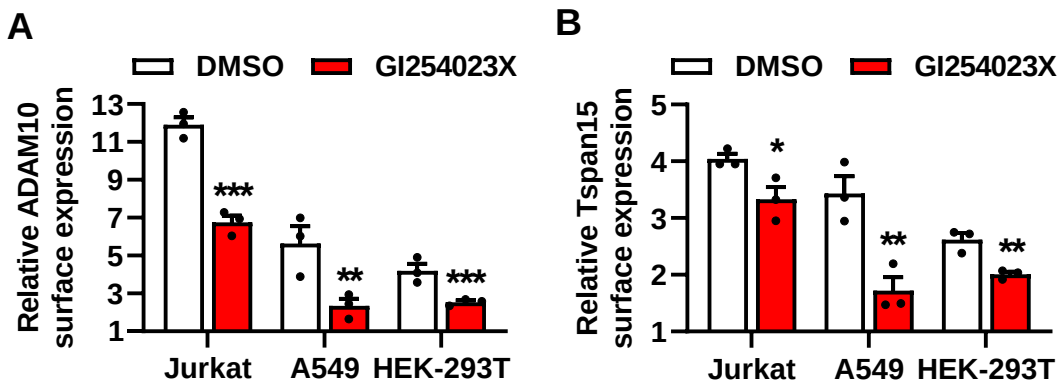

Figure 34. ADAM10 inhibition reduces ADAM10 and Tspan15 surface expression. Jurkat and A549 cells were treated with 2.5 μM of the ADAM10 inhibitor GI254023X, or DMSO as the vehicle control for 48 hours; inhibitor was reapplied every 24 hours. HEK-293T cells were treated with 10 μM of GI254023X for 24 hours for maximal ADAM10 reduction. Surface expression of (A) ADAM10 and (B) Tspan15 was assessed by flow cytometry. Expression was presented as geometric mean intensity of the target protein staining relative to the isotype control staining. Experiments for each cell type were done at different times but presented on the same graph for simplicity. Data were log-transformed and statistically analysed by a two-tailed *t*-test (**p*<0.05, ***p*<0.01, ****p*<0.001, compared to DMSO control). Error bars represent standard errors of the mean from three independent experiments.

5.3.5 Tspan15 minimises surface ADAM10 reduction following ADAM10 inhibition

Findings in the previous section prompted a follow-up investigation to determine whether TspanC8s differentially regulate GI254023X-mediated ADAM10 surface reduction. HEK-293T cells were chosen due to the availability of a range of TspanC8-knockout cells. ADAM10 surface expression was assessed by flow cytometry in control and GI254023X-treated wild-type, Tspan14-knockout, Tspan15-knockout, Tspan33-knockout and Tspan15/33 double knockout cells, in two different sets of knockout clones. In all cell types, GI254023X treatment led to substantial reduction in surface ADAM10 (Figure 35Ai and Bi). ADAM10 reduction was the greatest in the absence of Tspan15, as seen in Tspan15-knockout and Tspan15/33 double knockout cells (Figure 35Aii and Bii). Importantly, this difference was not due to differences in ADAM10 surface expression in the knockout cells; this was best demonstrated in the second set of knockout clones, which showed striking differences in the percentage of GI254023X-mediated ADAM10 reduction in cells deficient in Tspan14, Tspan15 or Tspan33 (Figure 35Bii), despite similar levels of ADAM10 in DMSO-treated control cells.

These data suggest that the presence of Tspan15 minimises ADAM10 downregulation on the cell surface following ADAM10 inhibition.

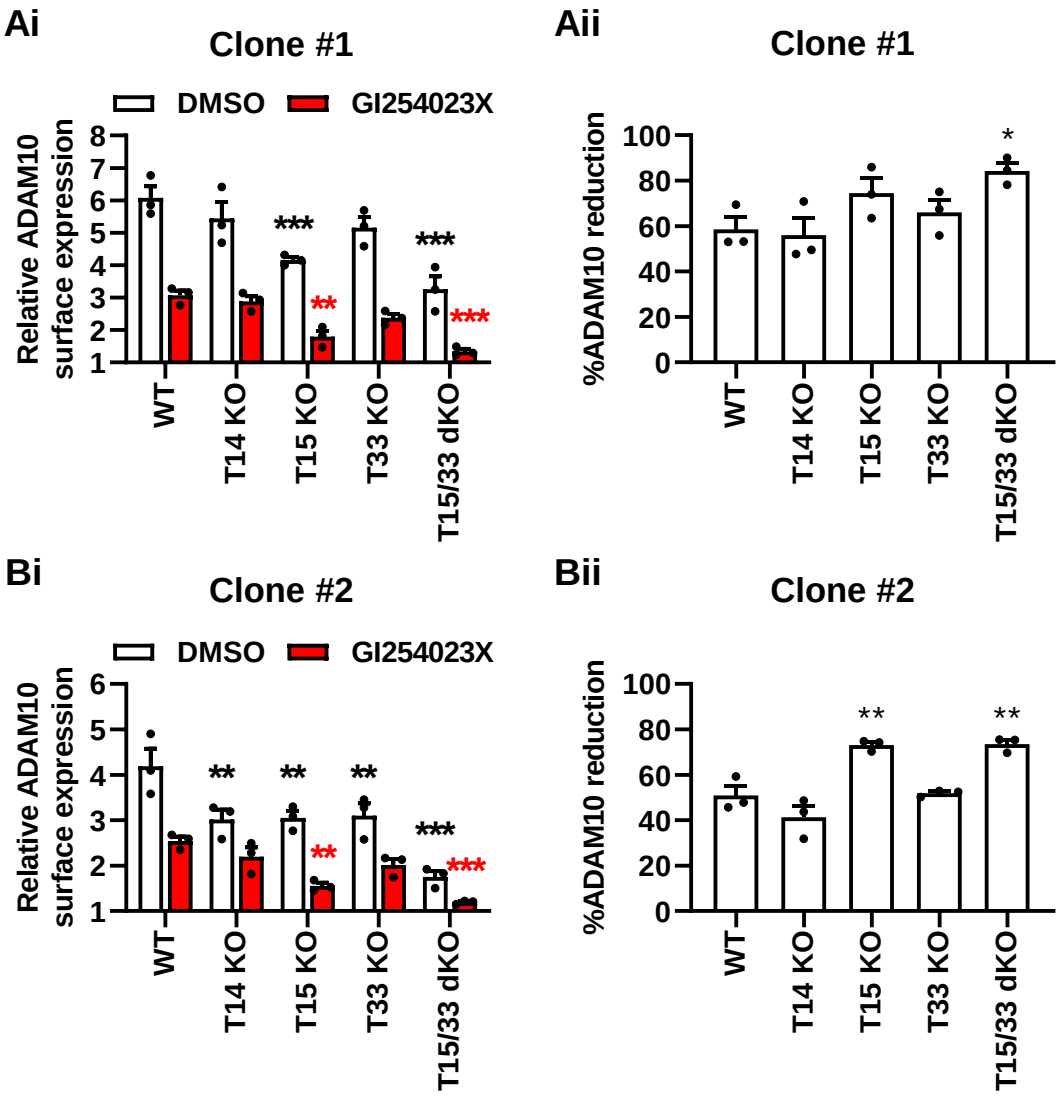

Figure 35. Tspan15 minimises surface ADAM10 reduction following ADAM10 inhibition. (Ai) Wild-type (WT), Tspan14-knockout (T14 KO), Tspan15-knockout (T15 KO), Tspan33-knockout (T33 KO) and Tspan15/33 double KO (T15/33 dKO) HEK-293T cells were treated with 10 μM of the ADAM10 inhibitor GI254023X, or DMSO as the vehicle control for 24 hours. Surface expression of ADAM10 was assessed by flow cytometry. Expression was presented as geometric mean intensity relative to the isotype control staining. Data were log-transformed and statistically analysed by a two-way ANOVA with Dunnett's multiple comparisons test (**p<0.01, ***p<0.001, compared to the respective WT controls). Error bars represent standard errors of the mean from three independent experiments. (Aii) The percentage of surface ADAM10 reduction following ADAM10 inhibition from panel Ai was quantitated. Data were arcsine-transformed and statistically analysed by a one-way ANOVA with Dunnett's multiple comparisons test (*p<0.05, **p<0.01, compared to WT). (Bi-ii) Experiment was as described in panel Ai-ii in a different set of knockout clones.

5.3.6 Tspan15/ADAM10 are dynamic complexes that can cluster on the cell surface

ADAM10 dynamics has been shown to be differentially regulated by TspanC8s, using Tspan5 and Tspan15 as model TspanC8s (Jouannet *et al.*, 2016; Eschenbrenner *et al.*, 2020). However, the dynamics of a TspanC8/ADAM10 complex has not been examined before. In this section, fluorescence correlation spectroscopy (FCS) was used to characterise Tspan15/ADAM10 bimolecular fluorescence complementation (BiFC) complexes on the cell surface. BiFC is a technique that generates a fluorescent dimer from two interacting proteins tagged separately with non-fluorescent halves of a fluorescent protein (Kerppola, 2006) (Figure 36A). FCS is a sensitive live-cell spectroscopy technique that measures the fluorescence fluctuations of molecules diffusing through a defined confocal volume of ~0.2 μm^3 and can provide metrics on the dynamics and brightness of fluorescent complexes when coupled with downstream statistical modelling (Briddon, Kilpatrick and Hill, 2018). Since cells are exposed to continuous high-power excitation laser during FCS, a more photostable superfolder GFP (sfGFP) was used for BiFC (Kilpatrick, Briddon and Holliday, 2012).

HEK-293T cells were transfected with expression constructs for ADAM10 tagged with the C-terminal half of sfGFP, Tspan15 tagged with N-terminal half of sfGFP, or both (Figure 36A). Flow cytometry confirmed the formation of the fluorescent Tspan15/ADAM10 BiFC complexes only when both constructs were expressed (Figure 36B). Confocal microscopy confirmed the expression and predominant localisation of the Tspan15/ADAM10 BiFC dimers on the cell surface, similar to Tspan15 labelling on the same cells (Figure 36C).

Using FCS, the lateral diffusion of Tspan15/ADAM10 complexes on the apical membrane of transfected HEK-293T cells was quantified with downstream autocorrelation analysis of the FCS data. On average, there were 48 fluorescent particles/μm^2 with an average diffusion

coefficient of 0.19 $\mu m^2/s$ (Figure 37A-B). Additionally, photon counting histogram (PCH) analysis of the FCS data was conducted to examine the average molecular brightness and oligomerisation status of Tspan15/ADAM10 BiFC complexes. This revealed that most of the FCS traces preferentially fitted to a one-component PCH model of a single average brightness value of 2.2×10^4 cpm/s; the remaining 42% preferentially fitted to a two-component model with two distinct brightness levels: a dimmer subcomponent with an average brightness of 1.4×10^4 cpm/s that was not statistically different ($p>0.05$) to the one-component brightness, and a brighter subcomponent with an average brightness of 5.4×10^4 cpm/s (Figure 37C). The distinct brightness grouping indicates that Tspan15/ADAM10 BiFC complexes can form clusters of different sizes. Taken together, the data suggest that Tspan15/ADAM10 complexes are dynamic and can cluster on the cell surface.

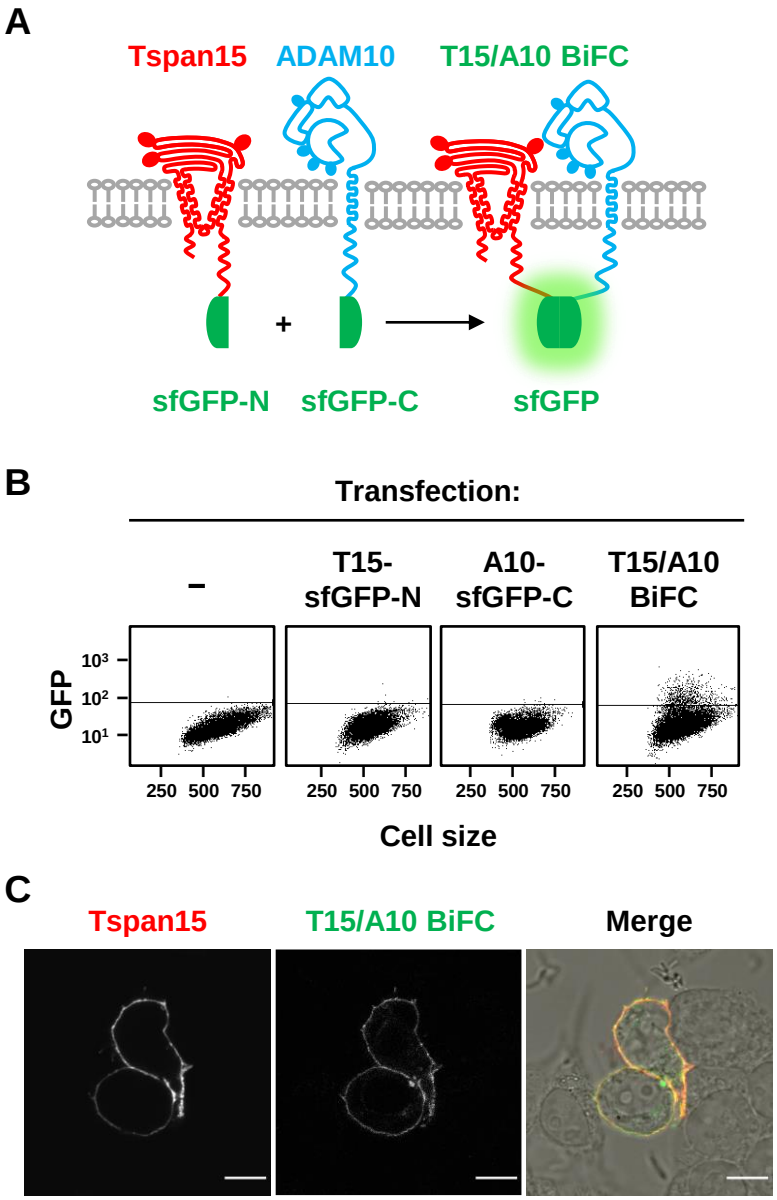

Figure 36. Validation of Tspan15/ADAM10 superfolder GFP (sfGFP) bimolecular fluorescence (BiFC) complexes. (A) Schematic representation of a Tspan15/ADAM10 (T15/A10) sfGFP BiFC dimer. The dimer is formed when Tspan15 tagged with the N-terminal half of sfGFP interacts with ADAM10 tagged with the C-terminal half of sfGFP. (B) HEK-293T cells were transfected with either of, or both, Tspan15 and ADAM10 sfGFP BiFC expression constructs, or empty vector control (–) for 24 hours and analysed by flow cytometry. Dot plots are representative of two independent experiments. (C) Cells transfected with both Tspan15 and ADAM10 sfGFP BiFC expression constructs were fixed and stained with Alexa Fluor 647-conjugated Tspan15 mAb for imaging of Tspan15 (red) and sfGFP (green) by confocal microscopy. The middle-plane images are representative of two independent experiments. Scale bar: 10 μm.

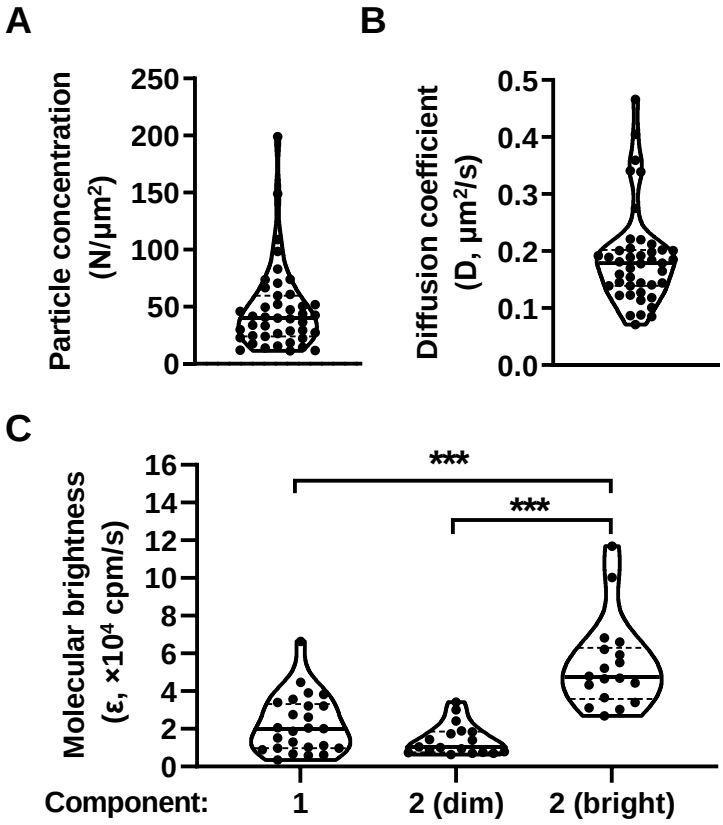

Figure 37. ADAM10/Tspan15 bimolecular fluorescence (BiFC) dimers are dynamic and can cluster on the cell surface. HEK-293T cells were transfected with both ADAM10 and Tspan15 superfolder GFP (sfGFP) BiFC expression constructs for 24 hours and analysed by fluorescence correlation spectroscopy (FCS) in live cells. Fluorescence fluctuation readings were collected from ADAM10/Tspan15 BiFC complexes on the apical membrane of transfected cells. Autocorrelation analysis of the FCS data was conducted to calculate the average (A) particle concentration (N: number of particles) and (B) diffusion coefficient of the complexes in the confocal volume. (C) The average molecular brightness of the complexes (cpm: counts per molecule) were calculated by photon counting histogram (PCH) analysis. The data preferentially fitted to two separate PCH models: a one-component model and a two-component model with two levels of brightness ('dim' and 'bright'). FCS traces were collected under the supervision of Dr. Joëlle Goulding, who also conducted the autocorrelation and PCH analyses. Data were from 43 cells in three independent experiments. Data were log-transformed and analysed by a one-way ANOVA with Tukey's multiple comparisons test (***p<0.001).

5.4 Discussion

How do TspanC8s and ADAM10 regulate each other? Using Tspan15 as the model TspanC8, findings in this chapter suggest that (1) ADAM10 promotes Tspan15 expression at the protein level, (2) the cytoplasmic tail of ADAM10 is required for Tspan15 surface expression, (3) ADAM10 inhibition downregulates ADAM10 and Tspan15 surface expression, but the presence of Tspan15 reduces surface ADAM10 downregulation, and (4) Tspan15/ADAM10 are dynamic complexes that can cluster on the cell surface.

The first aim of this chapter focused on how ADAM10 promotes Tspan15 expression. Similar to Tspan5, ADAM10 also promotes Tspan15 expression at the protein level because ADAM10 deficiency did not affect *TSPAN15* mRNA expression (Saint-Pol, Billard, *et al.*, 2017). Inhibiting lysosomes, but not proteasomes, partially restored intracellular Tspan15 expression in ADAM10-knockout cells but the rescued Tspan15 could not get to the cell surface. This suggests that Tspan15 may be unstable on the cell surface when not in complex with ADAM10, hence is rapidly internalised and targeted to lysosomes for degradation. Consistent with this, Tspan15 endocytosis increases in the absence of ADAM10 (Eschenbrenner *et al.*, 2020). Alternatively, Tspan15 may be trapped in the ER without ADAM10 and subsequently be targeted to the lysosomal degradation pathway for clearance (Fregno and Molinari, 2019). This is a possibility given that ADAM10 regulates Tspan5 exit from the ER (Saint-Pol, Billard, *et al.*, 2017).

Also similar to Tspan5 (Saint-Pol, Billard, *et al.*, 2017), Tspan15 N-glycosylation was altered in absence of ADAM10, as indicated by the presence of additional Tspan15 glycoforms in the absence of ADAM10. Tspan15 has three predicted N-glycosylation sites at N118, N189 and N230 on the large extracellular region, but comparisons with N-glycosylation mutants show

that Tspan15 is only glycosylated at N189 (Blacklow lab, unpublished). Therefore, it is possible that N118 and N230 are normally masked by ADAM10 interaction and can only be glycosylated in its absence. Since Tspan15 can be overexpressed on the cell surface in ADAM10-knockout cells (Koo *et al.*, 2020), it would be interesting to determine the predominant Tspan15 glycoform to examine this possibility, and whether the N-glycosylation of Tspan15 affects its interaction with ADAM10, hence its expression and function.

The discovery that the ADAM10 cytoplasmic tail is required for Tspan15 expression on the cell surface revealed another region on ADAM10, besides its extracellular region, that is important for Tspan15 regulation. The ADAM10 cytoplasmic tail has an arginine-rich ER-retention motif (Marcello *et al.*, 2010). Since ADAM10 and Tspan15 interact via their extracellular regions (Noy *et al.*, 2016), one would expect that deletion of the ADAM10 cytoplasmic tail would facilitate ER exit of both ADAM10 and Tspan15 and enhance expression of both proteins at the cell surface. In fact, it was shown that the ADAM10 tail-truncated mutant has a higher expression on the cell surface relative to its full-length counterpart (Maretzky *et al.*, 2015). Unexpectedly, the findings in this chapter suggest that ADAM10, but not Tspan15, can get to the cell surface efficiently without the ADAM10 cytoplasmic tail. As the level of endogenous Tspan15 in HEK-293T appears to be below the limit of detection for Western blotting of immunoprecipitates (Szyroka, 2019) and immunofluorescence microscopy (data not shown), it is currently not known whether the ADAM10 tail-truncated mutant restored Tspan15 expression intracellularly, and if so, whether their interaction was disrupted. Stable reconstitution of ADAM10-knockout cells with the tail-truncated mutant in another cell line with high Tspan15 expression, such as A549 or PC3, will be required to address this question. Nevertheless, this intriguing finding raises the possibility of ADAM10 and Tspan15 interaction at their cytoplasmic domains, which will be discussed further in Chapter 7.

The second aim of this chapter focused on how Tspan15 regulates ADAM10 surface expression. This was investigated in the context of ADAM10 activity inhibition by the preferential ADAM10 inhibitor GI254023X. Consistent with previous reports, surface ADAM10 was reduced in three different cell lines following prolonged treatment with GI254023X (Ezekwe, Weng and Duncan, 2016; Seifert *et al.*, 2021). This was accompanied by a reduction in surface Tspan15 in all three cell lines. However, Tspan15 surface downregulation in Jurkat cells was lower relative to ADAM10 in comparison to A549 and HEK-293T cells. This is in line with the previous finding in which ADAM10 surface expression was unaffected in Tspan15-knockout Jurkat cells, presumably due to presence of other more abundant TspanC8s, but contrasts with the finding that Tspan15 is reduced to the same extent as A549 and HEK-293T cells in ADAM10-knockout Jurkat cells (Koo *et al.*, 2020). In the latter, however, ADAM10 is completely depleted, and Tspan15 protein expression would already be inherently affected as discussed earlier in this chapter.

In contrast to the other two platelet TspanC8s, namely Tspan14 and Tspan33, the lack of Tspan15 alone enhanced the effect of ADAM10 downregulation on the surface following GI254023X treatment, therefore providing another piece of evidence demonstrating that Tspan15 promotes ADAM10 stability on the cell surface. It would be of interest to extend this finding to other cell lines, particularly Jurkat cells. Seifert *et al.* (2021) have demonstrated that the loss of ADAM10 from the cell surface following ADAM10 inhibition is accompanied by not only its internalisation and subsequent lysosomal degradation, but also its release into extracellular vesicles. In light of this, could the differential ADAM10 downregulation in TspanC8-knockout HEK-293T cells seen here be an effect of differential ADAM10 release into extracellular vesicles? This will be discussed in Chapter 7.

Finally, this chapter presents the first biophysical characterisation of the dynamics and organisation of a TspanC8 in complex with ADAM10 on the cell surface. Using BiFC in combination with FCS, the average lateral diffusion of Tspan15/ADAM10 BiFC complexes was found to be 0.19 $\mu m^2/s$. This is in the same order of magnitude as the diffusion coefficient reported for ADAM10 in Tspan15-transfected U2OS-N1 cells at 0.10 $\mu m^2/s$ using single-particle tracking (Jouannet *et al.*, 2016). In the same study, the diffusion coefficients of ADAM10 in Tspan5-transfected cells and non-transfected cells were lower, suggesting that ADAM10 diffusion speed is different depending on which TspanC8 it is in complex with. FCS of Tspan14/ADAM10 and Tspan33/ADAM10 BiFC complexes would be useful in determining whether there is any difference in their diffusion speed on the cell surface. Analysis of diffusion coefficient alone does not provide any indication on clustering because substantial changes will only be apparent with at least an eight-fold difference in size (Briddon, Kilpatrick and Hill, 2018). Therefore, another advantage of BiFC/FCS is the ability to extract information on the average molecular brightness of the particles. As brightness is proportional to the number of fluorescent units, the presence of particles of distinct brightness levels suggests that Tspan15/ADAM10 can form clusters of different sizes. With the use of controls of known oligomerisation states in future experiments, such as CD86, an obligate monomer and CD28, an obligate homodimer, the stoichiometry of TspanC8/ADAM10 complexes can be measured more accurately (Briddon, Kilpatrick and Hill, 2018).

In summary, this chapter provided further evidence that Tspan15 maintains ADAM10 surface expression and *vice versa*, and together they form a dynamic scissor complex on the cell surface.

CHAPTER 6
INVESTIGATING POTENTIAL TSPAN15 REDUNDANCY WITH OTHER TSPANC8S

6.1 Introduction

As introduced in Section 1.4.3.4, Tspan15 has emerged as an attractive therapeutic target for diseases such as cancer and arthritis. Findings in Chapter 3 suggests a potential novel anti-platelet strategy by inducing Tspan15/ADAM10-mediated GPVI shedding. Chapter 4 also suggests the potential for targeting Tspan15 in venous thrombosis. An important consideration in drug design is whether other proteins have redundant function with the target of interest. Functional compensation between the two closely related tetraspanins CD9 and CD81 in their roles in regulating cell-cell fusion has been well documented (Charrin *et al.*, 2014). In the TspanC8 subfamily, functional redundancies have been reported for all three *Drosophila* homologues (Tsp3A, 26A and 86D) in promoting Notch signalling (Dornier *et al.*, 2012). In a similar sense, Tspan5 and Tspan14 both promote Notch activation (Dornier *et al.*, 2012; Saint-Pol, Billard, *et al.*, 2017). Tspan5 and Tspan17, the two most closely related TspanC8s, have redundant roles in promoting lymphocyte transmigration through the downregulation of VE-cadherin on endothelial cells (Reyat *et al.*, 2017). Tspan15 and Tspan33 can both promote ADAM10 cleavage of GPVI (Matthews, 2019), although Chapter 3 has shown that Tspan15 is the more efficient TspanC8.

To evaluate the therapeutic potential of Tspan15, it was therefore important to address whether other closely related members in the TspanC8 subfamily can compensate for the loss of Tspan15, especially in a diseased state where other TspanC8s and ADAM10 may also be upregulated, such as in the case of pancreatic cancer, where transcriptomic data suggest the

upregulation of *TSPAN5, TSPAN14, TSPAN15, TSPAN17* and *ADAM10* (Tang *et al.,* 2019). The aim of this chapter is to emulate a potential extreme scenario in the diseased state by examining whether other TspanC8/ADAM10 scissors can cut Tspan15-dependent substrates when overexpressed in the absence of Tspan15. Three other Tspan15/ADAM10 substrates were tested alongside GPVI. These include RAGE and betacellulin, which showed loss of shedding in transfected ADAM10-knockout and Tspan15-knockout HEK-293T cells in recent studies in the Tomlinson lab, and N-cadherin, which is the best example of a Tspan15/ADAM10 substrate as demonstrated by several independent studies in different cell types (Prox *et al.*, 2012; Jouannet *et al.*, 2016; Noy *et al.*, 2016; Seipold *et al.*, 2018).

6.2 Results

6.2.1 Tspan15/ADAM10 is the strongest scissor for GPVI, RAGE and betacellulin in transfected HEK-293T cells

The potential for other TspanC8s to compensate for the loss of Tspan15 in shedding of Tspan15-dependent substrates was investigated for GPVI, RAGE and betacellulin in transfected HEK-293T cells in this section, and endogenous N-cadherin in the next section (Section 6.2.2). Shedding rescue by each TspanC8/ADAM10 scissor was assessed in Tspan15-knockout cells, except for GPVI, which was in Tspan15/33 double knockout cells since it has already been shown that Tspan33 can contribute to GPVI cleavage in Tspan15-knockout cells (Section 4.2.6) (Matthews, 2019). In all experiments, the cells were transfected with expression constructs for FLAG-tagged TspanC8s (Tspan5, 10, 14, 15, 17 or 33), at comparable expression levels, together with ADAM10 to ensure that the reduction of ADAM10 levels in TspanC8-knockout cells (Section 5.3.5) would not become a limiting factor in assessing shedding.

Cleavage of GPVI in transfected cells was assessed by measuring the percentage of C-terminal fragment generated by anti-myc Western blotting as described in previous chapters. Only the true scissors for GPVI, Tspan15/ADAM10 and Tspan33/ADAM10, rescued GPVI cleavage in Tspan15/33 double knockout cells beyond the level observed in wild-type cells, with a 3.1-fold and 2.4-fold increase, respectively (Figure 38). Tspan10/ADAM10 overexpression did not rescue GPVI cleavage, whereas the other three scissors rescued GPVI cleavage to a small extent (Figure 38).

The expression construct for RAGE has a GFP tag at the C-terminus. The membrane remnant of RAGE following ADAM10 cleavage is susceptible to subsequent γ-secretase cleavage

(Zhang *et al.*, 2008). Therefore, RAGE cleavage in transfected cells was assessed by anti-GFP Western blotting in the presence of the γ-secretase inhibitor DAPT to prevent loss of the C-terminal fragment. RAGE cleavage, which was almost completely abolished in Tspan15-knockout cells, was restored to a level comparable to wild-type cells by reintroducing ADAM10 alone (Figure 39). Overexpression of Tspan15/ADAM10 and Tspan33/ADAM10 increased RAGE cleavage rescue by 2-fold and 1.3-fold above the level seen in wild-type cells, respectively, whereas no further increase was seen with the other four scissors (Figure 39).

The expression construct for betacellulin has an alkaline phosphatase conjugated at the N-terminus. This allowed betacellulin shedding to be quantitated in transfected cells by measuring alkaline phosphatase activity of shed betacellulin in cell culture supernatant as a percentage of total, which included activity from intact betacellulin in cell lysates. Shedding differences were assessed in the presence of the metalloprotease activator NEM to increase the otherwise low levels of shedding (Figure 40). Betacellulin shedding was almost completely abolished in Tspan15-knockout cells, and overexpressing ADAM10 alone or Tspan10/ADAM10 did not increase shedding further (Figure 40). Tspan15/ADAM10 was the only scissor that increased shedding to a level above wild-type cells, by 1.5-fold, and this was 5.2-fold higher than the level seen in the ADAM10-transfected control, whereas the other four scissors rescued shedding partially by ~2.5-fold above the level seen in the ADAM10-transfected control (Figure 40).

Together, the results suggest that Tspan15/ADAM10 is the strongest scissor for GPVI, RAGE and betacellulin in transfected HEK-293T cells, with minor compensation of varying degrees from the other non-cutters, apart from Tspan10/ADAM10, when they are overexpressed in the absence of Tspan15.

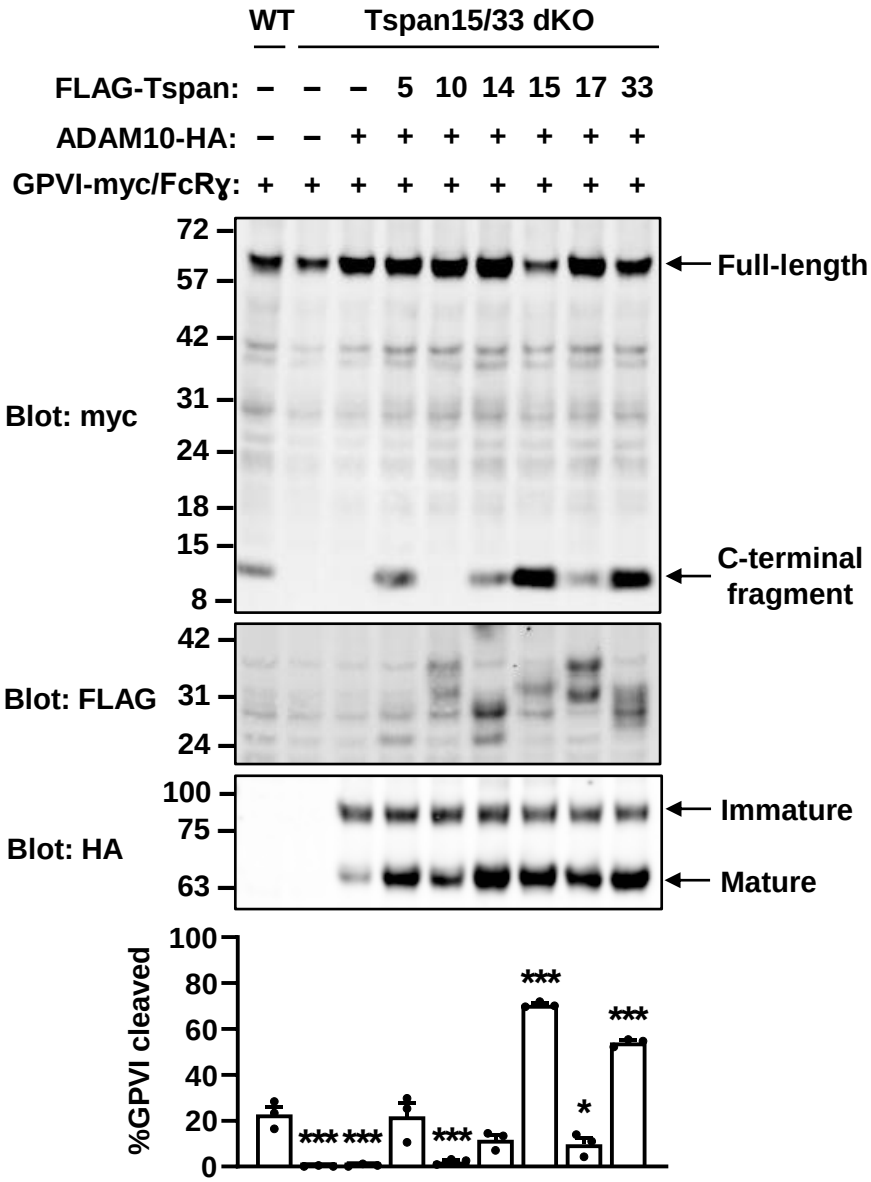

Figure 38. Tspan15/ADAM10 is the strongest scissor for GPVI. Wild-type (WT) and Tspan15/33 double knockout (dKO) HEK-293T cells were transfected with expression constructs for C-terminal myc-tagged human GPVI and FcRγ (+) for 24 hours. Tspan15/33 double knockout cells were also transfected with expression constructs for C-terminal HA-tagged ADAM10 and FLAG-tagged TspanC8s (Tspan5, 10, 14, 15, 17 or 33) or empty vector (–). Cells were lysed in 1% Triton X-100 lysis buffer. Lysates were subjected to anti-myc, anti-FLAG and anti-HA Western blotting (top panels). The percentage of GPVI cleaved was quantitated (bottom panel), arcsine-transformed and statistically analysed by a one-way ANOVA with Dunnett's multiple comparisons test (*p<0.05, ***p<0.001, compared to WT cells). Error bars represent standard errors of the mean from three independent experiments.

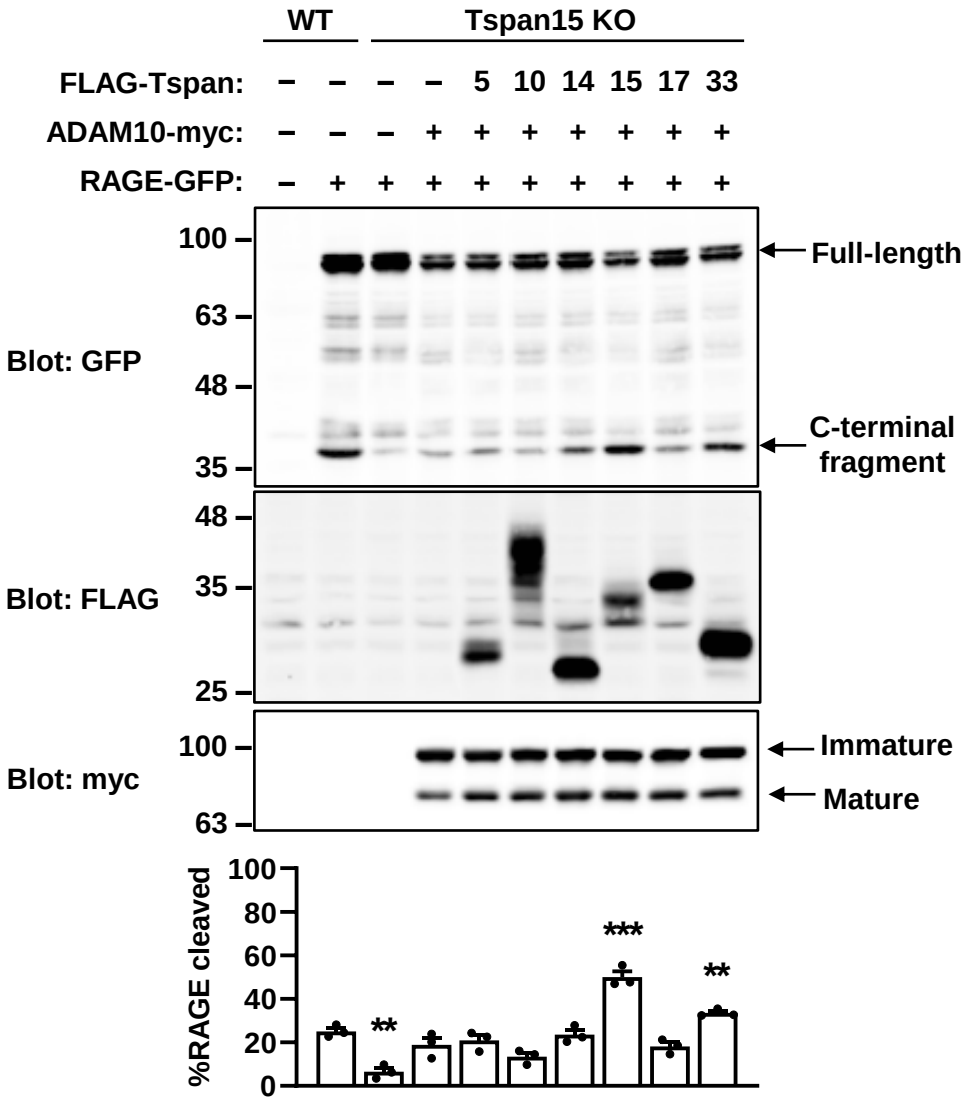

Figure 39. Tspan15/ADAM10 is the strongest scissor for RAGE. Wild-type (WT) and Tspan15-knockout (KO) HEK-293T cells were transfected with C-terminal GFP-tagged human RAGE expression construct for 24 hours. Tspan15-knockout cells were also transfected with expression constructs for C-terminal myc-tagged ADAM10 and FLAG-tagged TspanC8s (Tspan5, 10, 14, 15, 17 or 33) or empty vector (–). To prevent loss of the RAGE C-terminal fragment from subsequent γ-secretase cleavage, cells were treated with 10 μM of the γ-secretase inhibitor DAPT three hours post-transfection. Cells were lysed in 1% Triton X-100 lysis buffer. Lysates were subjected to anti-GFP, anti-FLAG and anti-myc Western blotting (top panels). The percentage of RAGE cleaved was quantitated (bottom panel), arcsine-transformed and statistically analysed by a one-way ANOVA with Dunnett's multiple comparisons test (**p<0.01, ***p<0.001, compared to cells transfected with ADAM10 only). Error bars represent standard errors of the mean from three independent experiments.

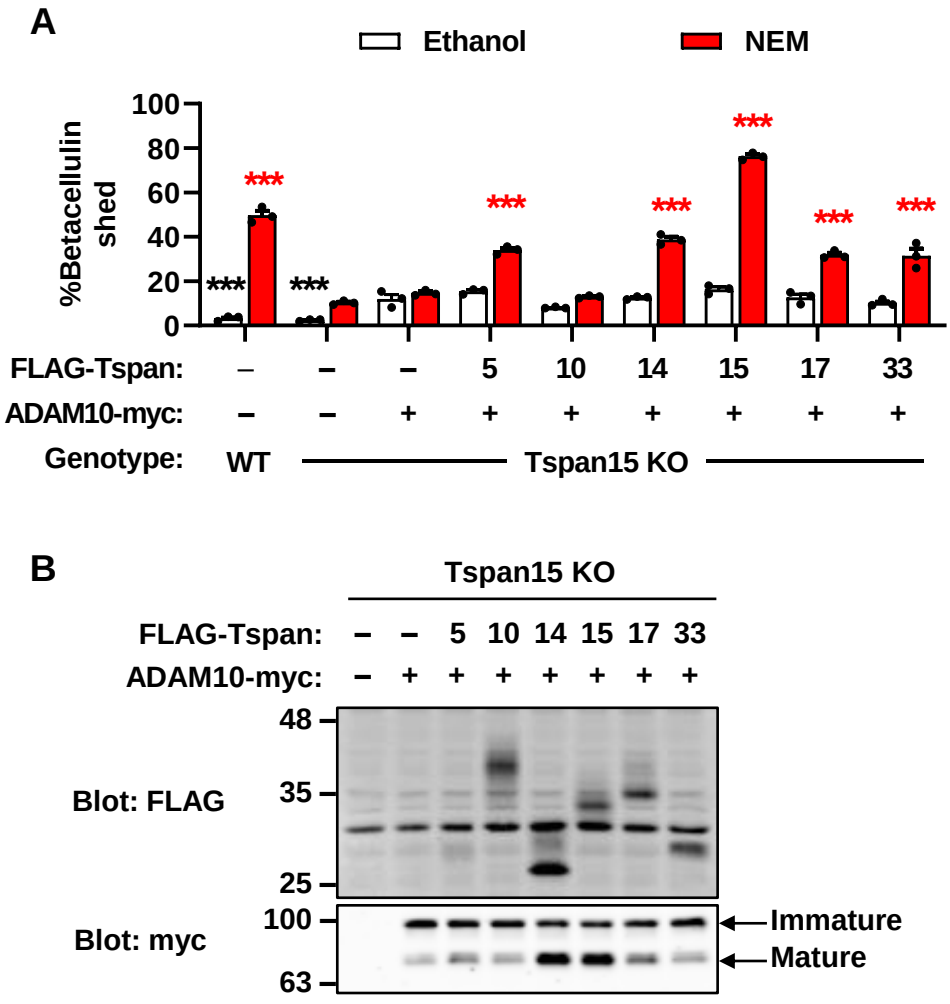

Figure 40. Tspan15/ADAM10 is the strongest scissor for betacellulin. Wild-type (WT) and Tspan15-knockout (KO) HEK-293T cells were transfected with an expression construct for human betacellulin conjugated to alkaline phosphatase at the N-terminus for 24 hours. Tspan15-knockout cells were also transfected with expression constructs for C-terminal myc-tagged ADAM10 and FLAG-tagged TspanC8s (Tspan5, 10, 14, 15, 17 or 33) or empty vector control (–). (A) Cells were washed with PBS and incubated with the reduced serum media Opti-MEM® for 30 minutes. To stimulate metalloprotease activity, cells were treated with 2 mM NEM or ethanol as vehicle control for 2.5 hours. To measure alkaline phosphatase activity, supernatant and lysate (extracted in 1% Triton X-100 lysis buffer) samples were harvested and incubated at 37 ºC with the alkaline phosphatase substrate pNPP at a final concentration of 1 mg/mL, and absorbance measured at 405 nm. The percentage of betacellulin shed was calculated from the absorbance of the supernatant sample as a percentage of total. Data were arcsine-transformed and statistically analysed by a two-way ANOVA with Dunnett's multiple comparisons test (***p<0.001, compared to the corresponding ADAM10-transfected Tspan15-knockout cells treated with ethanol (white) or NEM (red)). Error bars represent standard errors of the mean from three independent experiments. (B) Cells were lysed in 1% Triton X-100 lysis buffer. Lysates were subjected to anti-FLAG and anti-myc Western blotting. Blots are representative of three independent experiments.

6.2.2 Tspan15/ADAM10 is the strongest scissor for endogenous N-cadherin in HEK-293T cells

To extend the findings in the previous section to an endogenous substrate, rescue of shedding by each TspanC8/ADAM10 scissor was investigated in Tspan15-knockout HEK-293T cells for N-cadherin, which HEK-293T cells express endogenously. Shed N-cadherin released into cell culture supernatant was extracted by trichloroacetic acid (TCA) precipitation, whereas intact N-cadherin remaining on the cell surface was extracted in whole cell lysates. By Western blotting with an antibody against the extracellular region of N-cadherin, N-cadherin shedding can be quantitated by measuring the amount shed in the supernatant as a percentage of total N-cadherin from the supernatant and lysate samples.

In wild-type cells, full-length N-cadherin (~135 kDa) was substantially reduced in cell lysates and was accompanied by an accumulation of shed N-cadherin (~100 kDa) in the supernatant upon NEM stimulation, suggesting that N-cadherin was maximally shed (Figure 41). In contrast, no shed N-cadherin was detected in the supernatant sample of Tspan15-knockout cells, despite the detection of the full-length in cell lysates, suggesting that N-cadherin could not be shed in the absence of Tspan15 (Figure 41). Shedding was rescued maximally to ~50% of the level seen in wild-type cells with Tspan15/ADAM10 overexpression (Figure 41). Of note, the partial rescue was because not all cells were transfected (~50-70% transfection efficiency by flow cytometry; data not shown). Overexpressing Tspan10/ADAM10 and Tspan17/ADAM10 could not rescue shedding in Tspan15-knockout cells, similar to what was observed in the ADAM10-transfected control (Figure 41). Minimal rescue of ~30-50% of the level achieved with Tspan15/ADAM10 overexpression was seen with the other three scissors, with Tspan33/ADAM10 being the stronger of the three, which increased shedding significantly ($p<0.05$) compared to the ADAM10-transfected control (Figure 41).

Figure 42 summarises the shedding rescue data from Sections 6.2.1 and 6.2.2. Taken together, the results suggest that in an overexpression scenario, Tspan15/ADAM10 remains the strongest scissor for all Tspan15-dependent substrates, whereas there is no functional redundancy with Tspan10/ADAM10. Tspan17/ADAM10 can contribute to minimal rescue for all substrates except for N-cadherin. Tspan5/ADAM10, Tspan14/ADAM10 and Tspan33/ADAM10 can contribute to minimal rescue of all substrates; however, Tspan33/ADAM10 appears to be the stronger of the three as it can compensate for the loss of Tspan15 slightly better than other scissors in the case of RAGE and N-cadherin.

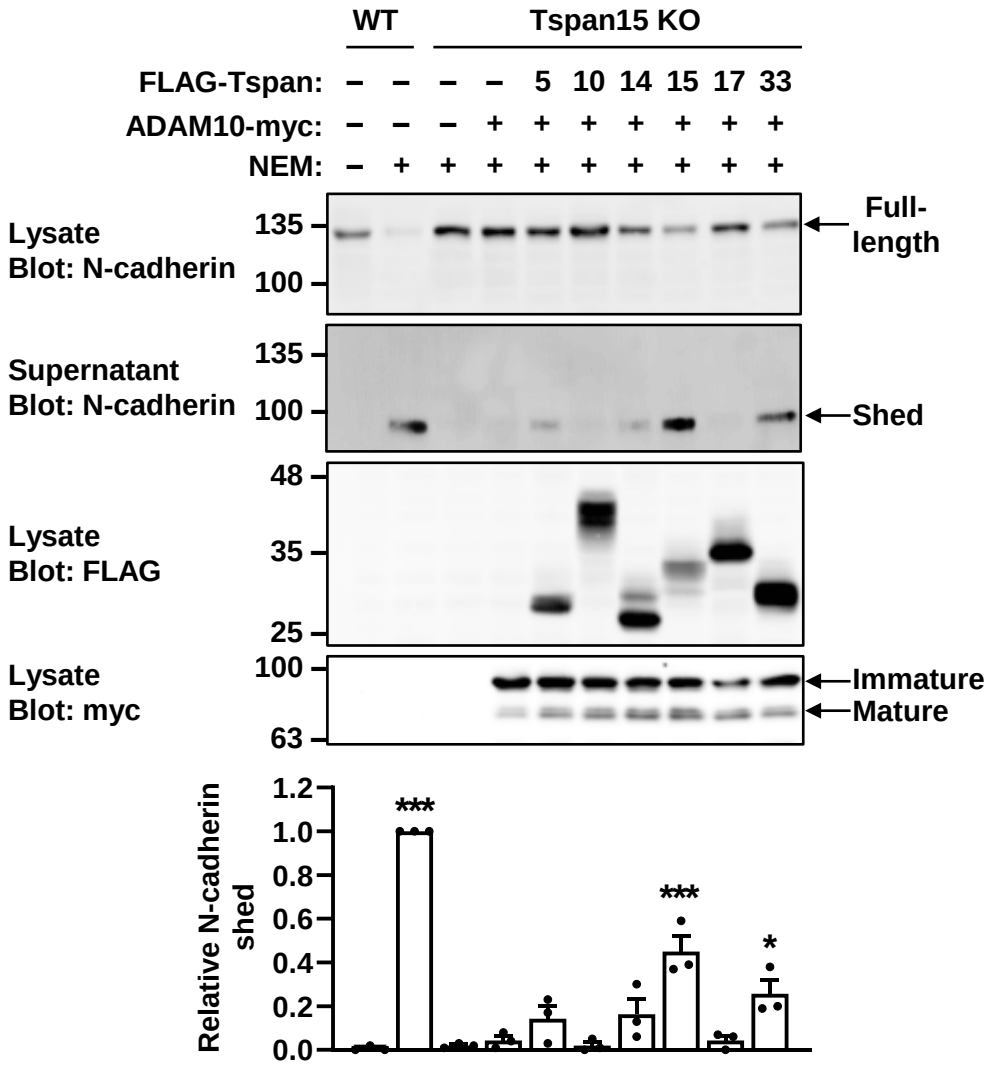

Figure 41. Tspan15/ADAM10 is the strongest scissor for N-cadherin. Wild-type (WT) and Tspan15-knockout (KO) HEK-293T cells were transfected with expression constructs for C-terminal myc-tagged ADAM10 and FLAG-tagged TspanC8s (Tspan5, 10, 14, 15, 17 or 33) or empty vector (–) for 24 hours. Cells were washed with PBS and incubated with the reduced serum media Opti-MEM® for 30 minutes. To stimulate metalloprotease activity, cells were treated with 2 mM NEM or ethanol as vehicle control for one hour. Protein was extracted from the supernatant by TCA precipitation. Cells were lysed in 1% Triton X-100 lysis buffer. Both the supernatant and lysate samples were subjected to Western blotting with an antibody against the extracellular region of N-cadherin; lysates were also blotted for FLAG and myc (top panels). The percentage of N-cadherin shed was calculated from the supernatant as a percentage of total and presented relative to NEM-stimulated WT cells (bottom panel). Data were arcsine-transformed and statistically analysed by a one-way ANOVA with Dunnett's multiple comparisons test (*p<0.05, ***p<0.001, compared to cells transfected with ADAM10 only). Error bars represent standard errors of the mean from three independent experiments.

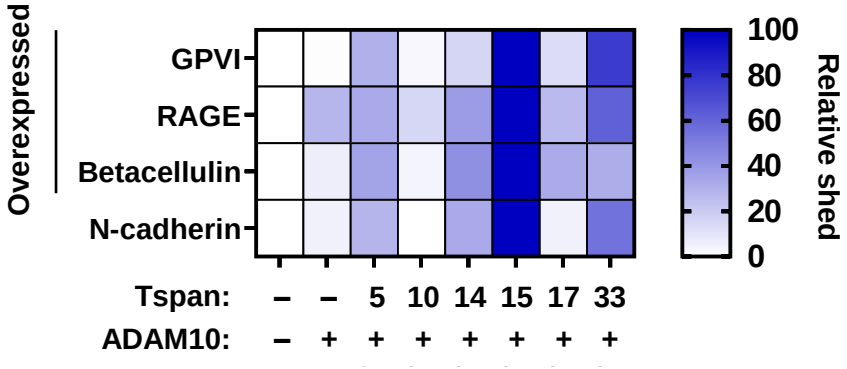

Figure 42. Summary of redundancy among TspanC8/ADAM10 scissors for Tspan15-dependent substrates. Data from the average percentage shedding rescue of GPVI, RAGE, betacellulin and N-cadherin in the absence of Tspan15 from Figure 38, Figure 39, Figure 40 and Figure 41 were combined. Data were normalised to a 0-100 scale based on the minimum and maximum values for each substrate.

6.2.3 Tspan15 shows the strongest colocalisation with N-cadherin

To investigate whether the subcellular localisation of an overexpressed TspanC8/ADAM10 scissor in relation to a Tspan15-dependent substrate would explain the differences in shedding compensation observed in previous sections, N-cadherin was selected as the model substrate. Dual-colour confocal imaging using an antibody against the cytoplasmic domain of N-cadherin and an anti-FLAG antibody was used to assess the degree of colocalisations between N-cadherin and FLAG-tagged TspanC8s in Tspan15-knockout cells co-transfected with expression constructs for ADAM10 and FLAG-tagged Tspan5, 10, 14, 15, 17 or 33. The experiment was done in the presence of the γ-secretase inhibitor DAPT to prevent γ-secretase cleavage of the membrane-bound remnant after ADAM10 shedding (Uemura *et al.*, 2006). N-cadherin showed predominant plasma membrane localisation (Figure 43A). In FLAG-positive, transfected cells, the percentage of colocalisation with N-cadherin was the highest with overexpressed Tspan15/ADAM10, which was also predominantly localised on the cell surface (Figure 43A-B). Comparisons with the other five scissors showed substantial reduction in colocalisation with N-cadherin, with most scissors showing predominant intracellular localisations; among these, Tspan33/ADAM10 showed stronger plasma membrane localisation and better colocalisation with N-cadherin (Figure 43A-B). Therefore, this suggests that for Tspan33/ADAM10, its greater ability to compensate for the loss of Tspan15 may be partly because of its stronger colocalisation with N-cadherin when overexpressed.

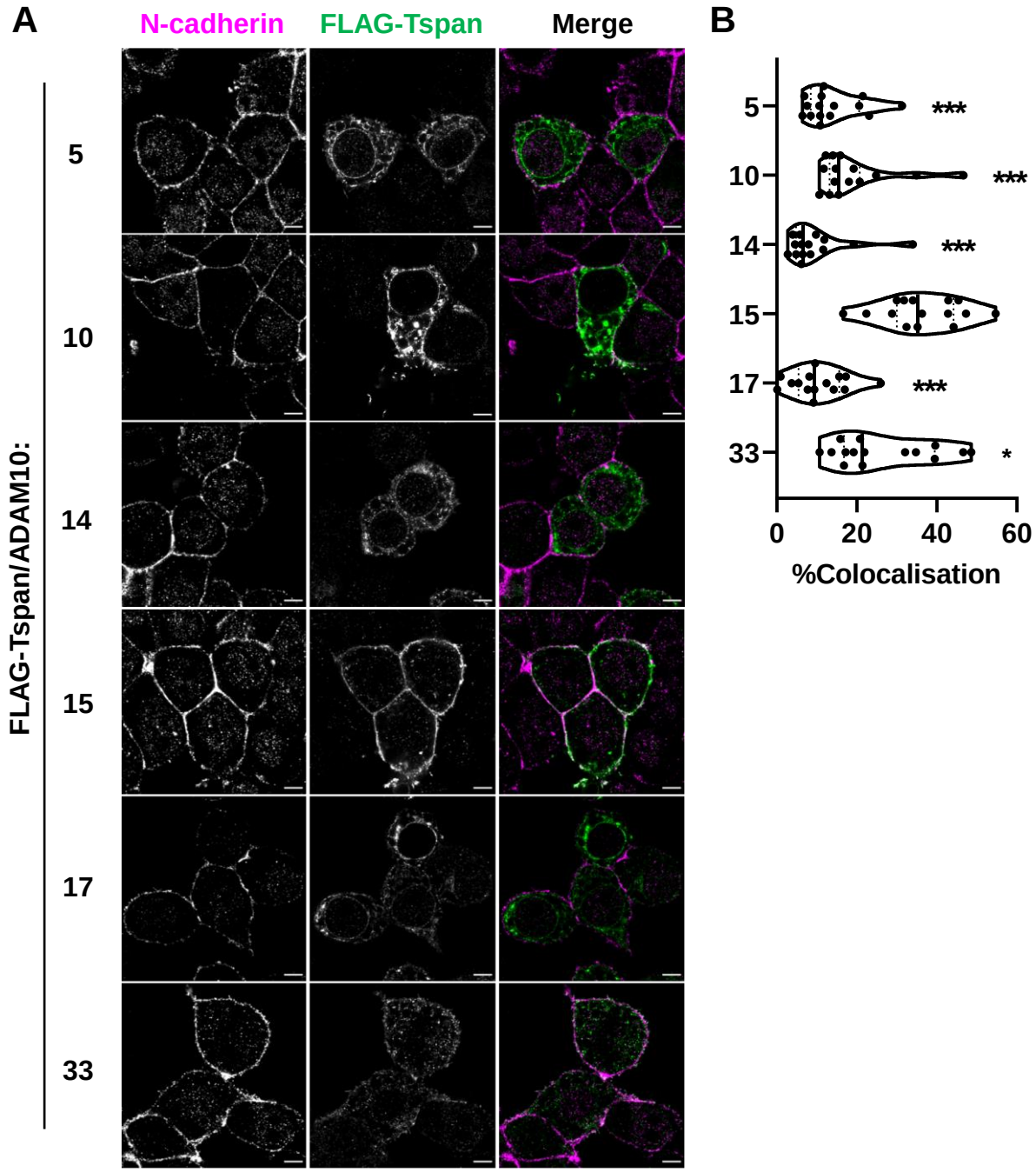

Figure 43. Tspan15 colocalises with N-cadherin. (A) Tspan15-knockout HEK-293T cells were transfected with expression constructs for ADAM10 and FLAG-tagged TspanC8s (Tspan5, 10, 14, 15, 17 or 33). To prevent loss of the N-cadherin C-terminal fragment, cells were treated with 10 μM of the γ-secretase inhibitor DAPT three hours post-transfection. After 24 hours, cells were fixed, permeabilised and immunostained for N-cadherin cytoplasmic tail (magenta) and FLAG (FLAG-Tspan; green). Cells were imaged at the middle plane using Airyscan confocal microscopy in super-resolution mode. No signal was detected in the magenta channel in cells stained with control mouse IgG, or in the green channel in empty vector-transfected cells stained with anti-FLAG (data not shown). Images are representative of 15 fields of view from three independent experiments. Scale bar: 5 μm. (B) The degree of colocalisation between N-cadherin and FLAG-TspanC8s was expressed as the percentage of overlapping pixels in FLAG-positive, transfected cells in the green channel. Data were arcsine-transformed and analysed by a one-way ANOVA, followed by Dunnett's multiple comparison tests (*p<0.05, ***p<0.001, compared to the cells transfected with Tspan15/ADAM10).

6.2.4 Tspan14/ADAM10 cannot outperform Tspan15/ADAM10 in shedding GPVI, RAGE and N-cadherin, but can do so to a small extent for betacellulin

Sections 6.2.1 and 6.2.2 assessed redundancies among TspanC8/ADAM10 scissors in cutting Tspan15-dependent substrates when overexpressed at high levels. Next, the effect of expression level on the extent of shedding rescue was investigated. Although functional redundancy with Tspan15/ADAM10 was the most prominent with the overexpression of Tspan33/ADAM10, proteomics data show that Tspan33 expression is restricted to B cells, platelets and kidney tissue, in contrast to the broad expression profile of Tspan14 (Section 1.4.3). Therefore, the ubiquitously expressed Tspan14, which showed some functional redundancies with Tspan15 when overexpressed was chosen as the representative TspanC8 for comparison.

The shedding assays for overexpressed GPVI, RAGE, betacellulin and endogenous N-cadherin were as described in Sections 6.2.1 and 6.2.2. To compare Tspan14 and Tspan15 directly, Tspan14/15 double knockout HEK-293T cells, which have a ~65% reduction in ADAM10 surface expression, were generated by CRISPR/Cas9 (Figure A1A, Appendix). Tspan14/15 double knockout cells were used for RAGE, betacellulin and N-cadherin shedding assays, whereas Tspan14/15/33 triple knockout cells (described in Section 3.2.2) were used to assess GPVI cleavage. The cells were transfected with expression constructs for ADAM10 and a titration of FLAG-tagged Tspan14 or Tspan15 with four-fold dilution steps to achieve four different expression levels, such that the FLAG signal would fall below the limit of detection at the lowest concentrations (Figure 44A).

A non-linear decrease in GPVI cleavage was seen in the titrations of both Tspan14 and Tspan15, with a noticeable decrease seen only in the lowest expression level (Figure 44A-B). Tspan14/ADAM10 cannot rescue GPVI cleavage to the same extent as Tspan15/ADAM10

because even Tspan15/ADAM10 at the lowest expression level was able to outperform the Tspan14/ADAM10 expressed at the highest level (Figure 44A-B). A steady reduction in RAGE cleavage was observed for both Tspan14 and Tspan15 titrations (Figure 45A-B). Titrating Tspan15/ADAM10 to the lowest expression level resulted in RAGE cleavage comparable to the level observed at maximal Tspan14/ADAM10 expression (Figure 45A-B). Similar to RAGE, betacellulin shedding was gradually reduced across the titrations of both Tspan14 and Tspan15 (Figure 46A-B). Titrating Tspan15/ADAM10 to the second lowest expression level was sufficient to yield shedding comparable to the level observed at maximal Tspan14/ADAM10 expression (Figure 46A-B). In the case of endogenous N-cadherin, shedding rescue by Tspan15/ADAM10 was lower compared to overexpressed substrates because not all cells would have been transfected. Nonetheless, Tspan15/ADAM10 still rescued shedding at its lowest expression level, in contrast to Tspan14/ADAM10 where no substantial shedding rescue was detected at any concentration (Figure 47A-B).

Figure 48 summarises the relative strengths of Tspan14/ADAM10 and Tspan15/ADAM10 in cutting overexpressed GPVI, RAGE, betacellulin and endogenous N-cadherin. Taken together, the data suggest that Tspan14/ADAM10, even at its highest expression level, cannot outperform Tspan15/ADAM10 at any expression level, except for betacellulin at the lowest Tspan15/ADAM10 expression level.

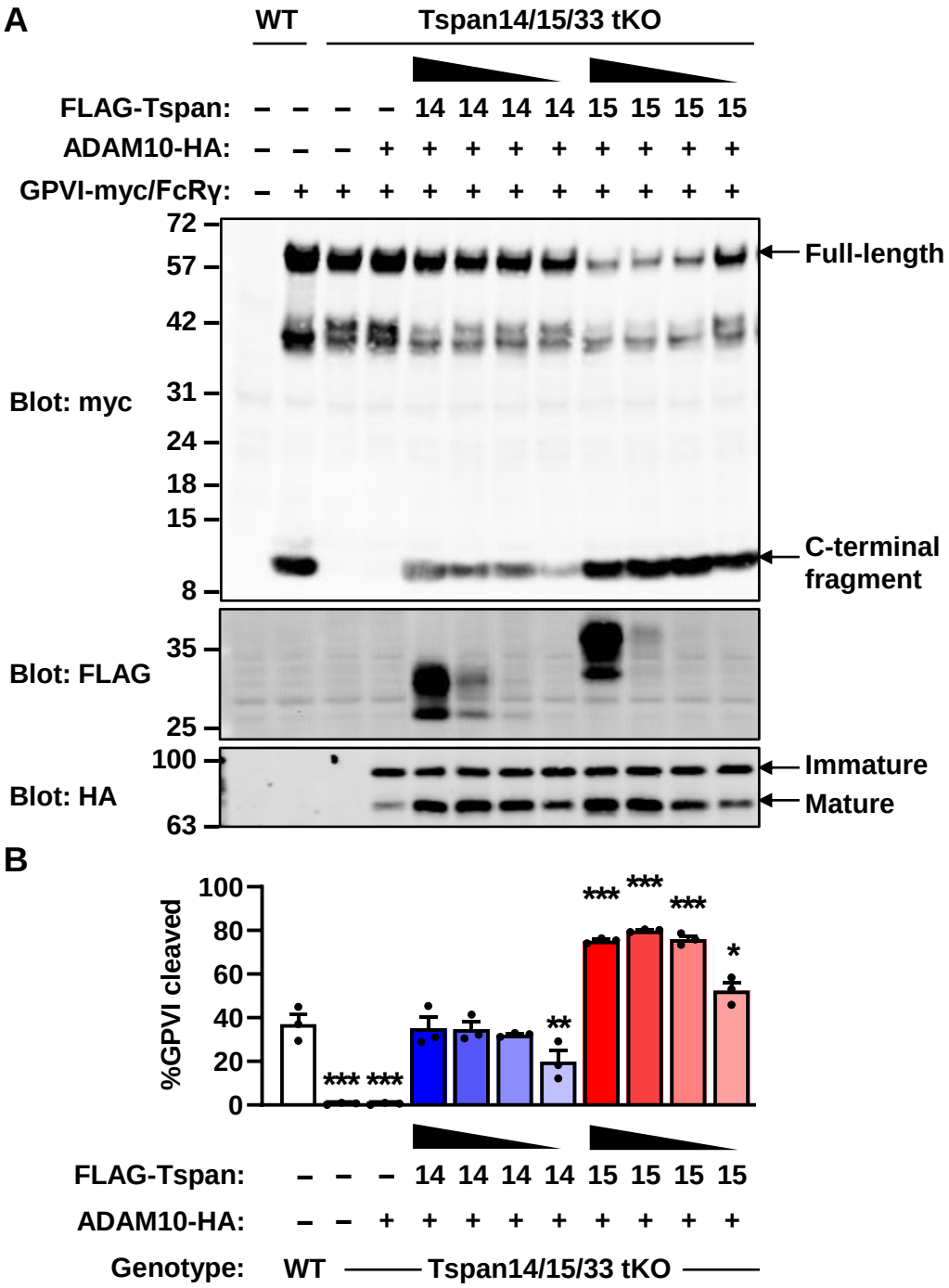

Figure 44. Tspan14/ADAM10 cannot rescue GPVI cleavage to the same extent as Tspan15/ADAM10 scissors. (A) Wild-type (WT) and Tspan14/15/33 triple knockout (tKO) HEK-293T cells were transfected with expression constructs for C-terminal myc-tagged human GPVI and FcRγ (+) for 24 hours. Tspan14/15/33 triple knockout cells were also transfected with expression constructs for C-terminal HA-tagged ADAM10 and a titration of FLAG-tagged Tspan14 or Tspan15 with four-fold dilution steps. Cells were lysed in 1% Triton X-100 lysis buffer. Lysates were subjected to anti-myc, anti-FLAG and anti-HA Western blotting. (B) The percentage of GPVI cleaved from panel A was quantitated. The titrations for Tspan14 and Tspan15 are represented by colour gradients of blue and red, respectively. Data were arcsine-transformed and statistically analysed by a one-way ANOVA with Dunnett's multiple comparisons test (*p<0.05, **p<0.01, ***p<0.001, compared to WT cells). Error bars represent standard errors of the mean from three independent experiments.

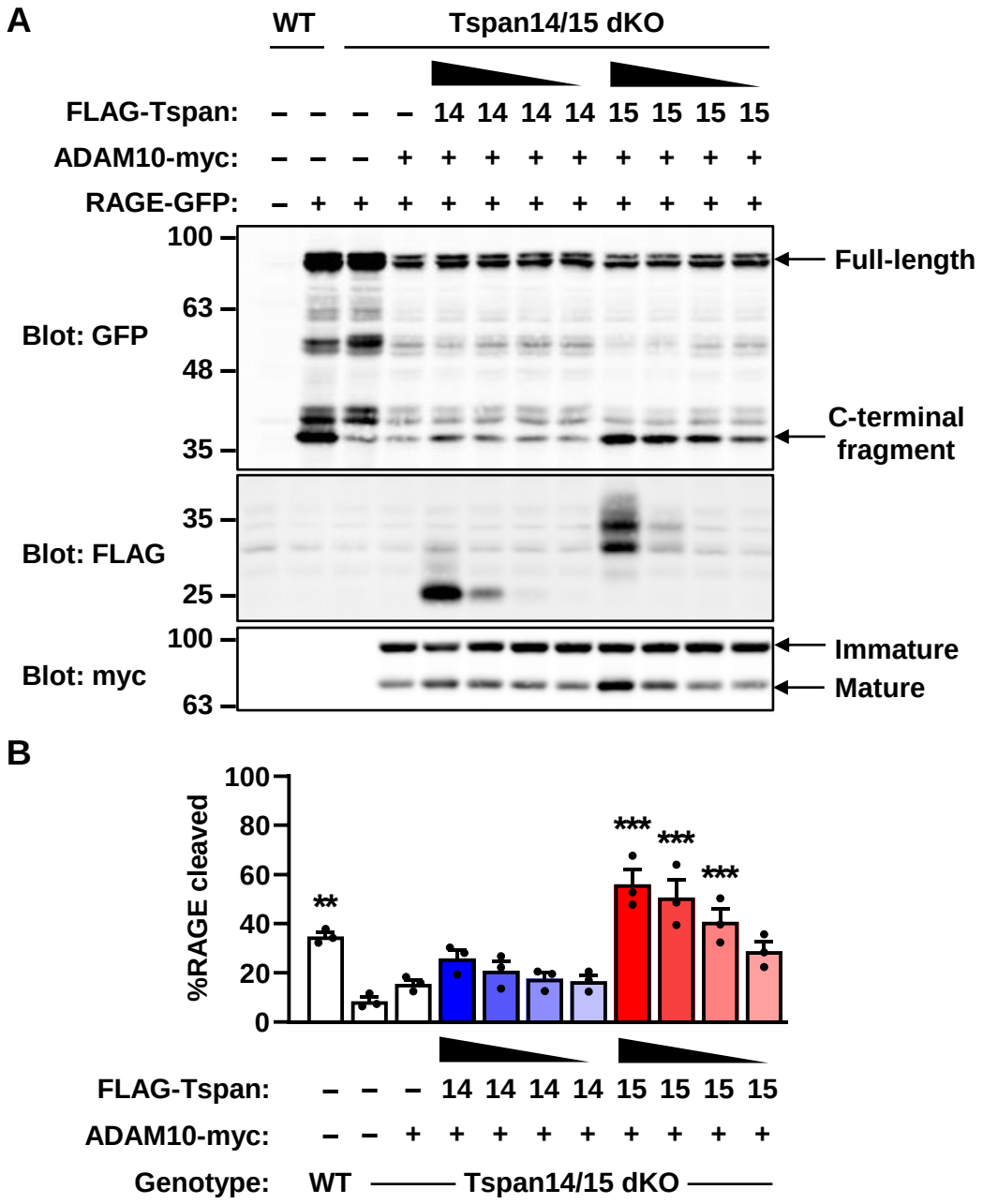

Figure 45. Tspan14/ADAM10 cannot rescue RAGE cleavage to the same extent as Tspan15/ADAM10 scissors. (A) Wild-type (WT) and Tspan14/15 double knockout (dKO) HEK-293T cells were transfected with expression constructs for C-terminal GFP-tagged RAGE for 24 hours. Tspan14/15 double knockout cells were also transfected with expression constructs for C-terminal myc-tagged ADAM10 and a titration of FLAG-tagged Tspan14 or Tspan15 with four-fold dilution steps. To prevent loss of the RAGE C-terminal fragment from subsequent γ-secretase cleavage, cells were treated with 10 μM of the γ-secretase inhibitor DAPT three hours post-transfection. Cells were lysed in 1% Triton X-100 lysis buffer. Lysates were subjected to anti-GFP, anti-FLAG and anti-myc Western blotting. (B) The percentage of RAGE cleaved from panel A was quantitated. Titrations for Tspan14 and Tspan15 are represented by colour gradients of blue and red, respectively. Data were arcsine-transformed and statistically analysed by a one-way ANOVA with Dunnett's multiple comparisons test (**p<0.01, ***p<0.001, compared to Tspan14/15 double knockout cells transfected with ADAM10 alone). Error bars represent standard errors of the mean from three independent experiments.

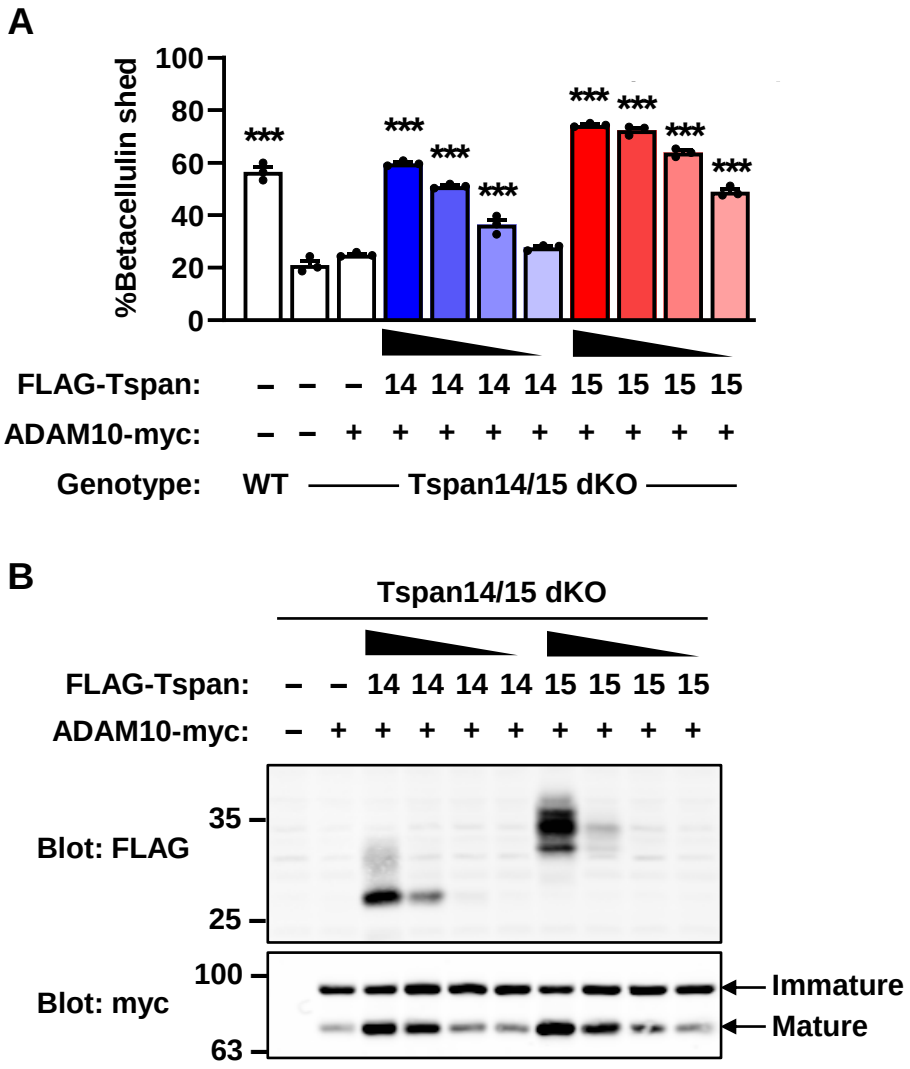

Figure 46. Tspan14/ADAM10 can outperform Tspan15/ADAM10 in shedding betacellulin to a small extent. Wild-type (WT) and Tspan14/15 double knockout (dKO) HEK-293T cells were transfected with an expression construct for human betacellulin conjugated to alkaline phosphatase at the N-terminus for 24 hours. Tspan14/15 double knockout cells were also transfected with expression constructs for C-terminal myc-tagged ADAM10 and a titration of FLAG-tagged Tspan14 or Tspan15 with four-fold dilution steps. (A) Cells were washed with PBS and incubated with the reduced serum media Opti-MEM® for 30 minutes. To stimulate metalloprotease activity, cells were treated with 2 mM NEM for 2.5 hours. To measure alkaline phosphatase activity, supernatant and lysate (extracted in 1% Triton X-100 lysis buffer) samples were harvested and incubated at 37 ºC with the alkaline phosphatase substrate pNPP at a final concentration of 1 mg/mL, and absorbance measured at 405 nm. The percentage of betacellulin shed was calculated from the absorbance of the supernatant sample as a percentage of total. Titrations for Tspan14 and Tspan15 are represented by colour gradients of blue and red, respectively. Data were arcsine-transformed and statistically analysed by a one-way ANOVA with Dunnett's multiple comparisons test (***p<0.001, compared to Tspan14/15 double knockout cells transfected with ADAM10 alone). Error bars represent standard errors of the mean from three independent experiments. (B) Cells were lysed in 1% Triton X-100 lysis buffer. Lysates were subjected to anti-FLAG and anti-myc Western blotting. Blots are representative of three independent experiments.

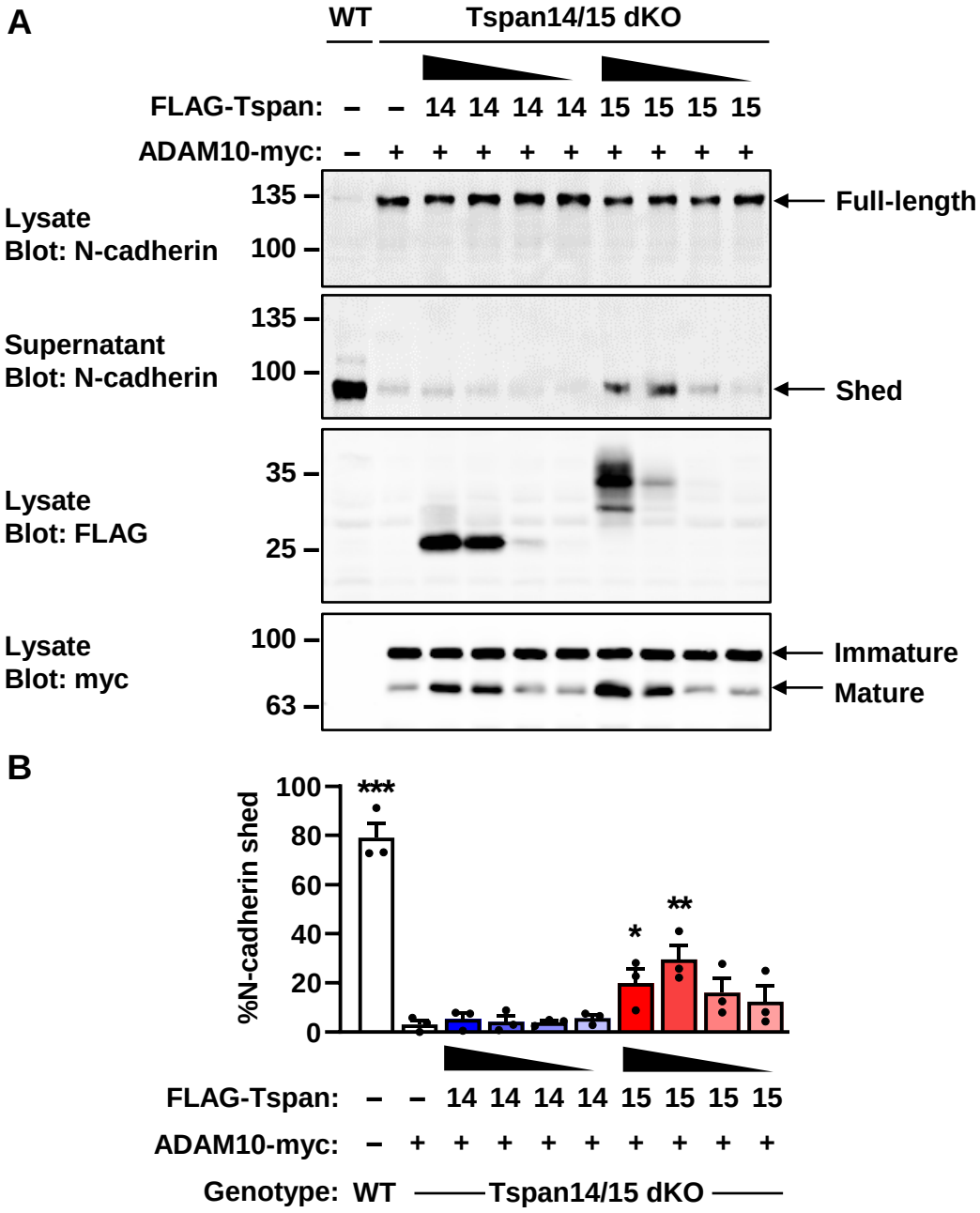

Figure 47. Tspan14/ADAM10 cannot rescue N-cadherin shedding to the same extent as Tspan15/ADAM10 scissors. (A) Wild-type (WT) and Tspan14/15 double knockout (KO) HEK-293T cells were transfected with expression constructs for C-terminal myc-tagged ADAM10 and a titration of FLAG-tagged Tspan14 or Tspan15 with four-fold dilution steps. Cells were washed with PBS and incubated with the reduced serum media Opti-MEM® for 30 minutes. To stimulate metalloprotease activity, cells were treated with 2 mM NEM for one hour. Protein was extracted from the supernatant by TCA precipitation. Cells were lysed in 1% Triton X-100 lysis buffer. Both the supernatant and lysate samples were subjected to Western blotting with an antibody against the extracellular region of N-cadherin; lysates were also blotted for FLAG and myc. (B) The percentage of N-cadherin shed was calculated from the supernatant as a percentage of total. Data were arcsine-transformed and statistically analysed by a one-way ANOVA with Dunnett's multiple comparisons test (*p<0.05, **p<0.01, ***p<0.001, compared to Tspan14/15 double knockout cells transfected with ADAM10 alone). Error bars represent standard errors of the mean from three independent experiments.

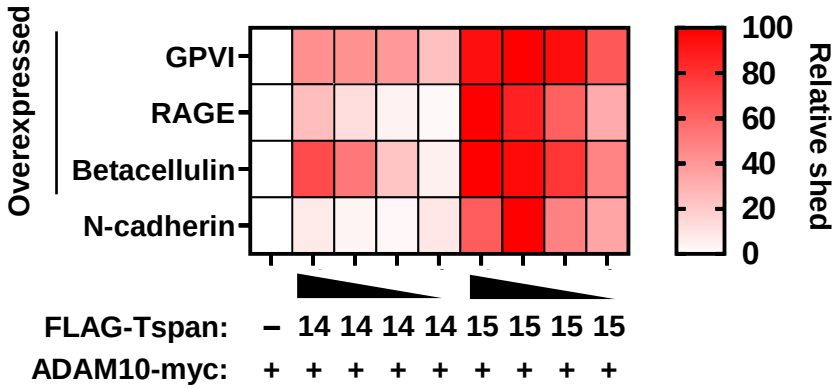

Figure 48. Summary of the relative strengths of Tspan14/ADAM10 and Tspan15/ADAM10 scissors for Tspan15-dependent substrates. Data from the average percentage shedding rescue of GPVI, RAGE, betacellulin and N-cadherin in the absence of Tspan14 and Tspan15 from Figure 44, Figure 45, Figure 46 and Figure 47 were combined. Data were normalised to a 0-100 scale based on the minimum and maximum values for each substrate.

6.3 Discussion

This chapter addressed a key question in validating Tspan15 as a drug target: can the scissor function of Tspan15/ADAM10 be compensated by the other five TspanC8/ADAM10 scissors in its absence? In addition to GPVI, RAGE, betacellulin and N-cadherin were selected as model Tspan15/ADAM10 substrates. The data revealed that (1) Tspan15/ADAM10 remains the strongest scissor for all substrates when expressed at either high or low expression levels and (2) other TspanC8/ADAM10 scissors, apart from Tspan10/ADAM10, can cut all substrates minimally to varying degrees when overexpressed.

The first part of this chapter focused on comparing TspanC8/ADAM10 scissors in their abilities in rescuing GPVI, RAGE, betacellulin and N-cadherin shedding when overexpressed in the absence of Tspan15 (and Tspan33 in the case of GPVI). In all cases, the maximum level of rescue was achieved with Tspan15/ADAM10 reconstitution, which was increased substantially beyond the level observed in wild-type cells. Compared to Tspan15, the amino acid sequences of Tspan5, 10, 14, 17 and 33 are 33%, 26%, 32%, 30% and 34% identical, respectively (Matthews, Szyroka, *et al.*, 2017). The most distantly related Tspan10/ADAM10 was not able to restore shedding of any substrate investigated, whereas the second most distantly related Tspan17/ADAM10 could only rescue GPVI and betacellulin shedding to a small extent, but not the other substrates. In addition to GPVI and betacellulin, Tspan5/ADAM10 and Tspan14/ADAM10 also rescued N-cadherin shedding to a small extent, but not RAGE. RAGE shedding was only rescued with Tspan33/ADAM10, the scissor most closely related to Tspan15/ADAM10, which also rescued the shedding of all other substrates. The pattern of shedding rescue described above suggests that any functional redundancy seen with the overexpression of a TspanC8/ADAM10 scissor may partly correlate with their sequence relatedness to Tspan15. This may arise from similarities and differences in their less conserved

regions, i.e., the small extracellular region and cytoplasmic tails (Matthews, Szyroka, *et al.*, 2017), which will be discussed in Chapter 7. Using N-cadherin as the representative substrate, colocalisation analysis revealed that Tspan15 showed the strongest colocalisation with N-cadherin, which were both predominantly localised to the plasma membrane, followed by Tspan33. Therefore, the observation that Tspan33/ADAM10 can rescue shedding better than other scissors could also be in part due to stronger colocalisation of overexpressed Tspan33 with substrates present on the cell surface. However, consistent with the findings in Chapter 3, degree of colocalisations of other scissors, at least at a steady state, do not associate with their ability to rescue shedding, suggesting that there may be other factors at play. Nevertheless, the results here show that even in an overexpression scenario, Tspan15/ADAM10 remains the major scissor for all Tspan15-dependent substrates examined because no other scissor can restore shedding to the same extent as Tspan15/ADAM10.

The next step in this investigation was to determine whether the expression level of a TspanC8/ADAM10 scissor affects the extent of shedding. Specifically, can Tspan14/ADAM10 cut a Tspan15/ADAM10 substrate more than Tspan15/ADAM10 expressed at a substantially lower level? As mentioned in Section 6.2.4, Tspan14 was chosen as the representative TspanC8 for comparison with Tspan15 because of its ubiquitous expression on many cell and tissue types. The generation of cell lines lacking both Tspan14 and Tspan15 (and Tspan33 for investigating GPVI) allowed the direct comparison between Tspan15 and Tspan14 at specific expression levels. A titration effect on the level of shedding was seen for all substrates with the reintroduction of Tspan14/ADAM10 or Tspan15/ADAM10, except for the rescue of endogenous N-cadherin by Tspan14/ADAM10 where no rescue was seen even at the highest expression of Tspan14/ADAM10. The effects on endogenous N-cadherin shedding rescue could be an underestimation because not all cells would have been transfected with the scissors

in a transient transfection system. Stable expression of TspanC8/ADAM10 scissors by lentiviral transduction would be useful in overcoming this limitation in future experiments. Nonetheless, it is clear from the data that minimal overexpression of Tspan15/ADAM10 at the lowest level was enough to rescue shedding of all substrates close to the level seen in wild-type cells, whereas Tspan14/ADAM10 could only achieve this at its maximum expression level. Betacellulin is the only exception to this, where Tspan15/ADAM10 scissor activity at its lowest expression level was outperformed by Tspan14/ADAM10 at its highest expression level by a small extent. The reason for this is unclear, but the presence of a bulky alkaline phosphatase tag on betacellulin, and potential sensitivity differences between Western blotting and colourimetric shedding assays are limitations to consider. Additionally, some residual betacellulin shedding was noticeable in Tspan15-knockout and Tspan14/15 double knockout cells, suggesting that even though Tspan15/ADAM10 may be the major scissor for betacellulin, other scissors may play minor roles, at least for overexpressed betacellulin. This is consistent with the observation that overexpressing ADAM10 alone was able to rescue betacellulin shedding to a small extent in Tspan15/ADAM10 double knockout HEK-293T cells (Koo *et al.*, 2020). There is a need to verify the scissor identities for betacellulin in a cell line expressing a good level of the endogenous protein, for example in the breast cancer cell line SK-BR-3 (Uhlén *et al.*, 2015; Human Protein Atlas, 2021).

It is worth mentioning that unlike other substrates, reintroduction of ADAM10 alone into Tspan15-knockout cells or Tspan14/15 double knockout cells could already rescue RAGE cleavage to a small extent, suggesting that like GPVI, more than one TspanC8/ADAM10 scissor may be involved in cutting RAGE. Based on the results here, Tspan33/ADAM10 may be the most likely candidate. In fact, this is possible because recent unpublished data from the Tomlinson lab show that RAGE cleavage in transfected single TspanC8-knockout HEK-293T

cells is strikingly similar to that of GPVI (Section 4.2.6). Although RAGE cleavage is substantially reduced in Tspan15-knockout cells, a small residual cleavage is still noticeable despite being completely abolished in ADAM10-knockout cells. Like GPVI, RAGE cleavage is also unaffected in transfected Tspan14-knockout and Tspan33-knockout HEK-293T cells. Future experiments should examine whether RAGE cleavage in Tspan15/33 double knockout cells is abolished to the extent seen in ADAM10-knockout cells and confirm this in a cell line expressing endogenous RAGE.

In summary, this chapter showed that except for Tspan10, there is minor functional redundancy of Tspan15 with other TspanC8s at varying degrees at high expression levels but the effect diminishes at low expression levels.

CHAPTER 7
GENERAL DISCUSSION

7.1 Overview

This project aimed to examine the 'six scissors' hypothesis by addressing the central question of how six TspanC8 tetraspanins regulate ADAM10 substrate specificity, using the platelet-activating receptor GPVI as a model substrate. Of the three scissors expressed on human platelets, Tspan15/ADAM10 and Tspan33/ADAM10 can cut GPVI but Tspan14/ADAM10 cannot (Matthews, 2019). Findings from Chapter 3 revealed that Tspan15/ADAM10 is the most efficient scissor for GPVI and investigated potential mechanisms of how TspanC8s regulate ADAM10 shedding of GPVI. The disease relevance of Tspan15/ADAM10 scissors is supported by data from Chapter 4 as high *TSPAN15* expression may contribute to lower venous thrombosis risk. Chapter 5 demonstrated the close relationship between Tspan15 and ADAM10 as their expression on the cell surface are regulated by each other. Finally, functional redundancy of Tspan15/ADAM10 with the other five scissors was assessed in Chapter 6 as a key step in evaluating whether Tspan15 is a druggable target. This thesis uncovered novel findings surrounding three main themes: (1) structure-function analysis of Tspan15 and ADAM10, (2) regulation of ADAM10 substrate specificity by TspanC8s and (3) therapeutic potential of Tspan15. These findings, along with new perspectives gained to guide future investigations, will be discussed in turn.

7.2 Structure-function analysis of Tspan15 and ADAM10

7.2.1 Tspan15 extracellular region has a major role in promoting plasma membrane localisation and ADAM10 activity

Previous structure-function studies have focused on the larger extracellular region of TspanC8s because this is the region important for interaction with ADAM10, as demonstrated by Tspan5 and Tspan14 (Noy *et al.*, 2016; Saint-Pol, Billard, *et al.*, 2017). The large extracellular region of Tspan14 on a CD9 backbone can co-immunoprecipitate ADAM10 but to a lesser extent compared to wild-type Tspan14 (Noy *et al.*, 2016). Using Tspan5 and Tspan15 chimeras, it has also been demonstrated that exchanging their large extracellular regions cannot exchange their opposite roles in regulating ADAM10 endocytosis, and it only modestly affected ADAM10 function in terms of promoting Notch activity (Eschenbrenner *et al.*, 2020). The crystal structure of tetraspanin CD53 captured in an open conformation capable of partner interaction (Yang *et al.*, 2020), and the cryo-EM structure of an extended, open conformation of tetraspanin CD81 in complex with its partner protein CD19 (Susa *et al.*, 2021), both revealed that the open conformations of these tetraspanins are stabilised by interactions between the small and large extracellular regions (Section 1.3.2). Therefore, the investigation in Chapter 3 considered the contribution from the small extracellular region by studying the role of the entire extracellular region to more accurately assess the function of the extracellular region of Tspan15, using Tspan14 and Tspan15 chimeras. In contrast to previous studies, the findings in this thesis provided striking, unambiguous phenotypes and showed that the large and small extracellular regions of Tspan15 on a Tspan14 backbone promoted plasma membrane localisation and promoted GPVI cleavage by ADAM10 to the same extent as wild-type Tspan15. This suggests that the extracellular region is the major regulator of Tspan15 subcellular localisation and Tspan15/ADAM10 scissor activity. A similar observation was also shown for the reverse

chimera, therefore providing some evidence that this may apply to all TspanC8s. It is particularly striking how the extracellular regions of Tspan14 and Tspan15 were important for their subcellular localisations. One possible mechanism for this intriguing finding is that ADAM10 may also reciprocally regulate TspanC8 subcellular localisation; binding of ADAM10 to different TspanC8s via the extracellular regions may cause subtle changes in the structure of an ADAM10 scissor complex, thus resulting in differences in binding affinities towards regulatory protein(s) that may control its localisation or stability.

Based on the results of Eschenbrenner *et al.* (2020), which showed that the large extracellular region of Tspan15 on a Tspan5 backbone was not sufficient to phenocopy wild-type Tspan15 and *vice versa*, perhaps because of aberrant conformation of the entire extracellular region, it is possible that the interaction between the large and small extracellular region of TspanC8s is important for their conformation and function. Indeed, the small extracellular region of TspanC8s is less conserved than the large extracellular region (Matthews, Szyroka, *et al.*, 2017), the latter of which contains residues highly conserved among TspanC8s that are important for interaction with ADAM10 (Section 1.4.5). This suggests that whilst the large extracellular regions of TspanC8s are needed for ADAM10 interaction, subtle distinctions among TspanC8s that contribute to their differential interactions with ADAM10 in the extracellular region (Noy *et al.*, 2016) may arise from their small extracellular regions. Therefore, to assess the finer details of how the Tspan15 extracellular region is important for promoting ADAM10 cleavage of GPVI, it may be of interest to investigate residues in the small extracellular region of Tspan15 that may be important for any potential interaction with the large extracellular region in future investigations.

Figure 49 shows the sequence alignment between TspanC8s and the tetraspanins CD9, CD53 and CD81 to highlight the potential residues of interests based on recent insights from the crystal structures of CD9 (Umeda *et al.*, 2020) and CD53 (Yang *et al.*, 2020). The small extracellular region of Tspan15 is predicted to be relatively short with 18 residues and is most similar to its closest relative Tspan33 (Figure 50) than the other TspanC8s, which are slightly longer and are more similar to each other (discussed further in Section 7.3.3). In the study by Umeda *et al.* (2020), Q40 on the small extracellular region of CD9 was identified as a putative residue that interacts with its large extracellular region to maintain a closed conformation. This most likely corresponds to Q50 on the Tspan15 small extracellular region based on sequence alignment with CD9. However, this putative residue on CD9 was identified based on molecular dynamics simulation with no further experimental evidence. In addition, this residue does not appear to be highly conserved in other less closely related tetraspanins. Unlike CD9, the interaction between the large and small extracellular region CD53 was predicted to support its open conformation in the study by Yang *et al.* (2020). Four residues (L43-N46) in the small extracellular region of CD53 were predicted to be involved in this interaction and mutating these residues impaired CD53 function in promoting B cell migration. In the same study, the authors modelled CD81 based on CD53 and showed that a similar four-residue stretch of hydrophobic residues (L44-L47) on the small extracellular region of CD81 is required to stabilise the open conformation on the basis that mutating these residues caused aberrant glycosylation of its partner protein CD19. Sequence alignment with CD53 did not reveal any strong candidate residues on Tspan15 because of poor sequence conservation. However, it is tantalizing to speculate that mutating these unknown key residues on the small extracellular region of Tspan15 would destabilise its conformation and disrupt ADAM10 function.

```
CD9          ----WLRFDSQTKSIFEQETNNNNSS-------- 22
CD81         ----WLRHDPQTTNLLYLELGDKPAPNTFYVGIY 30
CD53         YLLIHNNFGVLFHNLPSLTLGN------------ 22
Tspan15      ---AEVER--Q--KYKTLESAFLAP--------- 18
Tspan33      --YARLMK--H--AEAALACLAVDP--------- 19
Tspan10      --WGLAVKGSLG-----SDLGGPLPTDP------ 21
Tspan5       --WAWNEKGVLSNISSITDLGGFDP--------- 23
Tspan14      --WAWSEKGVLSDLTKVTRMHGIDP--------- 23
Tspan17      --WAWGEKGVLSNISALTDLGGLDP--------- 23
```

Figure 49. Sequence alignment of the small extracellular regions of TspanC8s, CD9, CD81 and CD53. Multiple sequence alignments were generated using Clustal Omega (Madeira *et al.*, 2019). Residues important for interaction with the large extracellular region identified in Umeda *et al.* (2020) and Yang *et al.* (2020) are highlighted in grey. The number of residues predicted to be in the small extracellular region is indicated at the end.

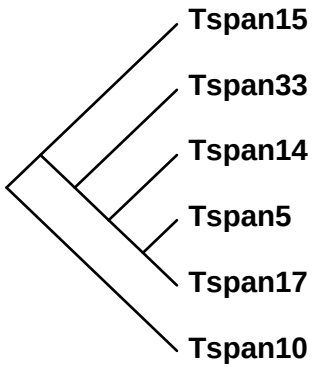

Figure 50. Sequence homology among the six TspanC8s. The TspanC8 subfamily branch from the tetraspanin superfamily tree depicted in Figure 5, Chapter 1 is displayed here to show the relationships among the six TspanC8s based on amino acid sequence identities.

7.2.2 Tspan15 cytoplasmic region may have a minor role in negatively regulating ADAM10 activity

Another highlight of Chapter 3 is the observation that the cytoplasmic region of Tspan15 may have a minor role in negatively regulating ADAM10 scissor activity. In particular, replacement of the C-terminus of Tspan14 by that of Tspan15 was sufficient to abolish the minimal GPVI cleavage rescue seen with the overexpression of wild-type Tspan14/ADAM10 in Tspan14/15/33 triple knockout cells. The Tspan15 C-terminus is relatively long with 38 residues compared to its N-terminus, which has 23 residues, and shares only as high as 26% identity with Tspan10, and as low as 13% with Tspan14 (Figure 51A). Tspan15 C-terminus

contains serine and threonine residues that can potentially be phosphorylated (Figure 51A). The C-terminus also has cysteine residues that can be palmitoylated, and the ability of Tspan15 to reduce ADAM10-mediated Notch signalling when overexpressed was not affected by the mutation of these cysteine residues (Eschenbrenner *et al.*, 2020). It would be of interest to investigate the effects of the same palmitoylation mutations on the shedding of GPVI and other Tspan15/ADAM10 substrates.

Binding of intracellular regulatory proteins to the cytoplasmic region of Tspan15 is another possibility. One potential candidate is 14-3-3 theta, a putative Tspan15-interacting protein identified from the proteomic analysis of Tspan15 immunoprecipitates extracted in the relatively stringent detergent digitonin from HEK-293T cells (Koo *et al.*, 2020). The 14-3-3 theta protein belongs to the highly conserved and ubiquitously expressed 14-3-3 family consisting of seven members in human (Pennington *et al.*, 2018). They act as signalling hubs to control a wide range of cellular processes as they can interact with at least 2000 proteins by binding to phosphorylated serine and threonine residues. Binding of 14-3-3 to its target protein can directly modulate its function by inciting a conformational change or by preventing interaction with other molecules or regulatory proteins, for example, kinases or phosphatases. Since 14-3-3s function as homo- or heterodimers, binding of 14-3-3 can also facilitate protein-protein interactions. Although proteins that can bind 14-3-3 proteins have consensus binding motifs, deviations from the classical consensus sequence also exist (Madeira *et al.*, 2015; Pennington *et al.*, 2018).

Using the 14-3-3-Pred tool, which can predict a diverse range of binding motifs based on known binding sites (Madeira *et al.*, 2015), a potential 14-3-3 binding motif centered around T269 was identified within the C-terminal tail of Tspan15 (Figure 51A). No putative binding sites were

identified in the cytoplasmic tails of other TspanC8s. T269 and neighbouring residues in Tspan15 are highly conserved in mammals, but not in other distant species (Figure 51B). In line with the potential negative regulatory role of the Tspan15 C-terminus, facilitation of Tspan15 interaction with ADAM10 at the cytoplasmic tail via 14-3-3 dimerisation is unlikely because there is no putative 14-3-3 binding site on the cytoplasmic tail of ADAM10. Therefore, perhaps a more likely scenario is the initiation of a negative feedback mechanism through binding of 14-3-3 theta to phosphorylated T269 on the Tspan15 C-terminus to inhibit its function. One potential consequence of 14-3-3 binding that can modulate protease activity had been described for ADAM17 and its partner iRhom2. Binding of 14-3-3 to phosphorylated iRhom2 disrupted its association with ADAM17, leading to ADAM17 activation (Cavadas *et al.*, 2017; Grieve *et al.*, 2017). Since a synthetic Tspan15/ADAM10 fusion protein is active (Koo *et al.*, 2020), the potential dissociation of ADAM10 from a Tspan15/ADAM10 complex upon binding of 14-3-3 theta to phosphorylated Tspan15 would be predicted to disrupt ADAM10 activity, which is the opposite effect of what had been described for iRhom2/ADAM17. This proposed mechanism is highly speculative at present given the diverse function of 14-3-3s and the possibility of other regulatory proteins that may bind to the cytoplasmic domain of Tspan15. To follow this up, it would be important to first confirm whether 14-3-3 theta can be co-immunoprecipitated with Tspan15, and whether mutation of T269 on Tspan15 would impact its binding to 14-3-3 theta. To broaden the scope of investigation, proteomic analysis of proteins that differentially bind Tspan15 in the absence or presence of its cytoplasmic region would also be useful in identifying other potential cytoplasmic-interacting proteins that may regulate ADAM10 activity.

A

```
Tspan15 -----TRVEDIIM-----EHSVTDGLLGPGAKPSVEAAGT-----------
Tspan10 -ARLLGALAA----------RSGAAYGPGAH-GEDRAGPQSPS-PGAPPAA
Tspan33 SQILVNQIKDQIKLQLYNQQHRADPWY-----------------------
Tspan14 ARTLISDIEAVKAGHHF-----------------------------------
Tspan5  AQNLVSDIEAVRASW-------------------------------------
Tspan17 AQNLVSDIKAVKANWSKWNDDFENHWLTPTISEVLSTAGPQQNSLTGAPGPA
              :

Tspan15 --------GCCLCYPN------ 38
Tspan10 KPARG---------------- 43
Tspan33 ---------------------- 27
Tspan14 ---------------------- 17
Tspan5  ---------------------- 15
Tspan17 PPSRHVFFGLGGLYPEPTFKNW 74
```

B

```
Human      TRVEDIIMEHSV-TDGLLG-PGAKPSVE--AAGTGCCLCYPN----- 38
Chimpanzee TRVEDIIMEHSV-TDGLLG-PGAKPSVE--AAGTGCCLCYPN----- 38
Bovine     TRVEDIITEHSV-TDGLLG-PGTKAGVE--AAGTGCCMCYPI----- 38
Mouse      TRVEDIILEHSV-TDGLLG-PGAKSRTD--TAGTGCCLCYPD----- 38
Chicken    TRVEDIIAEHKL-GESLFGGTRQHPDPE--FASPGCCMCYPG----- 39
Frog       TRIEDIINEWDS-SEVLLEGESVKREIE--FSKKGCCRCYPGMESTA 44
Zebrafish  TRVEDAIEEYGYYMDGLLQSDSVQPETKRQSKLAKCCKCMPLMD--- 44
           **:** * *     : *:     :   .       ** * *
```

Figure 51. Sequence alignment of the C-terminal tails of TspanC8s. Multiple sequence alignments of the C-terminal tails of (A) all six human TspanC8s and (B) Tspan15 from mammals (human, chimpanzee, bovine and mouse), chicken, frog and zebrafish were generated using Clustal Omega (Madeira *et al.*, 2019). The putative 14-3-3 binding motif on Tspan15 is highlighted in grey, and the central threonine (T269 on human Tspan15) is in bold. The number of residues predicted to be in C-terminal tail is indicated at the end. Residues that are conserved are indicated with '*'; highly similar residues are indicated with ':'; and residues that share weak similarities are indicated with '.'.

7.2.3 ADAM10 cytoplasmic tail is required for Tspan15 surface expression

Findings from Chapter 5 suggest the possibility that ADAM10 and Tspan15 may be interacting at their cytoplasmic regions because the ADAM10 cytoplasmic tail is required to rescue Tspan15 expression on the surface of ADAM10-knockout cells. Indeed, the cytoplasmic tail of ADAM10 has SH3 binding motifs and can bind to many SH3 domain-containing intracellular proteins (Section 1.2.1), some of which could be mutual binding proteins to both Tspan15 and ADAM10. One such potential candidate is the growth factor receptor-bound protein 2 (GRB2), which has been shown to bind ADAM10 (Ebsen *et al.*, 2014), and is also a potential Tspan15-interacting protein as it was enriched in Tspan15 immunoprecipitates from Tspan15-overexpressing HEK-293T cells (Tomlinson lab, unpublished). It would be useful to verify the interaction between Tspan15 and GRB2, and whether deficiency in GRB2 would affect Tspan15 and ADAM10 expression. However, ADAM10 does not appear to require the tails of Tspan15 to get to the cell surface because ADAM10 surface expression in Tspan15-knockout cells can be rescued by the tails-truncated Tspan15 mutant, suggesting that for ADAM10, interaction via the extracellular region may be sufficient to support the expression of Tspan15/ADAM10 on the cell surface (Szyroka, 2019). It is worth mentioning that the tails-truncated Tspan15 retains short stretches of residues near the predicted transmembrane regions at each terminus (5 and 14 residues for N- and C-terminus, respectively) as a preventive measure to limit potential disruption of the transmembrane helices (Table 4, Chapter 2), thus the possibility that these residues could facilitate Tspan15 and ADAM10 interaction cannot be excluded. Nevertheless, mechanisms other than cytoplasmic interactions should be considered.

It has been shown via cross-linking and co-immunoprecipitation experiments that ADAM10 can exist as homodimers on the cell surface, and that the truncation of its cytoplasmic domain disrupted dimerisation (Xu *et al.*, 2012). A follow-up study confirmed that ADAM10

dimerisation requires its cytoplasmic tail and support from the transmembrane domain (Deng *et al.*, 2014). Since the tail-truncated ADAM10, which cannot dimerise, failed to support Tspan15 expression on the cell surface, it raises the possibility that Tspan15 may preferentially bind to ADAM10 dimers. As a precedence, two recent independent studies reporting the cryo-EM structures of CD9 in complex with either of its partner proteins, EWI-F or EWI-2, revealed that each EWI homodimer is sandwiched between two CD9 molecules to form a linear tetrameric complex (Oosterheert *et al.*, 2020; Umeda *et al.*, 2020). Therefore, such an arrangement may also be favoured for the stabilisation of Tspan15/ADAM10 complexes on the cell surface. Moving forward, quantifying the stoichiometry of Tspan15/ADAM10 complexes using advanced microscopy techniques, such as BiFC-FCS established in Chapter 5, would be an attainable approach to examine this hypothesis.

7.3 Regulation of ADAM10 substrate specificity by TspanC8s

How is the substrate repertoire of each TspanC8/ADAM10 scissor determined? Taking together the findings from this thesis and evidence from other studies, a proposed model of this multi-level regulation is summarised in Figure 52.

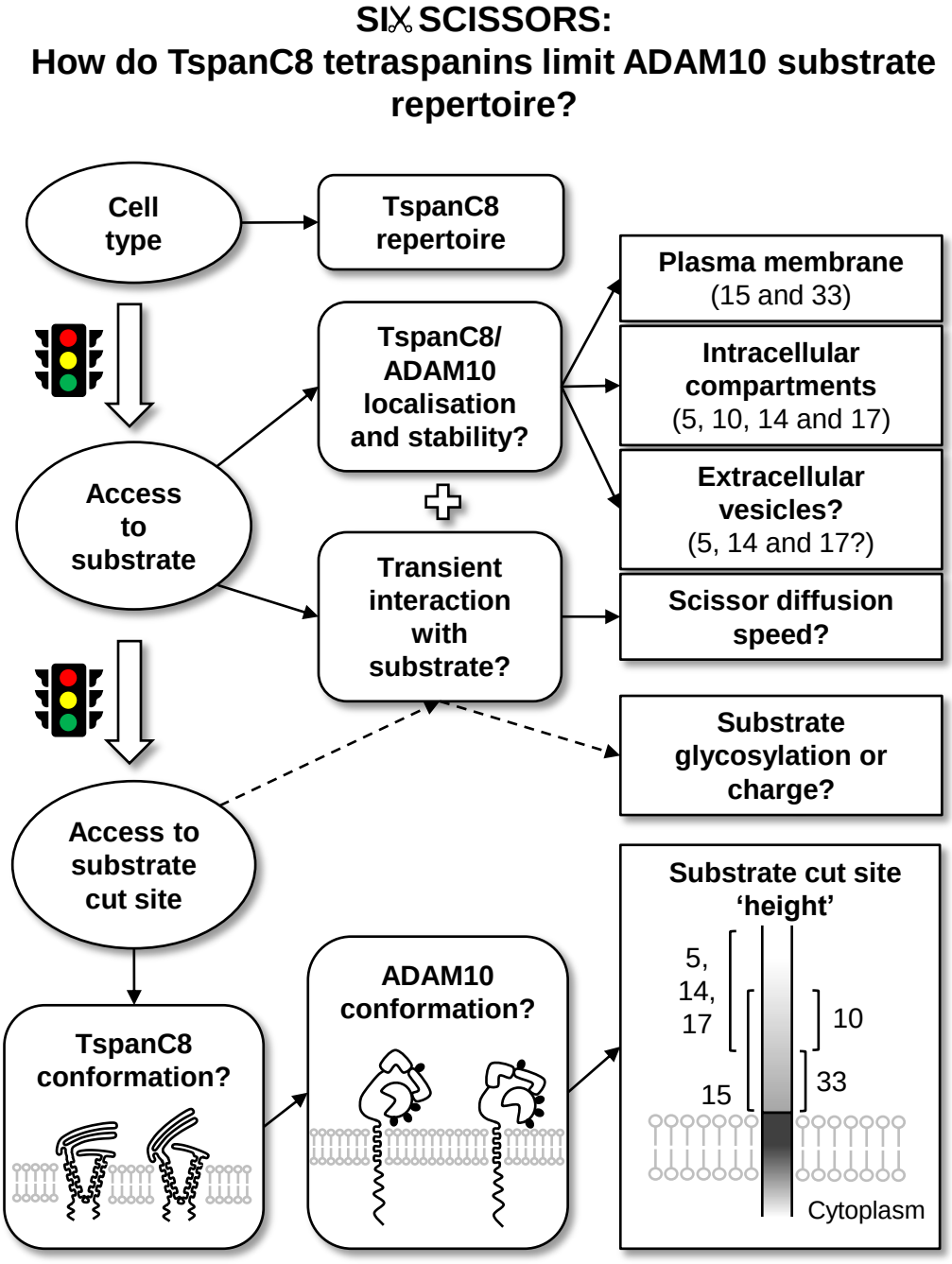

Figure 52. Proposed model of the mechanisms of TspanC8 regulation of ADAM10 substrate specificity. ADAM10 substrate specificity is controlled at three major checkpoints with tight regulation by TspanC8s and substrate properties at each level.

7.3.1 Substrate cleavage is limited by the TspanC8 repertoire in different cell types

As most ADAM10 cleavage events occur in *cis*, i.e., within the same cell, the first checkpoint that decides which TspanC8/ADAM10 scissor is important for cutting a substrate is whether the cell that the substrate is expressed in also expresses the TspanC8/ADAM10 scissor. This concept can be best illustrated by Notch. Notch activity has been shown to be promoted principally by Tspan5/ADAM10 or Tspan14/ADAM10 scissors in multiple cell types (Dornier *et al.*, 2012; Zhou *et al.*, 2014; Jouannet *et al.*, 2016; Saint-Pol, Billard, *et al.*, 2017; Eschenbrenner *et al.*, 2020). However, Tspan14-knockout mice, like ADAM10-knockout and Notch-knockout mice, are embryonic lethal (MRC Harwell and Tomlinson, unpublished), whereas Tspan5-knockout mice show no apparent phenotype (Saint-Pol, Billard, *et al.*, 2017). This discrepancy is likely because Tspan14 is ubiquitously expressed whereas Tspan5 expression is tissue-restricted (Section 1.4.3). Therefore, even though Tspan5/ADAM10 and Tspan14/ADAM10 may have the same capacities to cleave Notch, Tspan14/ADAM10 may be the more relevant scissor because of its broader expression profile.

Findings from Chapter 3 and Chapter 6 clearly showed that the cleavage capacity of each TspanC8/ADAM10 scissor was different for GPVI and other substrates, even when the TspanC8/ADAM10 scissors were expressed at comparable levels. This suggests that other key controls must exist downstream to fine-tune ADAM10 cleavage of ~100 different substrates.

7.3.2 TspanC8s regulate ADAM10's access to substrates

The most straightforward, logical mechanism as to how TspanC8s limit the substrate repertoire of ADAM10 is thought to be through membrane partitioning since it is well established that TspanC8s differentially ADAM10 localisation in different membrane compartments within the cell (Section 1.4.4). Although not included in this thesis, it was observed that in HEK-293T

cells overexpressing TspanC8/ADAM10 complexes, a small percentage of each TspanC8 was present in cell culture supernatant as detected by Western blotting. In addition, Tspan5, Tspan14 and Tspan17 were able to promote secretion of full-length mature ADAM10 into cell culture supernatant and were more efficient in doing so than the other TspanC8s (data not shown). Whether these signals originated from extracellular vesicles remains to be investigated, but may be the most likely possibility. This is because the release of mature ADAM10 into extracellular vesicles has been demonstrated (Stoeck *et al.*, 2006; Tosetti *et al.*, 2018; Seifert *et al.*, 2021). Tetraspanins are also well known for their enrichment in extracellular vesicles (Andreu and Yáñez-Mó, 2014). Among TspanC8s, Tspan14 is frequently detected in extracellular vesicles (Keerthikumar *et al.*, 2015; Dozio and Sanchez, 2017; Silva *et al.*, 2021). In fact, profiling of HEK-293T exosomes identified the presence of ADAM10, Tspan14, Tspan15 and Tspan33 (Li *et al.*, 2016). The lesser ability of Tspan15 to promote ADAM10 secretion may also partially contribute to why the absence of Tspan15 enhances the downregulation of ADAM10 on the cell surface following ADAM10 inhibition (Chapter 5), perhaps because ADAM10 can now bind to other TspanC8s, such as Tspan14, that are better at promoting ADAM10 release into the extracellular space. Therefore, the possibility that the TspanC8/ADAM10 scissor identity for a substrate is different in different compartments should be considered when examining cleavage of ADAM10 substrates known to occur in both intracellular compartments and in exosomes, for example, the IgE receptor CD23 (Mathews *et al.*, 2010; Padro *et al.*, 2013).

In contrast to the localisation hypothesis, Chapter 3 and Chapter 6 found no clear association between the degree of colocalisations of wild-type or mutant TspanC8/ADAM10 scissors with GPVI or N-cadherin and their scissor abilities, at least at a steady state when imaged in fixed cells. Although the study by Eschenbrenner *et al.* (2020) considered the effects of protein turnover when comparing the abilities of Tspan5/15 chimeras in promoting Notch activation,

the authors also did not find clear association between endocytosis and the extent of Notch activation. Although there is no clear evidence of direct interaction of ADAM10 or TspanC8s with its substrates from proteomics (Jouannet *et al.*, 2016; Sidahmed-Adrar *et al.*, 2019; Koo *et al.*, 2020) or from co-immunoprecipitation experiments (Matthews, 2019), the possibility of transient interactions cannot be excluded, especially since ectodomain shedding is a rapid and transient process. Together, these findings highlight the need to further improve spatio-temporal resolution in future studies by developing advanced live-cell single-molecule spectroscopy or microscopy techniques that are capable of capturing transient interactions and simultaneously quantifying shedding in real-time. For example, live-cell single-molecule total internal reflection (TIRF) microscopy (Sungkaworn *et al.*, 2017) may be suitable for tracking events at the surface of cells transfected with low levels of TspanC8/ADAM10 BiFC complexes and GPVI labelled with a small tag, for example by introducing fluorescent unnatural amino acids at the extracellular domain (Lee, Kang and Park, 2019), to monitor any transient interaction between each scissor and GPVI, and whether this interaction would affect the rate and extent of shedding by quantitating the loss of fluorescent signal from the tagged GPVI. As discussed in Chapter 5, it would also be useful to compare the lateral diffusion speeds of TspanC8/ADAM10 scissors, which may introduce another aspect that affect their capacities to cleave a substrate. Given that Tspan15 has a pro-invasive role in cancer (Harrison, Koo and Tomlinson, 2021), could it be that it is also the fastest travelling scissor, hence can capture and proceed to cleave a substrate quicker than the others? This could in part explain why Tspan15/ADAM10 appears to be the most efficient scissor for most substrates on the cell surface, including GPVI.

7.3.3 TspanC8s regulate ADAM10's access to substrate cut sites

Lastly, findings in Chapter 3 added another layer of regulation by providing the first evidence that TspanC8s may control ADAM10's access to substrate cut sites depending on the distance of ADAM10 cut site from the membrane surface. This could be because each TspanC8 interacts with ADAM10 differently as demonstrated by Noy *et al.* (2016), therefore positioning the metalloprotease domain at different angles such that each TspanC8/ADAM10 scissor has limited access to different substrate cut sites. Again, the most closely related Tspan5, Tspan14 and Tspan17 (Figure 50) behave similarly in that they allow ADAM10 to access cut sites located at a distance further away from the membrane, suggesting functional grouping by amino acid sequence similarities. Indeed, this is also evident from the alignment of their small extracellular regions alone, which showed that they are the most similar among TspanC8s (Figure 49). It was proposed that the length of the small extracellular region of tetraspanins may affect the shape of the open conformation and consequently partner interaction. This is because modelling comparison between the open conformations of CD81 and CD53 show that the large extracellular region of CD81 can extend further away from the membrane surface because of its longer small extracellular region (Figure 49), therefore explaining how it is able to interact with CD19 via a site located at a great distance from the membrane surface (Yang *et al.*, 2020). By the same logic, it is intriguing to note the association between the length of the small extracellular regions of TspanC8s and their preferred cut site distance ranges (Figure 49 and Figure 52). Specifically, Tspan5, Tspan14 and Tspan17, which have the longest small extracellular regions among TspanC8s, are also the TspanC8/ADAM10 scissors that prefer cut sites located at a greater distance away from the membrane surface. In contrast, Tspan15 and Tspan33 have shorter small extracellular regions, and this coincides with their preferences for cut sites located closer to the membrane surface. Therefore, it raises the exciting possibility that

the proposed stabilisation of the ADAM10 metalloprotease domain at different angles may be due to the subtle differences in the interactions between the small and large extracellular regions of TspanC8s in their open conformations. Ultimately, confirming this hypothesis would require high-resolution structures of each TspanC8/ADAM10 complex in its native environment, for example, by cryo-EM of the complexes solubilised in a detergent-free manner using styrene maleic acid lipid particles (SMALPs) (Pollock *et al.*, 2018).

Besides the distance of ADAM10 cut site from the membrane surface, alternative factors that could also contribute to the cleavage sequence specificity by each TspanC8/ADAM10 scissor observed in Chapter 3 should also be considered. O-glycans (Goth *et al.*, 2015; Shirakabe *et al.*, 2017) or negatively charged residues (Iwagishi *et al.*, 2020) surrounding the substrate cut site have been shown to reduce the susceptibility of substrates to ADAM17 cleavage. No such studies were reported for ADAM10 substrates, although some substrates appear to bind better to secondary substrate binding sites on ADAM10 when glycosylated (Madoux *et al.*, 2016). Notch1 has an O-glycosylation site close to the cleavage site at T1725, which is four residues downstream of its cleavage site, and interestingly, the glycopeptide has increased, rather than reduced susceptibility to ADAM17 cleavage (Boskovski *et al.*, 2013). Although not included in the current study, preliminary findings from a pilot investigation showed that cleavage of a presumed unglycosylated form of Notch1 cut site sequence by Tspan5/ADAM10 and Tspan14/ADAM10 scissors were reduced, and instead, favoured by Tspan15/ADAM10 scissor, compared to the glycosylated form (data not shown). Therefore, could charge interactions affect the affinity of a TspanC8/ADAM10 scissor towards a substrate? The preliminary data hinted at such a possibility but should be verified by comparing the cleavage of Notch1 and a T1725A mutant to remove the O-glycosylation site. Interestingly, GPVI also has an O-glycosylation site seven residues upstream of the ADAM10 cleavage site at S256 (King *et al.*, 2017); however,

none of the GPVI cleavage assays in this study revealed the possibility of its scissor identity being affected by changes in glycosylation. Therefore, this proposed mechanism is highly speculative at present unless transient interactions between TspanC8/ADAM10 and their substrates can be demonstrated in the future.

In summary, there is no single mechanism that can on its own, explain how TspanC8s regulate ADAM10 substrate specificity as it likely involves the interplay among different tightly regulated mechanisms.

7.4 Therapeutic potential of Tspan15

7.4.1 High *TSPAN15* expression level may protect against venous thrombosis

Chapter 4 revealed that an increased *TSPAN15* expression may explain why a minor *TSPAN15* haplotype consisting of 17 SNPs may have reduced venous thrombosis risk. Since Tspan15 is an essential subunit of an ADAM10 scissor complex, it is likely that Tspan15 may modulate venous thrombosis risk by affecting cleavage of ADAM10 substrates that are directly involved in the pathogenesis of venous thrombosis. A proposed mechanism involving GPVI and two other ADAM10 substrates, APP and the endothelial protein C receptor (EPCR), is summarised in Figure 53.

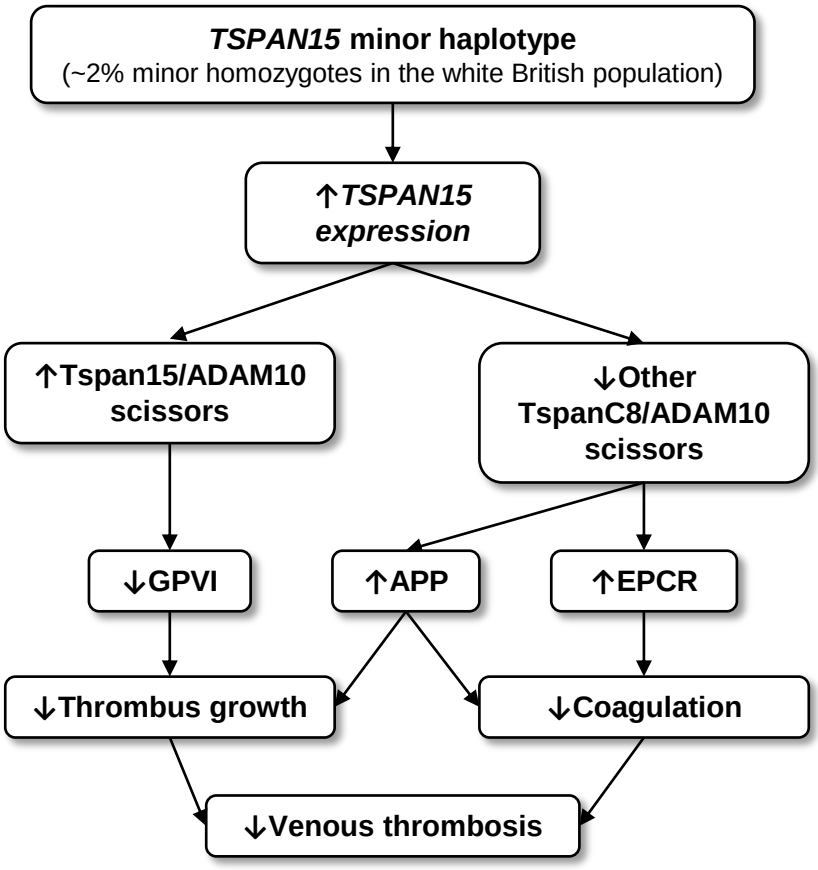

Figure 53. Proposed mechanism of how individuals with the *TSPAN15* minor haplotype may have lower venous thrombosis risk. High Tspan15 expression may downregulate the pro-thrombotic GPVI, upregulate the anti-thrombotic and anti-coagulant APP and anti-coagulant EPCR to reduce venous thrombosis risk.

7.4.1.1 GPVI

As discussed in Chapter 4, *GP6* polymorphisms may play little or no role in determining venous or arterial thrombosis risk. Setting aside any genetic link, the role of platelets in promoting thrombus growth via GPVI has been demonstrated experimentally, such as in an *in vitro* model of venous thrombosis using human blood (Lehmann *et al.*, 2018). Therefore, it is possible that a higher Tspan15 expression level may increase ADAM10-mediated GPVI cleavage, and subsequently reduce GPVI-dependent thrombus growth. It is important to note that mouse GPVI, which shares only ~65% sequence identity with human GPVI (Jandrot-Perrus *et al.*, 2000), does not appear to have a role in venous thrombosis formation in a mouse model (Payne, 2018), suggesting species differences which should be considered in the experimental design of future studies. Indeed, mouse platelets do not express Tspan15 (Matthews, Noy, *et al.*, 2017), which may limit the usefulness of mouse models in investigating the role of platelet Tspan15 in venous thrombosis.

7.4.1.2 APP

APP, which is abundantly expressed on platelets, may be another potential ADAM10 substrate. The role of platelet APP in protection against venous thrombosis has been demonstrated (Canobbio *et al.*, 2017). In this study, APP deficiency in mice showed marked increase in thrombus size, embolism and vessel occlusion in venous thrombosis models. The data suggest that this is mediated through the anti-coagulation and anti-inflammatory roles of APP. This study did not demonstrate the involvement of APP in haemostasis or arterial thrombosis, but a more recent study showed that APP-knockout mice have mild bleeding phenotypes, suggesting a minor role of platelet APP in haemostasis (Mazinani *et al.*, 2020). Nevertheless, it has become more apparent that full-length APP can have anti-coagulant and anti-thrombotic properties (Schmaier, 2017). This suggests that retaining full-length APP, perhaps through limiting

shedding, may be protective against venous thrombosis. As introduced in Section 1.4.2, it is unclear which TspanC8/ADAM10 scissors cleave APP because of conflicting observations in different cell types. However, combining all the evidence so far, it can be speculated that another TspanC8/ADAM10 scissor that is not Tspan15/ADAM10 is responsible for shedding APP. When Tspan15 expression is increased, less of this TspanC8/ADAM10 scissor may be available to cleave APP because of increased competition for ADAM10 binding. This is a plausible mechanism because downregulation of Tspan15 on the cell surface has been observed in cells overexpressing Tspan14 in two different cell lines, suggesting that TspanC8s compete for ADAM10 when ADAM10 is limited (data not shown). Therefore, more full-length APP may be available to limit venous thrombosis when Tspan15 expression is increased.

7.4.1.3 EPCR

EPCR, encoded by the *PROCR* gene, is another potential candidate ADAM10 substrate expressed primarily on endothelial cells (Gandrille, 2008; Rao, Esmon and Pendurthi, 2014; Pendurthi and Vijaya Mohan Rao, 2018). Of note, EPCR is palmitoylated (Pendurthi and Vijaya Mohan Rao, 2018), suggesting its potential association with tetraspanin nanodomains (van Deventer, Arp and van Spriel, 2021). Indeed, EPCR was identified as a tetraspanin-associated protein from mass spectrometry analysis of CD9 immunoprecipitates from HUVECs lysed in the relatively mild detergent Brij97 that preserves interactions among tetraspanin nanodomains (Tomlinson lab, unpublished). EPCR has a well-established role in venous thrombosis as a crucial player in the protein C anti-coagulant pathway (Gandrille, 2008; Rao, Esmon and Pendurthi, 2014; Pendurthi and Vijaya Mohan Rao, 2018). Indeed, mice deficient in EPCR are embryonic lethal due to excessive fibrin deposition, highlighting its key role as an anti-coagulant (Gu *et al.*, 2002). As its name suggests, EPCR primarily binds protein C, although it can also bind other ligands. Binding of protein C to EPCR stimulates its conversion to activated

protein C by thrombin to trigger downstream anti-coagulant and anti-inflammatory effects. In contrast, soluble EPCR, which can be generated through ectodomain shedding, has pro-coagulant and pro-inflammatory properties because it acts as a decoy by competing with its membrane-bound counterpart for ligand binding. Therefore, increased shedding of EPCR increases risk of thrombosis (Gandrille, 2008).

Indeed, more than 20 publications have identified venous thrombosis-associated SNPs in the *PROCR* locus. Of these, the coding SNP rs867186, with a minor allele frequency of ~0.1, results in a S219G substitution in the transmembrane domain and is associated with increased venous thrombosis risk (Lindström *et al.*, 2019). This amino acid change is associated with an increase in soluble EPCR levels in the plasma samples of patients (Saposnik *et al.*, 2004). Further studies have confirmed this and demonstrated *in vitro* that the risk variant is more susceptible to shedding in primary HUVECs and in transfected cells (Ireland *et al.*, 2005; Qu *et al.*, 2006). ADAM10 and ADAM17 were both shown to be the sheddases for EPCR. In one study, EPCR shedding was shown to be ADAM17-dependent because ADAM17 knockdown reduced PMA-induced EPCR shedding in HUVECs and in EPCR-transfected cells (Qu *et al.*, 2007). In a more recent study, ADAM10 was found to be the sole sheddase for EPCR on primary human endothelial cells when shedding was induced by bacterial infection, but ADAM17 can still shed EPCR in response to PMA in the absence of ADAM10 (Lécuyer *et al.*, 2018). This suggests that EPCR can be differentially cleaved by ADAM10 and ADAM17 depending on the stimulus, and the need to first verify whether ADAM10 is the principal sheddase in the context of venous thrombosis. Moreover, the fact that increased shedding of EPCR increases venous thrombosis risk contradicts with the initial hypothesis that increased substrate shedding by Tspan15/ADAM10 scissor protects against venous thrombosis. It is therefore tantalizing to speculate that like APP, another TspanC8/ADAM10 scissor may be responsible for shedding

EPCR, thus an increase in Tspan15 expression may lead to an indirect reduction in EPCR shedding.

Taking a step back, whilst the discovery that high *TSPAN15* mRNA expression associates with reduced venous thrombosis risk led to exciting hypotheses for future investigations as described above, it would be worthwhile to first confirm whether elevated Tspan15 expression is true at the protein level. Because of the availability of effective Tspan15 mAbs, this is now achievable by comparing Tspan15 expression in individuals with different *TSPAN15* haplotypes.

7.4.2 Feasibility of targeting Tspan15 to modulate ADAM10-mediated GPVI shedding

Chapter 6 showed that there is little functional redundancy of Tspan15/ADAM10 with the other TspanC8/ADAM10 scissors, apart from the most closely related Tspan33/ADAM10 scissors (Figure 50), but only to a small extent for some substrates in an overexpression system. In combination with the observation that shedding is substantially reduced or completely abolished in Tspan15-knockout cells for substrates known to be cleaved by Tspan15/ADAM10 only, the possibility that other TspanC8s may completely take over the role of Tspan15 when it is depleted is unlikely to be a concern. For GPVI, one could say that functional redundancy between Tspan15 and Tspan33 has already been demonstrated by the fact that it can be cleaved by both Tspan15/ADAM10 and Tspan33/ADAM10 scissors. However, Chapter 3 also revealed that Tspan15/ADAM10 is the more efficient scissor for GPVI, and in an anti-platelet strategy involving induction of GPVI shedding, the involvement of Tspan33/ADAM10 scissors would not be a concern.

Since Tspan15/ADAM10 is the most efficient scissor for GPVI, therapeutic targeting of Tspan15 to induce ADAM10-mediate GPVI shedding may be a better anti-platelet strategy than direct targeting of ADAM10. This is because one would predict that activating one scissor that

has a smaller substrate repertoire would lead to fewer side effects than activating all six TspanC8/ADAM10 scissors. However, one can also argue that targeting Tspan15 to modulate GPVI expression is less specific than directly targeting GPVI itself for two reasons. First, unlike GPVI, Tspan15 is not exclusively expressed on platelets; in the vasculature, for example, Tspan15 protein expression has also been confirmed on endothelial cells (Koo *et al.*, 2020). Second, other than GPVI, Tspan15/ADAM10 can cleave other substrates, for example, RAGE, which is also expressed on platelets (Gawlowski *et al.*, 2009). To overcome this challenge, specificity can be enhanced through drug design, for example, by engineering a bispecific antibody targeting both Tspan15 and GPVI to increase specificity towards platelet Tspan15 and which may also have the potential of bringing GPVI closer to Tspan15/ADAM10 scissors to enhance shedding. Indeed, preliminary proof-of-concept work suggests that a Tspan15/GPVI bispecific antibody retained the ability to recognise Tspan15 and GPVI, albeit at a lower affinity (data not shown). Whether this bispecific antibody brings Tspan15 and GPVI together has yet to be determined, but interestingly, it inhibited, rather than induced GPVI shedding in transfected cells (data not shown).

Although the Tspan15/GPVI bispecific antibody described above is only the beginning of a pilot experiment and more work is required before deeming the shedding-inducing strategy an impossible feat, it unquestionably highlighted the challenge of designing or obtaining functional antibodies that activate the function of the target of interest. From a therapeutic antibody design perspective, generating inhibitory antibodies are less challenging. This is because binding of an antibody to the target alone is usually sufficient to induce internalisation and target depletion, whereas activating antibodies would likely require targeting a specific epitope or conformation to enhance its function. This limitation may perhaps be overcome by recent advances in antibody display and screening technologies that can isolate activating

antibodies more efficiently from a wider selection of candidates with diverse epitopes (Lu *et al.*, 2020).

One counter-argument as to why targeting Tspan15/ADAM10 scissors may be more appealing than targeting GPVI itself is the additional effect of generating Revacept-like soluble GPVI (Section 1.5.4), which can compete with membrane-bound GPVI in binding collagen or fibrin. However, anti-GPVI antibodies can also induce its shedding, as demonstrated by several anti-GPVI mAbs, although these mAbs have limited therapeutic potential as they also induce platelet aggregation (Al-Tamimi *et al.*, 2009).

Considering the hurdles that need to be overcome to achieve a successful anti-platelet strategy involving activation of Tspan15/ADAM10-mediated shedding of GPVI, direct targeting of GPVI appears to be the path of least resistance to the already challenging task of drug development. Nevertheless, inhibiting Tspan15/ADAM10-mediated shedding of GPVI could still be useful in other scenarios when preventing GPVI shedding is favourable, such as in severely injured trauma patients who experience life-threatening trauma-induced haemorrhage due to loss of GPVI from excessive shedding (Vulliamy *et al.*, 2020).

7.5 Concluding remarks

Using the platelet-activating receptor GPVI as a model substrate, this thesis provided further evidence to the 'six scissors' hypothesis by unravelling several novel mechanisms that together orchestrate how six different TspanC8 tetraspanins differentially regulate ADAM10 expression, activity and substrate specificity. Tspan15 and ADAM10 reciprocally regulate each other's expression, and together they form the most efficient scissor complex for GPVI cleavage. Besides this, this thesis has demonstrated the relevance of Tspan15 in cardiovascular disease as high Tspan15 expression level may provide a molecular basis to how genetic variations in *TSPAN15* confer protection against venous thrombosis. Mechanistically, the activity of the Tspan15/ADAM10 scissor is supported by Tspan15 extracellular region, but the cytoplasmic region may have a minor negative regulatory role. Each TspanC8/ADAM10 complex may have differential access to substrate cut sites, depending on the distance of the cut site from the membrane surface. Despite the lack of evidence to support the hypothesis that scissor specificity is regulated by proximity of a substrate to its TspanC8/ADAM10 scissor, this research highlighted the need to consider the dynamics of transient interactions between a scissor and its substrate in future investigations. Future studies aiming to understand the biology of TspanC8s should focus on the interaction between their small and large extracellular regions, and regulatory proteins that may bind their cytoplasmic regions, to inform better decision in the design of therapeutics targeting TspanC8s.

APPENDIX

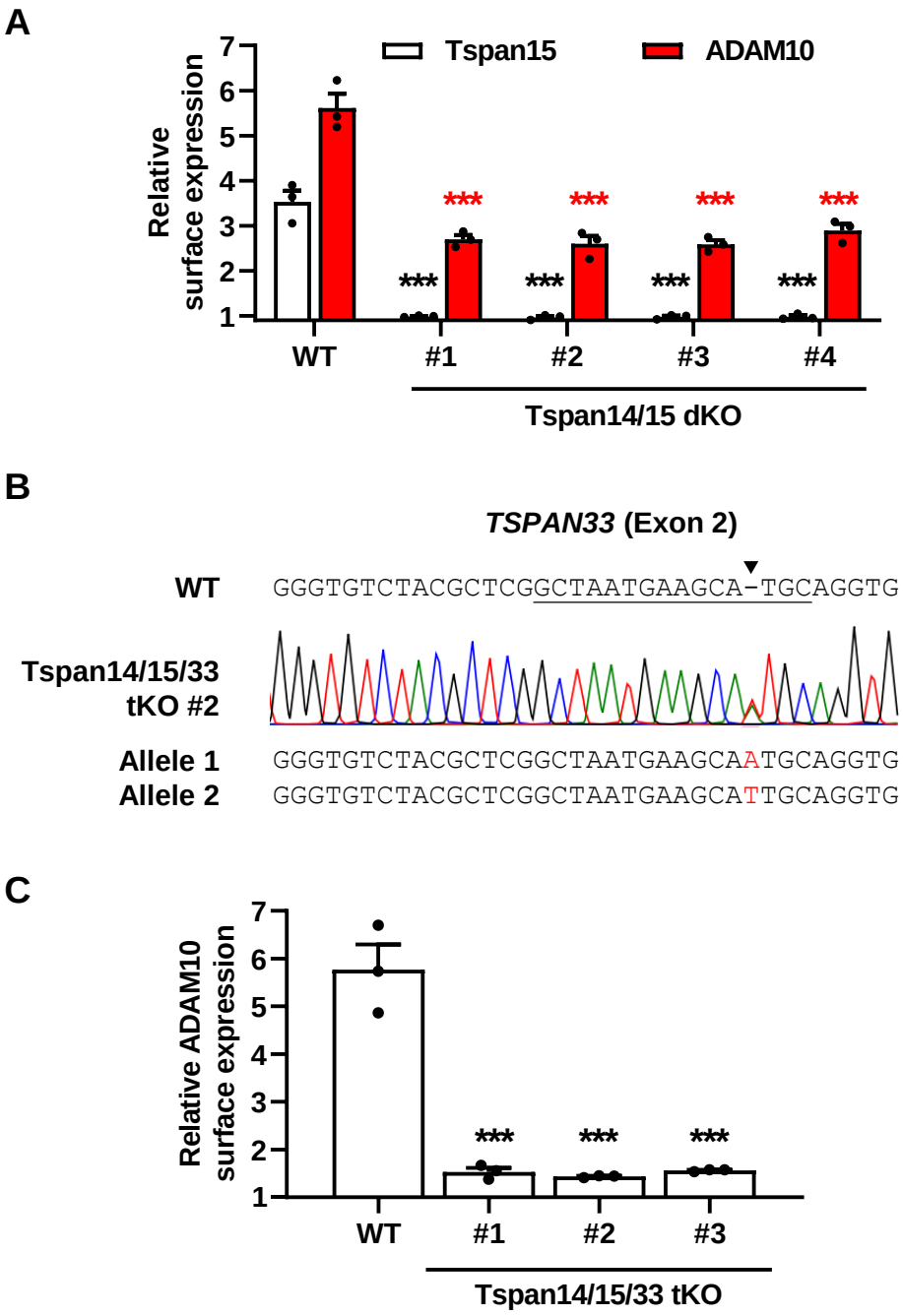

Figure A1. Validation of Tspan14/15 double knockout and Tspan14/15/33 triple knockout HEK-293T cells. (A) Tspan14-knockout HEK-293T cells were used to generate Tspan14/15 double KO (dKO) cells by CRISPR/Cas9. Tspan15 and ADAM10 surface expression in wild-type (WT) and four different Tspan14/15 dKO clones were analysed by flow cytometry. Surface expression level was presented as geometric mean intensity relative to the isotype control staining. Data were arcsine-transformed and analysed by ANOVA followed by Dunnett's multiple comparisons test (***p<0.001, compared to WT cells). Error bars represent standard errors of the mean from three independent experiments. (B) Representative *TSPAN33* sequence trace and alignment of Tspan14/15/33 triple knockout (tKO) HEK-293T (clone #2) generated from Tspan14/15 dKO cells (clone #3) in panel A. Base insertions are in red. The 20-nucleotide guide is underlined; arrow denotes Cas9 cut site. (C) Surface ADAM10 levels in three different clones of Tspan14/15/33 tKO cells were measured by flow cytometry as described in panel A.

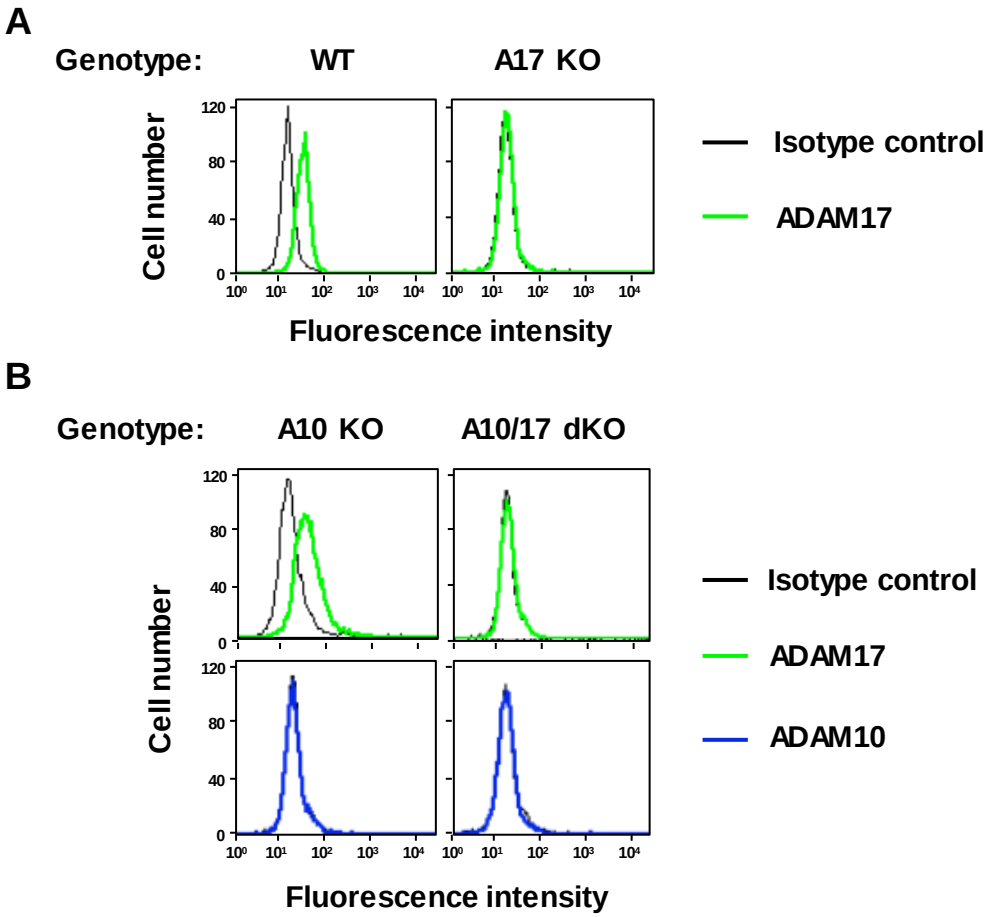

Figure A2. Validation of ADAM17-knockout and ADAM10/17 double knockout HEK-293T cells. Wild-type (WT) and ADAM10 (A10)-knockout (KO) HEK-293T cells were used to generate ADAM17 (A17) and ADAM10 and ADAM17 (A10/17) double KO (dKO) cells, respectively, by CRISPR/Cas9. (A) ADAM17 surface expression in WT and A17 KO cells were analysed by flow cytometry with an anti-ADAM17 mAb or mouse IgG1 isotype control. (B) ADAM17 and ADAM10 surface expression in A10 KO and A10/17 dKO cells were measured by flow cytometry with anti-ADAM17, anti-ADAM10 or the isotype control. Histograms are representative of two independent experiments from four different clones of each genotype from two different guides.

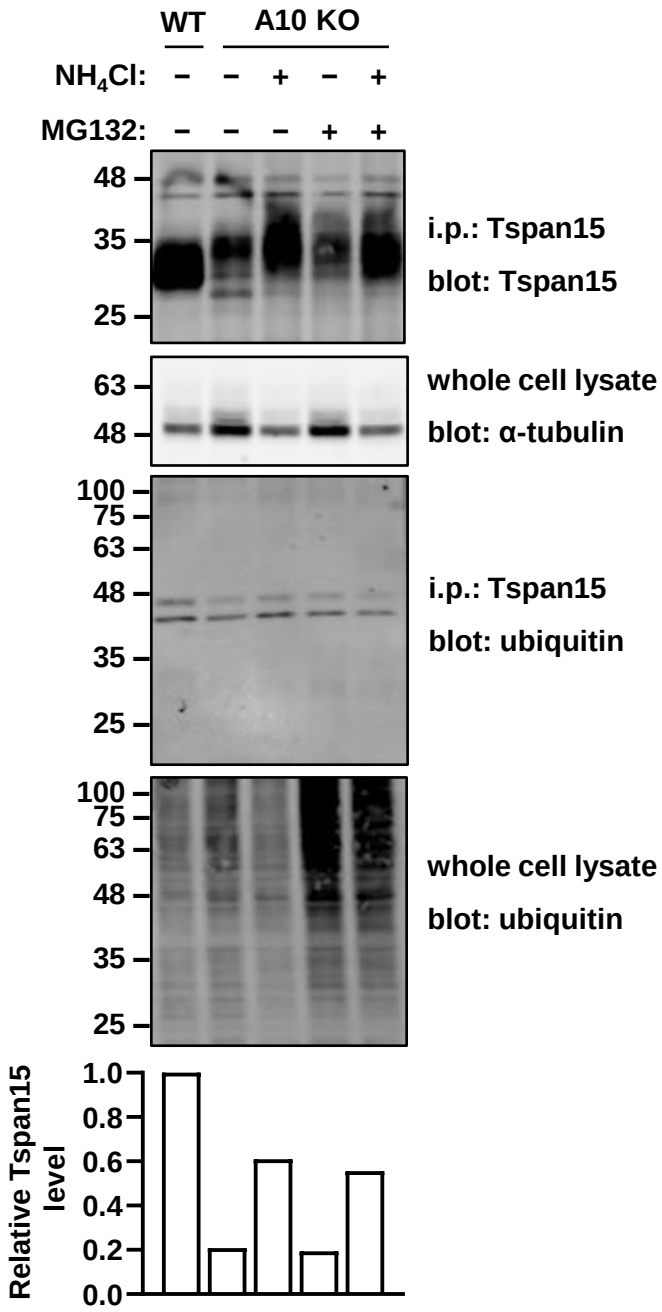

Figure A3. Proteosome inhibition does not rescue Tspan15 expression in ADAM10-knockout cells. Wild-type (WT) and ADAM10-knockout (A10 KO) A549 cells were treated with 50 mM NH_4Cl to inhibit lysosomes, 10 μM MG132 to inhibit proteasomes, or a combination of both for 20 hours. Cells were lysed in 1% Triton X-100 lysis buffer. Lysates were immunoprecipitated and Western blotted with Tspan15 mAb. Lysates were blotted for α-tubulin as a loading control. Tspan15 immunoprecipitates and lysates were also blotted for ubiquitin as a positive control for MG132 (top panels). The amount of immunoprecipitated Tspan15 was quantitated, normalised to tubulin expression, and presented relative to WT cells (bottom panel).

REFERENCES

Aguet, F., Barbeira, A. N., Bonazzola, R., Brown, A., Castel, S. E., Jo, B., Kasela, S., Kim-Hellmuth, S., Liang, Y., Oliva, M., Flynn, E. D., Parsana, P., Fresard, L., Gamazon, E. R., Hamel, A. R., He, Y., Hormozdiari, F., Mohammadi, P., Muñoz-Aguirre, M., Park, Y. S., Saha, A., Segrè, A. v., Strober, B. J., Wen, X., Wucher, V., Ardlie, K. G., Battle, A., Brown, C. D., Cox, N., Das, S., Dermitzakis, E. T., Engelhardt, B. E., Garrido-Martín, D., Gay, N. R., Getz, G. A., Guigó, R., Handsaker, R. E., Hoffman, P. J., Im, H. K., Kashin, S., Kwong, A., Lappalainen, T., Li, Xiao, MacArthur, D. G., Montgomery, S. B., Rouhana, J. M., Stephens, M., Stranger, B. E., Todres, E., Viñuela, A., Wang, G., Zou, Y., Anand, S., Gabriel, S., Graubert, A., Hadley, K., Huang, K. H., Meier, S. R., Nedzel, J. L., Nguyen, D. T., Balliu, B., Conrad, D. F., Cotter, D. J., DeGoede, O. M., Einson, J., Eskin, E., Eulalio, T. Y., Ferraro, N. M., Gloudemans, M. J., Hou, L., Kellis, M., Li, Xin, Mangul, S., Nachun, D. C., Nobel, A. B., Park, Y., Rao, A. S., Reverter, F., Sabatti, C., Skol, A. D., Teran, N. A., Wright, F., Ferreira, P. G., Li, G., Melé, M., Yeger-Lotem, E., Barcus, M. E., Bradbury, D., Krubit, T., McLean, J. A., Qi, L., Robinson, K., Roche, N. v., Smith, A. M., Sobin, L., Tabor, D. E., Undale, A., Bridge, J., Brigham, L. E., Foster, B. A., Gillard, B. M., Hasz, R., Hunter, M., Johns, C., Johnson, M., Karasik, E., Kopen, G., Leinweber, W. F., McDonald, A., Moser, M. T., Myer, K., Ramsey, K. D., Roe, B., Shad, S., Thomas, J. A., Walters, G., Washington, M., Wheeler, J., Jewell, S. D., Rohrer, D. C., Valley, D. R., Davis, D. A., Mash, D. C., Branton, P. A., Sobin, L., Barker, L. K., Gardiner, H. M., Mosavel, M., Siminoff, L. A., Flicek, P., Haeussler, M., Juettemann, T., Kent, W. J., Lee, C. M., Powell, C. C., Rosenbloom, K. R., Ruffier, M., Sheppard, D., Taylor, K., Trevanion, S. J., Zerbino, D. R., Abell, N. S., Akey, J., Chen, L., Demanelis, K., Doherty, J. A., Feinberg, A. P., Hansen, K. D., Hickey, P. F., Hou, L., Jasmine, F., Jiang, L., Kaul, R., Kellis, M., Kibriya, M. G., Li, J. B., Li, Q., Lin, S., Linder, S. E., Pierce, B. L., Rizzardi, L. F., Smith, K. S., Snyder, M., Stamatoyannopoulos, J., Tang, H., Wang, M., Branton, P. A., Carithers, L. J., Guan, P., Koester, S. E., Little, A. R., Moore, H. M., Nierras, C. R., Rao, A. K., Vaught, J. B. and Volpi, S. (2020) "The GTEx Consortium atlas of genetic regulatory effects across human tissues," *Science*, 369(6509), pp. 1318–1330. doi: 10.1126/SCIENCE.AAZ1776.

Aguet, F., Brown, A. A., Castel, S. E., Davis, J. R., He, Y., Jo, B., Mohammadi, P., Park, Y. S., Parsana, P., Segrè, A. v., Strober, B. J., Zappala, Z., Cummings, B. B., Gelfand, E. T., Hadley, K., Huang, K. H., Lek, M., Li, Xiao, Nedzel, J. L., Nguyen, D. Y., Noble, M. S., Sullivan, T. J., Tukiainen, T., MacArthur, D. G., Getz, G., Addington, A., Guan, P., Koester, S., Little, A. R., Lockhart, N. C., Moore, H. M., Rao, A., Struewing, J. P., Volpi, S., Brigham, L. E., Hasz, R., Hunter, M., Johns, C., Johnson, M., Kopen, G., Leinweber, W. F., Lonsdale, J. T., McDonald, A., Mestichelli, B., Myer, K., Roe, B., Salvatore, M., Shad, S., Thomas, J. A., Walters, G., Washington, M., Wheeler, J., Bridge, J., Foster, B. A., Gillard, B. M., Karasik, E., Kumar, R., Miklos, M., Moser, M. T., Jewell, S. D., Montroy, R. G., Rohrer, D. C., Valley, D., Mash, D. C., Davis, D. A.,

Sobin, L., Barcus, M. E., Branton, P. A., Abell, N. S., Balliu, B., Delaneau, O., Frésard, L., Gamazon, E. R., Garrido-Martín, D., Gewirtz, A. D. H., Gliner, G., Gloudemans, M. J., Han, B., He, A. Z., Hormozdiari, F., Li, Xin, Liu, B., Kang, E. Y., McDowell, I. C., Ongen, H., Palowitch, J. J., Peterson, C. B., Quon, G., Ripke, S., Saha, A., Shabalin, A. A., Shimko, T. C., Sul, J. H., Teran, N. A., Tsang, E. K., Zhang, H., Zhou, Y. H., Bustamante, C. D., Cox, N. J., Guigó, R., Kellis, M., McCarthy, M. I., Conrad, D. F., Eskin, E., Li, G., Nobel, A. B., Sabatti, C., Stranger, B. E., Wen, X., Wright, F. A., Ardlie, K. G., Dermitzakis, E. T., Lappalainen, T., Battle, A., Brown, C. D., Engelhardt, B. E., Montgomery, S. B., Handsaker, R. E., Kashin, S., Karczewski, K. J., Nguyen, D. T., Trowbridge, C. A., Barshir, R., Basha, O., Bogu, G. K., Chen, L. S., Chiang, C., Damani, F. N., Ferreira, P. G., Hall, I. M., Howald, C., Im, H. K., Kim, Y., Kim-Hellmuth, S., Mangul, S., Monlong, J., Muñoz-Aguirre, M., Ndungu, A. W., Nicolae, D. L., Oliva, M., Panousis, N., Papasaikas, P., Payne, A. J., Quan, J., Reverter, F., Sammeth, M., Scott, A. J., Sodaei, R., Stephens, M., Urbut, S., van de Bunt, M., Wang, G., Xi, H. S., Yeger-Lotem, E., Zaugg, J. B., Akey, J. M., Bates, D., Chan, J., Claussnitzer, M., Demanelis, K., Diegel, M., Doherty, J. A., Feinberg, A. P., Fernando, M. S., Halow, J., Hansen, K. D., Haugen, E., Hickey, P. F., Hou, L., Jasmine, F., Jian, R., Jiang, L., Johnson, A., Kaul, R., Kibriya, M. G., Lee, K., Li, J. B., Li, Q., Lin, J., Lin, S., Linder, S., Linke, C., Liu, Y., Maurano, M. T., Molinie, B., Nelson, J., Neri, F. J., Park, Y., Pierce, B. L., Rinaldi, N. J., Rizzardi, L. F., Sandstrom, R., Skol, A., Smith, K. S., Snyder, M. P., Stamatoyannopoulos, J., Tang, H., Wang, L., Wang, M., van Wittenberghe, N., Wu, F., Zhang, R., Nierras, C. R., Carithers, L. J., Vaught, J. B., Gould, S. E., Lockart, N. C., Martin, C., Addington, A. M., Koester, S. E., Undale, A. H., Smith, A. M., Tabor, D. E., Roche, N. v., McLean, J. A., Vatanian, N., Robinson, K. L., Valentino, K. M., Qi, L., Hunter, S., Hariharan, P., Singh, S., Um, K. S., Matose, T., Tomaszewski, M. M., Barker, L. K., Mosavel, M., Siminoff, L. A., Traino, H. M., Flicek, P., Juettemann, T., Ruffier, M., Sheppard, D., Taylor, K., Trevanion, S. J., Zerbino, D. R., Craft, B., Goldman, M., Haeussler, M., Kent, W. J., Lee, C. M., Paten, B., Rosenbloom, K. R., Vivian, J. and Zhu, J. (2017) "Genetic effects on gene expression across human tissues," *Nature*, 550(7675), pp. 204–213. doi: 10.1038/nature24277.

Alabi, R. O., Glomski, K., Haxaire, C., Weskamp, G., Monette, S. and Blobel, C. P. (2016) "ADAM10-dependent signaling through Notch1 and Notch4 controls development of organ-specific vascular beds," *Circulation Research*, 119(4), pp. 519–531. doi: 10.1161/CIRCRESAHA.115.307738.

Alabi, R. O., Lora, J., Celen, A. B., Maretzky, T. and Blobel, C. P. (2021) "Analysis of the conditions that affect the selective processing of endogenous Notch1 by ADAM10 and ADAM17," *International Journal of Molecular Sciences*, 22(4), pp. 1–17. doi: 10.3390/ijms22041846.

Alenazy, F. O. and Thomas, M. R. (2021) "Novel antiplatelet targets in the treatment of acute coronary syndromes," *Platelets*, 32(1), pp. 15–28. doi: 10.1080/09537104.2020.1763731.

Alshehri, O. M., Hughes, C. E., Montague, S., Watson, S. K., Frampton, J., Bender, M. and Watson, S. P. (2015) "Fibrin activates GPVI in human and mouse platelets," *Blood*, 126(13), pp. 1601–1608. doi: 10.1182/blood-2015-04-641654.

Al-Tamimi, M., Gardiner, E. E., Thom, J. Y., Shen, Y., Cooper, M. N., Hankey, G. J., Berndt, M. C., Baker, R. I. and Andrews, R. K. (2011) "Soluble glycoprotein VI is raised in the plasma of patients with acute ischemic stroke," *Stroke*, 42(2), pp. 498–500. doi: 10.1161/STROKEAHA.110.602532.

Al-Tamimi, M., Grigoriadis, G., Tran, H., Paul, E., Servadei, P., Berndt, M. C., Gardiner, E. E. and Andrews, R. K. (2011) "Coagulation-induced shedding of platelet glycoprotein VI mediated by factor Xa," *Blood*, 117(14), pp. 3912–3920. doi: 10.1182/blood-2010-08-301523.

Al-Tamimi, M., Mu, F. T., Arthur, J. F., Shen, Y., Moroi, M., Berndt, M. C., Andrews, R. K. and Gardiner, E. E. (2009) "Anti-glycoprotein VI monoclonal antibodies directly aggregate platelets independently of FcγRIIa and induce GPVI ectodomain shedding," *Platelets*, 20(2), pp. 75–82. doi: 10.1080/09537100802645029.

Al-Tamimi, M., Tan, C. W., Qiao, J., Pennings, G. J., Javadzadegan, A., Yong, A. S. C., Arthur, J. F., Davis, A. K., Jing, J., Mu, F. T., Hamilton, J. R., Jackson, S. P., Ludwig, A., Berndt, M. C., Ward, C. M., Kritharides, L., Andrews, R. K. and Gardiner, E. E. (2012) "Pathologic shear triggers shedding of vascular receptors: A novel mechanism for down-regulation of platelet glycoprotein VI in stenosed coronary vessels," *Blood*, 119(18), pp. 4311–4320. doi: 10.1182/blood-2011-10-386607.

Amour, A., Knight, C. G., Webster, A., Slocombe, P. M., Stephens, P. E., Knäuper, V., Docherty, A. J. P. and Murphy, G. (2000) "The in vitro activity of ADAM-10 is inhibited by TIMP-1 and TIMP-3," *FEBS Letters*, 473(3), pp. 275–279. doi: 10.1016/S0014-5793(00)01528-3.

Anders, A., Gilbert, S., Garten, W., Postina, R. and Fahrenholz, F. (2001) "Regulation of the α-secretase ADAM10 by its prodomain and proprotein convertases," *The FASEB Journal*, 15(10), pp. 1837–1839. doi: 10.1096/fj.01-0007fje.

André, M., le Caer, J. P., Greco, C., Planchon, S., el Nemer, W., Boucheix, C., Rubinstein, E., Chamot-Rooke, J. and le Naour, F. (2006) "Proteomic analysis of the tetraspanin web using LC-ESI-MS/MS and MALDI-FTICR-MS," *Proteomics*, 6(5), pp. 1437–1449. doi: 10.1002/pmic.200500180.

Andreu, Z. and Yáñez-Mó, M. (2014) "Tetraspanins in extracellular vesicle formation and function," *Frontiers in Immunology*, 5. doi: 10.3389/fimmu.2014.00442.

Andrews, R. K., Suzuki-Inoue, K., Shen, Y., Tulasne, D., Watson, S. P. and Berndt, M. C. (2002) "Interaction of calmodulin with the cytoplasmic domain of platelet glycoprotein VI," *Blood*, 99(11), pp. 4219–4221. doi: 10.1182/blood-2001-11-0008.

Arduise, C., Abache, T., Li, L., Billard, M., Chabanon, A., Ludwig, A., Mauduit, P., Boucheix, C., Rubinstein, E. and le Naour, F. (2008) "Tetraspanins regulate ADAM10-mediated cleavage of TNF-α and epidermal growth factor," *The Journal of Immunology*, 181(10), pp. 7002–7013. doi: 10.4049/jimmunol.181.10.7002.

Arima, T., Enokida, H., Kubo, H., Kagara, I., Matsuda, R., Toki, K., Nishimura, H., Chiyomaru, T., Tatarano, S., Idesako, T., Nishiyama, K. and Nakagawa, M. (2007) "Nuclear translocation of ADAM-10 contributes to the pathogenesis and progression of human prostate cancer," *Cancer Science*, 98(11), pp. 1720–1726. doi: 10.1111/j.1349-7006.2007.00601.x.

Arthur, J. F., Dunkley, S. and Andrews, R. K. (2007) "Platelet glycoprotein VI-related clinical defects," *British Journal of Haematology*, 139(3), pp. 363–372. doi: 10.1111/j.1365-2141.2007.06799.x.

Arthur, J. F., Shen, Y., Gardiner, E. E., Coleman, L., Kenny, D., Andrews, R. K. and Berndt, M. C. (2011) "TNF receptor-associated factor 4 (TRAF4) is a novel binding partner of glycoprotein Ib and glycoprotein VI in human platelets," *Journal of Thrombosis and Haemostasis*, 9(1), pp. 163–172. doi: 10.1111/j.1538-7836.2010.04091.x.

Auton, A., Abecasis, G. R., Altshuler, D. M., Durbin, R. M., Bentley, D. R., Chakravarti, A., Clark, A. G., Donnelly, P., Eichler, E. E., Flicek, P., Gabriel, S. B., Gibbs, R. A., Green, E. D., Hurles, M. E., Knoppers, B. M., Korbel, J. O., Lander, E. S., Lee, C., Lehrach, H., Mardis, E. R., Marth, G. T., McVean, G. A., Nickerson, D. A., Schmidt, J. P., Sherry, S. T., Wang, J., Wilson, R. K., Boerwinkle, E., Doddapaneni, H., Han, Y., Korchina, V., Kovar, C., Lee, S., Muzny, D., Reid, J. G., Zhu, Y., Chang, Y., Feng, Q., Fang, X., Guo, X., Jian, M., Jiang, H., Jin, X., Lan, T., Li, G., Li, J., Li, Yingrui, Liu, S., Liu, Xiao, Lu, Y., Ma, X., Tang, M., Wang, B., Wang, G., Wu, H., Wu, R., Xu, X., Yin, Y., Zhang, D., Zhang, W., Zhao, J., Zhao, M., Zheng, X., Gupta, N., Gharani, N., Toji, L. H., Gerry, N. P., Resch, A. M., Barker, J., Clarke, L., Gil, L., Hunt, S. E., Kelman, G., Kulesha, E., Leinonen, R., McLaren, W. M., Radhakrishnan, R., Roa, A., Smirnov, D., Smith, R. E., Streeter, I., Thormann, A., Toneva, I., Vaughan, B., Zheng-Bradley, X., Grocock, R., Humphray, S., James, T., Kingsbury, Z., Sudbrak, R., Albrecht, M. W., Amstislavskiy, V. S., Borodina, T. A., Lienhard, M., Mertes, F., Sultan, M., Timmermann, B., Yaspo, M. L., Fulton, L., Ananiev, V., Belaia, Z., Beloslyudtsev, D., Bouk, N., Chen, C., Church, D., Cohen, R., Cook, C., Garner, J., Hefferon, T., Kimelman, M., Liu, C., Lopez, J., Meric, P., O'Sullivan, C., Ostapchuk, Y., Phan, L., Ponomarov, S., Schneider, V., Shekhtman, E., Sirotkin, K., Slotta, D., Zhang, H., Balasubramaniam, S., Burton, J., Danecek, P., Keane, T. M., Kolb-Kokocinski, A., McCarthy, S., Stalker, J., Quail, M., Davies, C. J., Gollub, J., Webster, T., Wong, B., Zhan, Y., Campbell, C. L., Kong, Y., Marcketta, A., Yu, F., Antunes, L., Bainbridge, M., Sabo, A., Huang, Z., Coin, L. J. M., Fang, L., Li, Q., Li, Z., Lin, H., Liu, B., Luo, R., Shao, H., Xie, Y., Ye, C., Yu, C., Zhang, F., Zheng, H., Zhu, H., Alkan, C., Dal, E., Kahveci, F., Garrison, E. P., Kural, D., Lee, W. P., Leong, W. F., Stromberg, M., Ward, A. N., Wu, J., Zhang, M., Daly, M. J., DePristo, M. A., Handsaker, R. E., Banks, E., Bhatia, G., del Angel, G., Genovese, G., Li, H., Kashin, S., McCarroll, S. A., Nemesh, J. C., Poplin, R. E., Yoon, S. C., Lihm, J., Makarov, V., Gottipati, S., Keinan, A., Rodriguez-Flores, J. L., Rausch, T., Fritz, M. H., Stütz, A. M., Beal, K., Datta, A., Herrero, J., Ritchie, G. R. S., Zerbino, D., Sabeti, P. C., Shlyakhter, I., Schaffner, S. F., Vitti, J., Cooper, D. N., Ball, E. v., Stenson, P. D., Barnes, B., Bauer, M., Cheetham, R.

K., Cox, A., Eberle, M., Kahn, S., Murray, L., Peden, J., Shaw, R., Kenny, E. E., Batzer, M. A., Konkel, M. K., Walker, J. A., MacArthur, D. G., Lek, M., Herwig, R., Ding, L., Koboldt, D. C., Larson, D., Ye, Kai, Gravel, S., Swaroop, A., Chew, E., Lappalainen, T., Erlich, Y., Gymrek, M., Willems, T. F., Simpson, J. T., Shriver, M. D., Rosenfeld, J. A., Bustamante, C. D., Montgomery, S. B., de La Vega, F. M., Byrnes, J. K., Carroll, A. W., DeGorter, M. K., Lacroute, P., Maples, B. K., Martin, A. R., Moreno-Estrada, A., Shringarpure, S. S., Zakharia, F., Halperin, E., Baran, Y., Cerveira, E., Hwang, J., Malhotra, A., Plewczynski, D., Radew, K., Romanovitch, M., Zhang, C., Hyland, F. C. L., Craig, D. W., Christoforides, A., Homer, N., Izatt, T., Kurdoglu, A. A., Sinari, S. A., Squire, K., Xiao, C., Sebat, J., Antaki, D., Gujral, M., Noor, A., Ye, Kenny, Burchard, E. G., Hernandez, R. D., Gignoux, C. R., Haussler, D., Katzman, S. J., Kent, W. J., Howie, B., Ruiz-Linares, A., Dermitzakis, E. T., Devine, S. E., Kang, H. M., Kidd, J. M., Blackwell, T., Caron, S., Chen, W., Emery, S., Fritsche, L., Fuchsberger, C., Jun, G., Li, B., Lyons, R., Scheller, C., Sidore, C., Song, S., Sliwerska, E., Taliun, D., Tan, A., Welch, R., Wing, M. K., Zhan, X., Awadalla, P., Hodgkinson, A., Li, Yun, Shi, X., Quitadamo, A., Lunter, G., Marchini, J. L., Myers, S., Churchhouse, C., Delaneau, O., Gupta-Hinch, A., Kretzschmar, W., Iqbal, Z., Mathieson, I., Menelaou, A., Rimmer, A., Xifara, D. K., Oleksyk, T. K., Fu, Yunxin, Liu, Xiaoming, Xiong, M., Jorde, L., Witherspoon, D., Xing, J., Browning, B. L., Browning, S. R., Hormozdiari, F., Sudmant, P. H., Khurana, E., Tyler-Smith, C., Albers, C. A., Ayub, Q., Chen, Y., Colonna, V., Jostins, L., Walter, K., Xue, Y., Gerstein, M. B., Abyzov, A., Balasubramanian, S., Chen, J., Clarke, D., Fu, Yao, Harmanci, A. O., Jin, M., Lee, D., Liu, J., Mu, X. J., Zhang, J., Zhang, Yan, Hartl, C., Shakir, K., Degenhardt, J., Meiers, S., Raeder, B., Casale, F. P., Stegle, O., Lameijer, E. W., Hall, I., Bafna, V., Michaelson, J., Gardner, E. J., Mills, R. E., Dayama, G., Chen, K., Fan, X., Chong, Z., Chen, T., Chaisson, M. J., Huddleston, J., Malig, M., Nelson, B. J., Parrish, N. F., Blackburne, B., Lindsay, S. J., Ning, Z., Zhang, Yujun, Lam, H., Sisu, C., Challis, D., Evani, U. S., Lu, J., Nagaswamy, U., Yu, J., Li, W., Habegger, L., Yu, H., Cunningham, F., Dunham, I., Lage, K., Jespersen, J. B., Horn, H., Kim, D., Desalle, R., Narechania, A., Sayres, M. A. W., Mendez, F. L., Poznik, G. D., Underhill, P. A., Mittelman, D., Banerjee, R., Cerezo, M., Fitzgerald, T. W., Louzada, S., Massaia, A., Yang, F., Kalra, D., Hale, W., Dan, X., Barnes, K. C., Beiswanger, C., Cai, H., Cao, H., Henn, B., Jones, D., Kaye, J. S., Kent, A., Kerasidou, A., Mathias, R., Ossorio, P. N., Parker, M., Rotimi, C. N., Royal, C. D., Sandoval, K., Su, Y., Tian, Z., Tishkoff, S., Via, M., Wang, Y., Yang, H., Yang, L., Zhu, J., Bodmer, W., Bedoya, G., Cai, Z., Gao, Y., Chu, J., Peltonen, L., Garcia-Montero, A., Orfao, A., Dutil, J., Martinez-Cruzado, J. C., Mathias, R. A., Hennis, A., Watson, H., McKenzie, C., Qadri, F., LaRocque, R., Deng, X., Asogun, D., Folarin, O., Happi, C., Omoniwa, O., Stremlau, M., Tariyal, R., Jallow, M., Joof, F. S., Corrah, T., Rockett, K., Kwiatkowski, D., Kooner, J., Hien, T. T., Dunstan, S. J., ThuyHang, N., Fonnie, R., Garry, R., Kanneh, L., Moses, L., Schieffelin, J., Grant, D. S., Gallo, C., Poletti, G., Saleheen, D., Rasheed, A., Brooks, L. D., Felsenfeld, A. L., McEwen, J. E., Vaydylevich, Y., Duncanson, A., Dunn, M. and Schloss, J. A. (2015)

"A global reference for human genetic variation," *Nature*, pp. 68–74. doi: 10.1038/nature15393.

Ayling, L. J., Briddon, S. J., Halls, M. L., Hammond, G. R. V., Vaca, L., Pacheco, J., Hill, S. J. and Cooper, D. M. F. (2012) "Adenylyl cyclase AC8 directly controls its micro-environment by recruiting the actin cytoskeleton in a cholesterol-rich milieu," *Journal of Cell Science*, 125(4), pp. 869–886. doi: 10.1242/jcs.091090.

Baaten, C. C. F. M. J., Swieringa, F., Misztal, T., Mastenbroek, T. G., Feijge, M. A. H., Bock, P. E., Donners, M. M. P. C., Collins, P. W., Li, R., van der Meijden, P. E. J. and Heemskerk, J. W. M. (2018) "Platelet heterogeneity in activation-induced glycoprotein shedding: Functional effects," *Blood Advances*, 2(18), pp. 2320–2331. doi: 10.1182/bloodadvances.2017011544.

Becanovic, K., Nørremølle, A., Neal, S. J., Kay, C., Collins, J. A., Arenillas, D., Lilja, T., Gaudenzi, G., Manoharan, S., Doty, C. N., Beck, J., Lahiri, N., Portales-Casamar, E., Warby, S. C., Connolly, C., de Souza, R. A. G., Tabrizi, S. J., Hermanson, O., Langbehn, D. R., Hayden, M. R., Wasserman, W. W. and Leavitt, B. R. (2015) "A SNP in the HTT promoter alters NF-κB binding and is a bidirectional genetic modifier of Huntington disease," *Nature Neuroscience*, 18(6), pp. 807–816. doi: 10.1038/nn.4014.

Bender, M., Hofmann, S., Stegner, D., Chalaris, A., B??sl, M., Braun, A., Scheller, J., Rose-John, S. and Nieswandt, B. (2010) "Differentially regulated GPVI ectodomain shedding by multiple platelet-expressed proteinases," *Blood*, 116(17), pp. 3347–3355. doi: 10.1182/blood-2010-06-289108.

Berditchevski, F. (2001) "Complexes of tetraspanins with integrins: More than meets the eye," *Journal of Cell Science*, 114(23), pp. 4143–4151. doi: 10.1242/jcs.114.23.4143.

Berditchevski, F. and Odintsova, E. (2007) "Tetraspanins as regulators of protein trafficking," *Traffic*, 8(2), pp. 89–96. doi: 10.1111/j.1600-0854.2006.00515.x.

Berditchevski, F., Odintsova, E., Sawada, S. and Gilbert, E. (2002) "Expression of the palmitoylation-deficient CD151 weakens the association of α3β1 integrin with the tetraspanin-enriched microdomains and affects integrin-dependent signaling," *Journal of Biological Chemistry*, 277(40), pp. 36991–37000. doi: 10.1074/jbc.M205265200.

Berlanga, O., Bobe, R., Becker, M., Murphy, G., Leduc, M., Bon, C., Barry, F. A., Gibbins, J. M., Garcia, P., Frampton, J. and Watson, S. P. (2000) "Expression of the collagen receptor glycoprotein VI during megakaryocyte differentiation.," *Blood*, 96, pp. 2740–2745.

Berlanga, O., Bori-Sanz, T., James, J. R., Frampton, J., Davis, S. J., Tomlinson, M. G. and Watson, S. P. (2007) "Glycoprotein VI oligomerization in cell lines and platelets," *Journal of Thrombosis and Haemostasis*, 5(5), pp. 1026–1033. doi: 10.1111/j.1538-7836.2007.02449.x.

Berlanga, O., Tulasne, D., Bori, T., Snell, D. C., Miura, Y., Jung, S., Moroi, M., Frampton, J. and Watson, S. P. (2002) "The Fc receptor γ-chain is necessary and sufficient to initiate signalling through glycoprotein VI in transfected cells by the snake C-type lectin, convulxin," *European Journal of Biochemistry*, 269(12), pp. 2951–2960. doi: 10.1046/j.1432-1033.2002.02969.x.

Bezemer, I. D., Bare, L. A., Doggen, C. J. M., Arellano, A. R., Tong, C., Rowland, C. M., Catanese, J., Young, B. A., Reitsma, P. H., Devlin, J. J. and Rosendaal, F. R. (2008) "Gene variants associated with deep vein thrombosis," *JAMA - Journal of the American Medical Association*, 299(11), pp. 1306–1314. doi: 10.1001/jama.299.11.1306.

Bleibaum, F., Sommer, A., Veit, M., Rabe, B., Andrä, J., Kunzelmann, K., Nehls, C., Correa, W., Gutsmann, T., Grötzinger, J., Bhakdi, S. and Reiss, K. (2019) "ADAM10 sheddase activation is controlled by cell membrane asymmetry," *Journal of Molecular Cell Biology*, 11(11), pp. 979–993. doi: 10.1093/jmcb/mjz008.

Bori-Sanz, T., Inoue, K. S., Berndt, M. C., Watson, S. P. and Tulasne, D. (2003) "Delineation of the region in the glycoprotein VI tail required for association with the Fc receptor γ-chain," *Journal of Biological Chemistry*, 278(38), pp. 35914–35922. doi: 10.1074/jbc.M301826200.

Boskovski, M. T., Yuan, S., Pedersen, N. B., Goth, C. K., Makova, S., Clausen, H., Brueckner, M. and Khokha, M. K. (2013) "The heterotaxy gene GALNT11 glycosylates Notch to orchestrate cilia type and laterality," *Nature*, 504(7480), pp. 456–459. doi: 10.1038/nature12723.

Brækkan, S. K., Mathiesen, E. B., NjøLstad, I., Wilsgaard, T., StøRmer, J. and Hansen, J. B. (2010) "Mean platelet volume is a risk factor for venous thromboembolism: The Tromsø study," *Journal of Thrombosis and Haemostasis*, 8(1), pp. 157–162. doi: 10.1111/j.1538-7836.2009.03498.x.

Braley, A., Kwak, T., Jules, J., Harja, E., Landgraf, R. and Hudson, B. I. (2016) "Regulation of receptor for advanced glycation end products (RAGE) ectodomain shedding and its role in cell function," *Journal of Biological Chemistry*, 291(23), pp. 12057–12073. doi: 10.1074/jbc.M115.702399.

Brass, L. F., Diamond, S. L. and Stalker, T. J. (2016) "Platelets and hemostasis: a new perspective on an old subject," *Blood Advances*, 1(1), pp. 5–9. doi: 10.1182/bloodadvances.2016000059.

Braun, A., Anders, H. J., Gudermann, T. and Mammadova-Bach, E. (2021) "Platelet-cancer interplay: Molecular mechanisms and new therapeutic avenues," *Frontiers in Oncology*, 11, p. 665534. doi: 10.3389/fonc.2021.665534.

Briddon, S. J., Kilpatrick, L. E. and Hill, S. J. (2018) "Studying GPCR pharmacology in membrane microdomains: Fluorescence correlation spectroscopy comes of age," *Trends in Pharmacological Sciences*, 39(2), pp. 158–174. doi: 10.1016/j.tips.2017.11.004.

Brummer, T., Müller, S. A., Pan-Montojo, F., Yoshida, F., Fellgiebel, A., Tomita, T., Endres, K. and Lichtenthaler, S. F. (2019) "NrCAM is a marker for substrate-selective activation of ADAM10 in Alzheimer's disease," *EMBO Molecular Medicine*, 11(4), p. e9695. doi: 10.15252/emmm.201809695.

Brummer, T., Pigoni, M., Rossello, A., Wang, H., Noy, P. J., Tomlinson, M. G., Blobel, C. P. and Lichtenthaler, S. F. (2018) "The metalloprotease ADAM10 (a disintegrin and metalloprotease 10) undergoes rapid, postlysis autocatalytic degradation," *FASEB Journal*, 32(7), pp. 3560–3573. doi: 10.1096/fj.201700823RR.

Caescu, C. I., Jeschke, G. R. and Turk, B. E. (2009) “Active-site determinants of substrate recognition by the metalloproteinases TACE and ADAM10,” *Biochemical Journal*, 424(1), pp. 79–88. doi: 10.1042/BJ20090549.

Canela-Xandri, O., Rawlik, K. and Tenesa, A. (2018) “An atlas of genetic associations in UK Biobank,” *Nature Genetics*, 50(11), pp. 1593–1599. doi: 10.1038/s41588-018-0248-z.

Canobbio, I., Visconte, C., Momi, S., Guidetti, G. F., Zarà, M., Canino, J., Falcinelli, E., Gresele, P. and Torti, M. (2017) “Platelet amyloid precursor protein is a modulator of venous thromboembolism in mice,” *Blood*, 130(4), pp. 527–536. doi: 10.1182/blood-2017-01-764910.

Cavadas, M., Oikonomidi, I., Gaspar, C. J., Burbridge, E., Badenes, M., Félix, I., Bolado, A., Hu, T., Bileck, A., Gerner, C., Domingos, P. M., von Kriegsheim, A. and Adrain, C. (2017) “Phosphorylation of iRhom2 controls stimulated proteolytic shedding by the metalloprotease ADAM17/TACE,” *Cell Reports*, 21(3), pp. 745–757. doi: 10.1016/j.celrep.2017.09.074.

Chaimowitz, N. S., Martin, R. K., Cichy, J., Gibb, D. R., Patil, P., Kang, D.-J., Farnsworth, J., Butcher, E. C., McCright, B. and Conrad, D. H. (2011) “A Disintegrin and Metalloproteinase 10 Regulates Antibody Production and Maintenance of Lymphoid Architecture,” *The Journal of Immunology*, 187(10), pp. 5114–5122. doi: 10.4049/jimmunol.1102172.

Charrin, S., Jouannet, S., Boucheix, C. and Rubinstein, E. (2014) “Tetraspanins at a glance,” *Journal of Cell Science*, 127(17), pp. 3641–3648. doi: 10.1242/jcs.154906.

Charrin, S., Manié, S., Oualid, M., Billard, M., Boucheix, C. and Rubinstein, E. (2002) “Differential stability of tetraspanin/tetraspanin interactions: Role of palmitoylation,” *FEBS Letters*, 516(1–3), pp. 139–144. doi: 10.1016/S0014-5793(02)02522-X.

Charrin, S., Manié, S., Thiele, C., Billard, M., Gerlier, D., Boucheix, C. and Rubinstein, E. (2003) “A physical and functional link between cholesterol and tetraspanins,” *European Journal of Immunology*, 33(9), pp. 2479–2489. doi: 10.1002/eji.200323884.

Clark, J. C., Damaskinaki, F. N., Cheung, Y. F. H., Slater, A. and Watson, S. P. (2021) “Structure-function relationship of the platelet glycoprotein VI (GPVI) receptor: does it matter if it is a dimer or monomer?,” *Platelets*, 32(6), pp. 724–732. doi: 10.1080/09537104.2021.1887469.

Clark, J. C., Neagoe, R. A. I., Zuidscherwoude, M., Kavanagh, D. M., Slater, A., Martin, E. M., Soave, M., Stegner, D., Nieswandt, B., Poulter, N. S., Hummert, J., Herten, D. P., Tomlinson, M. G., Hill, S. J. and Watson, S. P. (2021) “Evidence that GPVI is expressed as a mixture of monomers and dimers, and that the D2 domain is not essential for GPVI activation,” *Thrombosis and Haemostasis*. doi: 10.1055/a-1401-5014.

Cole, V. J., Staton, J. M., Eikelboom, J. W., Hankey, G. J., Yi, Q., Shen, Y., Berndt, M. C. and Baker, R. I. (2003) “Collagen platelet receptor polymorphisms integrin α2β1 C807T and GPVI Q317L and risk of ischemic stroke,” *Journal of Thrombosis and Haemostasis*, 1(5), pp. 963–970. doi: 10.1046/j.1538-7836.2003.00179.x.

Crew, V. K., Burton, N., Kagan, A., Green, C. A., Levene, C., Flinter, F., Brady, R. L., Daniels, G. and Anstee, D. J. (2004) “CD151, the first member of the tetraspanin (TM4)

superfamily detected on erythrocytes, is essential for the correct assembly of human basement membranes in kidney and skin," *Blood*, 104(8), pp. 2217–2223. doi: 10.1182/blood-2004-04-1512.

Croft, A. P., Campos, J., Jansen, K., Turner, J. D., Marshall, J., Attar, M., Savary, L., Wehmeyer, C., Naylor, A. J., Kemble, S., Begum, J., Dürholz, K., Perlman, H., Barone, F., McGettrick, H. M., Fearon, D. T., Wei, K., Raychaudhuri, S., Korsunsky, I., Brenner, M. B., Coles, M., Sansom, S. N., Filer, A. and Buckley, C. D. (2019) "Distinct fibroblast subsets drive inflammation and damage in arthritis," *Nature*, 570(7760), pp. 246–251. doi: 10.1038/s41586-019-1263-7.

Croft, S. A., Samani, N. J., Teare, M. D., Hampton, K. K., Steeds, R. P., Channer, K. S. and Daly, M. E. (2001) "Novel platelet membrane glycoprotein VI dimorphism is a risk factor for myocardial infarction," *Circulation*, 104(13), pp. 1459–1463. doi: 10.1161/hc3801.096397.

Dehairs, J., Talebi, A., Cherifi, Y. and Swinnen, J. v. (2016) "CRISP-ID: Decoding CRISPR mediated indels by Sanger sequencing," *Scientific Reports*, 6(1), pp. 1–5. doi: 10.1038/srep28973.

Deng, W., Cho, S., Su, P.-C., Berger, B. W. and Li, R. (2014) "Membrane-enabled dimerization of the intrinsically disordered cytoplasmic domain of ADAM10," *Proceedings of the National Academy of Sciences of the United States of America*, 111(45), pp. 15987–92. doi: 10.1073/pnas.1409354111.

van Deventer, S., Arp, A. B. and van Spriel, A. B. (2021) "Dynamic Plasma Membrane Organization: A Complex Symphony," *Trends in Cell Biology*, pp. 119–129. doi: 10.1016/j.tcb.2020.11.004.

Dornier, E., Coumailleau, F., Ottavi, J. F., Moretti, J., Boucheix, C., Mauduit, P., Schweisguth, F. and Rubinstein, E. (2012) "TspanC8 tetraspanins regulate ADAM10/Kuzbanian trafficking and promote Notch activation in flies and mammals," *Journal of Cell Biology*, 199(3), pp. 481–496. doi: 10.1083/jcb.201201133.

Dozio, V. and Sanchez, J. C. (2017) "Characterisation of extracellular vesicle-subsets derived from brain endothelial cells and analysis of their protein cargo modulation after TNF exposure," *Journal of Extracellular Vesicles*, 6(1). doi: 10.1080/20013078.2017.1302705.

Dumont, B., Lasne, D., Rothschild, C., Bouabdelli, M., Ollivier, V., Oudin, C., Ajzenberg, N., Grandchamp, B. and Jandrot-Perrus, M. (2009) "Absence of collagen-induced platelet activation caused by compound heterozygous GPVI mutations," *Blood*, 114(9), pp. 1900–1903. doi: 10.1182/blood-2009-03-213504.

Dunn, C. D., Sulis, M. L., Ferrando, A. A. and Greenwald, I. (2010) "A conserved tetraspanin subfamily promotes Notch signaling in Caenorhabditis elegans and in human cells," *Proceedings of the National Academy of Sciences of the United States of America*, 107(13), pp. 5907–5912. doi: 10.1073/pnas.1001647107.

Düsterhöft, S., Babendreyer, A., Giese, A.A., Flasshove, C. and Ludwig, A. (2019) "Status update on iRhom and ADAM17: It's still complicated," *Biochimica et Biophysica Acta*

- *Molecular Cell Research*. Elsevier B.V., pp. 1567–1583. doi:10.1016/j.bbamcr.2019.06.017.

Dütting, S., Bender, M. and Nieswandt, B. (2012) "Platelet GPVI: A target for antithrombotic therapy?!," *Trends in Pharmacological Sciences*, 33(11), pp. 583–590. doi: 10.1016/j.tips.2012.07.004.

Ebsen, H., Lettau, M., Kabelitz, D. and Janssen, O. (2014) "Identification of SH3 domain proteins interacting with the cytoplasmic tail of the a Disintegrin and Metalloprotease 10 (ADAM10)," *PLoS ONE*, 9(7), p. e102899. doi: 10.1371/journal.pone.0102899.

Ehrhardt, C., Schmolke, M., Matzke, A., Knoblauch, A., Will, C., Wixler, V. and Ludwig, S. (2006) "Polyethylenimine, a cost-effective transfection reagent," *Signal Transduction*, 6(3), pp. 179–184. doi: 10.1002/sita.200500073.

Ellinghaus, D., Jostins, L., Spain, S. L., Cortes, A., Bethune, J., Han, B., Park, Y. R., Raychaudhuri, S., Pouget, J. G., Hübenthal, M., Folseraas, T., Wang, Y., Esko, T., Metspalu, A., Westra, H. J., Franke, L., Pers, T. H., Weersma, R. K., Collij, V., D'Amato, M., Halfvarson, J., Jensen, A. B., Lieb, W., Degenhardt, F., Forstner, A. J., Hofmann, A., Schreiber, S., Mrowietz, U., Juran, B. D., Lazaridis, K. N., Brunak, Sø., Dale, A. M., Trembath, R. C., Weidinger, S., Weichenthal, M., Ellinghaus, E., Elder, J. T., Barker, J. N. W. N., Andreassen, O. A., McGovern, D. P., Karlsen, T. H., Barrett, J. C., Parkes, M., Brown, M. A. and Franke, A. (2016) "Analysis of five chronic inflammatory diseases identifies 27 new associations and highlights disease-specific patterns at shared loci," *Nature Genetics*, 48(5), pp. 510–518. doi: 10.1038/ng.3528.

Eschenbrenner, E., Jouannet, S., Clay, D., Chaker, J., Boucheix, C., Brou, C., Tomlinson, M. G., Charrin, S. and Rubinstein, E. (2020) "TspanC8 tetraspanins differentially regulate ADAM10 endocytosis and half-life," *Life Science Alliance*, 3(1), p. e201900444. doi: 10.26508/lsa.201900444.

Essmann, F., Bantel, H., Totzke, G., Engels, I. H., Sinha, B., Schulze-Osthoff, K. and Jänicke, R. U. (2003) "Staphylococcus aureus α-toxin-induced cell death: Predominant necrosis despite apoptotic caspase activation," *Cell Death and Differentiation*, 10(11), pp. 1260–1272. doi: 10.1038/sj.cdd.4401301.

Ezekwe, E. A. D., Weng, C. and Duncan, J. A. (2016) "ADAM10 cell surface expression but not activity is critical for Staphylococcus aureus α-hemolysin-mediated activation of the NLRP3 inflammasome in human monocytes," *Toxins*, 8(4), pp. 1–14. doi: 10.3390/toxins8040095.

Facey, A., Pinar, I., Arthur, J. F., Qiao, J., Jing, J., Mado, B., Carberry, J., Andrews, R. K. and Gardiner, E. E. (2016) "A-disintegrin-and-metalloproteinase (ADAM)10 activity on resting and activated platelets," *Biochemistry*, 55(8), pp. 1187–1194. doi: 10.1021/acs.biochem.5b01102.

Fields, G. B. (2019) "The rebirth of matrix metalloproteinase inhibitors: Moving beyond the dogma," *Cells*, 8(9), p. 984. doi: 10.3390/cells8090984.

Fishilevich, S., Zimmerman, S., Kohn, A., Stein, T. I., Olender, T., Kolker, E., Safran, M. and Lancet, D. (2016) "Genic insights from integrated human proteomics in GeneCards," *Database*, 2016, p. baw030. doi: 10.1093/database/baw030.

Fregno, I. and Molinari, M. (2019) “Proteasomal and lysosomal clearance of faulty secretory proteins: ER-associated degradation (ERAD) and ER-to-lysosome-associated degradation (ERLAD) pathways,” *Critical Reviews in Biochemistry and Molecular Biology*, 54(2), pp. 153–163. doi: 10.1080/10409238.2019.1610351.

Fritsche, L. G., Igl, W., Bailey, J. N. C., Grassmann, F., Sengupta, S., Bragg-Gresham, J. L., Burdon, K. P., Hebbring, S. J., Wen, C., Gorski, M., Kim, I. K., Cho, D., Zack, D., Souied, E., Scholl, H. P. N., Bala, E., ELee, K., Hunter, D. J., Sardell, R. J., Mitchell, P., Merriam, J. E., Cipriani, V., Hoffman, J. D., Schick, T., Lechanteur, Y. T. E., Guymer, R. H., Johnson, M. P., Jiang, Y., Stanton, C. M., Buitendijk, G. H. S., Zhan, X., Kwong, A. M., Boleda, A., Brooks, M., Gieser, L., Ratnapriya, R., Branham, K. E., Foerster, J. R., Heckenlively, J. R., Othman, M. I., Vote, B. J., Liang, H. H., Souzeau, E., McAllister, I. L., Isaacs, T., Hall, J., Lake, S., Mackey, D. A., Constable, I. J., Craig, J. E., Kitchner, T. E., Yang, Z., Su, Z., Luo, H., Chen, D., Ouyang, H., Flagg, K., Lin, D., Mao, G., Ferreyra, H., Stark, K., von Strachwitz, C. N., Wolf, A., Brandl, C., Rudolph, G., Olden, M., Morrison, M. A., Morgan, D. J., Schu, M., Ahn, J., Silvestri, G., Tsironi, E. E., Park, K. H., Farrer, L. A., Orlin, A., Brucker, A., Li, M., Curcio, C. A., Mohand-Sa’d, S., Sahel, J. A., Audo, I., Benchaboune, M., Cree, A. J., Rennie, C. A., Goverdhan, S. v., Grunin, M., Hagbi-Levi, S., Campochiaro, P., Katsanis, N., Holz, F. G., Blond, F., Blanché, H., Deleuze, J. F. ois, Igo, R. P., Truitt, B., Peachey, N. S., Meuer, S. M., Myers, C. E., Moore, E. L., Klein, R., Hauser, M. A., Postel, E. A., Courtenay, M. D., Schwartz, S. G., Kovach, J. L., Scott, W. K., Liew, G., Tan, A. G., Gopinath, B., Merriam, J. C., Smith, R. T., Khan, J. C., Shahid, H., Moore, A. T., McGrath, J. A., Laux, R., Brantley, M. A., Agarwal, A., Ersoy, L., Caramoy, A., Langmann, T., Saksens, N. T. M., Jong, E. K., Hoyng, C. B., Cain, M. S., Richardson, A. J., Martin, T. M., Blangero, J., Weeks, D. E., Dhillon, B., van Duijn, C. M., Doheny, K. F., Romm, J., Klaver, C. C. W., Hayward, C., Gorin, M. B., Klein, M. L., Baird, P. N., den Hollander, A. I., Fauser, S., WYates, J. R., Allikmets, R., Wang, J. J., Schaumberg, D. A., Klein, B. E. K., Hagstrom, S. A., Chowers, I., Lotery, A. J., Léveillard, T., Zhang, K., Brilliant, M. H., Hewitt, A. W., Swaroop, A., Chew, E. Y., Pericak-Vance, M. A., DeAngelis, M., Stambolian, D., Haines, J. L., Iyengar, S. K., Weber, B. H. F., Abecasis, G. R. and Heid, I. M. (2016) “A large genome-wide association study of age-related macular degeneration highlights contributions of rare and common variants,” *Nature Genetics*, 48(2), pp. 134–143. doi: 10.1038/ng.3448.

Gandrille, S. (2008) “Endothelial cell protein C receptor and the risk of venous thrombosis,” *Haematologica*, 93(6), pp. 812–816. doi: 10.3324/haematol.13243.

Gardiner, E. E. (2018) “Proteolytic processing of platelet receptors,” *Research and Practice in Thrombosis and Haemostasis*, 2(2), pp. 240–250. doi: 10.1002/rth2.12096.

Gardiner, E. E., Arthur, J. F., Kahn, M. L., Berndt, M. C. and Andrews, R. K. (2004) “Regulation of platelet membrane levels of glycoprotein VI by a platelet-derived metalloproteinase,” *Blood*, 104(12), pp. 3611–3617. doi: 10.1182/blood-2004-04-1549.

Gardiner, E. E., Karunakaran, D., Shen, Y., Arthur, J. F., Andrews, R. K. and Berndt, M. C. (2007) “Controlled shedding of platelet glycoprotein (GP)VI and GPIb-IX-V by ADAM

family metalloproteinases," *Journal of Thrombosis and Haemostasis*, 5(7), pp. 1530–1537. doi: 10.1111/j.1538-7836.2007.02590.x.

Gawlowski, T., Stratmann, B., Ruetter, R., Buenting, C. E., Menart, B., Weiss, J., Vlassara, H., Koschinsky, T. and Tschoepe, D. (2009) "Advanced glycation end products strongly activate platelets," *European Journal of Nutrition*, 48(8), pp. 475–481. doi: 10.1007/s00394-009-0038-6.

van Geffen, J. P., Brouns, S. L. N., Batista, J., McKinney, H., Kempster, C., Nagy, M., Sivapalaratnam, S., Baaten, C. C. F. M. J., Bourry, N., Frontini, M., Jurk, K., Krause, M., Pillitteri, D., Swieringa, F., Verdoold, R., Cavill, R., Kuijpers, M. J. E., Ouweh, W. H., Downes, K. and Heemskerk, J. W. M. (2019) "High-throughput elucidation of thrombus formation reveals sources of platelet function variability," *Haematologica*, 104(6), pp. 1256–1267. doi: 10.3324/haematol.2018.198853.

Germain, M., Chasman, D. I., de Haan, H., Tang, W., Lindström, S., Weng, L. C., de Andrade, M., de Visser, M. C. H., Wiggins, K. L., Suchon, P., Saut, N., Smadja, D. M., le Gal, G., van Hylckama Vlieg, A., di Narzo, A., Hao, K., Nelson, C. P., Rocanin-Arjo, A., Folkersen, L., Monajemi, R., Rose, L. M., Brody, J. A., Slagboom, E., Aïssi, D., Gagnon, F., Deleuze, J. F., Deloukas, P., Tzourio, C., Dartigues, J. F., Berr, C., Taylor, K. D., Civelek, M., Eriksson, P., Psaty, B. M., Houwing-Duitermaat, J., Goodall, A. H., Cambien, F., Kraft, P., Amouyel, P., Samani, N. J., Basu, S., Ridker, P. M., Rosendaal, F. R., Kabrhel, C., Folsom, A. R., Heit, J., Reitsma, P. H., Trégouët, D. A., Smith, N. L. and Morange, P. E. (2015) "Meta-analysis of 65,734 individuals identifies TSPAN15 and SLC44A2 as two susceptibility loci for venous thromboembolism," *American Journal of Human Genetics*, 96(4), pp. 532–542. doi: 10.1016/j.ajhg.2015.01.019.

Gordón-Alonso, M., Sala-Valdés, M., Rocha-Perugini, V., Pérez-Hernández, D., López-Martín, S., Ursa, A., Álvarez, S., Kolesnikova, T. v., Vázquez, J., Sánchez-Madrid, F. and Yáñez-Mó, M. (2012) "EWI-2 association with α-actinin regulates T cell immune synapses and HIV viral infection," *The Journal of Immunology*, 189(2), pp. 689–700. doi: 10.4049/jimmunol.1103708.

Goth, C. K., Halim, A., Khetarpal, S. A., Rader, D. J., Clausen, H. and Schjoldager, K. T. B. G. (2015) "A systematic study of modulation of ADAM-mediated ectodomain shedding by site-specific O-glycosylation," *Proceedings of the National Academy of Sciences of the United States of America*, 112(47), pp. 14623–14628. doi: 10.1073/pnas.1511175112.

Grieve, A. G., Xu, H., Künzel, U., Bambrough, P., Sieber, B. and Freeman, M. (2017) "Phosphorylation of iRhom2 at the plasma membrane controls mammalian TACE-dependent inflammatory and growth factor signalling," *eLife*, 6, p. e23968. doi: 10.7554/eLife.23968.

Gu, J. M., Crawley, J. T. B., Ferrell, G., Zhang, F., Li, W., Esmon, N. L. and Esmon, C. T. (2002) "Disruption of the endothelial cell protein C receptor gene in mice causes placental thrombosis and early embryonic lethality," *Journal of Biological Chemistry*, 277(45), pp. 43335–43343. doi: 10.1074/jbc.M207538200.

Gu, R., Xu, J., Lin, Y., Sheng, W., Ma, D., Ma, X. and Huang, G. (2017) "The role of histone modification and a regulatory single-nucleotide polymorphism (rs2071166) in the Cx43 promoter in patients with TOF," *Scientific Reports*, 7(1), p. 10435. doi: 10.1038/s41598-017-10756-6.

Guo, X.-B., Zhang, X.-C., Chen, P., Ma, L.-M. and Shen, Z.-Q. (2019) "miR-378a-3p inhibits cellular proliferation and migration in glioblastoma multiforme by targeting tetraspanin 17," *Oncology Reports*, 42(5), p. 1957. doi: 10.3892/OR.2019.7283.

Gupta, M., Neavin, D., Liu, D., Biernacka, J., Hall-Flavin, D., Bobo, W. v., Frye, M. A., Skime, M., Jenkins, G. D., Batzler, A., Kalari, K., Matson, W., Bhasin, S. S., Zhu, H., Mushiroda, T., Nakamura, Y., Kubo, M., Wang, L., Kaddurah-Daouk, R. and Weinshilboum, R. M. (2016) "TSPAN5, ERICH3 and selective serotonin reuptake inhibitors in major depressive disorder: Pharmacometabolomics-informed pharmacogenomics," *Molecular Psychiatry*, 21(12), pp. 1717–1725. doi: 10.1038/mp.2016.6.

Haining, E. J., Yang, J., Bailey, R. L., Khan, K., Collier, R., Tsai, S., Watson, S. P., Frampton, J., Garcia, P. and Tomlinson, M. G. (2012) "The TspanC8 subgroup of tetraspanins interacts with a disintegrin and metalloprotease 10 (ADAM10) and regulates its maturation and cell surface expression," *Journal of Biological Chemistry*, 287(47), pp. 39753–39765. doi: 10.1074/jbc.M112.416503.

Hanley, S. C., Assouline-Thomas, B., Makhlin, J. and Rosenberg, L. (2011) "Epidermal growth factor induces adult human islet cell dedifferentiation," *Journal of Endocrinology*, 211(3), pp. 231–239. doi: 10.1530/JOE-11-0213.

Harbi, M. H., Smith, C. W., Nicolson, P. L. R., Watson, S. P. and Thomas, M. R. (2021) "Novel antiplatelet strategies targeting GPVI, CLEC-2 and tyrosine kinases," *Platelets*, 32(1), pp. 29–41. doi: 10.1080/09537104.2020.1849600.

Harris, B., Pereira, I. and Parkin, E. (2009) "Targeting ADAM10 to lipid rafts in neuroblastoma SH-SY5Y cells impairs amyloidogenic processing of the amyloid precursor protein," *Brain Research*, 1296, pp. 203–215. doi: 10.1016/j.brainres.2009.07.105.

Harrison, N., Koo, C. Z. and Tomlinson, M. G. (2021) "Regulation of ADAM10 by the TspanC8 family of tetraspanins and their therapeutic potential," *International Journal of Molecular Sciences*, 22(13), p. 6707. doi: 10.3390/ijms22136707.

van der Harst, P. and Verweij, N. (2018) "Identification of 64 novel genetic loci provides an expanded view on the genetic architecture of coronary artery disease," *Circulation Research*, 122(3), pp. 433–443. doi: 10.1161/CIRCRESAHA.117.312086.

Hartmann, D., de Strooper, B., Serneels, L., Craessaerts, K., Herreman, A., Annaert, W., Umans, L., Lübke, T., Illert, A. L., von Figura, K. and Saftig, P. (2002) "The disintegrin/metalloprotease ADAM 10 is essential for Notch signalling but not for α-secretase activity in fibroblasts," *Human Molecular Genetics*, 11(21), pp. 2615–2624. doi: 10.1093/hmg/11.21.2615.

Hayashida, K., Bartlett, A. H., Chen, Y. and Park, P. W. (2010) "Molecular and cellular mechanisms of ectodomain shedding," *Anatomical Record*, 293(6), pp. 925–937. doi: 10.1002/ar.20757.

Heikens, M. J., Cao, T. M., Morita, C., DeHart, S. L. and Tsai, S. (2007) "Penumbra encodes a novel tetraspanin that is highly expressed in erythroid progenitors and promotes effective erythropoiesis," *Blood*, 109(8), pp. 3244–3252. doi: 10.1182/blood-2006-09-046672.

Hemler, M. E. (2014) "Tetraspanin proteins promote multiple cancer stages," *Nature Reviews Cancer*, 14(1), pp. 49–60. doi: 10.1038/nrc3640.

Hermans, C., Wittevrongel, C., Thys, C., Smethurst, P. A., van Geet, C. and Freson, K. (2009) "A compound heterozygous mutation in glycoprotein VI in a patient with a bleeding disorder," *Journal of Thrombosis and Haemostasis*, 7(8), pp. 1356–1363. doi: 10.1111/j.1538-7836.2009.03520.x.

Hinds, D. A., Buil, A., Ziemek, D., Martinez-Perez, A., Malik, R., Folkersen, L., Germain, M., Mälarstig, A., Brown, A., Soria, J. M., Dichgans, M., Bing, N., Franco-Cereceda, A., Souto, J. C., Dermitzakis, E. T., Hamsten, A., Worrall, B. B., Tung, J. Y. and Sabater-Lleal, M. (2016) "Genome-wide association analysis of self-reported events in 6135 individuals and 252 827 controls identifies 8 loci associated with thrombosis," *Human Molecular Genetics*, 25(9), pp. 1867–1874. doi: 10.1093/hmg/ddw037.

Hiroshima, K., Shiiba, M., Oka, N., Hayashi, F., Ishida, S., Fukushima, R., Koike, K., Iyoda, M., Nakashima, D., Tanzawa, H. and Uzawa, K. (2019) "Tspan15 plays a crucial role in metastasis in oral squamous cell carcinoma," *Experimental Cell Research*, 384(2), p. 111622. doi: 10.1016/j.yexcr.2019.111622.

Ho, M. F., Zhang, C., Zhang, L., Wei, L., Zhou, Y., Moon, I., Geske, J. R., Choi, D. S., Biernacka, J., Frye, M., Wen, Z., Karpyak, V. M., Li, H. and Weinshilboum, R. (2020) "TSPAN5 influences serotonin and kynurenine: pharmacogenomic mechanisms related to alcohol use disorder and acamprosate treatment response," *Molecular Psychiatry*, pp. 1–12. doi: 10.1038/s41380-020-0855-9.

Hofmann, S., Vögtle, T., Bender, M., Rose-John, S. and Nieswandt, B. (2012) "The SLAM family member CD84 is regulated by ADAM10 and calpain in platelets," *Journal of Thrombosis and Haemostasis*, 10(12), pp. 2581–2592. doi: 10.1111/jth.12013.

Horii, K., Kahn, M. L. and Herr, A. B. (2006) "Structural basis for platelet collagen responses by the immune-type receptor glycoprotein VI," *Blood*, 108(3), pp. 936–942. doi: 10.1182/blood-2006-01-010215.

Horiuchi, K., le Gall, S., Schulte, M., Yamaguchi, T., Reiss, K., Murphy, G., Toyama, Y., Hartmann, D., Saftig, P. and Blobel, C. P. (2007) "Substrate selectivity of epidermal growth factor-receptor ligand sheddases and their regulation by phorbol esters and calcium influx," *Molecular Biology of the Cell*, 18(1), pp. 176–188. doi: 10.1091/mbc.E06-01-0014.

von Hoven, G., Rivas, A. J., Neukirch, C., Klein, S., Hamm, C., Qin, Q., Meyenburg, M., Fuser, S., Saftig, P., Hellmann, N., Postina, R. and Husmann, M. (2016) "Dissecting the

role of ADAM10 as a mediator of Staphylococcus aureus α-toxin action," *Biochemical Journal*, 473(13), pp. 1929–1940. doi: 10.1042/BCJ20160062.

Howe, K. L., Achuthan, P., Allen, James, Allen, Jamie, Alvarez-Jarreta, J., Ridwan Amode, M., Armean, I. M., Azov, A. G., Bennett, R., Bhai, J., Billis, K., Boddu, S., Charkhchi, M., Cummins, C., da Rin Fioretto, L., Davidson, C., Dodiya, K., el Houdaigui, B., Fatima, R., Gall, A., Giron, C. G., Grego, T., Guijarro-Clarke, C., Haggerty, L., Hemrom, A., Hourlier, T., Izuogu, O. G., Juettemann, T., Kaikala, V., Kay, M., Lavidas, I., Le, T., Lemos, D., Martinez, J. G., Marugán, J. C., Maurel, T., McMahon, A. C., Mohanan, S., Moore, B., Muffato, M., Oheh, D. N., Paraschas, D., Parker, A., Parton, A., Prosovetskaia, I., Sakthivel, M. P., Abdul Salam, A. I., Schmitt, B. M., Schuilenburg, H., Sheppard, D., Steed, E., Szpak, M., Szuba, M., Taylor, K., Thormann, A., Threadgold, G., Walts, B., Winterbottom, A., Chakiachvili, M., Chaubal, A., de Silva, N., Flint, B., Frankish, A., Hunt, S. E., IIsley, G. R., Langridge, N., Loveland, J. E., Martin, F. J., Mudge, J. M., Morales, J., Perry, E., Ruffier, M., Tate, J., Thybert, D., Trevanion, S. J., Cunningham, F., Yates, A. D., Zerbino, D. R. and Flicek, P. (2021) "Ensembl 2021," *Nucleic Acids Research*, 49(D1), pp. D884–D891. doi: 10.1093/nar/gkaa942.

Huang, C., Hays, F. A., Tomasek, J. J., Benyajati, S. and Zhang, X. A. (2020) "Tetraspanin CD82 interaction with cholesterol promotes extracellular vesicle–mediated release of ezrin to inhibit tumour cell movement," *Journal of Extracellular Vesicles*, 9(1), p. 1692417. doi: 10.1080/20013078.2019.1692417.

Huff, J., Bergter, A., Birkenbeil, J., Kleppe, I., Engelmann, R. and Krzic, U. (2017) "The new 2D superresolution mode for ZEISS Airyscan," *Nature Methods*, 14(12), pp. 1223–1223. doi: 10.1038/nmeth.f.404.

Human Protein Atlas (2021) *The Human Protein Atlas*. Available at: https://www.proteinatlas.org/ (Accessed: August 27, 2021).

Induruwa, I., Moroi, M., Bonna, A., Malcor, J. D., Howes, J. M., Warburton, E. A., Farndale, R. W. and Jung, S. M. (2018) "Platelet collagen receptor Glycoprotein VI-dimer recognizes fibrinogen and fibrin through their D-domains, contributing to platelet adhesion and activation during thrombus formation," *Journal of Thrombosis and Haemostasis*, 16(2), pp. 389–404. doi: 10.1111/jth.13919.

Ireland, H., Konstantoulas, C. J., Cooper, J. A., Hawe, E., Humphries, S. E., Mather, H., Goodall, A. H., Hogwood, J., Juhan-Vague, I., Yudkin, J. S., di Minno, G., Margaglione, M., Hamsten, A., Miller, G. J., Bauer, K. A., Kim, Y. T., Stearns-Kurosawa, D. J. and Kurosawa, S. (2005) "EPCR Ser219Gly: Elevated sEPCR, prothrombin F1+2, risk for coronary heart disease, and increased sEPCR shedding in vitro," *Atherosclerosis*, 183(2), pp. 283–292. doi: 10.1016/j.atherosclerosis.2005.02.028.

Ishigaki, K., Akiyama, M., Kanai, M., Takahashi, A., Kawakami, E., Sugishita, H., Sakaue, S., Matoba, N., Low, S. K., Okada, Y., Terao, C., Amariuta, T., Gazal, S., Kochi, Y., Horikoshi, M., Suzuki, Ken, Ito, K., Koyama, S., Ozaki, K., Niida, S., Sakata, Yasushi, Sakata, Yasuhiko, Kohno, T., Shiraishi, K., Momozawa, Y., Hirata, M., Matsuda, K.,

Ikeda, M., Iwata, N., Ikegawa, S., Kou, I., Tanaka, T., Nakagawa, H., Suzuki, A., Hirota, T., Tamari, M., Chayama, K., Miki, D., Mori, M., Nagayama, S., Daigo, Y., Miki, Y., Katagiri, T., Ogawa, O., Obara, W., Ito, H., Yoshida, T., Imoto, I., Takahashi, T., Tanikawa, C., Suzuki, T., Sinozaki, N., Minami, S., Yamaguchi, H., Asai, S., Takahashi, Y., Yamaji, K., Takahashi, K., Fujioka, T., Takata, R., Yanai, H., Masumoto, A., Koretsune, Y., Kutsumi, H., Higashiyama, M., Murayama, S., Minegishi, N., Suzuki, Kichiya, Tanno, K., Shimizu, A., Yamaji, T., Iwasaki, M., Sawada, N., Uemura, H., Tanaka, K., Naito, M., Sasaki, M., Wakai, K., Tsugane, S., Yamamoto, M., Yamamoto, K., Murakami, Y., Nakamura, Y., Raychaudhuri, S., Inazawa, J., Yamauchi, T., Kadowaki, T., Kubo, M. and Kamatani, Y. (2020) "Large-scale genome-wide association study in a Japanese population identifies novel susceptibility loci across different diseases," *Nature Genetics*, 52(7), pp. 669–679. doi: 10.1038/s41588-020-0640-3.

Iwagishi, R., Tanaka, R., Seto, M., Takagi, T., Norioka, N., Ueyama, T., Kawamura, T., Takagi, J., Ogawa, Y. and Shirakabe, K. (2020) "Negatively charged amino acids in the stalk region of membrane proteins reduce ectodomain shedding," *Journal of Biological Chemistry*, 295(35), pp. 12343–12352. doi: 10.1074/jbc.RA120.013758.

Jandrot-Perrus, M., Busfield, S., Lagrue, A. H., Xiong, X., Debili, N., Chickering, T., le Couedic, J. P., Goodearl, A., Dussault, B., Fraser, C., Vainchenker, W. and Villeval, J. L. (2000) "Cloning, characterization, and functional studies of human and mouse glycoprotein VI: A platelet-specific collagen receptor from the immunoglobulin superfamily," *Blood*, 96(5), pp. 1798–1807. doi: 10.1182/blood.v96.5.1798.

Jandrot-Perrus, M., Hermans, C. and Mezzano, D. (2019) "Platelet glycoprotein VI genetic quantitative and qualitative defects," *Platelets*, 30(6), pp. 708–713. doi: 10.1080/09537104.2019.1610166.

Jansen, I. E., Savage, J. E., Watanabe, K., Bryois, J., Williams, D. M., Steinberg, S., Sealock, J., Karlsson, I. K., Hägg, S., Athanasiu, L., Voyle, N., Proitsi, P., Witoelar, A., Stringer, S., Aarsland, D., Almdahl, I. S., Andersen, F., Bergh, S., Bettella, F., Bjornsson, S., Brækhus, A., Bråthen, G., de Leeuw, C., Desikan, R. S., Djurovic, S., Dumitrescu, L., Fladby, T., Hohman, T. J., Jonsson, P. v, Kiddle, S. J., Rongve, A., Saltvedt, I., Sando, S. B., Selbæk, G., Shoai, M., Skene, N. G., Snaedal, J., Stordal, E., Ulstein, I. D., Wang, Y., White, L. R., Hardy, J., Hjerling-Leffler, J., Sullivan, P. F., van der Flier, W. M., Dobson, R., Davis, L. K., Stefansson, H., Stefansson, K., Pedersen, N. L., Ripke, S., Andreassen, O. A. and Posthuma, D. (2019) "Genome-wide meta-analysis identifies new loci and functional pathways influencing Alzheimer's disease risk," *Nature Genetics*, 51(3), pp. 404–413. doi: 10.1038/s41588-018-0311-9.

Jin, E. J., Kiral, F. R. and Hiesinger, P. R. (2018) "The where, what, and when of membrane protein degradation in neurons," *Developmental Neurobiology*, 78(3), pp. 283–297. doi: 10.1002/dneu.22534.

Jones, C. I., Garner, S. F., Angenent, W., Bernard, A., Berzuini, C., Burns, P., Farndale, R. W., Hogwood, J., Rankin, A., Stephens, J. C., Tom, B. D., Walton, J., Dudbridge, F., Ouwehand, W. H. and Goodall, A. H. (2007) "Mapping the platelet profile for

functional genomic studies and demonstration of the effect size of the GP6 locus," *Journal of Thrombosis and Haemostasis*, 5(8), pp. 1756–1765. doi: 10.1111/j.1538-7836.2007.02632.x.

Jorissen, E., Prox, J., Bernreuther, C., Weber, S., Schwanbeck, R., Serneels, L., Snellinx, A., Craessaerts, K., Thathiah, A., Tesseur, I., Bartsch, U., Weskamp, G., Blobel, C. P., Glatzel, M., de Strooper, B. and Saftig, P. (2010) "The disintegrin/metalloproteinase ADAM10 is essential for the establishment of the brain cortex," *Journal of Neuroscience*, 30(14), pp. 4833–4844. doi: 10.1523/JNEUROSCI.5221-09.2010.

Jouannet, S., Saint-Pol, J., Fernandez, L., Nguyen, V., Charrin, S., Boucheix, C., Brou, C., Milhiet, P. E. and Rubinstein, E. (2016) "TspanC8 tetraspanins differentially regulate the cleavage of ADAM10 substrates, Notch activation and ADAM10 membrane compartmentalization," *Cellular and Molecular Life Sciences*, 73(9), pp. 1895–1915. doi: 10.1007/s00018-015-2111-z.

Joutsi-Korhonen, L., Smethurst, P. A., Rankin, A., Gray, E., IJsseldijk, M., Onley, C. M., Watkins, N. A., Williamson, L. M., Goodall, A. H., de Groot, P. G., Farndale, R. W. and Ouwehand, W. H. (2003) "The low-frequency allele of the platelet collagen signaling receptor glycoprotein VI is associated with reduced functional responses and expression," *Blood*, 101(11), pp. 4372–4379. doi: 10.1182/blood-2002-08-2591.

Jurkovitz, C. T., England, B. K., Ebb, R. G. and Mitch, W. E. (1992) "Influence of ammonia and pH on protein and amino acid metabolism in LLC-PK1 cells," *Kidney International*, 42(3), pp. 595–601. doi: 10.1038/ki.1992.323.

Jung, S.M., Takemura, Y., Imamura, Y., Hayashi, T., Adachi, E. and Moroi, M. (2008) "Collagen-type specificity of glycoprotein VI as a determinant of platelet adhesion," *Platelets*, 19(1), pp. 32–42. doi:10.1080/09537100701609027.

Kapur, R. and Semple, J. W. (2016) "Platelets as immune-sensing cells," *Blood Advances*, 1(1), pp. 10–14. doi: 10.1182/bloodadvances.2016000067.

Karlsson, M., Zhang, C., Méar, L., Zhong, W., Digre, A., Katona, B., Sjöstedt, E., Butler, L., Odeberg, J., Dusart, P., Edfors, F., Oksvold, P., von Feilitzen, K., Zwahlen, M., Arif, M., Altay, O., Li, X., Ozcan, M., Mardonoglu, A., Fagerberg, L., Mulder, J., Luo, Y., Ponten, F., Uhlén, M. and Lindskog, C. (2021) "A single–cell type transcriptomics map of human tissues," *Science Advances*, 7(31), p. eabh2169. doi: 10.1126/sciadv.abh2169.

Katoh, K. and Standley, D. M. (2013) "MAFFT multiple sequence alignment software version 7: Improvements in performance and usability," *Molecular Biology and Evolution*, 30(4), pp. 772–780. doi: 10.1093/molbev/mst010.

Keerthikumar, S., Gangoda, L., Liem, M., Fonseka, P., Atukorala, I., Ozcitti, C., Mechler, A., Adda, C. G., Ang, C. S. and Mathivanan, S. (2015) "Proteogenomic analysis reveals exosomes are more oncogenic than ectosomes," *Oncotarget*, 6(17), pp. 15375–15396. doi: 10.18632/oncotarget.3801.

Kelley, L. A., Mezulis, S., Yates, C. M., Wass, M. N. and Sternberg, M. J. E. (2015) "The Phyre2 web portal for protein modeling, prediction and analysis," *Nature Protocols*, 10(6), pp. 845–858. doi: 10.1038/nprot.2015.053.

Kerppola, T. K. (2006) “Visualization of molecular interactions by fluorescence complementation,” *Nature Reviews Molecular Cell Biology*, 7(6), pp. 449–456. doi: 10.1038/nrm1929.

Kilpatrick, L. E., Briddon, S. J. and Holliday, N. D. (2012) “Fluorescence correlation spectroscopy, combined with bimolecular fluorescence complementation, reveals the effects of β-arrestin complexes and endocytic targeting on the membrane mobility of neuropeptide Y receptors,” *Biochimica et Biophysica Acta - Molecular Cell Research*, 1823(6), pp. 1068–1081. doi: 10.1016/j.bbamcr.2012.03.002.

Kim, M., Suh, J., Romano, D., Truong, M.H., Mullin, K., Hooli, B., Norton, D., Tesco, G., Elliott, K., Wagner, S.L., Moir, R.D., Becker, K.D. and Tanzi, R.E. (2009) “Potential late-onset Alzheimer’s disease-associated mutations in the ADAM10 gene attenuate α-secretase activity,” *Human Molecular Genetics*, 18(20), pp. 3987–3996. doi:10.1093/hmg/ddp323.

Kim, M. S., Pinto, S. M., Getnet, D., Nirujogi, R. S., Manda, S. S., Chaerkady, R., Madugundu, A. K., Kelkar, D. S., Isserlin, R., Jain, S., Thomas, J. K., Muthusamy, B., Leal-Rojas, P., Kumar, P., Sahasrabuddhe, N. A., Balakrishnan, L., Advani, J., George, B., Renuse, S., Selvan, L. D. N., Patil, A. H., Nanjappa, V., Radhakrishnan, A., Prasad, S., Subbannayya, T., Raju, R., Kumar, M., Sreenivasamurthy, S. K., Marimuthu, A., Sathe, G. J., Chavan, S., Datta, K. K., Subbannayya, Y., Sahu, A., Yelamanchi, S. D., Jayaram, S., Rajagopalan, P., Sharma, J., Murthy, K. R., Syed, N., Goel, R., Khan, A. A., Ahmad, S., Dey, G., Mudgal, K., Chatterjee, A., Huang, T. C., Zhong, J., Wu, X., Shaw, P. G., Freed, D., Zahari, M. S., Mukherjee, K. K., Shankar, S., Mahadevan, A., Lam, H., Mitchell, C. J., Shankar, S. K., Satishchandra, P., Schroeder, J. T., Sirdeshmukh, R., Maitra, A., Leach, S. D., Drake, C. G., Halushka, M. K., Prasad, T. S. K., Hruban, R. H., Kerr, C. L., Bader, G. D., Iacobuzio-Donahue, C. A., Gowda, H. and Pandey, A. (2014) “A draft map of the human proteome,” *Nature*, 509(7502), pp. 575–581. doi: 10.1038/nature13302.

King, S.L., Joshi, H.J., Schjoldager, K.T., Halim, A., Madsen, T.D., Dziegiel, M.H., Woetmann, A., Vakhrushev, S.Y. and Wandall, H.H. (2017) “Characterizing the O-glycosylation landscape of human plasma, platelets, and endothelial cells,” *Blood Advances*, 1(7), pp. 429–442. doi:10.1182/bloodadvances.2016002121.

Kitadokoro, K., Bordo, D., Galli, G., Petracca, R., Falugi, F., Abrignani, S., Grandi, G. and Bolognesi, M. (2001) “CD81 extracellular domain 3D structure: Insight into the tetraspanin superfamily structural motifs,” *EMBO Journal*, 20(1–2), pp. 12–18. doi: 10.1093/emboj/20.1.12.

Klapproth, E., Kuenzel, S., Guenscht, M., Lorenz, K., Weber, S., Guan, K. and El-Armouche, A. (2020) “ADAM10 inhibition improves survival and augments cardiac function after myocardial infarction,” *European Heart Journal*, 41(Supplement_2), p. ehaa946.3640. doi: 10.1093/ehjci/ehaa946.3640.

Klarin, D., Busenkell, E., Judy, R., Lynch, J., Levin, M., Haessler, J., Aragam, K., Chaffin, M., Haas, M., Lindström, S., Assimes, T. L., Huang, J., Min Lee, K., Shao, Q., Huffman, J. E., Kabrhel, C., Huang, Y., Sun, Y. v., Vujkovic, M., Saleheen, D., Miller,

D. R., Reaven, P., DuVall, S., Boden, W. E., Pyarajan, S., Reiner, A. P., Trégouët, D. A., Henke, P., Kooperberg, C., Gaziano, J. M., Concato, J., Rader, D. J., Cho, K., Chang, K. M., Wilson, P. W. F., Smith, N. L., O'Donnell, C. J., Tsao, P. S., Kathiresan, S., Obi, A., Damrauer, S. M. and Natarajan, P. (2019) "Genome-wide association analysis of venous thromboembolism identifies new risk loci and genetic overlap with arterial vascular disease," *Nature Genetics*, 51(11), pp. 1574–1579. doi: 10.1038/s41588-019-0519-3.

Klarin, D., Emdin, C. A., Natarajan, P., Conrad, M. F. and Kathiresan, S. (2017) "Genetic analysis of venous thromboembolism in UK Biobank identifies the ZFPM2 locus and implicates obesity as a causal risk factor," *Circulation: Cardiovascular Genetics*, 10(2), p. e001643. doi: 10.1161/CIRCGENETICS.116.001643.

Kojro, E., Füger, P., Prinzen, C., Kanarek, A. M., Rat, D., Endres, K., Fahrenholz, F. and Postina, R. (2010) "Statins and the squalene synthase inhibitor zaragozic acid stimulate the non-amyloidogenic pathway of amyloid-β protein precursor processing by suppression of cholesterol synthesis," *Journal of Alzheimer's Disease*, 20(4), pp. 1215–1231. doi: 10.3233/JAD-2010-091621.

Kojro, E., Gimpl, G., Lammich, S., März, W. and Fahrenholz, F. (2001) "Low cholesterol stimulates the nonamyloidogenic pathway by its effect on the α-secretase ADAM 10," *Proceedings of the National Academy of Sciences of the United States of America*, 98(10), pp. 5815–5820. doi: 10.1073/pnas.081612998.

Kono, M., Sugiura, K., Suganuma, M., Hayashi, M., Takama, H., Suzuki, T., Matsunaga, Uk., Tomita, Y. and Akiyama, M. (2013) "Whole-exome sequencing identifies ADAM10 mutations as a cause of reticulate acropigmentation of Kitamura, a clinical entity distinct from Dowling-Degos disease," *Human Molecular Genetics*, 22(17), pp. 3524–3533. doi:10.1093/HMG/DDT207.

Koo, C. Z., Harrison, N., Noy, P. J., Szyroka, J., Matthews, A. L., Hsia, H. E., Müller, S. A., Tüshaus, J., Goulding, J., Willis, K., Apicella, C., Cragoe, B., Davis, E., Keles, M., Malinova, A., McFarlane, T. A., Morrison, P. R., Nguyen, H. T. H., Sykes, M. C., Ahmed, H., Maio, A. di, Seipold, L., Saftig, P., Cull, E., Pliotas, C., Rubinstein, E., Poulter, N. S., Briddon, S. J., Holliday, N. D., Lichtenthaler, S. F. and Tomlinson, M. G. (2020) "The tetraspanin Tspan15 is an essential subunit of an ADAM10 scissor complex," *Journal of Biological Chemistry*, 295(36), pp. 12822–12839. doi: 10.1074/jbc.ra120.012601.

Kotuličová, D., Chudý, P., Škereňová, M., Ivanková, J., Dobrotová, M. and Kubisz, P. (2012) "Variability of GP6 gene in patients with sticky platelet syndrome and deep venous thrombosis and/or pulmonary embolism," *Blood Coagulation and Fibrinolysis*, 23(6), pp. 543–547. doi: 10.1097/MBC.0b013e328355a808.

Koupenova, M., Kehrel, B. E., Corkrey, H. A. and Freedman, J. E. (2017) "Thrombosis and platelets: An update," *European Heart Journal*, 38(11), pp. 785–791. doi: 10.1093/eurheartj/ehw550.

Kovács, S., Csiki, Z., Zsóri, K. S., Bereczky, Z. and Shemirani, A. H. (2019) "Characteristics of platelet count and size and diagnostic accuracy of mean platelet volume in patients

with venous thromboembolism. A systematic review and meta-analysis," *Platelets*, 30(2), pp. 139–147. doi: 10.1080/09537104.2017.1414175.

Kuhn, P. H., Colombo, A. V., Schusser, B., Dreymueller, D., Wetzel, S., Schepers, U., Herber, J., Ludwig, A., Kremmer, E., Montag, D., Müller, U., Schweizer, M., Saftig, P., Bräse, S. and Lichtenthaler, S. F. (2016) "Systematic substrate identification indicates a central role for the metalloprotease ADAM10 in axon targeting and synapse function," *eLife*, 5, p. e12748. doi: 10.7554/eLife.12748.001.

Kuhn, P. H., Wang, H., Dislich, B., Colombo, A., Zeitschel, U., Ellwart, J. W., Kremmer, E., Roßner, S. and Lichtenthaler, S. F. (2010) "ADAM10 is the physiologically relevant, constitutive α-secretase of the amyloid precursor protein in primary neurons," *EMBO Journal*, 29(17), pp. 3020–3032. doi: 10.1038/emboj.2010.167.

Kunkle, B. W., Grenier-Boley, B., Sims, R., Bis, J. C., Damotte, V., Naj, A. C., Boland, A., Vronskaya, M., van der Lee, S. J., Amlie-Wolf, A., Bellenguez, C., Frizatti, A., Chouraki, V., Martin, E. R., Sleegers, K., Badarinarayan, N., Jakobsdottir, J., Hamilton-Nelson, K. L., Moreno-Grau, S., Olaso, R., Raybould, R., Chen, Y., Kuzma, A. B., Hiltunen, M., Morgan, T., Ahmad, S., Vardarajan, B. N., Epelbaum, J., Hoffmann, P., Boada, M., Beecham, G. W., Garnier, J. G., Harold, D., Fitzpatrick, A. L., Valladares, O., Moutet, M. L., Gerrish, A., Smith, A. v., Qu, L., Bacq, D., Denning, N., Jian, X., Zhao, Y., del Zompo, M., Fox, N. C., Choi, S. H., Mateo, I., Hughes, J. T., Adams, H. H., Malamon, J., Sanchez-Garcia, F., Patel, Y., Brody, J. A., Dombroski, B. A., Naranjo, M. C. D., Daniilidou, M., Eiriksdottir, G., Mukherjee, S., Wallon, D., Uphill, J., Aspelund, T., Cantwell, L. B., Garzia, F., Galimberti, D., Hofer, E., Butkiewicz, M., Fin, B., Scarpini, E., Sarnowski, C., Bush, W. S., Meslage, S., Kornhuber, J., White, C. C., Song, Y., Barber, R. C., Engelborghs, S., Sordon, S., Voijnovic, D., Adams, P. M., Vandenberghe, R., Mayhaus, M., Cupples, L. A., Albert, M. S., de Deyn, P. P., Gu, W., Himali, J. J., Beekly, D., Squassina, A., Hartmann, A. M., Orellana, A., Blacker, D., Rodriguez-Rodriguez, E., Lovestone, S., Garcia, M. E., Doody, R. S., Munoz-Fernadez, C., Sussams, R., Lin, H., Fairchild, T. J., Benito, Y. A., Holmes, C., Karamujić-Čomić, H., Frosch, M. P., Thonberg, H., Maier, W., Roschupkin, G., Ghetti, B., Giedraitis, V., Kawalia, A., Li, S., Huebinger, R. M., Kilander, L., Moebus, S., Hernández, I., Kamboh, M. I., Brundin, R. M., Turton, J., Yang, Q., Katz, M. J., Concari, L., Lord, J., Beiser, A. S., Keene, C. D., Helisalmi, S., Kloszewska, I., Kukull, W. A., Koivisto, A. M., Lynch, A., Tarraga, L., Larson, E. B., Haapasalo, A., Lawlor, B., Mosley, T. H., Lipton, R. B., Solfrizzi, V., Gill, M., Longstreth, W. T., Montine, T. J., Frisardi, V., Diez-Fairen, M., Rivadeneira, F., Petersen, R. C., Deramecourt, V., Alvarez, I., Salani, F., Ciaramella, A., Boerwinkle, E., Reiman, E. M., Fievet, N., Rotter, J. I., Reisch, J. S., Hanon, O., Cupidi, C., Andre Uitterlinden, A. G., Royall, D. R., Dufouil, C., Maletta, R. G., de Rojas, I., Sano, M., Brice, A., Cecchetti, R., George-Hyslop, P. S., Ritchie, K., Tsolaki, M., Tsuang, D. W., Dubois, B., Craig, D., Wu, C. K., Soininen, H., Avramidou, D., Albin, R. L., Fratiglioni, L., Germanou, A., Apostolova, L. G., Keller, L., Koutroumani, M., Arnold, S. E., Panza, F., Gkatzima, O., Asthana, S., Hannequin, D., Whitehead, P., Atwood, C. S., Caffarra, P., Hampel, H., Quintela, I., Carracedo, Á.,

Lannfelt, L., Rubinsztein, D. C., Barnes, L. L., Pasquier, F., Frölich, L., Barral, S., McGuinness, B., Beach, T. G., Johnston, J. A., Becker, J. T., Passmore, P., Bigio, E. H., Schott, J. M., Bird, T. D., Warren, J. D., Boeve, B. F., Lupton, M. K., Bowen, J. D., Proitsi, P., Boxer, A., Powell, J. F., Burke, J. R., Kauwe, J. S. K., Burns, J. M., Mancuso, M., Buxbaum, J. D., Bonuccelli, U., Cairns, N. J., McQuillin, A., Cao, C., Livingston, G., Carlson, C. S., Bass, N. J., Carlsson, C. M., Hardy, J., Carney, R. M., Bras, J., Carrasquillo, M. M., Guerreiro, R., Allen, M., Chui, H. C., Fisher, E., Masullo, C., Crocco, E. A., DeCarli, C., Bisceglio, G., Dick, M., Ma, L., Duara, R., Graff-Radford, N. R., Evans, D. A., Hodges, A., Faber, K. M., Scherer, M., Fallon, K. B., Riemenschneider, M., Fardo, D. W., Heun, R., Farlow, M. R., Kölsch, H., Ferris, S., Leber, M., Foroud, T. M., Heuser, I., Galasko, D. R., Giegling, I., Gearing, M., Hüll, M., Geschwind, D. H., Gilbert, J. R., Morris, J. C., Green, R. C., Mayo, K., Growdon, J. H., Feulner, T., Hamilton, R. L., Harrell, L. E., Drichel, D., Honig, L. S., Cushion, T. D., Huentelman, M. J., Hollingworth, P., Hulette, C. M., Hyman, B. T., Marshall, R., Jarvik, G. P., Meggy, A., Abner, E., Menzies, G. E., Jin, L. W., Leonenko, G., Real, L. M., Jun, G. R., Baldwin, C. T., Grozeva, D., Karydas, A., Russo, G., Kaye, J. A., Kim, R., Jessen, F., Kowall, N. W., Vellas, B., Kramer, J. H., Vardy, E., LaFerla, F. M., Jöckel, K. H., Lah, J. J., Dichgans, M., Leverenz, J. B., Mann, D., Levey, A. I., Pickering-Brown, S., Lieberman, A. P., Klopp, N., Lunetta, K. L., Wichmann, H. E., Lyketsos, C. G., Morgan, K., Marson, D. C., Brown, K., Martiniuk, F., Medway, C., Mash, D. C., Nöthen, M. M., Masliah, E., Hooper, N. M., McCormick, W. C., Daniele, A., McCurry, S. M., Bayer, A., McDavid, A. N., Gallacher, J., McKee, A. C., van den Bussche, H., Mesulam, M., Brayne, C., Miller, B. L., Riedel-Heller, S., Miller, C. A., Miller, J. W., Al-Chalabi, A., Shaw, C. E., Myers, A. J., Wiltfang, J., O'Bryant, S., Olichney, J. M., Alvarez, V., Parisi, J. E., Singleton, A. B., Paulson, H. L., Collinge, J., Perry, W. R., Mead, S., Peskind, E., Cribbs, D. H., Rossor, M., Pierce, A., Ryan, N. S., Poon, W. W., Nacmias, B., Potter, H., Sorbi, S., Quinn, J. F., Sacchinelli, E., Raj, A., Spalletta, G., Raskind, M., Caltagirone, C., Bossù, P., Orfei, M. D., Reisberg, B., Clarke, R., Reitz, C., Smith, A. D., Ringman, J. M., Warden, D., Roberson, E. D., Wilcock, G., Rogaeva, E., Bruni, A. C., Rosen, H. J., Gallo, M., Rosenberg, R. N., Ben-Shlomo, Y., Sager, M. A., Mecocci, P., Saykin, A. J., Pastor, P., Cuccaro, M. L., Vance, J. M., Schneider, J. A., Schneider, L. S., Slifer, S., Seeley, W. W., Smith, A. G., Sonnen, J. A., Spina, S., Stern, R. A., Swerdlow, R. H., Tang, M., Tanzi, R. E., Trojanowski, J. Q., Troncoso, J. C., van Deerlin, V. M., van Eldik, L. J., Vinters, H. v., Vonsattel, J. P., Weintraub, S., Welsh-Bohmer, K. A., Wilhelmsen, K. C., Williamson, J., Wingo, T. S., Woltjer, R. L., Wright, C. B., Yu, C. E., Yu, L., Saba, Y., Pilotto, A., Bullido, M. J., Peters, O., Crane, P. K., Bennett, D., Bosco, P., Coto, E., Boccardi, V., de Jager, P. L., Lleo, A., Warner, N., Lopez, O. L., Ingelsson, M., Deloukas, P., Cruchaga, C., Graff, C., Gwilliam, R., Fornage, M., Goate, A. M., Sanchez-Juan, P., Kehoe, P. G., Amin, N., Ertekin-Taner, N., Berr, C., Debette, S., Love, S., Launer, L. J., Younkin, S. G., Dartigues, J. F., Corcoran, C., Ikram, M. A., Dickson, D. W., Nicolas, G., Campion, D., Tschanz, J. A., Schmidt, H., Hakonarson, H., Clarimon, J., Munger,

R., Schmidt, R., Farrer, L. A., van Broeckhoven, C., C. O'Donovan, M., DeStefano, A. L., Jones, L., Haines, J. L., Deleuze, J. F., Owen, M. J., Gudnason, V., Mayeux, R., Escott-Price, V., Psaty, B. M., Ramirez, A., Wang, L. S., Ruiz, A., van Duijn, C. M., Holmans, P. A., Seshadri, S., Williams, J., Amouyel, P., Schellenberg, G. D., Lambert, J. C. and Pericak-Vance, M. A. (2019) "Genetic meta-analysis of diagnosed Alzheimer's disease identifies new risk loci and implicates Aβ, tau, immunity and lipid processing," *Nature Genetics*, 51(3), pp. 414–430. doi: 10.1038/s41588-019-0358-2.

Latysheva, N., Muratov, G., Rajesh, S., Padgett, M., Hotchin, N. A., Overduin, M. and Berditchevski, F. (2006) "Syntenin-1 is a new component of tetraspanin-enriched microdomains: Mechanisms and consequences of the interaction of syntenin-1 with CD63," *Molecular and Cellular Biology*, 26(20), pp. 7707–7718. doi: 10.1128/mcb.00849-06.

Lebozec, K., Jandrot-Perrus, M., Avenard, G., Favre-Bulle, O. and Billiald, P. (2017) "Design, development and characterization of ACT017, a humanized Fab that blocks platelet's glycoprotein VI function without causing bleeding risks," *mAbs*, 9(6), pp. 945–958. doi: 10.1080/19420862.2017.1336592.

Lecut, C., Arocas, V., Ulrichts, H., Elbaz, A., Villeval, J. L., Lacapère, J. J., Deckmynll, H. and Jandrot-Perrus, M. (2004) "Identification of residues within human glycoprotein VI involved in the binding to collagen: Evidence for the existence of distinct binding sites," *Journal of Biological Chemistry*, 279(50), pp. 52293–52299. doi: 10.1074/jbc.M406342200.

Lécuyer, H., Virion, Z., Barnier, J. P., Matczak, S., Bourdoulous, S., Bianchini, E., Saller, F., Borgel, D., Nassif, X. and Coureuil, M. (2018) "An ADAM10-dependent EPCR shedding links meningococcal interaction with endothelial cells to purpura fulminans," *PLoS Pathogens*, 14(4). doi: 10.1371/journal.ppat.1006981.

Lee, K. J., Kang, D. and Park, H. S. (2019) "Site-specific labeling of proteins using unnatural amino acids," *Molecules and Cells*, 42(5), pp. 386–396. doi: 10.14348/molcells.2019.0078.

Lehmann, M., Schoeman, R. M., Krohl, P. J., Wallbank, A. M., Samaniuk, J. R., Jandrot-Perrus, M. and Neeves, K. B. (2018) "Platelets drive thrombus propagation in a hematocrit and glycoprotein VI-dependent manner in an in vitro venous thrombosis model," *Arteriosclerosis, Thrombosis, and Vascular Biology*, 38(5), pp. 1052–1062. doi: 10.1161/ATVBAHA.118.310731.

Lepäntalo, A., Mikkelsson, J., Reséndiz, J. C., Viiri, L., Backman, J. T., Kankuri, E., Karhunen, P. J. and Lassila, R. (2006) "Polymorphisms of COX-I and GPVI associate with the antiplatelet effect of aspirin in coronary artery disease patients," *Thrombosis and Haemostasis*, 95(2), pp. 253–259. doi: 10.1160/TH05-07-0516.

Letunic, I. and Bork, P. (2021) "Interactive tree of life (iTOL) v5: An online tool for phylogenetic tree display and annotation," *Nucleic Acids Research*, 49(W1), pp. W293–W296. doi: 10.1093/nar/gkab301.

Levy, S. (2014) "Function of the tetraspanin molecule CD81 in B and T cells," *Immunologic Research*, 58(2–3), pp. 179–185. doi: 10.1007/s12026-014-8490-7.

Li, J., Chen, X., Yi, J., Liu, Y., Li, D., Wang, Jifeng, Hou, D., Jiang, X., Zhang, J., Wang, Jin, Zen, K., Yang, F., Zhang, C. Y. and Zhang, Y. (2016) "Identification and characterization of 293t cell-derived exosomes by profiling the protein, mRNA and microrna components," *PLoS ONE*, 11(9), p. e0163043. doi: 10.1371/journal.pone.0163043.

Lichtenthaler, S. F., Lemberg, M. K. and Fluhrer, R. (2018) "Proteolytic ectodomain shedding of membrane proteins in mammals—hardware, concepts, and recent developments," *The EMBO Journal*, 37(15), p. 99456. doi: 10.15252/embj.201899456.

Lindström, S., Wang, L., Smith, E. N., Gordon, W., van Hylckama Vlieg, A., de Andrade, M., Brody, J. A., Pattee, J. W., Haessler, J., Brumpton, B. M., Chasman, D. I., Suchon, P., Chen, M. H., Turman, C., Germain, M., Wiggins, K. L., MacDonald, J., Braekkan, S. K., Armasu, S. M., Pankratz, N., Jackson, R. D., Nielsen, J. B., Giulianini, F., Puurunen, M. K., Ibrahim, M., Heckbert, S. R., Damrauer, S. M., Natarajan, P., Klarin, D., de Vries, P. S., Sabater-Lleal, M., Huffman, J. E., Bammler, T. K., Frazer, K. A., McCauley, B. M., Taylor, K., Pankow, J. S., Reiner, A. P., Gabrielsen, M. E., Deleuze, J. F., O'Donnell, C. J., Kim, J., McKnight, B., Kraft, P., Hansen, J. B., Rosendaal, F. R., Heit, J. A., Psaty, B. M., Tang, W., Kooperberg, C., Hveem, K., Ridker, P. M., Morange, P. E., Johnson, A. D., Kabrhel, C., Trégouët, D. A. and Smith, N. L. (2019) "Genomic and transcriptomic association studies identify 16 novel susceptibility loci for venous thromboembolism," *Blood*, 134(19), pp. 1645–1657. doi: 10.1182/blood.2019000435.

Lippi, G., Buonocore, R. and Cervellin, G. (2016) "The mean platelet volume is decreased in patients diagnosed with venous thromboembolism in the emergency department," *Seminars in Thrombosis and Hemostasis*, 42(6), pp. 632–635. doi: 10.1055/s-0036-1571335.

Lippi, G., Sanchis-Gomar, F. and Favaloro, E. J. (2020) "Mean platelet volume in arterial and venous thrombotic disorders," *Journal of Laboratory Medicine*. De Gruyter, pp. 305–312. doi: 10.1515/labmed-2019-0201.

Liu, C., Xu, P., Lamouille, S., Xu, J. and Derynck, R. (2009) "TACE-mediated ectodomain shedding of the type I TGF-β receptor downregulates TGF-β signaling," *Molecular Cell*, 35(1), pp. 26–36. doi: 10.1016/j.molcel.2009.06.018.

Liu, J. Z., van Sommeren, S., Huang, H., Ng, S. C., Alberts, R., Takahashi, A., Ripke, S., Lee, J. C., Jostins, L., Shah, T., Abedian, S., Cheon, J. H., Cho, J., Daryani, N. E., Franke, L., Fuyuno, Y., Hart, A., Juyal, R. C., Juyal, G., Kim, W. H., Morris, A. P., Poustchi, H., Newman, W. G., Midha, V., Orchard, T. R., Vahedi, H., Sood, A., Sung, J. J. Y., Malekzadeh, R., Westra, H. J., Yamazaki, K., Yang, S. K., Barrett, J. C., Franke, A., Alizadeh, B. Z., Parkes, M., Thelma, B. K., Daly, M. J., Kubo, M., Anderson, C. A. and Weersma, R. K. (2015) "Association analyses identify 38 susceptibility loci for inflammatory bowel disease and highlight shared genetic risk across populations," *Nature Genetics*, 47(9), pp. 979–986. doi: 10.1038/ng.3359.

Livak, K. J. and Schmittgen, T. D. (2001) “Analysis of relative gene expression data using real-time quantitative PCR and the 2-ΔΔCT method,” *Methods*, 25(4), pp. 402–408. doi: 10.1006/meth.2001.1262.

Lu, R. M., Hwang, Y. C., Liu, I. J., Lee, C. C., Tsai, H. Z., Li, H. J. and Wu, H. C. (2020) “Development of therapeutic antibodies for the treatment of diseases,” *Journal of Biomedical Science*. doi: 10.1186/s12929-019-0592-z.

Ludwig, A., Hundhausen, C., Lambert, M., Broadway, N., Andrews, R., Bickett, D., Leesnitzer, M. and Becherer, J. (2005) “Metalloproteinase inhibitors for the disintegrin-Like metalloproteinases ADAM10 and ADAM17 that differentially block constitutive and phorbol ester-inducible shedding of cell surface molecules,” *Combinatorial Chemistry & High Throughput Screening*, 8(2), pp. 161–171. doi: 10.2174/1386207053258488.

Luu, V. P., Hevezi, P., Vences-Catalan, F., Maravillas-Montero, J. L., White, C. A., Casali, P., Llorente, L., Jakez-Ocampo, J., Lima, G., Vilches-Cisneros, N., Flores-Gutiérrez, J. P., Santos-Argumedo, L. and Zlotnik, A. (2013) “TSPAN33 is a novel marker of activated and malignant B cells,” *Clinical Immunology*, 149(3 PB), pp. 388–399. doi: 10.1016/j.clim.2013.08.005.

Lyon, C. A., Johnson, J. L., Williams, H., Sala-Newby, G. B. and George, S. J. (2009) “Soluble N-cadherin overexpression reduces features of atherosclerotic plaque instability,” *Arteriosclerosis, Thrombosis, and Vascular Biology*, 29(2), pp. 195–201. doi: 10.1161/ATVBAHA.108.178087.

Lyon, C. A., Wadey, K. S. and George, S. J. (2016) “Soluble N-cadherin: A novel inhibitor of VSMC proliferation and intimal thickening,” *Vascular Pharmacology*, 78, pp. 53–62. doi: 10.1016/j.vph.2015.11.040.

Ma, W. T., Gao, F., Gu, K. and Chen, D. K. (2019) “The role of monocytes and macrophages in autoimmune diseases: A comprehensive review,” *Frontiers in Immunology*, 10(MAY), p. 1140. doi: 10.3389/fimmu.2019.01140.

Machiela, M. J. and Chanock, S. J. (2015) “LDlink: A web-based application for exploring population-specific haplotype structure and linking correlated alleles of possible functional variants,” *Bioinformatics*, 31(21), pp. 3555–3557. doi: 10.1093/bioinformatics/btv402.

Mackman, N., Bergmeier, W., Stouffer, G. A. and Weitz, J. I. (2020) “Therapeutic strategies for thrombosis: new targets and approaches,” *Nature Reviews Drug Discovery*, 19(5), pp. 333–352. doi: 10.1038/s41573-020-0061-0.

Madeira, F., Park, Y. M., Lee, J., Buso, N., Gur, T., Madhusoodanan, N., Basutkar, P., Tivey, A. R. N., Potter, S. C., Finn, R. D. and Lopez, R. (2019) “The EMBL-EBI search and sequence analysis tools APIs in 2019,” *Nucleic Acids Research*, 47(W1), pp. W636–W641. doi: 10.1093/nar/gkz268.

Madeira, F., Tinti, M., Murugesan, G., Berrett, E., Stafford, M., Toth, R., Cole, C., MacKintosh, C. and Barton, G. J. (2015) “14-3-3-Pred: Improved methods to predict 14-3-3-binding phosphopeptides,” *Bioinformatics*, 31(14), pp. 2276–2283. doi: 10.1093/bioinformatics/btv133.

Madoux, F., Dreymuller, D., Pettiloud, J. P., Santos, R., Becker-Pauly, C., Ludwig, A., Fields, G. B., Bannister, T., Spicer, T. P., Cudic, M., Scampavia, L. D. and Minond, D. (2016) "Discovery of an enzyme and substrate selective inhibitor of ADAM10 using an exosite-binding glycosylated substrate," *Scientific Reports*, 6(1), pp. 1–17. doi: 10.1038/s41598-016-0013-4.

Mammadova-Bach, E., Ollivier, V., Loyau, S., Schaff, M., Dumont, B., Favier, R., Freyburger, G., Latger-Cannard, V., Nieswandt, B., Gachet, C., Mangin, P. H. and Jandrot-Perrus, M. (2015) "Platelet glycoprotein VI binds to polymerized fibrin and promotes thrombin generation," *Blood*, 126(5), pp. 683–691. doi: 10.1182/blood-2015-02-629717.

Manders, E. M. M., Verbeek, F. J. and Aten, J. A. (1993) "Measurement of co-localization of objects in dual-colour confocal images," *Journal of Microscopy*, 169(3), pp. 375–382. doi: 10.1111/j.1365-2818.1993.tb03313.x.

Mangin, P. H., Tang, C. J., Bourdon, C., Loyau, S., Freund, M., Hechler, B., Gachet, C. and Jandrot-Perrus, M. (2012) "A humanized glycoprotein VI (GPVI) mouse model to assess the antithrombotic efficacies of anti-GPVI agents," *Journal of Pharmacology and Experimental Therapeutics*, 341(1), pp. 156–163. doi: 10.1124/jpet.111.189050.

Manzine, P. R., Ettcheto, M., Cano, A., Busquets, O., Marcello, E., Pelucchi, S., di Luca, M., Endres, K., Olloquequi, J., Camins, A. and Cominetti, M. R. (2019) "ADAM10 in Alzheimer's disease: Pharmacological modulation by natural compounds and its role as a peripheral marker," *Biomedicine and Pharmacotherapy*, 113, p. 108661. doi: 10.1016/j.biopha.2019.108661.

Marcello, E., Gardoni, F., di Luca, M. and Pérez-Otan, I. (2010) "An arginine stretch limits ADAM10 exit from the endoplasmic reticulum," *Journal of Biological Chemistry*, 285(14), pp. 10376–10384. doi: 10.1074/jbc.M109.055947.

Maretzky, T., Evers, A., Gall, S. le, Alabi, R. O., Speck, N., Reiss, K. and Blobel, C. P. (2015) "The cytoplasmic domain of a disintegrin and metalloproteinase 10 (ADAM10) regulates its constitutive activity but is dispensable for stimulated ADAM10-dependent shedding," *Journal of Biological Chemistry*, 290(12), pp. 7416–7425. doi: 10.1074/jbc.M114.603753.

Maretzky, T., Reiss, K., Ludwig, A., Buchholz, J., Scholz, F., Proksch, E., de Strooper, B., Hartmann, D. and Saftig, P. (2005) "ADAM10 mediates E-cadherin shedding and regulates epithelial cell-cell adhesion, migration, and β-catenin translocation," *Proceedings of the National Academy of Sciences of the United States of America*, 102(26), pp. 9182–9187. doi: 10.1073/pnas.0500918102.

Maretzky, T., Schulte, M., Ludwig, A., Rose-John, S., Blobel, C., Hartmann, D., Altevogt, P., Saftig, P. and Reiss, K. (2005) "L1 Is Sequentially Processed by Two Differently Activated Metalloproteases and Presenilin/γ-Secretase and Regulates Neural Cell Adhesion, Cell Migration, and Neurite Outgrowth," *Molecular and Cellular Biology*, 25(20), pp. 9040–9053. doi: 10.1128/mcb.25.20.9040-9053.2005.

Marioni, R. E., Harris, S. E., Zhang, Q., McRae, A. F., Hagenaars, S. P., Hill, W. D., Davies, G., Ritchie, C. W., Gale, C. R., Starr, J. M., Goate, A. M., Porteous, D. J., Yang, J.,

Evans, K. L., Deary, I. J., Wray, N. R. and Visscher, P. M. (2018) "GWAS on family history of Alzheimer's disease," *Translational Psychiatry*, 8(1). doi: 10.1038/s41398-018-0150-6.

Massberg, S., Konrad, I., Bültmann, A., Schulz, C., Münch, G., Peluso, M., Lorenz, M., Schneider, S., Besta, F., Müller, I., Hu, B., Langer, H., Kremmer, E., Rudelius, M., Heinzmann, U., Ungerer, M. and Gawaz, M. (2004) "Soluble glycoprotein VI dimer inhibits platelet adhesion and aggregation to the injured vessel wall in vivo," *The FASEB journal*, 18(2), pp. 397–399. doi: 10.1096/fj.03-0464fje.

Mathews, J. A., Gibb, D. R., Chen, B. H., Scherle, P. and Conrad, D. H. (2010) "CD23 sheddase a disintegrin and metalloproteinase 10 (ADAM10) is also required for CD23 sorting into B cell-derived exosomes," *Journal of Biological Chemistry*, 285(48), pp. 37531–37541. doi: 10.1074/jbc.M110.141556.

Matthews, A. L. (2019) *Regulation of the major platelet collagen and fibrin receptor GPVI by ADAM10 and TspanC8 tetraspanins*. Available at: https://etheses.bham.ac.uk//id/eprint/9464/.

Matthews, A. L., Koo, C. Z., Szyroka, J., Harrison, N., Kanhere, A. and Tomlinson, M. G. (2018) "Regulation of leukocytes by TspanC8 tetraspanins and the 'molecular scissor' ADAM10," *Frontiers in Immunology*, 9(JUL), p. 1451. doi: 10.3389/fimmu.2018.01451.

Matthews, A. L., Noy, P. J., Reyat, J. S. and Tomlinson, M. G. (2017) "Regulation of A disintegrin and metalloproteinase (ADAM) family sheddases ADAM10 and ADAM17: The emerging role of tetraspanins and rhomboids," *Platelets*, 28(4), pp. 333–341. doi: 10.1080/09537104.2016.1184751.

Matthews, A. L., Szyroka, J., Collier, R., Noy, P. J. and Tomlinson, M. G. (2017) "Scissor sisters: regulation of ADAM10 by the TspanC8 tetraspanins," *Biochemical Society Transactions*, 45(3), pp. 719–730. doi: 10.1042/BST20160290.

Matthews, V., Schuster, B., Schütze, S., Bussmeyer, I., Ludwig, A., Hundhausen, C., Sadowski, T., Saftig, P., Hartmann, D., Kallen, K. J. and Rose-John, S. (2003) "Cellular cholesterol depletion triggers shedding of the human interleukin-6 receptor by ADAM10 and ADAM17 (TACE)," *Journal of Biological Chemistry*, 278(40), pp. 38829–38839. doi: 10.1074/jbc.M210584200.

Maurer, S., Kopp, H. G., Salih, H. R. and Kropp, K. N. (2020) "Modulation of immune responses by platelet-derived ADAM10," *Frontiers in Immunology*, 11, p. 44. doi: 10.3389/fimmu.2020.00044.

Mayer, K., Hein-Rothweiler, R., Schüpke, S., Janisch, M., Bernlochner, I., Ndrepepa, G., Sibbing, D., Gori, T., Borst, O., Holdenrieder, S., Kupka, D., Petzold, T., Bradaric, C., Okrojek, R., Leistner, D. M., Trippel, T. D., Münzel, T., Landmesser, U., Pieske, B., Zeiher, A. M., Gawaz, M. P., Hapfelmeier, A., Laugwitz, K. L., Schunkert, H., Kastrati, A. and Massberg, S. (2021) "Efficacy and safety of Revacept, a novel lesion-directed competitive antagonist to platelet glycoprotein VI, in patients undergoing elective percutaneous coronary intervention for stable ischemic heart disease: the randomized,

double-blind, placebo-contro," *JAMA Cardiology*, 6(7), pp. 753–761. doi: 10.1001/jamacardio.2021.0475.

Mazinani, N., Strilchuk, A. W., Baylis, J. R., Hur, W. S., Jefferies, W. A. and Kastrup, C. J. (2020) "Bleeding is increased in amyloid precursor protein knockout mouse," *Research and Practice in Thrombosis and Haemostasis*, 4(5), pp. 823–828. doi: 10.1002/rth2.12375.

Mentrup, T., Theodorou, K., Cabrera-Cabrera, F., Helbig, A. O., Happ, K., Gijbels, M., Gradtke, A. C., Rabe, B., Fukumori, A., Steiner, H., Tholey, A., Fluhrer, R., Donners, M. and Schröder, B. (2019) "Atherogenic LOX-1 signaling is controlled by SPPL2-mediated intramembrane proteolysis," *Journal of Experimental Medicine*, 216(4), pp. 807–830. doi: 10.1084/jem.20171438.

Mizuno, S., Yoda, M., Shimoda, M., Tohmonda, T., Okada, Y., Toyama, Y., Takeda, S., Nakamura, M., Matsumoto, M. and Horiuchi, K. (2015) "A disintegrin and metalloprotease 10 (ADAM10) is indispensable for maintenance of the muscle satellite cell pool," *Journal of Biological Chemistry*, 290(47), pp. 28456–28464. doi: 10.1074/jbc.M115.653477.

Mohammadi, P., Castel, S. E., Brown, A. A. and Lappalainen, T. (2017) "Quantifying the regulatory effect size of cis-acting genetic variation using allelic fold change," *Genome Research*, 27(11), pp. 1872–1884. doi: 10.1101/gr.216747.116.

Montague, S. J., Andrews, R. K. and Gardiner, E. E. (2018) "Mechanisms of receptor shedding in platelets," *Blood*, 132(24), pp. 2535–2545. doi: 10.1182/blood-2018-03-742668.

Montague, S. J., Delierneux, C., Lecut, C., Layios, N., Dinsdale, R. J., Lee, C. S.-M., Poulter, N. S., Andrews, R. K., Hampson, P., Wearn, C. M., Maes, N., Bishop, J., Bamford, A., Gardiner, C., Lee, W. M., Iqbal, T., Moiemen, N., Watson, S. P., Oury, C., Harrison, P. and Gardiner, E. E. (2018) "Soluble GPVI is elevated in injured patients: shedding is mediated by fibrin activation of GPVI," *Blood Advances*, 2(3), pp. 240–251. doi: 10.1182/bloodadvances.2017011171.

Montague, S. J., Hicks, S. M., Lee, C. S. M., Coupland, L. A., Parish, C. R., Lee, W. M., Andrews, R. K. and Gardiner, E. E. (2020) "Fibrin exposure triggers αIIbβ3-independent platelet aggregate formation, ADAM10 activity and glycoprotein VI shedding in a charge-dependent manner," *Journal of Thrombosis and Haemostasis*, 18(6), pp. 1447–1458. doi: 10.1111/jth.14797.

Montoro-García, S., Schindewolf, M., Stanford, S., Larsen, O. H. and Thiele, T. (2016) "The role of platelets in venous thromboembolism," *Seminars in Thrombosis and Hemostasis*, 42(3), pp. 242–251. doi: 10.1055/s-0035-1570079.

Moretto, E., Longatti, A., Murru, L., Chamma, I., Sessa, A., Zapata, J., Hosy, E., Sainlos, M., Saint-Pol, J., Rubinstein, E., Choquet, D., Broccoli, V., Schiavo, G., Thoumine, O. and Passafaro, M. (2019) "TSPAN5 Enriched Microdomains Provide a Platform for Dendritic Spine Maturation through Neuroligin-1 Clustering," *Cell Reports*, 29(5), pp. 1130-1146.e8. doi: 10.1016/j.celrep.2019.09.051.

Moroi, M., Induruwa, I., Farndale, R. W. and Jung, S. M. (2021) "Dimers of the platelet collagen receptor glycoprotein VI bind specifically to fibrin fibers during clot formation, but not to intact fibrinogen," *Journal of Thrombosis and Haemostasis*, 19(8), pp. 2056–2067. doi: 10.1111/jth.15399.

Moroi, M., Jung, S. M., Okuma, M. and Shinmyozu, K. (1989) "A patient with platelets deficient in glycoprotein VI that lack both collagen-induced aggregation and adhesion," *Journal of Clinical Investigation*, 84(5), pp. 1440–1445. doi: 10.1172/JCI114318.

Moss, M. L., Bomar, M., Liu, Q., Sage, H., Dempsey, P., Lenhart, P. M., Gillispie, P. A., Stoeck, A., Wildeboer, D., Bartsch, J. W., Palmisano, R. and Zhou, P. (2007) "The ADAM10 prodomain is a specific inhibitor of ADAM10 proteolytic activity and inhibits cellular shedding events," *Journal of Biological Chemistry*, 282(49), pp. 35712–35721. doi: 10.1074/jbc.M703231200.

Mrozik, K. M., Blaschuk, O. W., Cheong, C. M., Zannettino, A. C. W. and Vandyke, K. (2018) "N-cadherin in cancer metastasis, its emerging role in haematological malignancies and potential as a therapeutic target in cancer," *BMC Cancer*, 18(1), p. 939. doi: 10.1186/s12885-018-4845-0.

Mumm, J. S., Schroeter, E. H., Saxena, M. T., Griesemer, A., Tian, X., Pan, D. J., Ray, W. J. and Kopan, R. (2000) "A ligand-induced extracellular cleavage regulates γ-secretase-like proteolytic activation of Notch1," *Molecular Cell*, 5(2), pp. 197–206. doi: 10.1016/S1097-2765(00)80416-5.

Muraguchi, T., Takegami, Y., Ohtsuka, T., Kitajima, S., Chandana, E. P. S., Omura, A., Miki, T., Takahashi, R., Matsumoto, N., Ludwig, A., Noda, M. and Takahashi, C. (2007) "RECK modulates Notch signaling during cortical neurogenesis by regulating ADAM10 activity," *Nature Neuroscience*, 10(7), pp. 838–845. doi: 10.1038/nn1922.

Murai, T., Maruyama, Y., Mio, K., Nishiyama, H., Suga, M. and Sato, C. (2011) "Low cholesterol triggers membrane microdomain-dependent CD44 shedding and suppresses tumor cell migration," *Journal of Biological Chemistry*, 286(3), pp. 1999–2007. doi: 10.1074/jbc.M110.184010.

Nagata, S., Suzuki, J., Segawa, K. and Fujii, T. (2016) "Exposure of phosphatidylserine on the cell surface," *Cell Death and Differentiation*, 23(6), pp. 952–961. doi: 10.1038/cdd.2016.7.

Nakamura, H., Suenaga, N., Taniwaki, K., Matsuki, H., Yonezawa, K., Fujii, M., Okada, Y. and Seiki, M. (2004) "Constitutive and induced CD44 shedding by ADAM-like proteases and membrane-type 1 matrix metalloproteinase," *Cancer Research*, 64(3), pp. 876–882. doi: 10.1158/0008-5472.CAN-03-3502.

le Naour, F., André, M., Greco, C., Billard, M., Sordat, B., Emile, J. F., Lanza, F., Boucheix, C. and Rubinstein, E. (2006) "Profiling of the tetraspanin web of human colon cancer cells," *Molecular and Cellular Proteomics*, 5(5), pp. 845–857. doi: 10.1074/mcp.M500330-MCP200.

Navarro-Hernandez, I. C., López-Ortega, O., Acevedo-Ochoa, E., Cervantes-Díaz, R., Romero-Ramírez, S., Sosa-Hernández, V. A., Meza-Sánchez, D. E., Juárez-Vega, G., Pérez-Martínez, C. A., Chávez-Munguía, B., Galván-Hernández, A., Antillón, A.,

Ortega-Blake, I., Santos-Argumedo, L., Hernández-Hernández, J. M. and Maravillas-Montero, J. L. (2020) "Tetraspanin 33 (TSPAN33) regulates endocytosis and migration of human B lymphocytes by affecting the tension of the plasma membrane," *FEBS Journal*, 287(16), pp. 3449–3471. doi: 10.1111/febs.15216.

Noris, P., Melazzini, F. and Balduini, C. L. (2016) "New roles for mean platelet volume measurement in the clinical practice?," *Platelets*, 27(7), pp. 607–612. doi: 10.1080/09537104.2016.1224828.

Noy, P. J., Yang, J., Reyat, J. S., Matthews, A. L., Charlton, A. E., Furmston, J., Rogers, D. A., Ed Rainger, G. and Tomlinson, M. G. (2016) "TspanC8 tetraspanins and a disintegrin and metalloprotease 10 (ADAM10) interact via their extracellular regions: Evidence for distinct binding mechanisms for different TspanC8 proteins," *Journal of Biological Chemistry*, 291(7), pp. 3145–3157. doi: 10.1074/jbc.M115.703058.

Ollikainen, E., Mikkelsson, J., Perola, M., Penttilä, A. and Karhunen, P. J. (2004) "Platelet membrane collagen receptor glycoprotein VI polymorphism is associated with coronary thrombosis and fatal myocardial infarction in middle-aged men," *Atherosclerosis*, 176(1), pp. 95–99. doi: 10.1016/j.atherosclerosis.2004.03.021.

Onselaer, M.-B., Hardy, A. T., Wilson, C., Sanchez, X., Babar, A. K., Miller, J. L. C., Watson, C. N., Watson, S. K., Bonna, A., Philippou, H., Herr, A. B., Mezzano, D. and As, R. (2017) "Fibrin and D-dimer bind to monomeric GPVI," *Blood Advances*, 1(19), pp. 1495–1504. doi: 10.1182/bloodadvances.2017007732.The.

Oosterheert, W., Xenak, K. T., Neviani, V., Pos, W., Doulkeridou, S., Manshande, J., Pearce, N. M., Kroon-Batenburg, L. M. J., Lutz, M., van Bergen En Henegouwen, P. M. P. and Gros, P. (2020) "Implications for tetraspanin-enriched microdomain assembly based on structures of CD9 with EWI-F," *Life Science Alliance*, 3(11), p. 2020.06.02.130047. doi: 10.26508/LSA.202000883.

Oren, R., Takahashi, S., Doss, C., Levy, R. and Levy, S. (1990) "TAPA-1, the target of an antiproliferative antibody, defines a new family of transmembrane proteins," *Molecular and Cellular Biology*, 10(8), pp. 4007–4015. doi: 10.1128/mcb.10.8.4007-4015.1990.

Padro, C. J., Shawler, T. M., Gormley, M. G. and Sanders, V. M. (2013) "Adrenergic regulation of IgE involves modulation of CD23 and ADAM10 expression on exosomes," *The Journal of Immunology*, 191(11), pp. 5383–5397. doi: 10.4049/jimmunol.1301019.

Pallini, C., Pike, J. A., O'Shea, C., Andrews, R. K., Gardiner, E. E., Watson, S. P. and Poulter, N. S. (2021) "Immobilized collagen prevents shedding and induces sustained GPVI clustering and signaling in platelets," *Platelets*, 32(1), pp. 59–73. doi: 10.1080/09537104.2020.1849607.

Palor, M., Stejskal, L., Mandal, P., Lenman, A., Alberione, M. P., Kirui, J., Moeller, R., Ebner, S., Meissner, F., Gerold, G., Shepherd, A. J. and Grove, J. (2020) "Cholesterol sensing by CD81 is important for hepatitis C virus entry," *Journal of Biological Chemistry*, 295(50), pp. 16931–16948. doi: 10.1074/jbc.RA120.014761.

Pandey, C., Misra, A., Negi, M., Kanuri, B., Chhonker, Y., Bhatta, R., Narain, V. and Dikshit, M. (2019) "Aspirin and clopidogrel non-responsiveness and its association with genetic

polymorphisms in patients with myocardial infarction," *Indian Journal of Medical Research*, 150(1), pp. 50–61. doi: 10.4103/ijmr.IJMR_782_17.

Panova-Noeva, M., Wagner, B., Nagler, M., Koeck, T., Cate, V. ten, Prochaska, J. H., Heitmeier, S., Meyer, I., Gerdes, C., Laux, V., Konstantinides, S., Spronk, H. M., Münzel, T., Lackner, K. J., Leineweber, K., Cate, H. ten and Wild, P. S. (2020) "Comprehensive platelet phenotyping supports the role of platelets in the pathogenesis of acute venous thromboembolism – results from clinical observation studies," *EBioMedicine*, 60, p. 102978. doi: 10.1016/J.EBIOM.2020.102978.

Payne, H. (2018) *Novel insights into the mechanisms of venous thrombosis*. Available at: https://etheses.bham.ac.uk//id/eprint/8172/.

Pendurthi, U. R. and Vijaya Mohan Rao, L. (2018) "Endothelial cell protein C receptor-dependent signaling," *Current Opinion in Hematology*, 25(3), pp. 219–226. doi: 10.1097/MOH.0000000000000416.

Pennington, K., Chan, T., Torres, M. and Andersen, J. (2018) "The dynamic and stress-adaptive signaling hub of 14-3-3: emerging mechanisms of regulation and context-dependent protein–protein interactions," *Oncogene*, 37(42), pp. 5587–5604. doi: 10.1038/s41388-018-0348-3.

Pérez-Martínez, C. A., Maravillas-Montero, J. L., Meza-Herrera, I., Vences-Catalán, F., Zlotnik, A. and Santos-Argumedo, L. (2017) "Tspan33 is expressed in transitional and memory B Cells, but is not responsible for high ADAM10 expression," *Scandinavian Journal of Immunology*, 86(1), pp. 23–30. doi: 10.1111/sji.12559.

Petersen, R., Lambourne, J. J., Javierre, B. M., Grassi, L., Kreuzhuber, R., Ruklisa, D., Rosa, I. M., Tomé, A. R., Elding, H., van Geffen, J. P., Jiang, T., Farrow, S., Cairns, J., Al-Subaie, A. M., Ashford, S., Attwood, A., Batista, J., Bouman, H., Burden, F., Choudry, F. A., Clarke, L., Flicek, P., Garner, S. F., Haimel, M., Kempster, C., Ladopoulos, V., Lenaerts, A. S., Materek, P. M., McKinney, H., Meacham, S., Mead, D., Nagy, M., Penkett, C. J., Rendon, A., Seyres, D., Sun, B., Tuna, S., van der Weide, M. E., Wingett, S. W., Martens, J. H., Stegle, O., Richardson, S., Vallier, L., Roberts, D. J., Freson, K., Wernisch, L., Stunnenberg, H. G., Danesh, J., Fraser, P., Soranzo, N., Butterworth, A. S., Heemskerk, J. W., Turro, E., Spivakov, M., Ouwehand, W. H., Astle, W. J., Downes, K., Kostadima, M. and Frontini, M. (2017) "Platelet function is modified by common sequence variation in megakaryocyte super enhancers," *Nature Communications*, 8(1), p. 16058. doi: 10.1038/ncomms16058.

Pike, J. A., Styles, I. B., Rappoport, J. Z. and Heath, J. K. (2017) "Quantifying receptor trafficking and colocalization with confocal microscopy," *Methods*, 115, pp. 42–54. doi: 10.1016/j.ymeth.2017.01.005.

Pirinen, M., Donnelly, P. and Spencer, C. C. A. (2013) "Efficient computation with a linear mixed model on large-scale data sets with applications to genetic studies," *Annals of Applied Statistics*, 7(1), pp. 369–390. doi: 10.1214/12-AOAS586.

Plotnikov, D., Shah, R. L., Rodrigues, J. N., Cumberland, P. M., Rahi, J. S., Hysi, P. G., Atan, D., Williams, C. and Guggenheim, J. A. (2019) "A commonly occurring genetic variant

within the NPLOC4–TSPAN10–PDE6G gene cluster is associated with the risk of strabismus," *Human Genetics*, 138(7), pp. 723–737. doi: 10.1007/s00439-019-02022-8.

Pollock, N. L., Lee, S. C., Patel, J. H., Gulamhussein, A. A. and Rothnie, A. J. (2018) "Structure and function of membrane proteins encapsulated in a polymer-bound lipid bilayer," *Biochimica et Biophysica Acta - Biomembranes*, 1860(4), pp. 809–817. doi: 10.1016/j.bbamem.2017.08.012.

Postina, R., Schroeder, A., Dewachter, I., Bohl, J., Schmitt, U., Kojro, E., Prinzen, C., Endres, K., Hiemke, C., Blessing, M., Flamez, P., Dequenne, A., Godaux, E., van Leuven, F. and Fahrenholz, F. (2004) "A disintegrin-metalloproteinase prevents amyloid plaque formation and hippocampal defects in an Alheizmer disease mouse model," *Journal of Clinical Investigation*, 113(10), pp. 1456–1464. doi: 10.1172/JCI20864.

Poulter, N. S., Pollitt, A. Y., Owen, D. M., Gardiner, E. E., Andrews, R. K., Shimizu, H., Ishikawa, D., Bihan, D., Farndale, R. W., Moroi, M., Watson, S. P. and Jung, S. M. (2017) "Clustering of glycoprotein VI (GPVI) dimers upon adhesion to collagen as a mechanism to regulate GPVI signaling in platelets," *Journal of Thrombosis and Haemostasis*, 15(3), pp. 549–564. doi: 10.1111/jth.13613.

Powers, M. E., Kim, H. K., Wang, Y. and Wardenburg, J. B. (2012) "ADAM10 mediates vascular injury induced by staphylococcus aureus α-hemolysin," *Journal of Infectious Diseases*, 206(3), pp. 352–356. doi: 10.1093/infdis/jis192.

Prox, J., Willenbrock, M., Weber, S., Lehmann, T., Schmidt-Arras, D., Schwanbeck, R., Saftig, P. and Schwake, M. (2012) "Tetraspanin15 regulates cellular trafficking and activity of the ectodomain sheddase ADAM10," *Cellular and Molecular Life Sciences*, 69(17), pp. 2919–2932. doi: 10.1007/s00018-012-0960-2.

Pruessmeyer, J. and Ludwig, A. (2009) "The good, the bad and the ugly substrates for ADAM10 and ADAM17 in brain pathology, inflammation and cancer," *Seminars in Cell and Developmental Biology*, 20(2), pp. 164–174. doi: 10.1016/j.semcdb.2008.09.005.

Qu, D., Wang, Y., Esmon, N. L. and Esmon, C. T. (2007) "Regulated endothelial protein C receptor shedding is mediated by tumor necrosis factor-α converting enzyme/ADAM17," *Journal of Thrombosis and Haemostasis*, 5(2), pp. 395–402. doi: 10.1111/j.1538-7836.2007.02347.x.

Qu, D., Wang, Y., Song, Y., Esmon, N. L. and Esmon, C. T. (2006) "The Ser219->Gly dimorphism of the endothelial protein C receptor contributes to the higher soluble protein levels observed in individuals with the A3 haplotype," *Journal of Thrombosis and Haemostasis*, 4(1), pp. 229–235. doi: 10.1111/j.1538-7836.2005.01676.x.

Radice, G. L. (2013) "N-Cadherin-mediated adhesion and signaling from development to disease: Lessons from mice," *Progress in Molecular Biology and Translational Science*, 116, pp. 263–289. doi: 10.1016/B978-0-12-394311-8.00012-1.

Rajesh, S., Sridhar, P., Tews, B. A., Fénéant, L., Cocquerel, L., Ward, D. G., Berditchevski, F. and Overduin, M. (2012) "Structural basis of ligand interactions of the large extracellular domain of tetraspanin CD81," *Journal of Virology*, 86(18), pp. 9606–9616. doi: 10.1128/jvi.00559-12.

Ran, F. A., Hsu, P. D., Wright, J., Agarwala, V., Scott, D. A. and Zhang, F. (2013) "Genome engineering using the CRISPR-Cas9 system," *Nature*, 8(11), pp. 2281–2308.

Rao, L. V. M., Esmon, C. T. and Pendurthi, U. R. (2014) "Endothelial cell protein C receptor: A multiliganded and multifunctional receptor," *Blood*, pp. 1553–1562. doi: 10.1182/blood-2014-05-578328.

Raucci, A., Cugusi, S., Antonelli, A., Barabino, S. M., Monti, L., Bierhaus, A., Reiss, K., Saftig, P. and Bianchi, M. E. (2008) "A soluble form of the receptor for advanced glycation endproducts (RAGE) is produced by proteolytic cleavage of the membrane-bound form by the sheddase a disintegrin and metalloprotease 10 (ADAM10)," *The FASEB Journal*, 22(10), pp. 3716–3727. doi: 10.1096/fj.08-109033.

Rausch, T., Fritz, M. H. Y., Untergasser, A. and Benes, V. (2020) "Tracy: Basecalling, alignment, assembly and deconvolution of sanger chromatogram trace files," *BMC Genomics*, 21(1), pp. 1–9. doi: 10.1186/s12864-020-6635-8.

Reiss, K., Maretzky, T., Ludwig, A., Tousseyn, T., de Strooper, B., Hartmann, D. and Saftig, P. (2005) "ADAM10 cleavage of N-cadherin and regulation of cell-cell adhesion and β-catenin nuclear signalling," *EMBO Journal*, 24(4), pp. 742–752. doi: 10.1038/sj.emboj.7600548.

Reyat, J. S. (2016) *Regulation of lymphocyte transmigration by ADAM10 and TspanC8 tetraspanins*. Available at: https://etheses.bham.ac.uk//id/eprint/6650/.

Reyat, J. S., Chimen, M., Noy, P. J., Szyroka, J., Rainger, G. E. and Tomlinson, M. G. (2017) "ADAM10-Interacting tetraspanins Tspan5 and Tspan17 regulate VE-Cadherin expression and promote T Lymphocyte transmigration," *The Journal of Immunology*, 199(2), pp. 666–676. doi: 10.4049/jimmunol.1600713.

Riethmueller, S., Ehlers, J. C., Lokau, J., Düsterhöft, S., Knittler, K., Dombrowsky, G., Grötzinger, J., Rabe, B., Rose-John, S. and Garbers, C. (2016) "Cleavage Site Localization Differentially Controls Interleukin-6 Receptor Proteolysis by ADAM10 and ADAM17," *Scientific Reports*, 6(1), p. 25550. doi: 10.1038/srep25550.

Roy, D., Ramasamy, R. and Schmidt, A. M. (2021) "Journey to a Receptor for Advanced Glycation End Products Connection in Severe Acute Respiratory Syndrome Coronavirus 2 Infection with Stops along the Way in the Lung, Heart, Blood Vessels, and Adipose Tissue," *Arteriosclerosis, Thrombosis, and Vascular Biology*. Lippincott Williams & Wilkins Hagerstown, MD, pp. 614–627. doi: 10.1161/ATVBAHA.120.315527.

Rubinstein, E. (2011) "The complexity of tetraspanins," *Biochemical Society Transactions*, 39(2), pp. 501–505. doi: 10.1042/BST0390501.

Rubinstein, E., Charrin, S. and Tomlinson, M. G. (2013) "Organisation of the tetraspanin web," in Berditchevski, F. and Rubinstein, E. (eds) *Tetraspanins*. 1st edn. Springer, Dordrecht, pp. 47–90. doi: 10.1007/978-94-007-6070-7_3.

Ruiz-García, A., López-López, S., García-Ramírez, J. J., Baladrón, V., Ruiz-Hidalgo, M. J., López-Sanz, L., Ballesteros, Á., Laborda, J., Monsalve, E. M. and Díaz-Guerra, M. J. M. (2016) "The tetraspanin TSPAN33 controls TLR-triggered macrophage activation

through modulation of NOTCH signaling," *The Journal of Immunology*, 197(8), pp. 3371–3381. doi: 10.4049/jimmunol.1600421.

Sachs, N., Claessen, N., Aten, J., Kreft, M., Teske, G. J. D., Koeman, A., Zuurbier, C. J., Janssen, H. and Sonnenberg, A. (2012) "Blood pressure influences end-stage renal disease of Cd151 knockout mice," *Journal of Clinical Investigation*, 122(1), pp. 348–358. doi: 10.1172/JCI58878.

Sachs, N., Kreft, M., van den Bergh Weerman, M. A., Beynon, A. J., Peters, T. A., Weening, J. J. and Sonnenberg, A. (2006) "Kidney failure in mice lacking the tetraspanin CD151," *Journal of Cell Biology*, 175(1), pp. 33–39. doi: 10.1083/jcb.200603073.

Sahin, U., Weskamp, G., Kelly, K., Zhou, H. M., Higashiyama, S., Peschon, J., Hartmann, D., Saftig, P. and Blobel, C. P. (2004) "Distinct roles for ADAM10 and ADAM17 in ectodomain shedding of six EGFR ligands," *Journal of Cell Biology*, 164(5), pp. 769–779. doi: 10.1083/jcb.200307137.

Saint-Pol, J., Billard, M., Dornier, E., Eschenbrenner, E., Danglot, L., Boucheix, C., Charrin, S. and Rubinstein, E. (2017) "New insights into the tetraspanin Tspan5 using novel monoclonal antibodies," *Journal of Biological Chemistry*, 292(23), pp. 9551–9566. doi: 10.1074/jbc.M116.765669.

Saint-Pol, J., Eschenbrenner, E., Dornier, E., Boucheix, C., Charrin, S. and Rubinstein, E. (2017) "Regulation of the trafficking and the function of the metalloprotease ADAM10 by tetraspanins," *Biochemical Society Transactions*, 45(4), pp. 937–944. doi: 10.1042/BST20160296.

Santosa, M. M., Low, B. S. J., Pek, N. M. Q. and Teo, A. K. K. (2016) "Knowledge gaps in rodent pancreas biology: Taking human pluripotent stem cell-derived pancreatic beta cells into our own hands," *Frontiers in Endocrinology*, 6, p. 194. doi: 10.3389/fendo.2015.00194.

Saposnik, B., Reny, J. L., Gaussem, P., Emmerich, J., Aiach, M. and Gandrille, S. (2004) "A haplotype of the EPCR gene is associated with increased plasma levels of sEPCR and is a candidate risk factor for thrombosis," *Blood*, 103(4), pp. 1311–1318. doi: 10.1182/blood-2003-07-2520.

Scharfenberg, F., Helbig, A., Sammel, M., Benzel, J., Schlomann, U., Peters, F., Wichert, R., Bettendorff, M., Schmidt-Arras, D., Rose-John, S., Moali, C., Lichtenthaler, S. F., Pietrzik, C. U., Bartsch, J. W., Tholey, A. and Becker-Pauly, C. (2020) "Degradome of soluble ADAM10 and ADAM17 metalloproteases," *Cellular and Molecular Life Sciences*, 77(2), pp. 331–350. doi: 10.1007/s00018-019-03184-4.

Schindelin, J., Arganda-Carreras, I., Frise, E., Kaynig, V., Longair, M., Pietzsch, T., Preibisch, S., Rueden, C., Saalfeld, S., Schmid, B., Tinevez, J. Y., White, D. J., Hartenstein, V., Eliceiri, K., Tomancak, P. and Cardona, A. (2012) "Fiji: An open-source platform for biological-image analysis," *Nature Methods*, 9(7), pp. 676–682. doi: 10.1038/nmeth.2019.

Schmaier, A. H. (2017) "The amyloid beta-precursor protein—The unappreciated cerebral anticoagulant," *Thrombosis Research*, 155, pp. 149–151. doi: 10.1016/j.thromres.2017.05.037.

Schönberger, T., Ziegler, M., Borst, O., Konrad, I., Nieswandt, B., Massberg, S., Ochmann, C., Jürgens, T., Seizer, P., Langer, H., Münch, G., Ungerer, M., Preissner, K. T., Elvers, M. and Gawaz, M. (2012) "The dimeric platelet collagen receptor GPVI-Fc reduces platelet adhesion to activated endothelium and preserves myocardial function after transient ischemia in mice," *American Journal of Physiology - Cell Physiology*, 303(7), pp. 757–766. doi: 10.1152/ajpcell.00060.2012.

Schulz, B., Pruessmeyer, J., Maretzky, T., Ludwig, A., Blobel, C. P., Saftig, P. and Reiss, K. (2008) "ADAM10 regulates endothelial permeability and T-cell transmigration by proteolysis of vascular endothelial cadherin," *Circulation Research*, 102(10), pp. 1192–1201. doi: 10.1161/CIRCRESAHA.107.169805.

Schwartzentruber, J., Cooper, S., Liu, J. Z., Barrio-Hernandez, I., Bello, E., Kumasaka, N., Young, A. M. H., Franklin, R. J. M., Johnson, T., Estrada, K., Gaffney, D. J., Beltrao, P. and Bassett, A. (2021) "Genome-wide meta-analysis, fine-mapping and integrative prioritization implicate new Alzheimer's disease risk genes," *Nature Genetics*, 53(3), pp. 392–402. doi: 10.1038/s41588-020-00776-w.

Seegar, T. C. M., Killingsworth, L. B., Saha, N., Meyer, P. A., Patra, D., Zimmerman, B., Janes, P. W., Rubinstein, E., Nikolov, D. B., Skiniotis, G., Kruse, A. C. and Blacklow, S. C. (2017) "Structural Basis for regulated proteolysis by the α-Secretase ADAM10," *Cell*, 171(7), pp. 1638-1648.e7. doi: 10.1016/j.cell.2017.11.014.

Seifert, A., Düsterhöft, S., Wozniak, J., Koo, C. Z., Tomlinson, M. G., Nuti, E., Rossello, A., Cuffaro, D., Yildiz, D. and Ludwig, A. (2021) "The metalloproteinase ADAM10 requires its activity to sustain surface expression," *Cellular and Molecular Life Sciences*, 78(2), pp. 715–732. doi: 10.1007/s00018-020-03507-w.

Seipold, L., Altmeppen, H., Koudelka, T., Tholey, A., Kasparek, P., Sedlacek, R., Schweizer, M., Bär, J., Mikhaylova, M., Glatzel, M. and Saftig, P. (2018) "In vivo regulation of the A disintegrin and metalloproteinase 10 (ADAM10) by the tetraspanin 15," *Cellular and Molecular Life Sciences*, 75(17), pp. 3251–3267. doi: 10.1007/s00018-018-2791-2.

Seipold, L., Damme, M., Prox, J., Rabe, B., Kasparek, P., Sedlacek, R., Altmeppen, H., Willem, M., Boland, B., Glatzel, M. and Saftig, P. (2017) "Tetraspanin 3: A central endocytic membrane component regulating the expression of ADAM10, presenilin and the amyloid precursor protein," *Biochimica et Biophysica Acta - Molecular Cell Research*, 1864(1), pp. 217–230. doi: 10.1016/j.bbamcr.2016.11.003.

Servier Laboratories (2020) *SMART Servier Medical Art*. Available at: https://smart.servier.com/ (Accessed: August 31, 2021).

Shah, J., Rouaud, F., Guerrera, D., Vasileva, E., Popov, L. M., Kelley, W. L., Rubinstein, E., Carette, J. E., Amieva, M. R. and Citi, S. (2018) "A dock-and-lock mechanism clusters ADAM10 at cell-cell junctions to promote α-toxin cytotoxicity," *Cell Reports*, 25(8), pp. 2132-2147.e7. doi: 10.1016/j.celrep.2018.10.088.

Shah, R. L. and Guggenheim, J. A. (2018) "Genome-wide association studies for corneal and refractive astigmatism in UK Biobank demonstrate a shared role for myopia susceptibility loci," *Human Genetics*, 137(11–12), pp. 881–896. doi: 10.1007/s00439-018-1942-8.

Shapiro, V. S., Mollenauer, M. N., Greene, W. C. and Weiss, A. (1996) "c-Rel regulation of IL-2 gene expression may be mediated through activation of AP-1," *Journal of Experimental Medicine*, 184(5), pp. 1663–1669. doi: 10.1084/jem.184.5.1663.

Sherry, S. T., Ward, M. and Sirotkin, K. (1999) "dbSNP - database for single nucleotide polymorphisms and other classes of minor genetic variation," *Genome Research*, 9(8), pp. 677–679. doi: 10.1101/gr.9.8.677.

Shirakabe, K., Omura, T., Shibagaki, Y., Mihara, E., Homma, K., Kato, Y., Yoshimura, A., Murakami, Y., Takagi, J., Hattori, S. and Ogawa, Y. (2017) "Mechanistic insights into ectodomain shedding: Susceptibility of CADM1 adhesion molecule is determined by alternative splicing and O-glycosylation," *Scientific Reports*, 7(1), pp. 1–12. doi: 10.1038/srep46174.

Sidahmed-Adrar, N., Ottavi, J. F., Benzoubir, N., Ait Saadi, T., Bou Saleh, M., Mauduit, P., Guettier, C., Desterke, C. and le Naour, F. (2019) "Tspan15 is a new stemness-related marker in hepatocellular carcinoma," *Proteomics*, 19(21–22), p. 1900025. doi: 10.1002/pmic.201900025.

Silva, A. M., Lázaro-Ibáñez, E., Gunnarsson, A., Dhande, A., Daaboul, G., Peacock, B., Osteikoetxea, X., Salmond, N., Friis, K. P., Shatnyeva, O. and Dekker, N. (2021) "Quantification of protein cargo loading into engineered extracellular vesicles at single-vesicle and single-molecule resolution," *Journal of Extracellular Vesicles*, 10(10), p. e12130. doi: 10.1002/jev2.12130.

Silvie, O., Charrin, S., Billard, M., Franetich, J. F., Clark, K. L., van Gemert, G. J., Sauerwein, R. W., Dautry, F., Boucheix, C., Mazier, D. and Rubinstein, E. (2006) "Cholesterol contributes to the organization of tetraspanin-enriched microdomains and to CD81-dependent infection by malaria sporozoites," *Journal of Cell Science*, 119(10), pp. 1992–2002. doi: 10.1242/jcs.02911.

Siney, E. J., Holden, A., Casselden, E., Bulstrode, H., Thomas, G. J. and Willaime-Morawek, S. (2017) "Metalloproteinases ADAM10 and ADAM17 Mediate Migration and Differentiation in Glioblastoma Sphere-Forming Cells," *Molecular Neurobiology*, 54(5), pp. 3893–3905. doi: 10.1007/s12035-016-0053-6.

Skille, H., Paulsen, B., Hveem, K., Gabrielsen, M. E., Brumpton, B., Hindberg, K., Gran, O. v., Rosendaal, F. R., Brækkan, S. K. and Hansen, J. B. (2020) "Genetic variation of platelet glycoprotein VI and the risk of venous thromboembolism," *Haematologica*, 105(7), pp. E359–E360. doi: 10.3324/haematol.2019.231225.

Slater, A., Di, Y., Clark, J. C., Jooss, N. J., Martin, E. M., Alenazy, F., Thomas, M. R., Ariëns, R. A. S., Herr, A. B., Poulter, N. S., Emsley, J. and Watson, S. P. (2021) "Structural characterization of a novel GPVI-nanobody complex reveals a biologically active domain-swapped GPVI dimer," *Blood*, 137(24), pp. 3443–3453. doi: 10.1182/blood.2020009440.

Slater, A., Perrella, G., Onselaer, M.-B., Martin, E. M., Gauer, J. S., Xu, R.-G., Heemskerk, J. W., Ariëns, R. A. S. and Watson, S. P. (2018) "Does fibrin(ogen) bind to monomeric or dimeric GPVI, or not at all?," *Platelets*, pp. 1–9. doi: 10.1080/09537104.2018.1508649.

Smethurst, P. A., Joutsi-Korhonen, L., O'Connor, M. N., Wilson, E., Jennings, N. S., Garner, S. F., Zhang, Y., Knight, C. G., Dafforn, T. R., Buckle, A., IJsseldijk, M. J. W., de Groot, P. G., Watkins, N. A., Farndale, R. W. and Ouwehand, W. H. (2004) "Identification of the primary collagen-binding surface on human glycoprotein VI by site-directed mutagenesis and by a blocking phage antibody," *Blood*, 103(3), pp. 903–911. doi: 10.1182/blood-2003-01-0308.

Smith, T. M., Tharakan, A. and Martin, R. K. (2020) "Targeting ADAM10 in cancer and autoimmunity," *Frontiers in Immunology*, 11, p. 499. doi: 10.3389/fimmu.2020.00499.

Sogorb-Esteve, A., García-Ayllón, M. S., Gobom, J., Alom, J., Zetterberg, H., Blennow, K. and Sáez-Valero, J. (2018) "Levels of ADAM10 are reduced in Alzheimer's disease CSF," *Journal of Neuroinflammation*, 15(1), pp. 1–9. doi: 10.1186/s12974-018-1255-9.

Sokol, J., Skerenova, M., Biringer, K., Simurda, T., Kubisz, P. and Stasko, J. (2018) "Glycoprotein VI gene variants affect pregnancy loss in patients with platelet hyperaggregability," *Clinical and Applied Thrombosis/Hemostasis*, 24(9_suppl), pp. 202S-208S. doi: 10.1177/1076029618802358.

Sorci, G., Riuzzi, F., Giambanco, I. and Donato, R. (2013) "RAGE in tissue homeostasis, repair and regeneration," *Biochimica et Biophysica Acta - Molecular Cell Research*. Elsevier, pp. 101–109. doi: 10.1016/j.bbamcr.2012.10.021.

Spracklen, C. N., Horikoshi, M., Kim, Y. J., Lin, K., Bragg, F., Moon, S., Suzuki, K., Tam, C. H. T., Tabara, Y., Kwak, S. H., Takeuchi, F., Long, J., Lim, V. J. Y., Chai, J. F., Chen, C. H., Nakatochi, M., Yao, J., Choi, H. S., Iyengar, A. K., Perrin, H. J., Brotman, S. M., van de Bunt, M., Gloyn, A. L., Below, J. E., Boehnke, M., Bowden, D. W., Chambers, J. C., Mahajan, A., McCarthy, M. I., Ng, M. C. Y., Petty, L. E., Zhang, W., Morris, A. P., Adair, L. S., Akiyama, M., Bian, Z., Chan, J. C. N., Chang, L. C., Chee, M. L., Chen, Y. D. I., Chen, Y. T., Chen, Z., Chuang, L. M., Du, S., Gordon-Larsen, P., Gross, M., Guo, X., Guo, Y., Han, S., Howard, A. G., Huang, W., Hung, Y. J., Hwang, M. Y., Hwu, C. M., Ichihara, S., Isono, M., Jang, H. M., Jiang, G., Jonas, J. B., Kamatani, Y., Katsuya, T., Kawaguchi, T., Khor, C. C., Kohara, K., Lee, M. S., Lee, N. R., Li, L., Liu, J., Luk, A. O., Lv, J., Okada, Y., Pereira, M. A., Sabanayagam, C., Shi, J., Shin, D. M., So, W. Y., Takahashi, A., Tomlinson, B., Tsai, F. J., van Dam, R. M., Xiang, Y. B., Yamamoto, K., Yamauchi, T., Yoon, K., Yu, C., Yuan, J. M., Zhang, L., Zheng, W., Igase, M., Cho, Y. S., Rotter, J. I., Wang, Y. X., Sheu, W. H. H., Yokota, M., Wu, J. Y., Cheng, C. Y., Wong, T. Y., Shu, X. O., Kato, N., Park, K. S., Tai, E. S., Matsuda, F., Koh, W. P., Ma, R. C. W., Maeda, S., Millwood, I. Y., Lee, J., Kadowaki, T., Walters, R. G., Kim, B. J., Mohlke, K. L. and Sim, X. (2020) "Identification of type 2 diabetes loci in 433,540 East Asian individuals," *Nature*, 582(7811), pp. 240–245. doi: 10.1038/s41586-020-2263-3.

Stack, J. R., Madigan, A., Helbert, L., Dunne, E., Gardiner, E. E., Andrews, R. K., Finan, R., Smyth, E., Kenny, D. and McCarthy, G. M. (2017) "Soluble glycoprotein VI, a specific marker of platelet activation is increased in the plasma of subjects with seropositive rheumatoid arthritis," *PLoS ONE*, 12(11). doi: 10.1371/journal.pone.0188027.

Stipp, C. S., Kolesnikova, T. v. and Hemler, M. E. (2003) "Functional domains in tetraspanin proteins," *Trends in Biochemical Sciences*, 28(2), pp. 106–112. doi: 10.1016/S0968-0004(02)00014-2.

Stoeck, A., Keller, S., Riedle, S., Sanderson, M. P., Runz, S., le Naour, F., Gutwein, P., Ludwig, A., Rubinstein, E. and Altevogt, P. (2006) "A role for exosomes in the constitutive and stimulus-induced ectodomain cleavage of L1 and CD44," *Biochemical Journal*, 393(3), pp. 609–618. doi: 10.1042/BJ20051013.

Sugiyama, T., Okuma, M., Ushikubi, F., Sensaki, S., Kanaji, K. and Uchino, H. (1987) "A novel platelet aggregating factor found in a patient with defective collagen-induced platelet aggregation and autoimmune thrombocytopenia," *Blood*, 69(6), pp. 1712–1720. doi: 10.1182/blood.v69.6.1712.1712.

Suh, J., Choi, S.H., Romano, D.M., Gannon, M.A., Lesinski, A.N., Kim, D.Y. and Tanzi, R.E. (2013) "ADAM10 missense mutations potentiate β-amyloid accumulation by impairing prodomain chaperone function," *Neuron*, 80(2), pp. 385–401. doi:10.1016/j.neuron.2013.08.035.

Sungkaworn, T., Jobin, M. L., Burnecki, K., Weron, A., Lohse, M. J. and Calebiro, D. (2017) "Single-molecule imaging reveals receptor-G protein interactions at cell surface hot spots," *Nature*, 550(7677), pp. 543–547. doi: 10.1038/nature24264.

Sunnarborg, S. W., Leann Hinkle, C., Stevenson, M., Russell, W. E., Raska, C. S., Peschon, J. J., Castner, B. J., Gerhart, M. J., Paxton, R. J., Black, R. A. and Lee, D. C. (2002) "Tumor necrosis factor-α converting enzyme (TACE) regulates epidermal growth factor receptor ligand availability," *Journal of Biological Chemistry*, 277(15), pp. 12838–12845. doi: 10.1074/jbc.M112050200.

Susa, K. J., Rawson, S., Kruse, A. C. and Blacklow, S. C. (2021) "Cryo-EM structure of the B cell co-receptor CD19 bound to the tetraspanin CD81," *Science*, 371(6526), pp. 300–305. doi: 10.1126/science.abd9836.

Suzuki-Inoue, K., Tulasne, D., Shen, Y., Bori-Sanz, T., Inoue, O., Jung, S. M., Moroi, M., Andrews, R. K., Berndt, M. C. and Watson, S. P. (2002) "Association of Fyn and Lyn with the proline-rich domain of glycoprotein VI regulates intracellular signaling," *Journal of Biological Chemistry*, 277(24), pp. 21561–21566. doi: 10.1074/jbc.M201012200.

Szyroka, J. (2019) *Regulation of the "molecular scissor" ADAM10 by tetraspanin Tspan15*. Available at: https://etheses.bham.ac.uk/id/eprint/9182/ (Accessed: February 17, 2020).

Takagi, S., Iwai, N., Baba, S., Mannami, T., Ono, K., Tanaka, C., Miyata, T., Miyazaki, S., Nonogi, H. and Goto, Y. (2002) "A GPVI polymorphism is a risk factor for myocardial infarction in Japanese," *Atherosclerosis*, 165(2), pp. 397–398. doi: 10.1016/S0021-9150(02)00241-1.

Takahashi, M., Yamashita, A., Moriguchi-Goto, S., Marutsuka, K., Sato, Y., Yamamoto, H., Koshimoto, C. and Asada, Y. (2009) "Critical role of von willebrand factor and platelet interaction in venous thromboembolism," *Histology and Histopathology*, 24(11), pp. 1391–1398. doi: 10.14670/HH-24.1391.

Tang, Z., Kang, B., Li, C., Chen, T. and Zhang, Z. (2019) "GEPIA2: an enhanced web server for large-scale expression profiling and interactive analysis," *Nucleic Acids Research*, 47(W1), pp. W556–W560. doi: 10.1093/nar/gkz430.

Tarrant, J. M., Robb, L., van Spriel, A. B. and Wright, M. D. (2003) "Tetraspanins: Molecular organisers of the leukocyte surface," *Trends in Immunology*, 24(11), pp. 610–617. doi: 10.1016/j.it.2003.09.011.

van Tetering, G., van Diest, P., Verlaan, I., van der Wall, E., Kopan, R. and Vooijs, M. (2009) "Metalloprotease ADAM10 is required for Notch1 site 2 cleavage," *Journal of Biological Chemistry*, 284(45), pp. 31018–31027. doi: 10.1074/jbc.M109.006775.

van Wart, H.E. and Birkedal-Hansent, H. (1990) "The cysteine switch: A principle of regulation of metalloproteinase activity with potential applicability to the entire matrix metalloproteinase gene family (collagenase/gelatinase/stromelysin/zinc enzyme)," *Proc. Natl. Acad. Sci. USA*, 87, pp. 5578–5582.

Tien, W. S., Chen, J. H. and Wu, K. P. (2017) "SheddomeDB: The ectodomain shedding database for membrane-bound shed markers," *BMC Bioinformatics*, 18(3), pp. 31–48. doi: 10.1186/s12859-017-1465-7.

Tomlinson, M. G. (2009) "Platelet tetraspanins: Small but interesting," *Journal of Thrombosis and Haemostasis*, 7(12), pp. 2070–2073. doi: 10.1111/j.1538-7836.2009.03613.x.

Tomlinson, M. G., Calaminus, S. D., Berlanga, O., Auger, J. M., Bori-Sanz, T., Meyaard, L. and Watson, S. P. (2007) "Collagen promotes sustained glycoprotein VI signaling in platelets and cell lines," *Journal of Thrombosis and Haemostasis*, 5(11), pp. 2274–2283. doi: 10.1111/j.1538-7836.2007.02746.x.

Tosetti, F., Venè, R., Camodeca, C., Nuti, E., Rossello, A., D'Arrigo, C., Galante, D., Ferrari, N., Poggi, A. and Zocchi, M. R. (2018) "Specific ADAM10 inhibitors localize in exosome-like vesicles released by Hodgkin lymphoma and stromal cells and prevent sheddase activity carried to bystander cells," *OncoImmunology*, 7(5). doi: 10.1080/2162402X.2017.1421889.

Tousseyn, T., Thathiah, A., Jorissen, E., Raemaekers, T., Konietzko, U., Reiss, K., Maes, E., Snellinx, A., Serneels, L., Nyabi, O., Annaert, W., Saftig, P., Hartmann, D. and de Strooper, B. (2009) "ADAM10, the rate-limiting protease of regulated intramembrane proteolysis of notch and other proteins, is processed by ADAMS-9, ADAMS-15, and the γ-secretase," *Journal of Biological Chemistry*, 284(17), pp. 11738–11747. doi: 10.1074/jbc.M805894200.

Trégouët, D. A., Heath, S., Saut, N., Biron-Andreani, C., Schved, J. F., Pernod, G., Galan, P., Drouet, L., Zelenika, D., Juhan-Vague, I., Alessi, M. C., Tiret, L., Lathrop, M., Emmerich, J. and Morange, P. E. (2009) "Common susceptibility alleles are unlikely to contribute as strongly as the FV and ABO loci to VTE risk: Results from aGWAS approach," *Blood*, 113(21), pp. 5298–5303. doi: 10.1182/blood-2008-11-190389.

Trifiro, E., Williams, S. A., Cheli, Y., Furihata, K., Pulcinelli, F. M., Nugent, D. J. and Kunicki, T. J. (2009) "The low-frequency isoform of platelet glycoprotein VIb attenuates ligand-mediated signal transduction but not receptor expression or ligand binding," *Blood*, 114(9), pp. 1893–1899. doi: 10.1182/blood-2009-03-209510.

Tsai, Y. H., Vandussen, K. L., Sawey, E. T., Wade, A. W., Kasper, C., Rakshit, S., Bhatt, R. G., Stoeck, A., Maillard, I., Crawford, H. C., Samuelson, L. C. and Dempsey, P. J. (2014) "ADAM10 regulates notch function in intestinal stem cells of mice," *Gastroenterology*, 147(4), pp. 822-834.e13. doi: 10.1053/j.gastro.2014.07.003.

Tsuji, M., Ezumi, Y., Arai, M. and Takayama, H. (1997) "A novel association of Fc receptor γ-chain with glycoprotein VI and their co-expression as a collagen receptor in human platelets," *Journal of Biological Chemistry*, 272(38), pp. 23528–23531. doi: 10.1074/jbc.272.38.23528.

Tucher, J., Linke, D., Koudelka, T., Cassidy, L., Tredup, C., Wichert, R., Pietrzik, C., Becker-Pauly, C. and Tholey, A. (2014) "LC-MS based cleavage site profiling of the proteases ADAM10 and ADAM17 using proteome-derived peptide libraries," *Journal of Proteome Research*, 13(4), pp. 2205–2214. doi: 10.1021/pr401135u.

Tüshaus, J., Müller, S. A., Kataka, E. S., Zaucha, J., Sebastian Monasor, L., Su, M., Güner, G., Jocher, G., Tahirovic, S., Frishman, D., Simons, M. and Lichtenthaler, S. F. (2020) "An optimized quantitative proteomics method establishes the cell type-resolved mouse brain secretome," *The EMBO Journal*, 39(20). doi: 10.15252/embj.2020105693.

Uemura, K., Kihara, T., Kuzuya, A., Okawa, K., Nishimoto, T., Ninomiya, H., Sugimoto, H., Kinoshita, A. and Shimohama, S. (2006) "Characterization of sequential N-cadherin cleavage by ADAM10 and PS1," *Neuroscience Letters*, 402(3), pp. 278–283. doi: 10.1016/j.neulet.2006.04.018.

Uhlén, M., Fagerberg, L., Hallström, B. M., Lindskog, C., Oksvold, P., Mardinoglu, A., Sivertsson, Å., Kampf, C., Sjöstedt, E., Asplund, A., Olsson, I. M., Edlund, K., Lundberg, E., Navani, S., Szigyarto, C. A. K., Odeberg, J., Djureinovic, D., Takanen, J. O., Hober, S., Alm, T., Edqvist, P. H., Berling, H., Tegel, H., Mulder, J., Rockberg, J., Nilsson, P., Schwenk, J. M., Hamsten, M., von Feilitzen, K., Forsberg, M., Persson, L., Johansson, F., Zwahlen, M., von Heijne, G., Nielsen, J. and Pontén, F. (2015) "Tissue-based map of the human proteome," *Science*, 347(6220). doi: 10.1126/science.1260419.

Umeda, R., Satouh, Y., Takemoto, M., Nakada-Nakura, Y., Liu, K., Yokoyama, T., Shirouzu, M., Iwata, S., Nomura, N., Sato, K., Ikawa, M., Nishizawa, T. and Nureki, O. (2020) "Structural insights into tetraspanin CD9 function," *Nature Communications*, 11(1). doi: 10.1038/s41467-020-15459-7.

US National Library of Medicine (2020) *INCB7839 in Treating Children With Recurrent/Progressive High-Grade Gliomas*. Available at: https://clinicaltrials.gov/ct2/show/NCT04295759 (Accessed: August 27, 2021).

US National Library of Medicine (2021a) *ACT017 (glenzocimab) clinical trials*. Available at: https://clinicaltrials.gov/ct2/results?term=act017 (Accessed: September 1, 2021).

US National Library of Medicine (2021b) *Revacept in Symptomatic Carotid Stenosis*. Available at: https://www.clinicaltrials.gov/ct2/show/results/NCT01645306 (Accessed: September 1, 2021).

Vanatabe, I. P., Peron, R., Grigoli, M. M., Pelucchi, S., de Cesare, G., Magalhães, T., Manzine, P. R., Balthazar, M. L. F., di Luca, M., Marcello, E. and Cominetti, M. R. (2021) "ADAM10 plasma and CSF levels are increased in mild Alzheimer's disease,"

International Journal of Molecular Sciences, 22(5), pp. 1–13. doi: 10.3390/ijms22052416.

Venkatesh, H. S., Johung, T. B., Caretti, V., Noll, A., Tang, Y., Nagaraja, S., Gibson, E. M., Mount, C. W., Polepalli, J., Mitra, S. S., Woo, P. J., Malenka, R. C., Vogel, H., Bredel, M., Mallick, P. and Monje, M. (2015) "Neuronal activity promotes glioma growth through neuroligin-3 secretion," *Cell*, 161(4), pp. 803–816. doi: 10.1016/j.cell.2015.04.012.

Voors-Pette, C., Lebozec, K., Dogterom, P., Jullien, L., Billiald, P., Ferlan, P., Renaud, L., Favre-Bulle, O., Avenard, G., Machacek, M., Plétan, Y. and Jandrot-Perrus, M. (2019) "Safety and Tolerability, Pharmacokinetics, and Pharmacodynamics of ACT017, an Antiplatelet GPVI (Glycoprotein VI) Fab: First-in-Human Healthy Volunteer Trial," *Arteriosclerosis, Thrombosis, and Vascular Biology*, 39(5), pp. 956–964. doi: 10.1161/ATVBAHA.118.312314.

Vujkovic, M., Keaton, J. M., Lynch, J. A., Miller, D. R., Zhou, J., Tcheandjieu, C., Huffman, J. E., Assimes, T. L., Lorenz, K., Zhu, X., Hilliard, A. T., Judy, R. L., Huang, J., Lee, K. M., Klarin, D., Pyarajan, S., Danesh, J., Melander, O., Rasheed, A., Mallick, N. H., Hameed, S., Qureshi, I. H., Afzal, M. N., Malik, U., Jalal, A., Abbas, S., Sheng, X., Gao, L., Kaestner, K. H., Susztak, K., Sun, Y. v., DuVall, S. L., Cho, K., Lee, J. S., Gaziano, J. M., Phillips, L. S., Meigs, J. B., Reaven, P. D., Wilson, P. W., Edwards, T. L., Rader, D. J., Damrauer, S. M., O'Donnell, C. J., Tsao, P. S., Atkinson, M. A., Powers, A. C., Naji, A., Kaestner, K. H., Abecasis, G. R., Baras, A., Cantor, M. N., Coppola, G., Economides, A. N., Lotta, L. A., Overton, J. D., Reid, J. G., Shuldiner, A. R., Beechert, C., Forsythe, C., Fuller, E. D., Gu, Z., Lattari, M., Lopez, A. E., Schleicher, T. D., Padilla, M. S., Toledo, K., Widom, L., Wolf, S. E., Pradhan, M., Manoochehri, K., Ulloa, R. H., Bai, X., Balasubramanian, S., Barnard, L., Blumenfeld, A. L., Eom, G., Habegger, L., Hawes, A., Khalid, S., Maxwell, E. K., Salerno, W. J., Staples, J. C., Yadav, A., Jones, M. B., Mitnaul, L. J., Aguayo, S. M., Ahuja, S. K., Ballas, Z. K., Bhushan, S., Boyko, E. J., Cohen, D. M., Concato, J., Constans, J. I., Dellitalia, L. J., Fayad, J. M., Fernando, R. S., Florez, H. J., Gaddy, M. A., Gappy, S. S., Gibson, G., Godschalk, M., Greco, J. A., Gupta, S., Gutierrez, S., Hammer, K. D., Hamner, M. B., Harley, J. B., Hung, A. M., Huq, M., Hurley, R. A., Iruvanti, P. R., Ivins, D. J., Jacono, F. J., Jhala, D. N., Kaminsky, L. S., Kinlay, S., Klein, J. B., Liangpunsakul, S., Lichy, J. H., Mastorides, S. M., Mathew, R. O., Mattocks, K. M., McArdle, R., Meyer, P. N., Meyer, L. J., Moorman, J. P., Morgan, T. R., Murdoch, M., Nguyen, X. M. T., Okusaga, O. O., Oursler, K. A. K., Ratcliffe, N. R., Rauchman, M. I., Robey, R. B., Ross, G. W., Servatius, R. J., Sharma, S. C., Sherman, S. E., Sonel, E., Sriram, P., Stapley, T., Striker, R. T., Tandon, N., Villareal, G., Wallbom, A. S., Wells, J. M., Whittle, J. C., Whooley, M. A., Xu, J., Yeh, S. S., Aslan, M., Brewer, J. v., Brophy, M. T., Connor, T., Argyres, D. P., Do, N. v., Hauser, E. R., Humphries, D. E., Selva, L. E., Shayan, S., Stephens, B., Whitbourne, S. B., Zhao, H., Moser, J., Beckham, J. C., Breeling, J. L., Romero, J. P. C., Huang, G. D., Ramoni, R. B., Pyarajan, S., Sun, Y. v., Cho, K., Wilson, P. W., O'Donnell, C. J., Tsao, P. S., Chang,

K. M., Gaziano, J. M., Muralidhar, S., Chang, K. M., Voight, B. F. and Saleheen, D. (2020) “Discovery of 318 new risk loci for type 2 diabetes and related vascular outcomes among 1.4 million participants in a multi-ancestry meta-analysis,” *Nature Genetics*, 52(7), pp. 680–691. doi: 10.1038/s41588-020-0637-y.

Vulliamy, P., Montague, S. J., Gillespie, S., Chan, M. v., Coupland, L. A., Andrews, R. K., Warner, T. D., Gardiner, E. E., Brohi, K. and Armstrong, P. C. (2020) “Loss of GPVI and GPIbα contributes to trauma-induced platelet dysfunction in severely injured patients,” *Blood Advances*, 4(12), pp. 2623–2630. doi: 10.1182/bloodadvances.2020001776.

Wang, H., Zang, C., Liu, X. S. and Aster, J. C. (2015) “The role of notch receptors in transcriptional regulation,” *Journal of Cellular Physiology*, pp. 982–988. doi: 10.1002/jcp.24872.

Wang, M., Hao, H., Leeper, N. J. and Zhu, L. (2018) “Thrombotic regulation from the endothelial cell perspectives,” *Arteriosclerosis, Thrombosis, and Vascular Biology*, 38(6), pp. E90–E95. doi: 10.1161/ATVBAHA.118.310367.

Weber, S., Niessen, M. T., Prox, J., Lüllmann-Rauch, R., Schmitz, A., Schwanbeck, R., Blobel, C. P., Jorissen, E., de Strooper, B., Niessen, C. M. and Saftig, P. (2011) “The disintegrin/metalloproteinase Adam10 is essential for epidermal integrity and Notch-mediated signaling,” *Development*, 138(3), pp. 495–505. doi: 10.1242/dev.055210.

Wilke, G. A. and Wardenburg, J. B. (2010) “Role of a disintegrin and metalloprotease 10 in Staphylococcus aureus α-hemolysin - Mediated cellular injury,” *Proceedings of the National Academy of Sciences of the United States of America*, 107(30), pp. 13473–13478. doi: 10.1073/pnas.1001815107.

Williams, E. J., Williams, G., Howell, F. v., Skaper, S. D., Walsh, F. S. and Doherty, P. (2001) “Identification of an N-cadherin motif that can interact with the fibroblast growth factor receptor and is required for axonal growth,” *Journal of Biological Chemistry*, 276(47), pp. 43879–43886. doi: 10.1074/jbc.M105876200.

Wong, E., Maretzky, T., Peleg, Y., Blobel, C. P. and Sagi, I. (2015) “The functional maturation of a disintegrin and metalloproteinase (ADAM) 9, 10, and 17 requires processing at a newly identified proprotein convertase (PC) cleavage site,” *Journal of Biological Chemistry*, 290(19), pp. 12135–12146. doi: 10.1074/jbc.M114.624072.

Xie, Q., Guo, H., He, P., Deng, H., Gao, Y., Dong, N., Niu, W., Liu, T., Li, M., Wang, S., Wu, Y. and Li, J.-L. (2021) “Tspan5 promotes epithelial–mesenchymal transition and tumour metastasis of hepatocellular carcinoma by activating Notch signalling,” *Molecular Oncology*, pp. 1–19. doi: 10.1002/1878-0261.12980.

Xu, D., Sharma, C. and Hemler, M. E. (2009) “Tetraspanin12 regulates ADAM10-dependent cleavage of amyloid precursor protein,” *FASEB Journal*, 23(11), pp. 3674–3681. doi: 10.1096/fj.09-133462.

Xu, P., Liu, J., Sakaki-Yumoto, M. and Derynck, R. (2012) “TACE activation by MAPK-mediated regulation of cell surface dimerization and TIMP3 association,” *Science Signaling*, 5(222), p. ra34. doi: 10.1126/scisignal.2002689.

Xu, X. R., Carrim, N., Neves, M. A. D., McKeown, T., Stratton, T. W., Coelho, R. M. P., Lei, X., Chen, P., Xu, J., Dai, X., Li, B. X. and Ni, H. (2016) "Platelets and platelet adhesion molecules: Novel mechanisms of thrombosis and anti-thrombotic therapies," *Thrombosis Journal*, 14(Suppl 1), p. 29. doi: 10.1186/s12959-016-0100-6.

Yalcin Kehribar, D., Cihangiroglu, M., Sehmen, E., Avci, B., Capraz, A., Yildirim Bilgin, A., Gunaydin, C. and Ozgen, M. (2021) "The receptor for advanced glycation end product (RAGE) pathway in COVID-19," *Biomarkers*, 26(2), pp. 114–118. doi: 10.1080/1354750X.2020.1861099.

Yamashita, Y., Naitoh, K., Wada, H., Ikejiri, M., Mastumoto, T., Ohishi, K., Hosaka, Y., Nishikawa, M. and Katayama, N. (2014) "Elevated plasma levels of soluble platelet glycoprotein VI (GPVI) in patients with thrombotic microangiopathy," *Thrombosis Research*, 133(3), pp. 440–444. doi: 10.1016/j.thromres.2013.11.023.

Yang, X., Claas, C., Kraeft, S. K., Chen, L. B., Wang, Z., Kreidberg, J. A. and Hemler, M. E. (2002) "Palmitoylation of tetraspanin proteins: Modulation of CD151 lateral interactions, subcellular distribution, and integrin-dependent cell morphology," *Molecular Biology of the Cell*, 13(3), pp. 767–781. doi: 10.1091/mbc.01-05-0275.

Yang, Y., Liu, X. R., Greenberg, Z. J., Zhou, F., He, P., Fan, L., Liu, S., Shen, G., Egawa, T., Gross, M. L., Schuettpelz, L. G. and Li, W. (2020) "Open conformation of tetraspanins shapes interaction partner networks on cell membranes," *The EMBO Journal*, 39(18). doi: 10.15252/embj.2020105246.

Yauch, R. L., Berditchevski, F., Harler, M. B., Reichner, J. and Hemler, M. E. (1998) "Highly stoichiometric, stable, and specific association of integrin α3β1 with CD151 provides a major link to phosphatidylinositol 4-kinase, and may regulate cell migration," *Molecular Biology of the Cell*, 9(10), pp. 2751–2765. doi: 10.1091/mbc.9.10.2751.

van Zelm, M. C., Smet, J., Adams, B., Mascart, F., Schandené, L., Janssen, F., Ferster, A., Kuo, C. C., Levy, S., van Dongen, J. J. M. and van der Burg, M. D. (2010) "CD81 gene defect in humans disrupts CD19 complex formation and leads to antibody deficiency," *Journal of Clinical Investigation*, 120(4), pp. 1265–1274. doi: 10.1172/JCI39748.

Zhang, B., Zhang, Z., Li, L., Qin, Y.-R., Liu, H., Jiang, C., Zeng, T.-T., Li, M.-Q., Xie, D., Li, Y., Guan, X.-Y. and Zhu, Y.-H. (2018) "TSPAN15 interacts with BTRC to promote oesophageal squamous cell carcinoma metastasis via activating NF-κB signaling," *Nature Communications*, 9(1), p. 1423. doi: 10.1038/s41467-018-03716-9.

Zhang, L., Bukulin, M., Kojro, E., Roth, A., Metz, V. v., Fahrenholz, F., Nawroth, P. P., Bierhaus, A. and Postina, R. (2008) "Receptor for advanced glycation end products is subjected to protein ectodomain shedding by metalloproteinases," *Journal of Biological Chemistry*, 283(51), pp. 35507–35516. doi: 10.1074/jbc.M806948200.

Zhou, J., Fujiwara, T., Ye, S., Li, X. and Zhao, H. (2014) "Downregulation of Notch modulators, tetraspanin 5 and 10, inhibits osteoclastogenesis in vitro," *Calcified Tissue International*, 95(3), pp. 209–217. doi: 10.1007/s00223-014-9883-2.

Zimmerman, B., Kelly, B., McMillan, B. J., Seegar, T. C. M., Dror, R. O., Kruse, A. C. and Blacklow, S. C. (2016) "Crystal structure of a full-length human tetraspanin reveals a

cholesterol-binding pocket," *Cell*, 167(4), pp. 1041-1051.e11. doi: 10.1016/j.cell.2016.09.056.

Zuidscherwoude, M., Göttfert, F., Dunlock, V. M. E., Figdor, C. G., van den Bogaart, G. and van Spriel, A. B. (2015) "The tetraspanin web revisited by super-resolution microscopy," *Scientific Reports*, 5(1), p. 12201. doi: 10.1038/srep12201.